Heat Transfer Coefficient Using Liquid Heat Transfer Fluids for use in Active Magnetic Regenerative Refrigeration

by

Michael Frischmann

A thesis submitted in partial fulfillment of the requirements for the degree of

Master of Science

(Mechanical Engineering)

at the

UNIVERSITY OF WISCONSIN-MADISON

2009

Abstract

Active magnetic regenerative refrigeration (AMRR) is an alternative and environmentally friendly refrigeration technology with some potential advantages including quiet operation and high part-load and full-load efficiency. As research continues to break down the technical barriers associated with magnetic refrigeration, there is a need for high-fidelity and computationally efficient AMRR computer models. One-dimensional models are often used for this purpose; these models depend on correlations from the literature in order to determine the Nusselt number, axial dispersion coefficient, and friction factor which lead to the heat transfer coefficient, dispersive heat transfer, and pressure drop, respectively.

Nusselt number correlations are of particular interest because the performance of an AMRR system is critically-dependent on the heat transfer coefficient. There is are large discrepancies between the correlations available in the literature. This is particularly true when the correlations are applied to high Prandtl number fluids at low Reynolds number flows; these are the conditions associated with many of the AMRR systems that are being developed for near room temperature operation. Therefore, there is a need for careful measurement of Nusselt number for packed beds of various types at high Prandtl number and low Reynolds number. One technique used to measure the Nusselt number associated with a packed bed uses a passive single-blow test facility. During a single-blow test, a regenerator is cooled to a uniform temperature (i.e., cold-soaked) and then exposed to a step change in fluid temperature entering the bed. By measuring the temperature at the outlet of the regenerator as a function of time it is possible to infer the Nusselt number within the regenerator.

The University of Wisconsin has constructed a single-blow test facility and obtained data for a bed of packed spheres for Reynolds number flows ranging from 1 to 100 and for fluids with Prandtl numbers that range from 7 to 35 using two separate regenerator beds. The experimental data is reduced using two different numerical models. The results from the experiment confirms that they correlation developed by Wakao and Kaguei (1982) is accurate for low Reynolds number high Prandtl number flow through packed sphere regenerators.

Acknowledgements

First and foremost I would like to thank my advisors, Professor Greg Nellis and Professor Sanford Klein for the technical guidance and support on this project. I have learned a great deal over the past year and a half, and am greatly appreciative for it. I would also like to thank Astronautics Corporation for providing the funding for my research, and in particular Steve Jacobs, Carl Zimm, and Andre Boeder for their technical support. Special thanks to Professor Jay Martin for participating on my defense committee.

I would also like to thank my dad Tom, mom Beth, brother Bryan, and sister Katie for their support during my education. I could not have gotten through the last six years without your encouragement. I would also like to thank my grandparents for the never ending supply of support.

I would also like to thank Gabe Bernhardt and Ed Dreir for their assistance in the lab. Thanks to Ryan Taylor and Mike Cheadle for their technical assistance and guidance. Special thanks to Nick Guldan, and Kevin Myers for their ability to keep things in the office fun and relaxed. Finally, I would like to thank everyone in the SEL. The experience I had during my work here has been unforgettable. Thank you all.

Table of contents

Abstract ..... **i**
Acknowledgements ..... **ii**
Table of contents ..... **iii**
List of Figures ..... **v**
List of Tables ..... **ix**
Nomenclature ..... **x**
CHAPER 1 INTRODUCTION 1
1.1 Magnetic Refrigeration 1
1.1.1 The Magnetocaloric Effect 1
1.1.2 The Magnetic Refrigeration Cycle 6
1.2 Astronautics AMRR Prototype 9
1.3 UW AMRR Model Results 10
1.4 Methods of Measuring Nusselt Number 14
1.4.1 Steady State Method 14
1.4.2 Mass Transfer Analog Method 15
1.4.3 Transient Method 16
1.5 Project Description 18
1.6 Thesis Organization 19
CHAPTER 2 PASSIVE REGENERATOR TEST FACILITY 20
2.1 Single-Blow Operation 21
2.2 Second Generation Regenerator 25
2.2.1 Second Generation Regnerator Design 25
2.2.2 Second Generation Regenerator Fabrication 29
2.2.3 Additional Thermocouple Placement 36
2.3 Third Generation Regnerator 42
2.3.1 Third Generation Regenerator Design 42
2.3.2 Third Generation Regenerator Fabrication 46
2.3.3 Initial Trials 50
2.4 Instrumentation and Data Acquisition 52
CHAPTER 3 NUMERICAL MODELS 59
3.1 UW AMRR Model 59
3.1.1 Governing Equations 61
3.1.2 Correlations Used 64
3.1.3 Single Blow Adjustments 66
3.1.4 Determining Nusselt Number with the UW AMRR Model 67
3.2 Astronautics Dispersion Concentric Model 71
3.2.1 Governing Equations 72
3.2.2 Determing Nusselt Number with the DC Model 75
CHAPTER 4 SECOND GENERATION EXPERIMENT RESULTS **79**
4.1 Experiment Data 79
4.2 Repeatability Trials 81
4.3 Second Generation Results 87

4.4 Investigation of Results 92
4.4.1 Heat Transfer with the Environment 92
4.4.2 Nusselt Number as a Function of Re and Pr 98
4.4.3 Flow Maldistribution 102
CHAPTER 5 THIRD GENERATION EXPERIMENT RESULTS 109
5.1 Experiemental Data 109
5.2 Repeatability Experiment 111
5.3 Nusselt Number Results 114
5.3.1 Third Regenerator Results 115
5.3.2 Second Regenerator Results 118
5.4 Friction Factor 120
5.4.1 Uncertaintyin the Friction Factor 122
CHAPTER 6 CONCLUSIONS and Future Work 131
References 133
Appendix A 135
Appendix B 149
Appendix C 172

List of Figures

Figure 1.1 Analogy between magnetic work and mechanical work. 3
Figure 1.2 Temperature – entropy diagram for $Gd_{0.94}Er_{0.06}$ with lines of constant applied magnetic field. 4
Figure 1.3 Adiabatic temperature change with magnetization for $Gd_{0.94}Er_{0.06.}$ 5
Figure 1.4 Active magnetic regenerative refrigeration cycle. 8
Figure 1.5 Rotary AMRR experiment at Astronautics. 10
Figure 1.6 Predicted cooling power versus experimental cooling power. 11
Figure 1.7 Nusselt number correlations from the literature using a Prandtl number of 30 and a bed porosity of 0.36. 14
Figure 2.1 Flow schematic of the single - blow test facility. 20
Figure 2.2 Photograph of the single - blow test facility with the test section, cold and hot temperature baths indicated. 21
Figure 2.3 Flow schematic of the single - blow experiment during cold soak operation. 23
Figure 2.4 Flow schematic of the single - blow experiment during hot blow operation. 25
Figure 2.5 Heat capacity ratio as a function of housing diameter and wall thickness. 27
Figure 2.6 NTU as a function of housing outer diameter for a fluid flow rate of 1.0 L/min. 28
Figure 2.7 Finished regenerator caps. 30
Figure 2.8 The completed screen plugs used to pack the regenerator. 31
Figure 2.9 Stainless steel screen plug tack-welded to the regenerator housing. 31
Figure 2.10 The inside of the regenerator with the foam rubber adhered to the inner walls of the housing and the lower screen plug welded into place. 32
Figure 2.11 Hand press used to compress the spheres in the regenerator housing. 33
Figure 2.12 The regenerator has been fully packed and is clamped so the top screen plug can be tack-welded into place. 34
Figure 2.13 The tack-welds used to secure the second screen plug. Note the slightly convex shape of the screen due to compressing the plug against the spheres. 34
Figure 2.14 One of the thermocouple banks with the thermocouples extending through the rod and the small amount of epoxy used to stabilize the setup. 35
Figure 2.15 The completed second generation regenerator. 36
Figure 2.16 An initial set of test data taken with the new regenerator using a fluid flow rate of 1.0 L/min. The thermocouples at the outlet are numbered. 37
Figure 2.17 Cross section of the regenerator outlet. 38

Figure 2.18 Two additional thermocouples placed at the beginning of the outlet tube. The thermocouples at the inlet were positioned similarly on the inlet tube. 39
Figure 2.19 Experimental results using water with a flow rate of 1.0 L/min with the additional thermocouples in place. 40
Figure 2.20 Measured Nusselt number as a function of Reynolds number for water based on a single thermocouple and the average of all three thermocouples. 41
Figure 2.21 HCR as a function of housing outer diameter and wall thickness for the third generation regenerator. 43
Figure 2.22 Computer model of a cross section of the third generation regenerator. 45
Figure 2.23 Photograph of one of the screen plugs after it was set in place with epoxy. 47
Figure 2.24 Thermocouple placement inside of the regenerator housing. 49
Figure 2.25 Completed third generation regenerator with the external thermocouples exposed and the fiberglass insulation removed. 50
Figure 2.26 Experimental temperature measurements as a function of time for the inlet and outlet thermocouples during a test with a Reynolds number of 2. 51
Figure 2.27 Thermocouple measurements after a sufficiently long period of time with a flow rate of 4.0 L/min. 52
Figure 2.28 Photograph of the magnetic flow meter placement. 53
Figure 2.29 Thermocouple response over a 20 degree. 56
Figure 2.30 The SCXI chassis with the thermocouple, flow meter, and pressure transducer connections highlighted. 57
Figure 3.1 Differential segment of the fluid with all of the energy transfers indicated. 61
Figure 3.2 Differential segment of the regenerator material with all of the associated energy transfers shown. 63
Figure 3.3 RMS error as a function of Nusslet number for a test corresponding to a Reynolds number of 100 with water. 70
Figure 3.4 RMS error as a function of Nusselt number for a Reynolds number of 1.5 with water as the working fluid. 71
Figure 3.5 Computational domains of the dispersion concentric model including the spherical particles. 73
Figure 3.6 Experimental inlet temperature and the curve fit using equation (3.22). 76
Figure 3.7 Experimental volumetric flow rate. 77
Figure 3.8 RMSE as a function of Nusselt number guess for a test with a Reynolds number of 5. 78
Figure 4.1 Maximum attainable Reynolds number of the test facility as a function of the Prandtl number of the fluid used. The fluids that are used in the experiment are indicated. 81
Figure 4.2 Nusselt numbers derived from ten individual sets of data using water at 1.0 L/min. 82
Figure 4.3 Nusselt numbers derived from data using water at 1.0 L/min with Engelbrecht's regenerator. 83

Figure 4.4 Nusselt numbers derived from ten sets of data using water with a flow rate of 1.0 L/min. Five sets of data were taken one day, and five more were taken the next two days. 84
Figure 4.5 Measured Nusselt numbers for temperature spans of 9 K, 19 K, and 28 K. 86
Figure 4.6 Experimentally determined Nusselt numbers for all data sets taken. 87
Figure 4.7 Experimental data along with Nusselt numbers predicted by Wakao and Kaguei. 88
Figure 4.8 Experimental data along with Nusselt numbers predicted by Engelbrecht. 89
Figure 4.9 Average Nusselt number as a function of average Reynolds number. 90
Figure 4.10 Average Nusselt number as a function of average Reynolds number using the range uncertainty. 91
Figure 4.11 Energy balance on one node of the regenerator material including heat loss to the surroundings. 93
Figure 4.12 Diagram of the regenerator showing conduction heat loss through the thermal resistance network associated with the regenerator housing. 94
Figure 4.13 Heat loss to surrounding as a function of time for Re = 100 with water. 97
Figure 4.14 Nusselt numbers for water before and after the heat loss term is included. 98
Figure 4.15 RMS error as a function of Nusselt number guess for both the constant Nusselt number and Nu=f(Re,Pr) for experimental data taken with a Reynolds number of 100 with A and B taken from Wakao and Kaguei. 100
Figure 4.16 RMS error as a function of Nusselt number guess for both the constant Nusselt number and Nu=f(Re,Pr) for experimental data taken with a Reynolds number of 1.5 with A and B taken from Wakao and Kaguei. 100
Figure 4.17 RMS error as a function of Nusselt number guess for constant Nusselt number and Nu=f(Re,Pr) for experimental data taken with a Reynolds number of 100 with A=0.8 and B=0.1. 101
Figure 4.18 RMS error as a function of Nusselt number guess for constant Nusselt number and Nu=f(Re,Pr) for experimental data taken with a Reynolds number of 1.5 with A=0.8 and B=0.1. 102
Figure 4.19 CFD model of the passive regenerator used to study flow maldistribution effects. 104
Figure 4.20 Total pressure drop across the bed predicted by the CFD model and experimentally measured as a function of Reynolds number. 105
Figure 4.21 Fluid velocity in m/s inside regenerator for a Reynolds number of 100. 106
Figure 4.22 Fluid velocity in m/s inside regenerator for a Reynolds number of 38. 107
Figure 4.23 Fluid velocity in m/s inside regenerator for a Reynolds number of 1. 108
Figure 5.1 Maximum achievable Reynolds number for the second and third generation experiment. 111
Figure 5.2 Nusselt number results for 10 individual tests performed at a flow rate of 0.3 L/min (Re = 10). 112
Figure 5.3 Nusselt numbers derived from data using water at 1.0 L/min with Engelbrecht's regenerator. 112

Figure 5.4 Nusselt number derived from 10 sets of data taken on separate days with a flow rate of 0.3 L/min. 114
Figure 5.5 Best fit Nusselt number as a function of average Reynolds number for all data sets taken on the third regenerator. 115
Figure 5.6 Best fit Nusselt numbers along with the Nusselt number predicted by the Wakao and Kaguei correlation. 116
Figure 5.7 Average Nusselt number as a function of average Reynolds number. 117
Figure 5.8 Best fit Nusselt number as a function of average Reynolds number for all data sets taken on the third regenerator. 118
Figure 5.9 Average Nusselt number as a function of average Reynolds number compared with the Wakao and Kaguei correlation. 119
Figure 5.10 Experimental friction factor as a function of Reynolds number for all fluids tested. 121
Figure 5.11 Average friction factor as a function of average Reynolds number along with the Macdonal *et al.* correlation. 122
Figure 5.12 Experimental friction factors using a bed porosity of 0.31 instead of the measured value of 0.368. 124
Figure 5.13 Friction factor as a function of Reynolds number after the diameter of the regenerator has been adjusted from 0.0482 m to 0.0366 m (24 % change). 126
Figure 5.14 Friction factor as a function of average Reynolds number. 129

List of Tables

Table 2.1	Parameters used to re-design the regenerator housing	27
Table 4.1	Required flow rates in L/min. Entries that are grayed out exceed the maximum flow rate of the test facility	80
Table 4.2	Temperature Spans Summary	85
Table 4.3	Variable values used in equation (4.7)	96
Table 4.4	Nominal thermal resistances	96
Table 5.1	Required flow rates in L/min. Entries that are grayed out exceed the maximum flow rate of the test facility	110
Table 5.2	Summary of uncertainty values.	128

Nomenclature

A_c	cross-sectional area (m^2)
a_s	specific surface area (m^2/m^3)
b	half thickness of a plate in a parallel plate regenerator (m)
Bi	Biot number
c	specific heat capacity (J/kg-K)
$c_{\mu_o H}$	specific heat capacity at constant magnetic field (J/kg-K)
DF	heat transfer degradation factor
d_h	hydraulic diameter (m)
d_p	particle diameter in a packed sphere or crushed particle regenerator (m)
e_{Nu}	uncertainty in the mean Nusselt number
f	friction factor
Fo	Fourier number
k	thermal conductivity (W/m-K)
k_{eff}	effective static thermal conductivity of regenerator and fluid (W/m-K)
k_{disp}	thermal conductivity of the fluid due to axial dispersion (W/m-K)
h	heat transfer coefficient (W/m^2-K) or enthalpy (J/kg-K)
h^*	modified heat transfer coefficient (W/m^2-K)
j_D	Chilton-Colburn *j*-factor for mass transfer
j_H	Chilton-Colburn *j*-factor for heat transfer
L	length (m)
m	mass (kg)
$\dot{m}$	mass flow rate (kg/s)
M	magnetic intensity (A/m)
NTU	number of transfer units
Nu	Nusselt number
P	pressure (Pa)
Pe	Peclet number
Pr	Prandtl number
r	radial position of regenerator bed (m)
$\hat{r}$	radial position inside a spherical particle (m)
Re	Reynolds number
s	entropy (J/kg-K)
t	time (s)
T	temperature (K)
T_{Curie}	Curie temperature (K)
u	specific internal energy (J/kg)
U	internal energy (J) or utilization factor
v	specific volume (m^3/kg)
W	work (J)
x	axial position (m)

Greek

ε	porosity of the regenerator bed
μ	viscosity (N-s/m^2) or magnetic permeability (H/m)
$\mu_o H$	applied field (Tesla)
ρ	density (kg/m^3)
σ	standard deviation
τ	cycle duration (s)

Subscripts

C	cold or refrigeration temperature
eff	effective
f	fluid
H	hot or heat rejection temperature
hd	based on hydraulic diameter
i	spatial subscript
j	temporal subscript
P	particle
r	regenerator material
ref	reference
s	surface
w	wall

Chapter 1 - Introduction

1.1 Magnetic Refrigeration

Active magnetic regenerative refrigeration (AMRR) systems have emerged as a possible alternative to vapor compression refrigeration cycles. AMRR systems use solid refrigerants instead of a fluorocarbon working fluid. The solid refrigerant communicates with the environment via a heat transfer fluid. A solid refrigerant would have essentially zero vapor pressure, and therefore have no Ozone Depletion Potential (ODP) and no direct Global Warming Potential (GWP). The heat transfer fluids are typically aqueous solutions, such as ethylene glycol and water, and therefore will have a minimal impact on the environment. In addition to these environmental advantages, AMRR systems have the potential to provide performance that is competitive with vapor compression cycles. This thesis experimentally addresses one specific technical aspect of AMRR systems: the Nusselt number and friction factor correlations associated with the flow of the working fluid through the regenerator composed of the solid refrigerant.

1.1.1 The magnetocaloric effect

The driving phenomenon for magnetic refrigeration is the magnetocaloric effect, which is the entropy change of a material that is induced by magnetization. The internal energy (U) of a thermodynamic substance can change as a result of either work or heat transfer, as shown in equation 1.1.

$$dU = T\,dS + dW \tag{1.1}$$

The first term in equation 1.1 represents the heat transfer to or from the system, while the second term refers to the work performed on the system or extracted from it. Kitanovski and Egolf (2005) explain that through use of the four Maxwell equations, the work for a magnetic material can be described as a function of the applied magnetic field strength ($\mu_o H$) and the magnetic moment (*dM*) assuming that the magnetic field is uniform throughout the entire specimen. Substituting these definitions into equation 1.1 results in an equation including work transfer that is suitable for describing magnetic materials, shown in equation 1.2.

$$dU = T\,dS - \mu_o H\,dM \tag{1.2}$$

Isothermal magnetization of a ferromagnetic solid aligns the magnetic moments of the material, which reduces the magnetic portion of the material's entropy. Similarly, in the reverse process, isothermal demagnetization returns the material to its zero field entropy. An analogous process would be the isothermal compression and expansion of a gas, shown in Figure 1.1 (Engelbrecht, 2005). When a gas is isothermally compressed, the positional disorder, and therefore entropy, is reduced. Isothermal expansion of the gas then returns the entropy to its original uncompressed value.

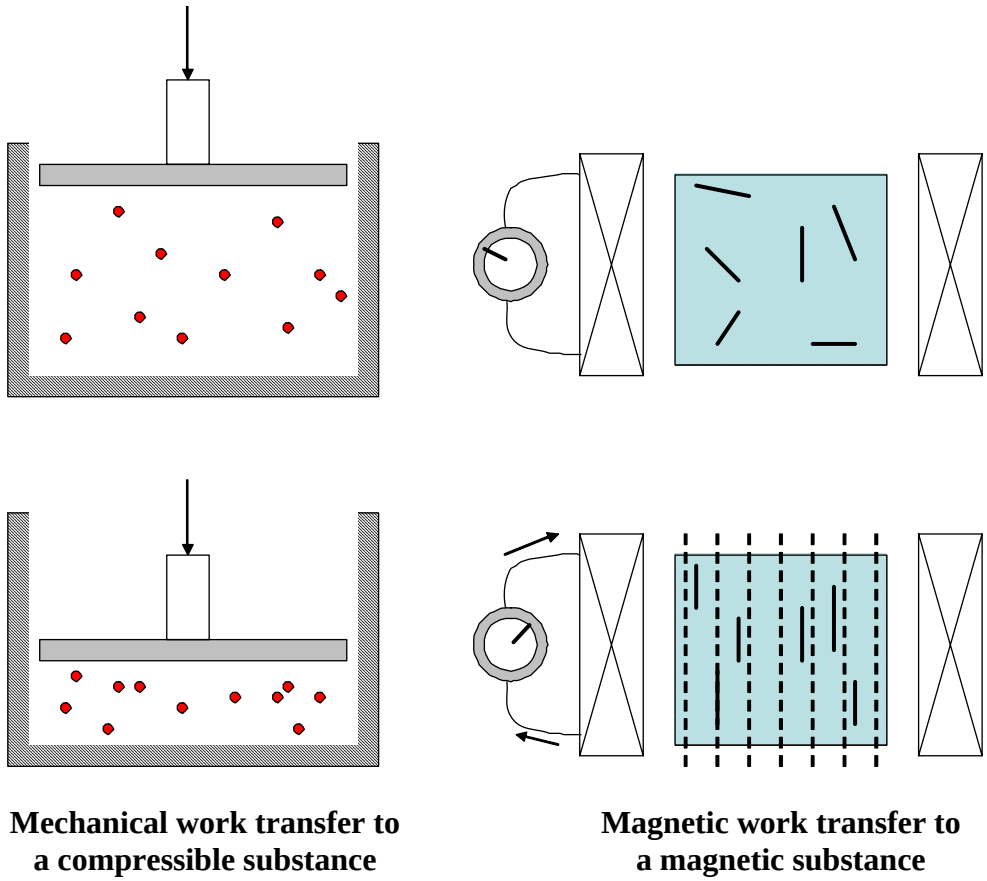

Figure 1.1: Analogy between magnetic work and mechanical work (Engelbrecht, 2005).

Using the relationship between entropy, applied magnetic field and internal energy, it is possible to apply thermodynamic identities to magnetocaloric substances. A temperature – entropy diagram for a magnetocaloric material includes lines of constant applied magnetic field instead of isobars. Figure 1.2 shows a temperature – entropy plot for a Gadolinium – Erbium alloy ($Gd_{0.94}Er_{0.06}$) (Engelbrecht, 2008). Another method of quantifying the magnetocaloric effect is through the adiabatic temperature change. If a magnetocaloric material is adiabatically magnetized, the temperature of the material will increase. Figure 1.3 shows the adiabatic temperature change for $Gd_{0.94}Er_{0.06}$ as a function of the initial temperature of the material (Engelbrecht, 2008). For example, Figure 1.3 shows that when a

piece of $Gd_{0.94}Er_{0.06}$ that is initially at 250 K is magnetized from 0 Tesla to 2 Tesla, its temperature will rise by approximately 2.5 K to 252.5 K.

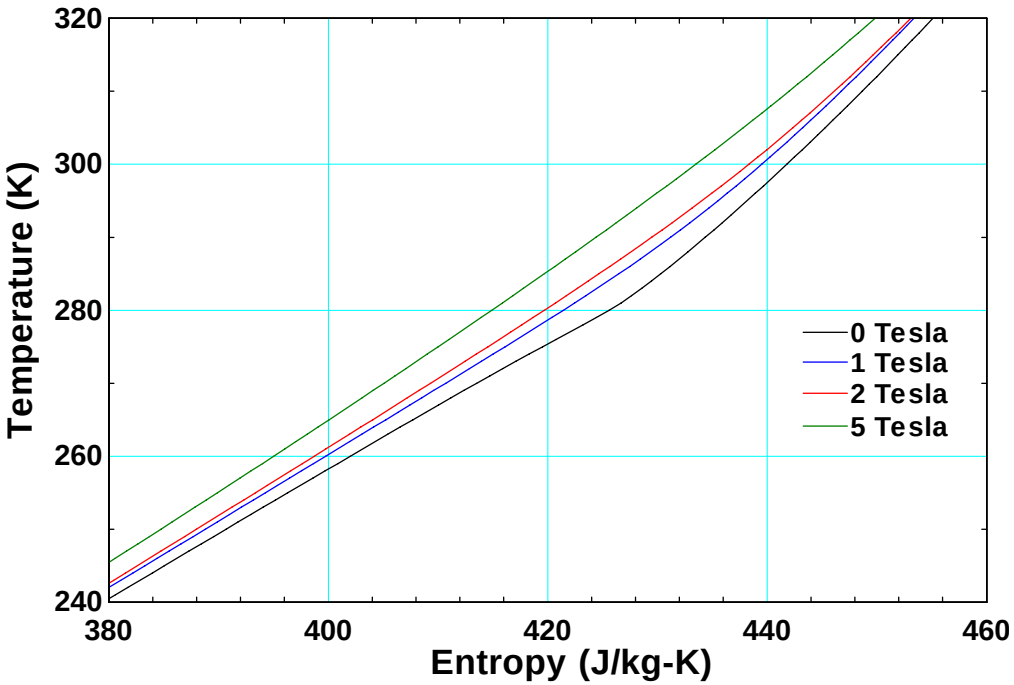

Figure 1.2: Temperature – entropy diagram for $Gd_{0.94}Er_{0.06}$ with lines of constant applied magnetic field (Redrawn from Engelbrecht, 2008).

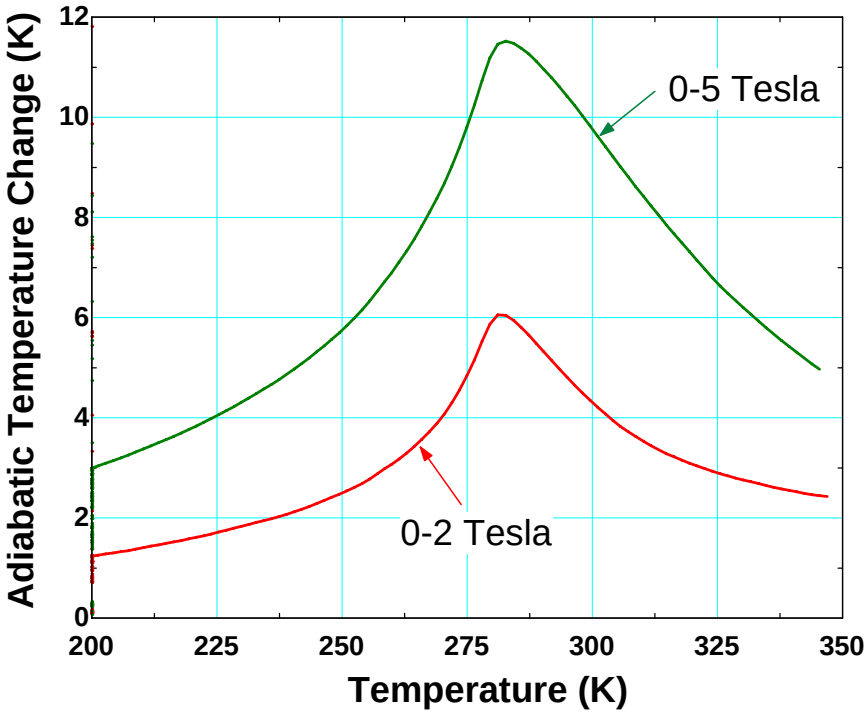

Figure 1.3: Adiabatic temperature change with magnetization for $Gd_{0.94}Er_{0.06}$ (Engelbrecht, 2008)

Examination of Figure 1.3 reveals that a significant temperature change only occurs over a limited temperature span. The magnitude of the magnetocaloric effect is highly sensitive to the initial temperature and, for most materials, a large magnetocaloric effect only occurs near the Curie temperature where the material changes from a ferromagnetic state to a paramagnetic state. Another observation is that the magnitude of the adiabatic temperature change is small compared to the temperature difference that must be covered by a practical cooling system. This necessitates the use of a regenerative cycle in order to provide cooling over a more useful temperature span.

1.1.2 The Magnetic Refrigeration Cycle

The concept of magnetic refrigeration has existed since 1933 when Giauque and MacDougall (1933) used an adiabatic demagnetization refrigeration (ADR) cycle to break the 1 K temperature barrier. The active magnetic regenerative refrigeration (AMRR) overcomes the limited temperature span associated with the ADR cycle and therefore enables magnetic refrigeration for near room temperature applications. A proof of concept AMRR cycle was first developed by Brown (1976).

During an AMRR cycle, a porous media that is composed of the magnetocaloric material is exposed to a time varying magnetic field and a time varying flow of a heat transfer fluid. There are several mechanical realizations of this process, but they are all similar to the example shown in Figure 1.4. The process begins at state (1) where the porous bed (i.e., the regenerator) initially has a temperature distribution that extends, approximately, from the cold reservoir temperature (T_C) at one end to the hot reservoir temperature (T_H) at the other. As the cycle moves from state (1) to state (2), the bed is magnetized with no fluid flow; this causes the material everywhere in the bed to increase in temperature due to the magnetocaloric effect. The new temperature distribution is shown qualitatively in Figure 1.4 as state (2), notice that the highest temperature in the bed has risen above the hot reservoir temperature. Heat transfer fluid then flows from the cold reservoir to the hot reservoir during the cold-to-hot blow process. The bed temperature decreases as it comes into contact with the colder fluid. The temperature distribution at the conclusion of the cold-to-hot blow process is shown qualitatively in Figure 1.4 as state (3). During the cold-to-hot blow process, fluid at a temperature that is greater than T_H enters the hot reservoir and therefore a heat

rejection is accomplished. Next, the bed is demagnetized with no flow which causes the temperature of the entire bed to decrease. The temperature distribution at the conclusion of the demagnetization process is shown qualitatively in Figure 1.4 as state (4). Notice that the temperature at the cold end has fallen below T_C. Therefore, during the ensuing hot-to-cold blow process, the heat transfer fluid flows into the cold reservoir at a temperature that is below T_C which induces a cooling load. At the conclusion of the hot-to-cold blow process the temperature of the bed has returned to state (1) and the cycle repeats.

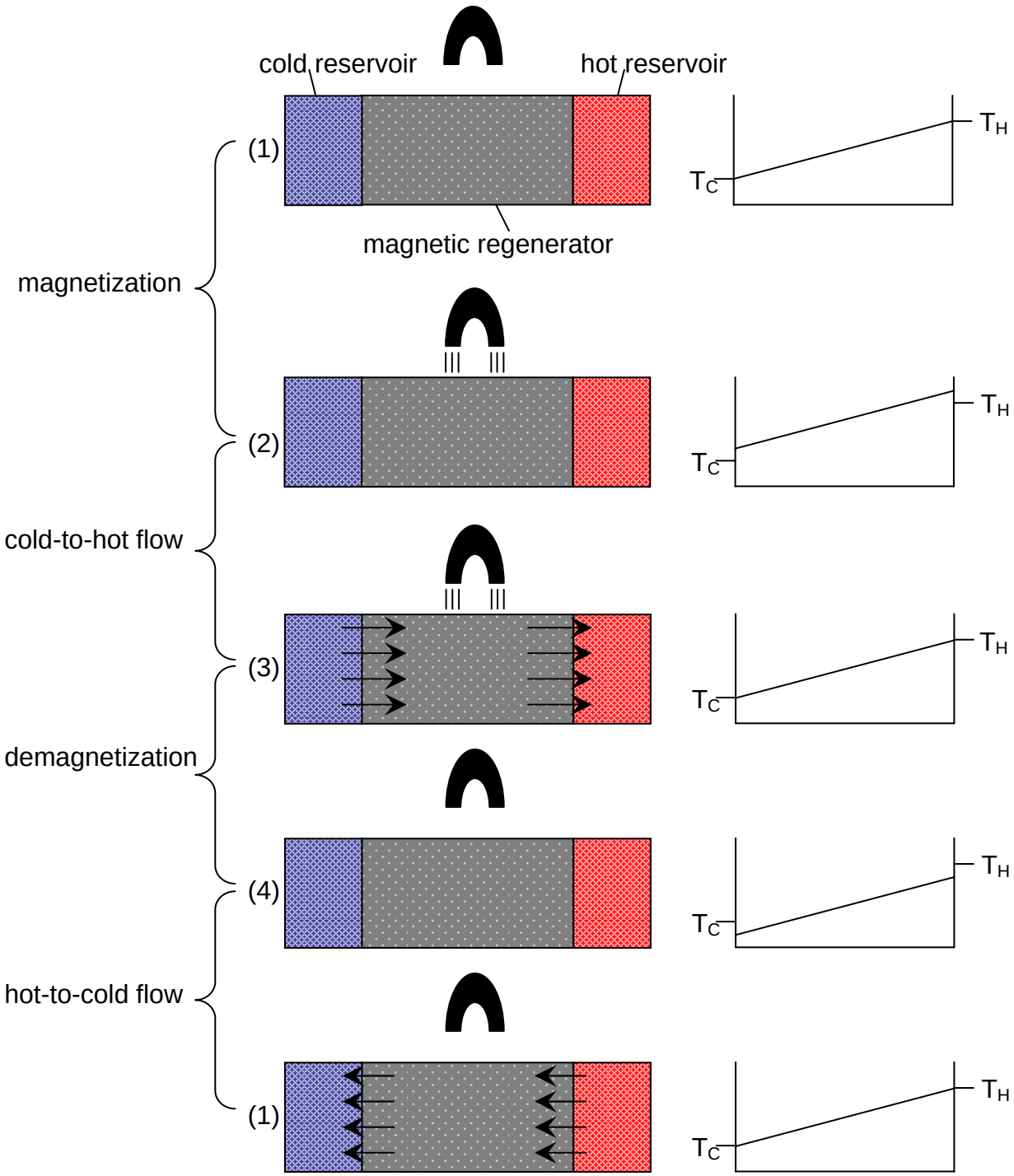

Figure 1.4: Active magnetic regenerative refrigeration cycle

1.2 Astronautics AMRR Prototype

There are several different AMRR system configurations that can accomplish the cycle shown in Figure 1.4 and various prototypes have been constructed. One configuration utilizes a stationary regenerator bed and varies the magnetic field by controlling the current to a solenoid. This type of system configuration is only practical if a superconducting solenoid can be used to handle the large currents that are required to supply a large magnetic field. These systems are therefore not practical near room temperatures because the power required to operate the auxiliary cryogenic refrigeration system that must be used to maintain the superconducting magnets at very low temperature will likely exceed the cooling power obtained from the AMR itself.

AMRR systems for use in residential or other small scale applications will have to use more practical permanent magnets in order to generate the required magnetic field. Permanent magnet systems require some relative motion of the bed with respect to the magnet in order to vary the magnetic field. The bed may physically move into and out of the magnetic field or the magnet may move with respect to the regenerator bed. One example of a rotating bed, stationary magnet system is the rotary AMRR experimental apparatus built by Astronautics Corporation and described by Zimm *et al.* (2006). The rotary device is composed of a regenerator wheel that rotates in the presence of a stationary permanent magnet. The wheel contains six individual regenerator beds that are arranged back-to-back, i.e., the hot ends of each bed share a separating wall. These six beds are arranged on a wheel that rotates through a 1.5 Tesla $Ne_2Fe_{14}B$ permanent magnet. Each regenerator bed completes one AMRR cycle

during one revolution of the regenerator wheel. A photograph of the Astronautics device is shown in Figure 1.5 (Zimm *et al.,* 2006).

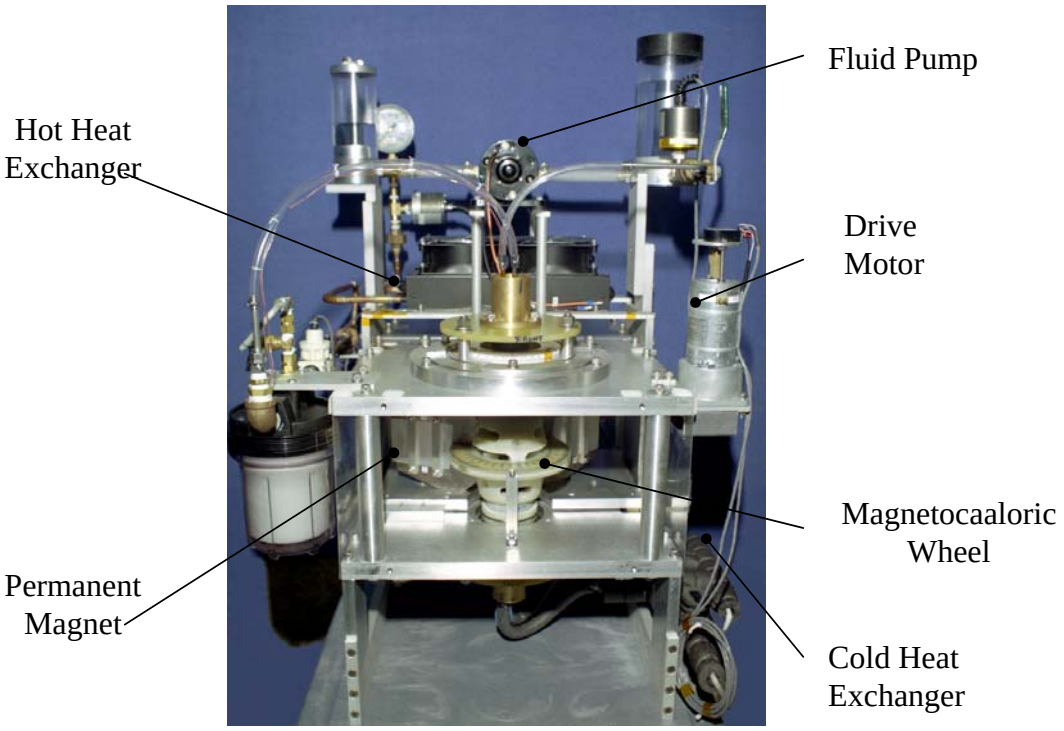

Figure 1.5: Rotary AMRR experiment at Astronautics (Zimm *et al.*, 2006)

1.3 UW AMRR Model Results

Astronautics has taken experimental data measured using the rotary AMRR prototype described in Section 1.2. The rotary bed used to generate the experimental data consisted of packed spherical particles of commercial grade gadolinium (Gd). Figure 1.6 illustrates the predicted cooling power as a function of measured cooling power for these data. Note that each data point represents a unique operating condition corresponding to an experimentally measured mass flow rate, bed temperatures, and cycle frequency. These same conditions were simulated using the AMRR model developed at the University of Wisconsin by Engelbrecht (2008). A detailed description of the model is located in section 3.1.

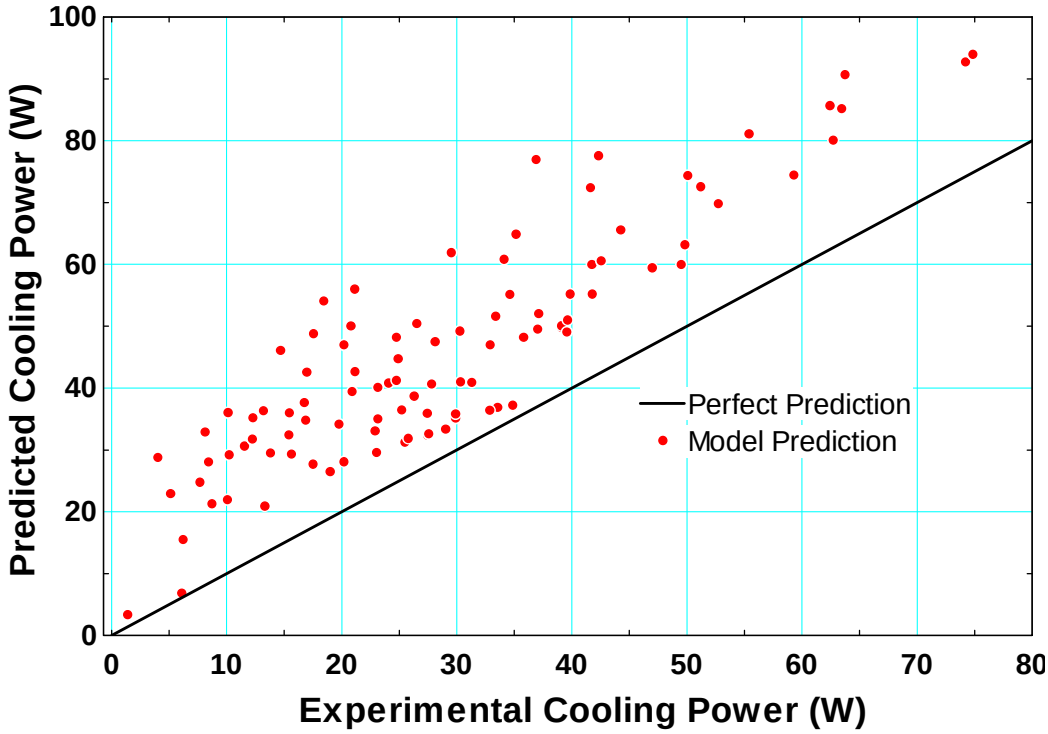

Figure 1.6: Predicted cooling power versus experimental cooling power (Engelbrecht, 2008)

Figure 1.6 shows that the model consistently over predicts the cooling power by, on average, 20 W. One of the possible reasons for this discrepancy is that the Nusselt number correlation used by the model may not be accurate for the flow of the high Prandtl number working fluid that is used to generate the data. Nusselt number is defined as the ratio of convection heat transfer to conduction into a fluid, and is defined in equation 1.3.

$$Nu = \frac{h\,d_p}{k_f} \tag{1.3}$$

where h is the heat transfer coefficient, d_p is the particle diameter, and k_f is the thermal conductivity of the fluid. Most commonly, the Nusselt number is found as a function of the

Reynolds number and Prandtl number of the heat transfer fluid. The Reynolds number (Re_f) is the ratio of inertia to viscous forces, and is shown in equation 1.4.

$$Re_f = \frac{\rho_f v_f d_p}{\mu_f} \tag{1.4}$$

where ρ_f is the density of the fluid, v_f is the superficial velocity of the fluid, d_p is the particle diameter, and μ_f is the dynamic viscosity of the fluid. Prandtl number (Pr_f), defined in equation 1.5, is the ratio of molecular momentum to thermal diffusivity.

$$Pr_f = \frac{\nu_f}{\alpha_f} \tag{1.5}$$

where ν_f is the kinematic viscosity, and α_f is the thermal diffusivity.

Several correlations can be found in the literature for heat transfer inside a packed sphere regenerator. The data used to generate these correlations have been developed in a variety of ways; however, the typical data was collected using a gaseous test fluid and therefore is limited to moderate Prandtl number. As a result, there is significant uncertainty in these correlations when applied to the high Prandtl number fluids used in an AMRR system. This uncertainty shows up most clearly as discrepancies between the various correlations when they are implemented at a high Prandtl number condition. The AMRR model currently uses a correlation developed by Wakao and Kaguei (1982), which is given in equation (1.6).

$$Nu_f = 2 + 1.1 \mathrm{Re}_f^{0.6} \mathrm{Pr}_f^{1/3} \tag{1.6}$$

The Wakao and Kaguei correlation was developed from data measured using single - blow tests with a gaseous heat transfer fluid in a variety of regenerator geometries. An alternative

correlation that is also derived from data is described by Kunii and Levenspiel (1969) and given by equation (1.7).

$$Nu_{Kunii} = 2 + 1.8\left(\frac{Re_f}{\varepsilon}\right)^{1/2} \Pr_f^{1/3} \tag{1.7}$$

The correlation described by Kunii and Levenspiel was intended for use with a Reynolds number based on particle diameter and interstitial fluid velocity. As previously shown in equation 1.4, Reynolds number is defined in this thesis as a function of the superficial fluid velocity. Therefore, in order to keep the definitions in agreement, the Reynolds number from equation 1.4 must be divided by the regenerator bed porosity (ε). Macias – Mechin *et al.* (1991) developed still another correlation using data obtained from a hot wire immersed in a packed sphere regenerator operating with a liquid heat transfer fluid. Once again, the bed porosity adjustment is applied to maintain the proper definition of Reynolds number.

$$Nu_{Macias} = 1.27 + 2.66\left(\frac{Re_f}{\varepsilon}\right)^{0.56} Pr_f^{-0.41}\left(\frac{1-\varepsilon}{\varepsilon}\right)^{0.29} \tag{1.8}$$

where ε is the porosity of the regenerator bed (the ratio of the void volume to the total volume). The correlations shown in equations (1.6) to (1.8) all have a similar form, but they predict very different Nusselt numbers when applied to high Prandtl number. Figure 1.7 shows the Nusselt numbers predicted by these three correlations as a function of Reynolds number for a constant Prandtl number of 30 (which corresponds approximately to a mixture of 50% water and 50% propylene glycol) and bed porosity of 0.36. Notice that the three correlations from the literature differ by approximately a factor of 5 under these conditions

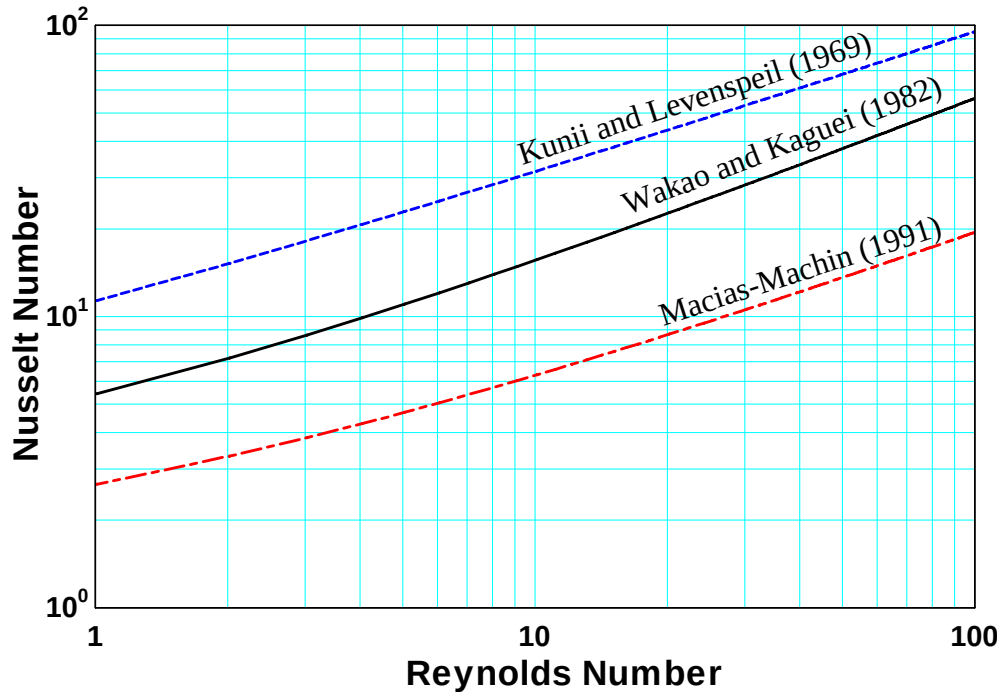

Figure 1.7: Nusselt number correlations from the literature using a Prandtl number of 30 and a bed porosity of 0.36

1.4 Methods of Measuring Nusselt Number

There are many possible experimental techniques used for measuring the heat transfer inside of packed beds. These techniques can be classified into three main categories; the steady state method, the mass transfer analog method, and the transient method. The wide range of experimental techniques may explain the large variability in the correlations in the literature (Heggs and Burns, 1988).

1.4.1 Steady State Method

During the steady state method, the outer temperature of the test section is held at a constant temperature, and fluid is then forced through the test section. Knowing the outlet and inlet temperatures make it possible to determine the heat transfer coefficient present inside the test

section. Maintaining the outer surface temperature can be done a variety of ways, such as a ceramic heater used by Wen *et al.* (2007), or a steam jacket described by Balakrishnan and Pei (1978). The heat transfer coefficient can then be calculated using the equation suggested by Wen *et al.* (2007), shown below as equation (1.9)

$$h_m = \frac{(\dot{m}c)(T_{g,out} - T_{g,in})}{A_{ht}} \Delta T_{lm} \tag{1.9}$$

where h_m is the overall heat transfer coefficient, $\dot{m}$ is the total mass flow rate through the system, c is the specific heat of the heat transfer fluid, $T_{g,out}$ is the temperature of the fluid at the outlet, $T_{g,in}$ is the temperature of the fluid at the inlet, A_{ht} is the total heat transfer surface area, and ΔT_{lm} is the log mean temperature difference.

1.4.2 Mass Transfer Analog Method

The mass transfer method involves measuring the amount of mass transferred from the test section over a period of time. This process can be achieved by soaking the bed and drying it with a gas as described by Balakrishnan and Pei (1978), or constructing the bed out of an evaporative material such as Naphthalene (Carley, 1995). By measuring the initial mass of the test section and its final mass after a known period of time, the amount of mass transfer and the mass transfer rate can be determined. From this information it is possible to calculate the Chilton-Colburn *j*-factor for mass transfer, which is equal to the analogous *j*-factor for heat transfer which is used to find the heat transfer coefficient (Carley, 1995). The Chilton-Colburn *j*-factor for heat transfer is defined in equation 1.10

$$j_D = j_H = \frac{h}{c_p V \rho} \left(\frac{c_p \mu}{k} \right)^{2/3} \tag{1.10}$$

where j_D is the j-factor for mass transfer, j_H is the j-factor for heat transfer, h is the heat transfer coefficient, c_p is the constant pressure specific heat of the gas, V is the characteristic velocity, μ is the gas velocity, and k is the thermal conductivity of the gas.

1.4.3 Transient Method

One technique in the transient method category is single-blow analysis. During a single-blow experiment, a regenerator test section is exposed to a step change in the temperature of the heat transfer fluid and the resulting temperature profiles at the inlet and outlet are measured (Balakrishnan and Pei, 1978). The temperature profile at the outlet can then be used to determine the heat transfer coefficient. The single-blow technique has several advantages over the steady state and mass transfer analog methods in that the apparatus is relatively simple to construct, and the time required for each data point is relatively short (Heggs and Burns, 1988).

Reducing the data obtained from a single-blow test can be done in many different ways. The four most common methods are the maximum slope, shape factor, differential fluid enthalpy, and direct curve matching methods (Heggs and Burns, 1988). The maximum slope method involves finding the unique maximum slope of a breakthrough curve as a function of NTU (number of transfer units). The NTU is then used to predict the heat transfer coefficient (Locke, 1950). While this method greatly reduces the computational effect in the analysis, it is limited to systems in which the NTU is less than 3. A second NTU related technique is proposed by Drabi (1982) in which the time interval between the 20 and 80% breakthrough

points correlates with the shape factor/NTU relationship. Similar to the maximum slope technique, the NTU of the system is restricted to 1.8 < NTU < 20. The third method is the differential fluid enthalpy method. During this type of analysis, it is necessary to measure the time constant of the inlet forcing function as well as the difference between the inlet and outlet temperatures of the test section. Baclic *et al.* (1986) developed a mathematical method of relating the fluid inlet and outlet temperature, and the inlet forcing function time constant to the differential enthalpy change for a true step input. Once again, the differential enthalpy change is given as a function of NTU from which the heat transfer coefficient can be determined.

Heggs and Burns (1988) suggest that the most effective way to reduce the data obtained on a single-blow test facility is by direct shape matching. During direct shape matching, a numerical model of the single-blow test facility is used, and the heat transfer coefficient used by the model is varied to minimize some functional relationship between the theoretical and experimental curves. This is the technique used during data reduction for this project, and is discussed further in section 3.3.1. The functional relationship used is the root mean square error (RMSE) given in equation (1.11)

$$RMSE = \sqrt{\frac{\sum_{i=1}^{N_{exp}} \left(T_{exp,i} - T_{pre,i} \right)^2}{N_{exp}}} \tag{1.11}$$

Where N_{exp} is the number of experimental data points, $T_{exp,i}$ is the ith experimental temperature data point, $T_{pre,i}$ is the ith model predicted temperature.

1.5 Project Description

The main goal of this project was to either experimentally verify one of the existing correlations in the literature at high Prandtl number or, if necessary, develop a new one. The resulting correlation can be used to improve the accuracy of AMRR models, including the model developed at the University of Wisconsin.

In order to examine the heat transfer coefficient associated with flow through a packed sphere regenerator, several passive regenerators have been constructed and tested using a single - blow test procedure. A passive regenerator has geometry that is consistent with those regenerators used in AMRR systems; however, it is not packed with a magnetocaloric material. A single - blow experiment was chosen because of its simplicity and the ability to precisely control the experimental conditions and accurately measure the results.

The experimental measurements from the single - blow test consist of the exit temperature of the fluid as a function of time. The single - blow experimental apparatus was specifically designed so that the temperature variation at the exit is sensitive to the Nusselt number. In order to relate the data to the underlying Nusselt number, it is necessary to use a numerical model. The experimental results have been reduced using two separate models. The first is the one-dimensional University of Wisconsin AMRR model, modified to analyze a single - blow experiment instead of the magnetic refrigeration cycle. This model neglects several phenomena (such as fluid interactions with the heat capacity of the walls of the regenerator); however, the passive regenerator was designed to minimize these affects. The second model used to reduce the data is the Astronautics dispersion concentric model. This model is two

dimensional and is capable of account for many of the phenomena that the one-dimensional UW model neglects.

1.6 Thesis Organization

Chapter 2 describes the single - blow test facility, including the hardware, instrumentation, operating procedure, and the design and construction of both passive regenerators. A detailed descriptions of the two numerical models used to reduce the data are found in Chapter 3. The data associated with the first generation regenerator was reduced using the University of Wisconsin model; the Nusselt number relationship inferred from the data exhibited some unexpected trends. The details of these results and the supplemental investigation into potential causes are presented in Chapter 4. Results obtained using the two dimensional dispersion concentric model are more consistent with expectations and are discussed thoroughly in Chapter 5. Conclusions and other recommendations are presented in Chapter 6.

CHAPTER 2 – Passive Regenerator Test Facility

As discussed in Section 1.4, there are several methods that can be used to experimentally determine the Nusselt number associated with flow through a regenerator packing. The University of Wisconsin has developed a single-blow test facility (Marconnet, 2007) in order to accomplish this task. A single - blow experiment was chosen because of its simplicity and because of the ability to precisely control the experimental conditions and accurately measure the results associated with this type of test. Figure 2.1 shows a detailed schematic of the test facility, and Figure 2.2 is a photograph of the test facility.

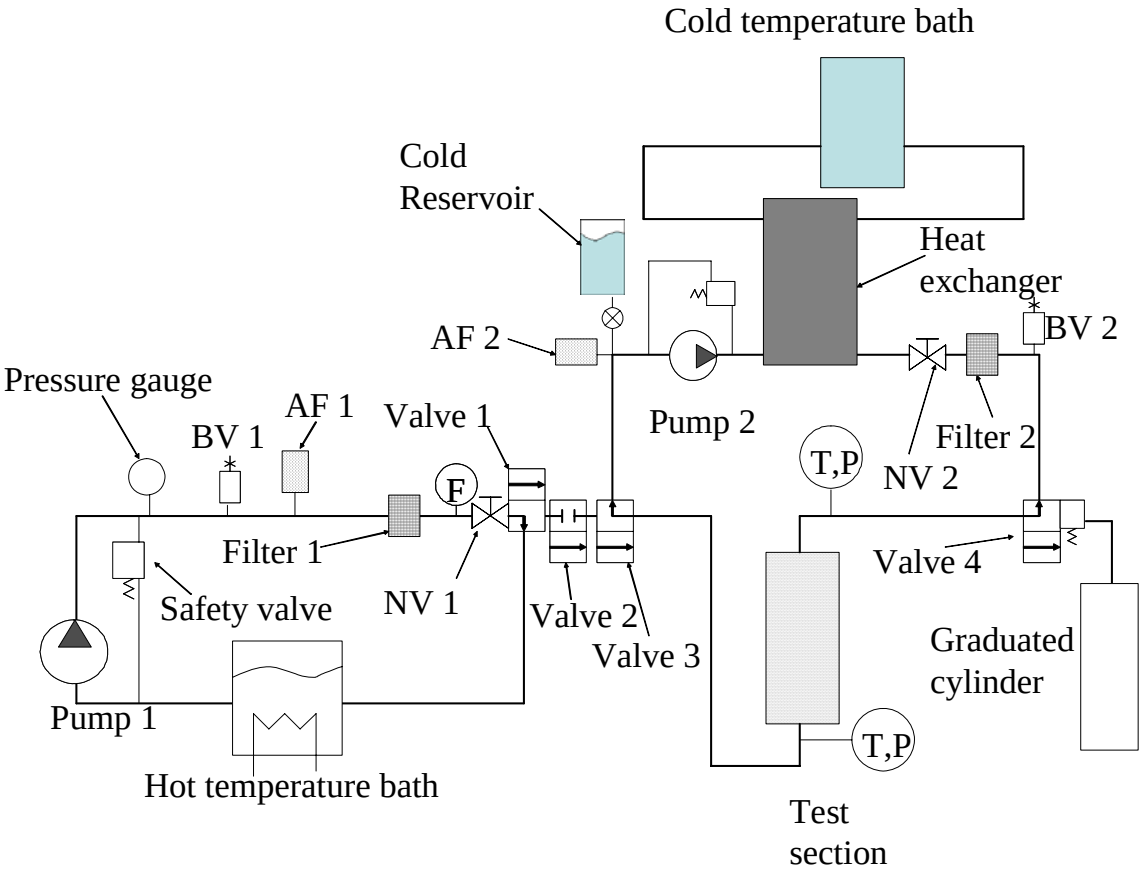

Figure 2.1: Flow schematic of the single - blow test facility.

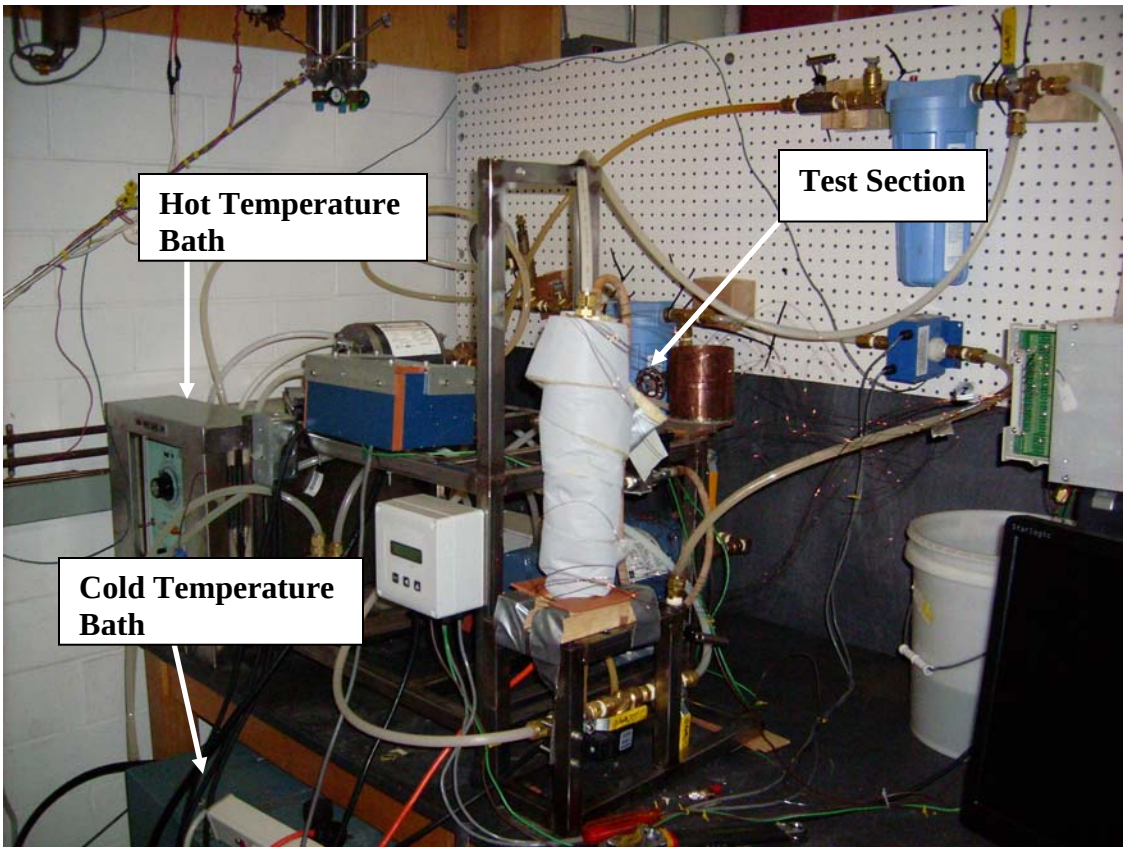

Figure 2.2: Photograph of the single - blow test facility with the test section, cold and hot temperature baths indicated.

2.1 Single - blow Operation

In order to run a single-blow experiment, fluid that has been heat exchanged with coolant from a cold temperature bath is pumped through the regenerator until a uniform cold temperature has been reached (this is referred to as the cold soak process). By activating a sequence of solenoid valves, fluid at an elevated temperature is drawn from a hot temperature bath and diverted through the regenerator in order to accomplish the blow process (this is referred to as the hot blow process). Once the entire regenerator has achieved at least a 90% breakthrough (i.e., the outlet temperature has changed by 90% of its total eventual variation), the test is terminated and the regenerator is cold-soaked again in order to prepare for the next

test. The breakthrough time of the experiment is defined as the time required for the temperature at the outlet of the regenerator to increase from 20% to 80% of the total temperature difference between the cold soak and hot blow.

The cold soak process is initiated by directing fluid from the cold fluid pump (Pump 2), through the test section and then back to the pump using the 3-way valves labeled Valve 3 and Valve 4. The cold soak process is illustrated in Figure 2.3. Fluid flows from Pump 2 (a STA-RITE centrifugal pump model 6HB-61HL) through a heat exchanger that is coupled to the coolant obtained from a Model 575 Poly Science Refrigerated Recirculator which is used to provide the required cooling for the experiment. A needle valve (NV 2) is used to control the flow rate during the cold soak process. The cold fluid passes through a 10 micron sediment filter in order to remove any particulates before traveling through the test section. The flow leaving the test section is directed through Valve 3 and returns to the pump.

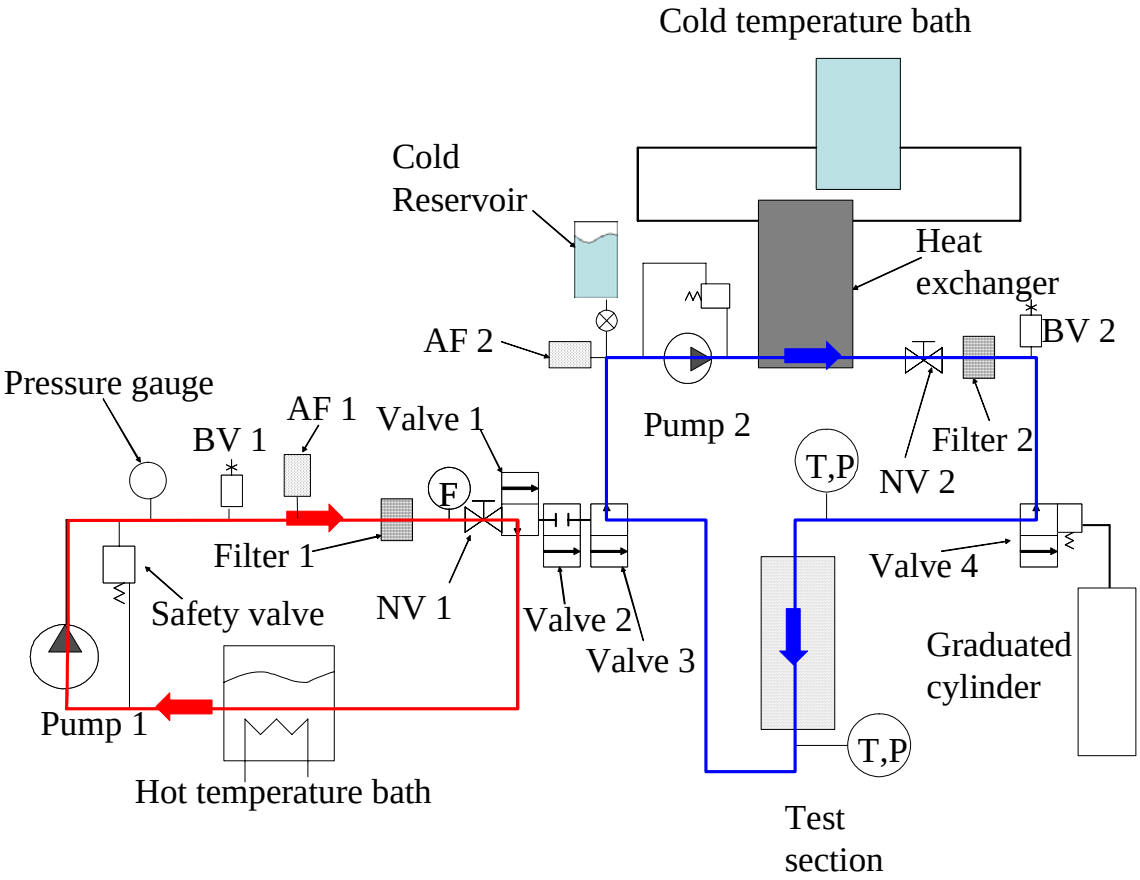

Figure 2.3: Flow schematic of the single - blow experiment during cold soak operation.

Figure 2.3 also illustrates the fluid flow that occurs in the hot loop during the cold soak process. The hot loop is energized using Pump 1 (an Emerson S55-JXNSM-7296 Gear Pump). Flow is obtained from the hot temperature bath (Blue M Magni Whirl 543H constant temperature bath) through a 0-100 psi pressure gauge, an additional 10 micron sediment filter, the volumetric flow meter, a needle valve (NV 1), Valve 1, and finally back to the hot fluid reservoir. The pressure gauge is used to monitor the pressure inside of the plastic lines to insure that it stays below the rated pressure of 120 psi. These components are all required for efficient and effective experimental operation. However, these hot soak components represent a large thermal mass within the experimental system. Therefore, it is necessary to

continually circulate hot fluid through these components during the cold soak process in order to ensure that they are thermally fixed at the hot reservoir temperature. This process reduces the thermal impact that these components have on the experimental results and allows more nearly a step change in the temperature provided to the regenerator. The bleed valves (BV 1 and BV 2) aid in removing air pockets or bubbles that are trapped in the lines. The safety valve ensures that the overall pressure in the system does not exceed the physical limits of the system components.

Once a steady state temperature has been reached during the cold soak process, Valve 1, Valve 3, and Valve 4 are switched simultaneously. This action stops the flow of cold fluid through the test section. The data acquisition system (discussed in Section 2.4) is activated at this point in order to establish the initial temperature distribution associated with the current experiment test. After approximately five seconds of data collection, Valve 2 (a Granzow BDU08110AW Solenoid Valve) is switched on and fluid is routed from the hot reservoir, through the test section and into a graduated cylinder, as illustrated in Figure 2.4. The graduated cylinder is used as a supplemental method of measuring the volumetric flow rate in order to ensure that the flow meter is accurate at least on an average basis. The experiment is run until the regenerator outlet temperature reaches at least 90% breakthrough. At this point, data acquisition is halted, Valve 2 is closed, Valve 3 and Valve 4 are switched to their original positions, and the cold soak process is repeated in order to prepare for the next test. Figure 2.4 also shows that Pump 2 is left operating during the hot blow process in order to ease in switching between the two operating conditions. Step-by-step operating instructions are available in Appendix C.

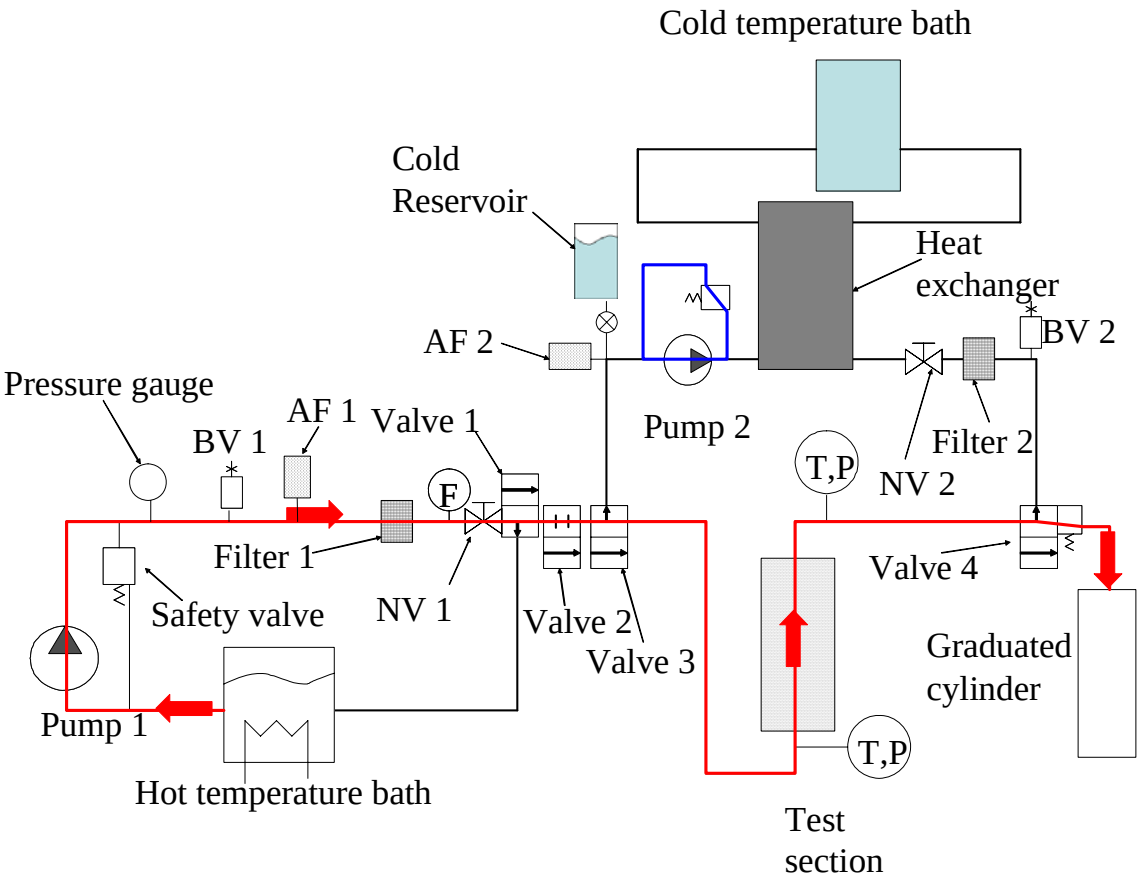

Figure 2.4: Flow schematic of the single - blow experiment during hot blow operation.

2.2 Second Generation Regenerator

2.2.1 Second Generation Regenerator Design

It was observed by Engelbrecht et. al. (2006) that the breakthrough time and temperature distribution inside a regenerator during a single - blow process are most sensitive to the underlying fluid-to-solid heat transfer characteristics (i.e., the Nusselt number) when the number of transfer units associated with the regenerator (*NTU*) is small. Furthermore, the characteristics of the breakthrough curve can be measured most accurately when the overall

breakthrough time is relatively long compared to the resolution of the data acquisition system and the timing of the events required to run an experiment. These observations drove the design of the passive single-blow regenerator test facility, as discussed by Marconnet (2007). Many of the details of the new regenerator were based on the analysis performed by Marconnet (2007) and then verified to ensure that they agreed.

The main goal of the redesign was to reduce the heat capacity of the regenerator housing so that it is a smaller fraction of the heat capacity of the matrix material. This redesign reduces the impact that the fluid to housing thermal interaction has on the experimental results. This thermal interaction was not accounted for explicitly in the UW Model used to reduce the data and therefore the presence of the housing heat capacity tended to reduce the accuracy of the experimental results. The heat capacity ratio (HCR) is defined as the ratio of the heat capacity of the regenerator housing to the heat capacity of the regenerator matrix. The second generation regenerator was designed to minimize the heat capacity ratio by varying the regenerator housing wall thickness and diameter while keeping all other parameters constant at the values that are summarized in Table 2.1. The values listed in Table 2.1 follow the recommendations discussed by Marcnonnet (2007) with the exception of the regenerator length. The regenerator length was chosen in order to reduce fabrication difficulty. Figure 2.5 illustrates contours of the heat capacity ratio in the parameter space of housing diameter and wall thickness.

Table 2.1: Parameters used to re-design the regenerator housing.

Regenerator Material	Type 304 Stainless Steel
Regenerator Length (L_r)	279.4 mm
Regenerator Density (ρ_r)	7903 kg/m^3
Regenerator Specific Heat (c_r)	471 J/kg-K
Housing Material	Type 304 Stainless Steel
Housing Density (ρ_{wall})	7903 kg/m^3
Housing Specific Heat (c_{wall})	471 J/kg-K
Bed Porosity (ψ)	0.36
Foam Rubber Thickness (th_{ins})	0.79 mm

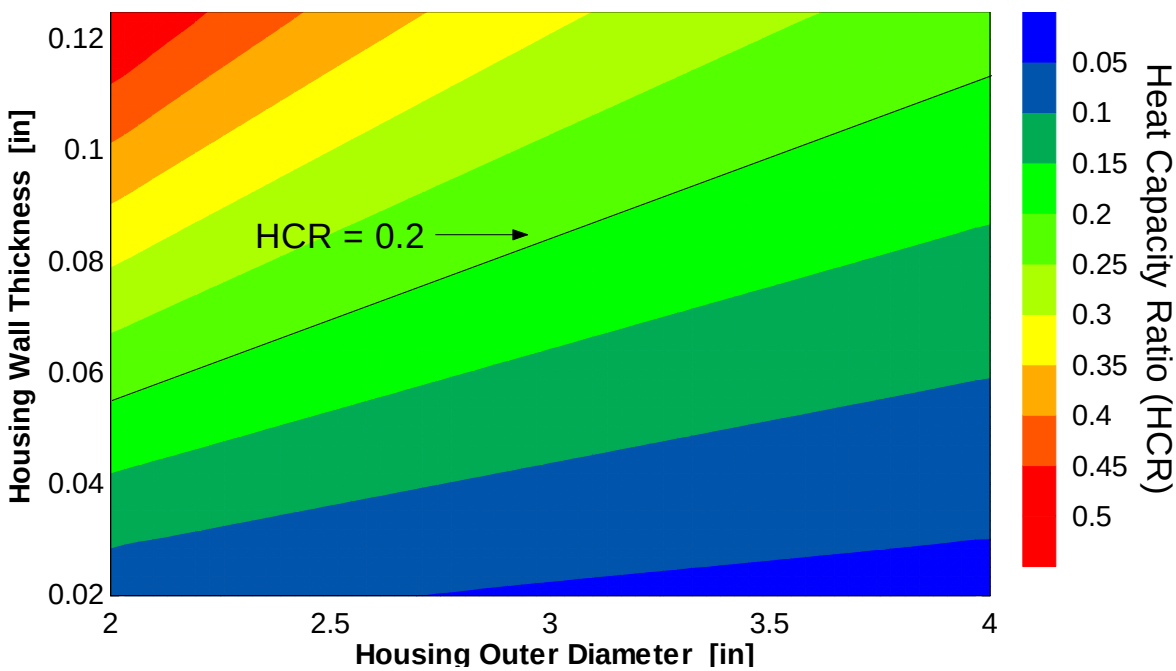

Figure 2.5: Heat capacity ratio as a function of housing diameter and wall thickness.

Examination of Figure 2.5 shows that for any housing diameter larger than 2.5 inch, a wall thickness of 0.065 inch (which is commercially available) keeps the heat capacity ratio below the desired value of 0.2. Marconnet (2007) and others have shown that the breakthrough time and the sensitivity of the shape of the breakthrough curve to the heat transfer coefficient

is high when the number of transfer units (*NTU*) is less than 50. Figure 2.6 shows a plot of the *NTU* of the regenerator as a function of housing outer diameter for a constant fluid flow rate of 1.0 L/min, packed spheres nominally 0.156 inch (3.97 mm) in diameter, and a length that is selected in order to provide a large and therefore measurable breakthrough time of 26.1 seconds.

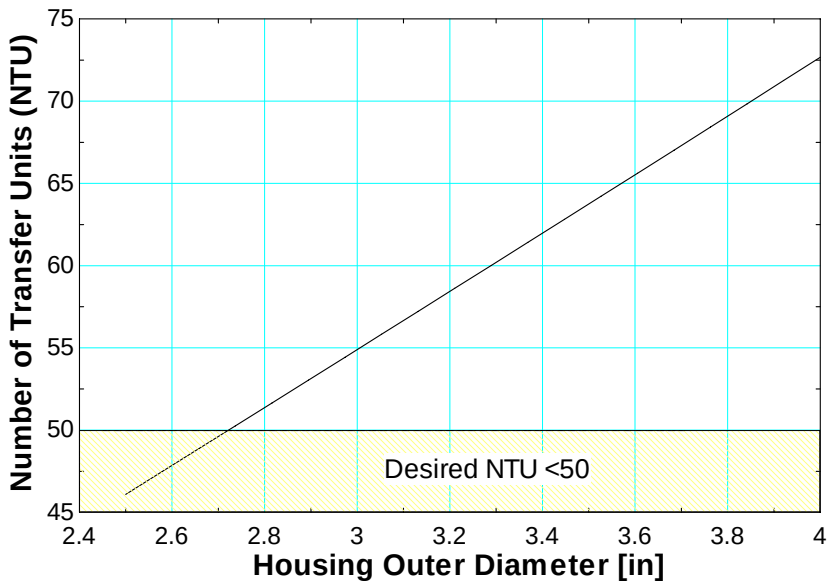

Figure 2.6: NTU as a function of housing outer diameter for a fluid flow rate of 1.0 L/min.

According to Figure 2.6, the maximum allowable outer diameter of the housing is 2.75 inch in order to keep the *NTU* below the desired value of 50. The results of this analysis show that the best design of the housing is a 2.5 inch outer diameter tube with a 0.065 inch wall thickness; this combination results in a *HCR* of 0.18 and *NTU* of 46.1 while keeping the breakthrough time large.

The particles used in the regenerator are 1.56 inch nominal diameter, type 304 stainless steel spheres. These particles are identical to those used in the previous regenerator and were

selected in order to meet the design constraints discussed by Marconnet (2007). One of these is that the Fourier number (*Fo*) characterizing the particle-to-fluid interaction is greater than 10 so that the entire particle participates in the process. The model that was developed by Engelbrecht (2008) is one-dimensional and cannot explicitly model flow non-uniformities in the radial direction. Thus, it is also important to reduce flow maldistribution in the test apparatus (as well as in any real regenerative heat exchanger). Chu and Ng (1989) show that if the ratio of the diameter of a regenerator to the diameter of the spheres is larger than 15, then the permeability (i.e. the ability of the substance to transmit a fluid) approaches that of a regenerator with an infinite diameter ratio. This constraint is satisfied with the 2.5 inch outer diameter tube and the 0.156 inch spheres, which results in a diameter ratio of 15.2.

2.2.2 Second Generation Regenerator Fabrication

The caps of the regenerator were machined from solid discs of type 304 stainless steel that were 3 inch in diameter and 0.75 inch thick. Each cap has a centered circular inset that is 2.5 inch in diameter and 0.375 inch deep and accepts the regenerator housing. There are three holes drilled in the caps. The largest, centered hole is 0.375 inch in diameter and accommodates the fluid flow (inlet or exit); this hole is tapped for 0.375 inch NPT thread in order to accept a fluid fitting. The two smaller holes allow access to the thermocouples and a pressure tap. These are each drilled and tapped for 0.125 inch NPT thread. Figure 2.7 shows a photograph of the completed caps.

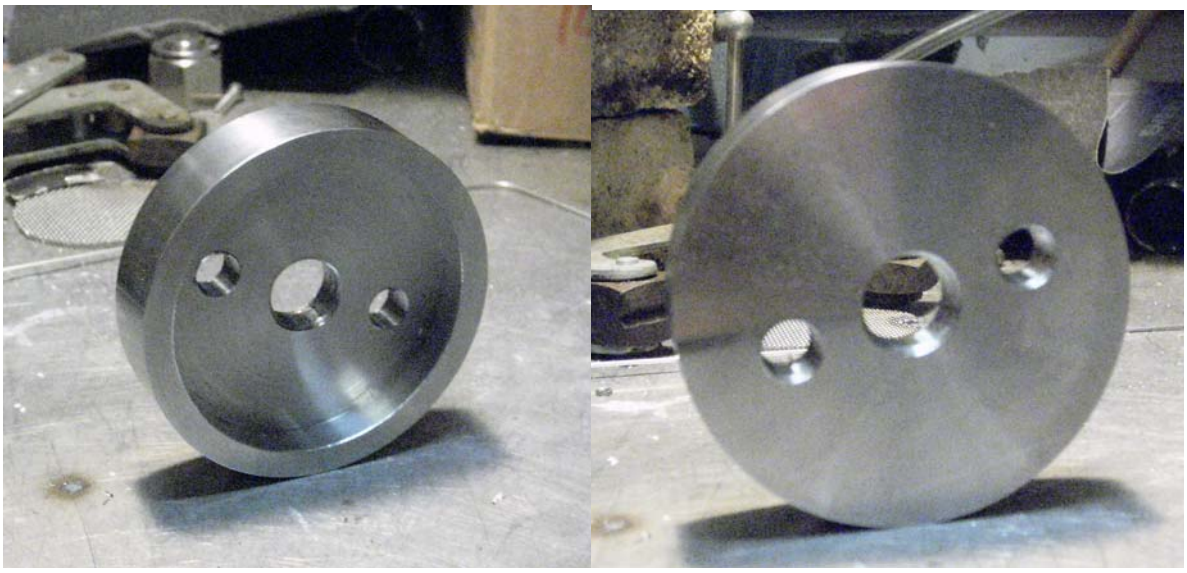

Figure 2.7: Finished regenerator caps. Left – The inside of the cap showing the inset for the regenerator housing. Right – The top of the cap.

The two ends of the regenerator also require a plug to hold the spheres in place. The plugs are made of a 0.5 inch long piece of 2.375 inch outer diameter stainless steel pipe that has been machined so that it fits smoothly within the regenerator housing. Both plugs have a piece of 20x 20 stainless steel screen with 0.020 inch wire diameter attached to one side. The completed screen plugs are shown in Figure 2.8. One of the stainless steel plugs with the screen attached is tack welded into one end of the stainless steel regenerator housing, as shown in Figure 2.9.

Figure 2.8: The completed screen plugs used to pack the regenerator.

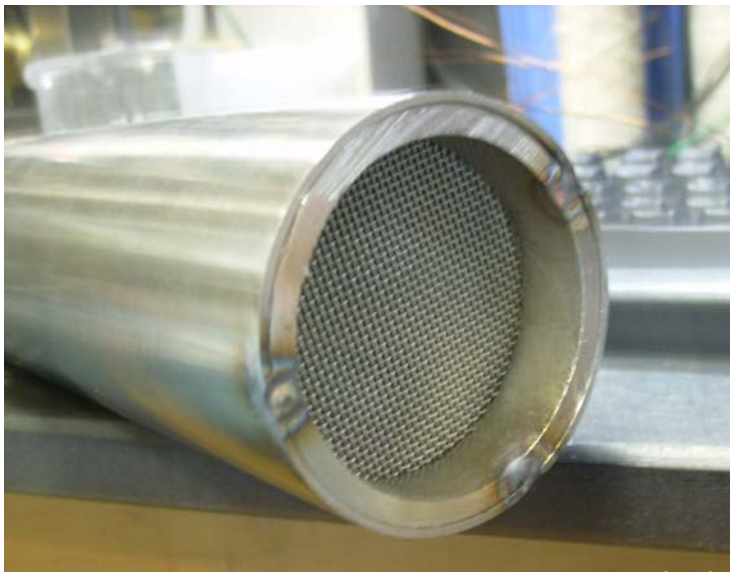

Figure 2.9: Stainless steel screen plug tack-welded to the regenerator housing.

After the plug is welded in place, the foam rubber liner is cut to length so that does not interfere with the second plug that will be installed once the regenerator is fully packed. The foam rubber has an adhesive backing that is used to secure it to the inside of the regenerator housing, as shown in Figure 2.10.

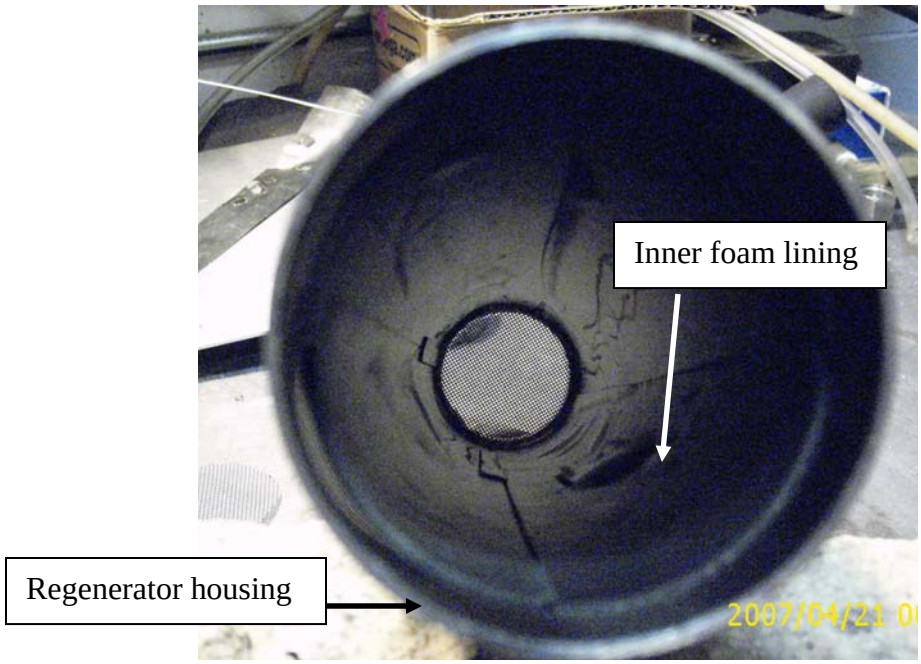

Figure 2.10: The inside of the regenerator with the foam rubber adhered to the inner walls of the housing and the lower screen plug welded into place.

Stainless steel spheres are then placed into the housing two to three layers at a time. After each set of spheres are added, they are compressed using two different plugs and a hand press, as shown in Figure 2.11. The first plug is smaller than the housing and therefore forces the spheres towards the wall of the regenerator. The second plug is nominally same diameter as the inside of the housing and forces the spheres against the lower layers and into the foam lining the wall of the housing. This packing procedure ensures uniform porosity and structure throughout the regenerator.

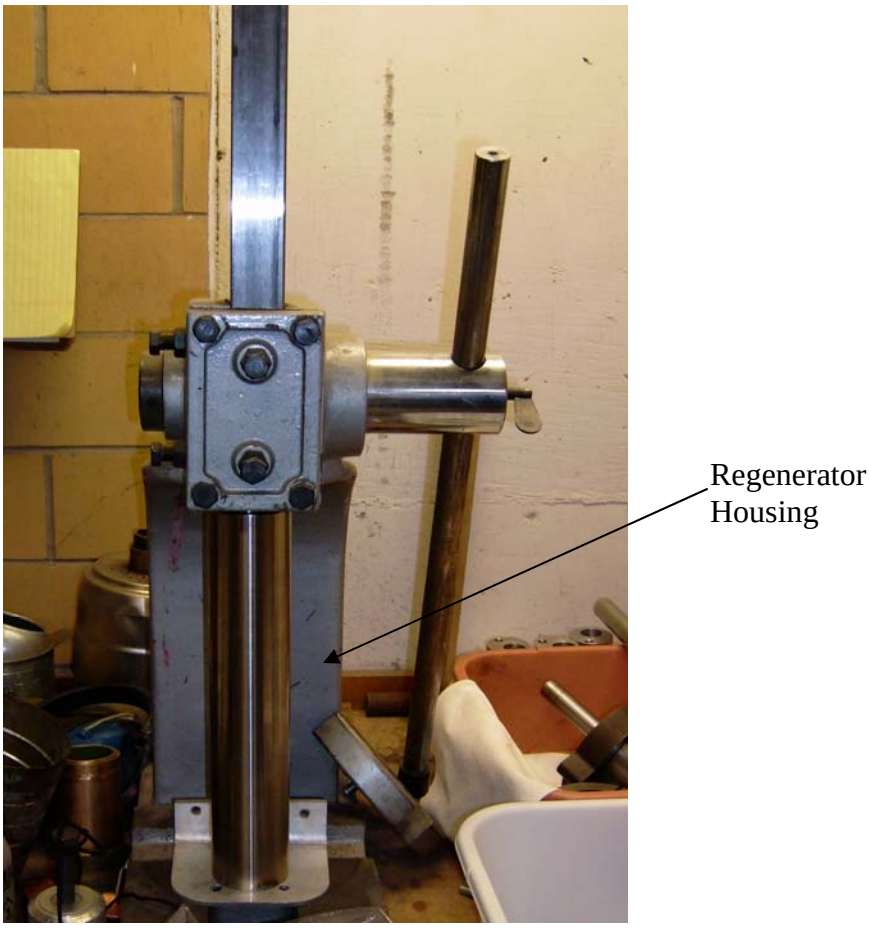

Figure 2.11: Hand press used to compress the spheres in the regenerator housing.

Once the regenerator is fully packed, the second stainless steel screen plug is installed to contain the spheres. The final layers of spheres are packed using the screen plug instead of the metal plug in order to ensure that the entire regenerator is fully compacted. Once the last row of spheres is added, the screen plug is clamped into place for welding as shown in Figure 2.12. The final regenerator tack-welds are shown in Figure 2.13.

Figure 2.12: The regenerator has been fully packed and is clamped so the top screen plug can be tack-welded into place.

Figure 2.13: The tack-welds used to secure the second screen plug. Note the slightly convex shape of the screen due to compressing the plug against the spheres.

The regenerator has two thermocouple banks, one at the inlet plenum and the other at the outlet plenum; these plenums are the void volume that exists between the plug and the cap at each end. Each thermocouple bank is composed of five type-E (chromel–constantan) thermocouples attached to a 0.125 inch diameter acetyl copolymer rod (a material that is similar to DuPont's Delrin), as shown in Figure 2.14. The rod has five small holes that are slightly larger than the thermocouple wire. The thermocouples pass through the holes and protrude into the flow stream. The leads pass through a second hole at the end of the rod for additional stability. A small amount of epoxy is placed on the underside of the rod in order to retain the thermocouples.

Figure 2.14: One of the thermocouple banks with the thermocouples extending through the rod and the small amount of epoxy used to stabilize the setup.

Each of the thermocouple banks is attached to the inside of the screen plug with a small amount of epoxy. Finally, the outside of the regenerator housing and the inside of the

stainless steel caps are polished and cleaned with acetone. Epoxy is used to join these parts and create a water tight seal. A picture of the final assembly is shown in Figure 2.15.

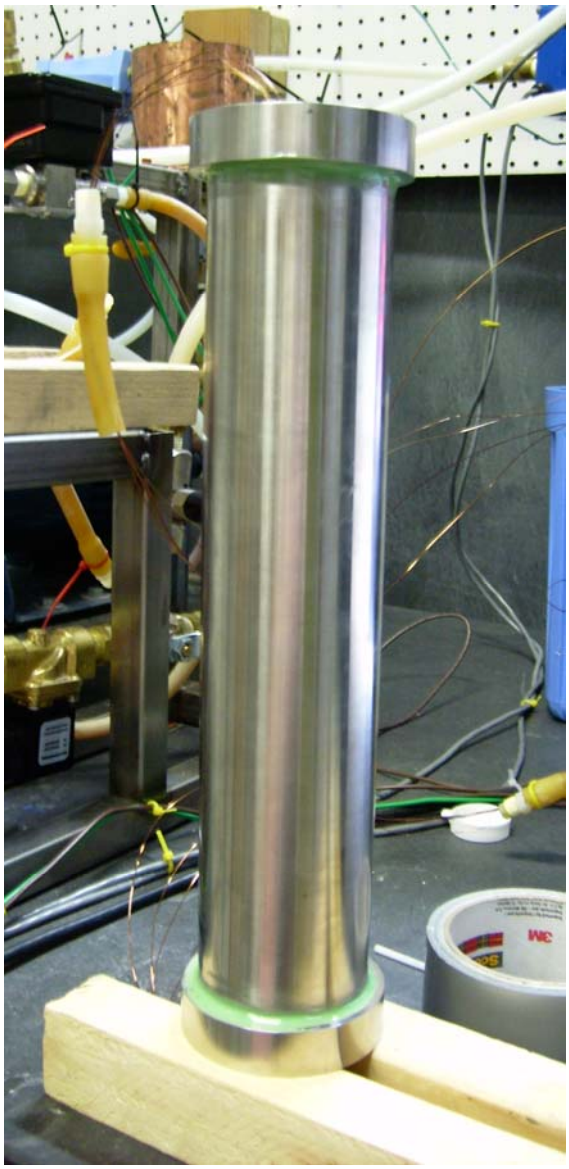

Figure 2.15: The completed second generation regenerator.

2.2.3 Additional Thermocouple Placement

Initial tests were carried out using water as the working fluid in order to confirm that the test facility was functioning properly. Results from a test carried out at a flow rate of 1.0 L/min

(which is a very low flow rate that corresponds to a low Reynolds number data point) are shown in Figure 2.16.

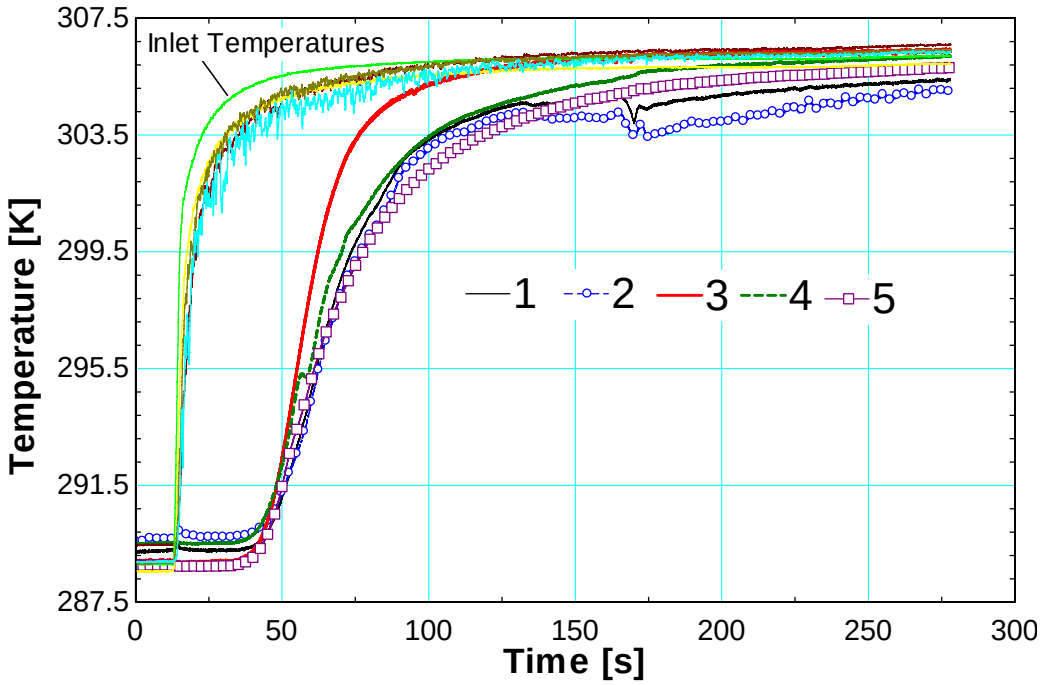

Figure 2.16: An initial set of test data taken with the new regenerator using a fluid flow rate of 1.0 L/min. The thermocouples at the outlet are numbered.

Examination of Figure 2.16 reveals two very important flaws in the experimental data; there is large variation between the thermocouples during a test, and all of the thermocouples do not start and end at the same temperature which suggests a calibration error. The thermocouples are mounted radially across the entire cross section of the inlet and outlet plenums. The numbers in Figure 2.16 are used to identify the thermocouples that are located at the outlet; thermocouples 1 and 5 are located near the walls of the regenerator, thermocouples 2 and 4 are at a mid-radius, and thermocouple 3 is located in the center. Note that thermocouple 3 produces the cleanest temperature profile because it is directly in line

with the outlet tube and is therefore exposed to the highest velocity of fluid. At the very low flow rates associated with the low Reynolds number data, the velocity experienced by thermocouples 1, 2, 4, and 5 is small and therefore they exhibit substantial noise and, perhaps, lag the true temperature of the fluid. The thermocouples are mounted radially in order to measure the radial temperature variation. However, because some of the thermocouples are located in relatively stagnant fluid it seems likely that they do not measure the radial temperature distribution accurately.

Also, the thermocouples are not located exactly at the end of the packed sphere. Figure 2.17 shows a cross section of the regenerator.

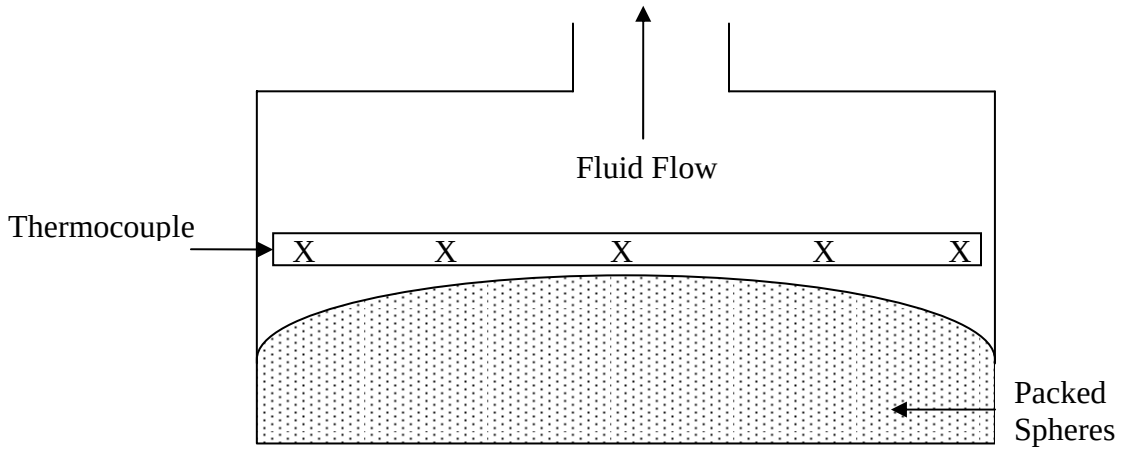

Figure 2.17: Cross section of the regenerator outlet.

When the spheres are packed into the regenerator, they caused the screen used to retain them to curve slightly. It is therefore not possible to locate all of the thermocouples directly adjacent to the screen. Some of the noise observed in the temperature measurements may be caused by fluid that is circulating inside the top of the regenerator. Therefore, it is difficult to

determine if the temperature reading is from the actual exiting fluid, or from the mixing fluid. The middle thermocouple however is located immediately at the end of the packed spheres and is not exposed to the fluid circulation in the same way that the other thermocouples are. The same argument can be applied to the inlet of the test facility as well. Therefore, there is only one useful thermocouple at the center of the regenerator at the inlet and outlet. In order to provide some redundant and reliable temperature sensors, two additional thermocouples (TC 6 and TC 7) have been added near the center at both the inlet and outlet. These additional thermocouples are placed at the end of the inlet tube, and the beginning of the outlet tube, as shown in Figure 2.18.

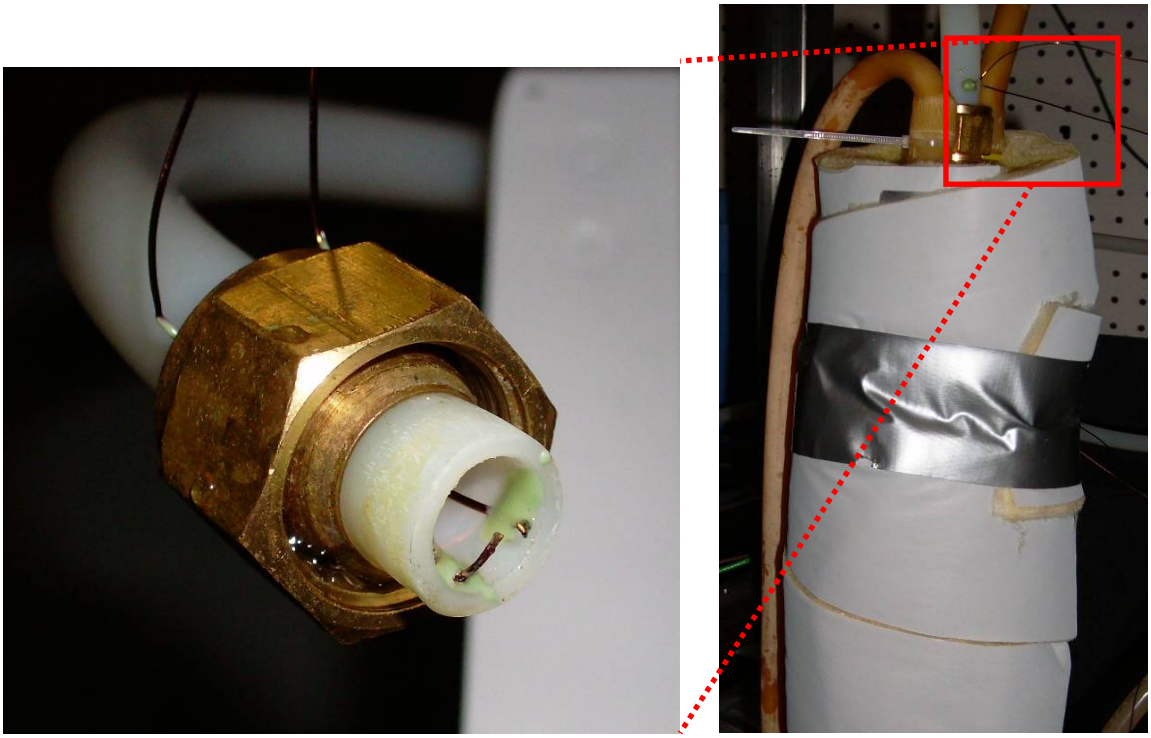

Figure 2.18: Two additional thermocouples placed at the beginning of the outlet tube. The thermocouples at the inlet were positioned similarly on the inlet tube.

The thermocouples are attached to the inside of the tube with epoxy, and positioned so that they are exposed to the relatively high velocity fluid flowing in the tube. Additionally, all of the thermocouples have been re-calibrated between 273 K and 373 K in order to eliminate the measurement error at the start and end of the test seen in Figure 2.16. Figure 2.18 also shows that insulation that has been placed on the outside of the regenerator test facility. The insulation is 1 inch thick fiberglass with a vinyl backing. Figure 2.19 shows the results obtained from a test using water with a flow rate of 1.0 L/min with the new thermocouples in place. The results are much cleaner at the inlet. The measurements at the outlet are improved but there is still some discrepancy at very low flow rates. It is also important to note the improved agreement between all of the thermocouples at the start and end of the test due to the recalibration.

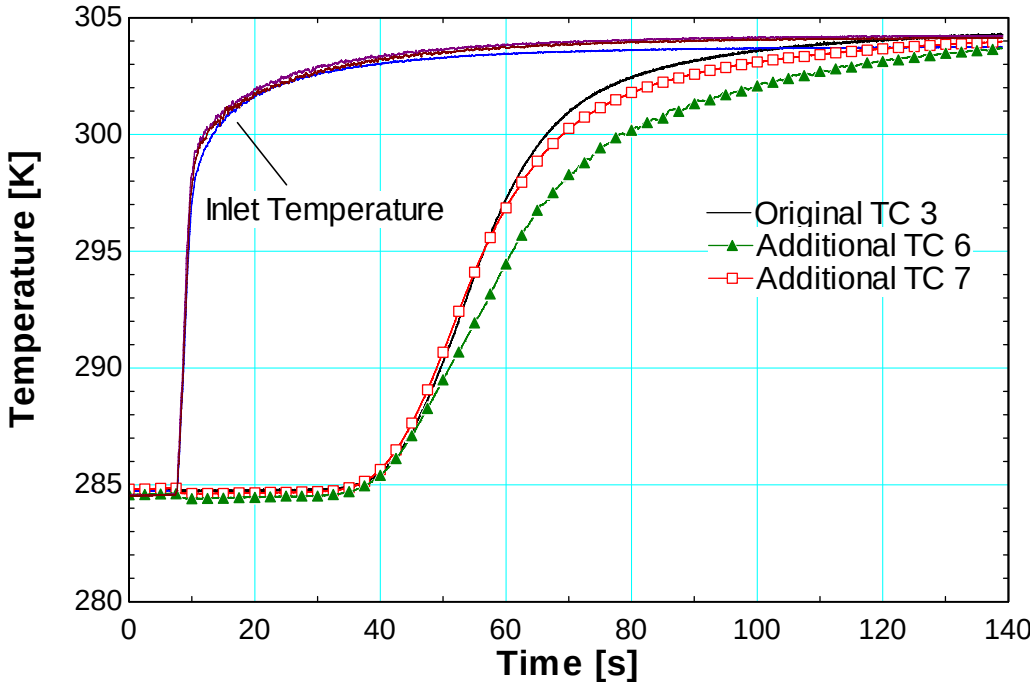

Figure 2.19: Experimental results using water with a flow rate of 1.0 L/min with the additional thermocouples in place.

Because the model requires only one temperature input, the average of the two new thermocouples and the original middle thermocouple are used when reducing the data in order to determine the Nusselt number. Averaging the three central thermocouples does not significantly impact the results, even at very low flow rates. Figure 2.20 illustrates the measured Nusselt number as a function of Reynolds number for the water tests based on a single thermocouple and also based on the average of three thermocouples.

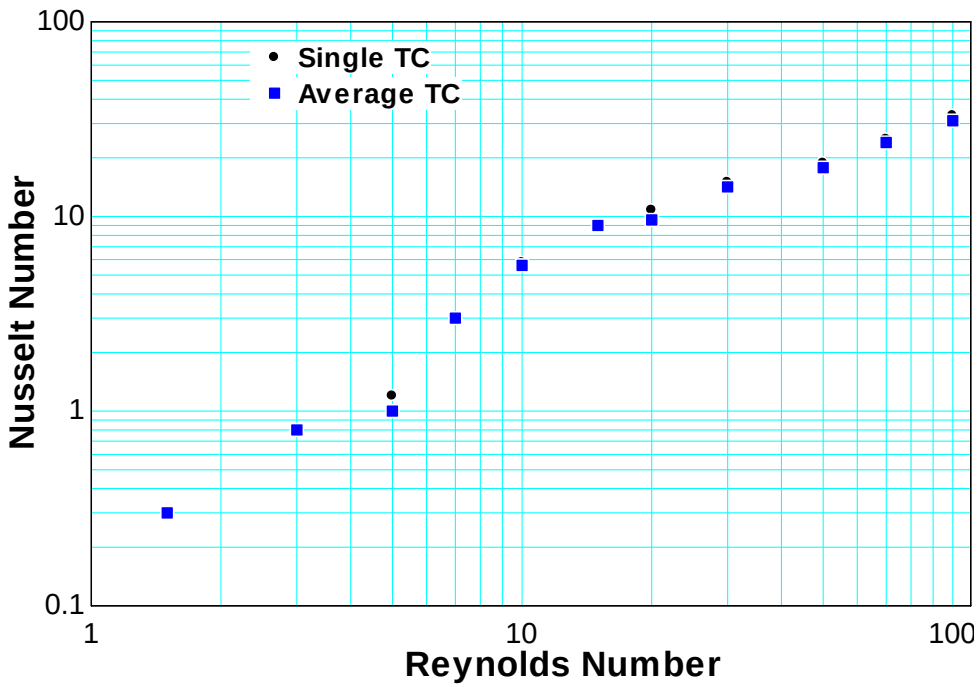

Figure 2.20: Measured Nusselt number as a function of Reynolds number for water based on a single thermocouple and the average of all three thermocouples.

When the Reynolds number is small (i.e., Re < 10) there is essentially no difference in the model predicted Nusselt number. As the flow rate increases there is a more noticeable change, but not of a significant magnitude. When deriving the best fit Nusselt number, the temperature data between the 20% and 80% breakthrough is examined. Therefore, when all three thermocouples are averaged the temperature profile between the 20 and 80%

breakthrough region does not change significantly. This small change in temperature profile only results in a small change in the predicted Nusselt number.

2.3 Third Generation Regenerator

The results reduced from the data obtained using the second generation regenerator exhibit a sharp decrease in the Nusselt number at low Reynolds number. This phenomenon is non-physical and therefore suggests that there are some issues with either the facility or the data reduction. This problem is discussed further in Section 4.2. As part of an effort to identify the source of the underlying problem, a third regenerator was constructed with the objective of further reduce the heat capacity of the regenerator housing. A secondary objective was to provide additional data with an entirely different test section in order to confirm the unusual behavior of the second generation regenerator data.

2.3.1 Third Generation Regenerator Design

The design procedure used for the third generation regenerator is identical to the design procedure used for the second generation regenerator. Marconnet (2007) performed an in depth regenerator design experiment, and many of those recommendations are again used in the design of the third generation regenerator.

As with the second generation regenerator, a primary goal of the third generation regenerator was to reduce the impact of the heat capacity of the housing. The end cap heat capacity was also found to be significant and therefore another goal was to reduce the size of the end caps. In order to provide a geometry that is different from the other regenerators (and therefore

determine whether the unusual behavior is consistent across geometries), the overall outside diameter and length of the test section is reduced. The parameters shown in Table 2.1 are used in the design of this regenerator; notice that the housing outer diameter is 50.8 mm, and the length of the regenerator is 152.4 mm. Figure 2.21 shows the *HCR* in the parameter space of housing outer diameter and wall thickness.

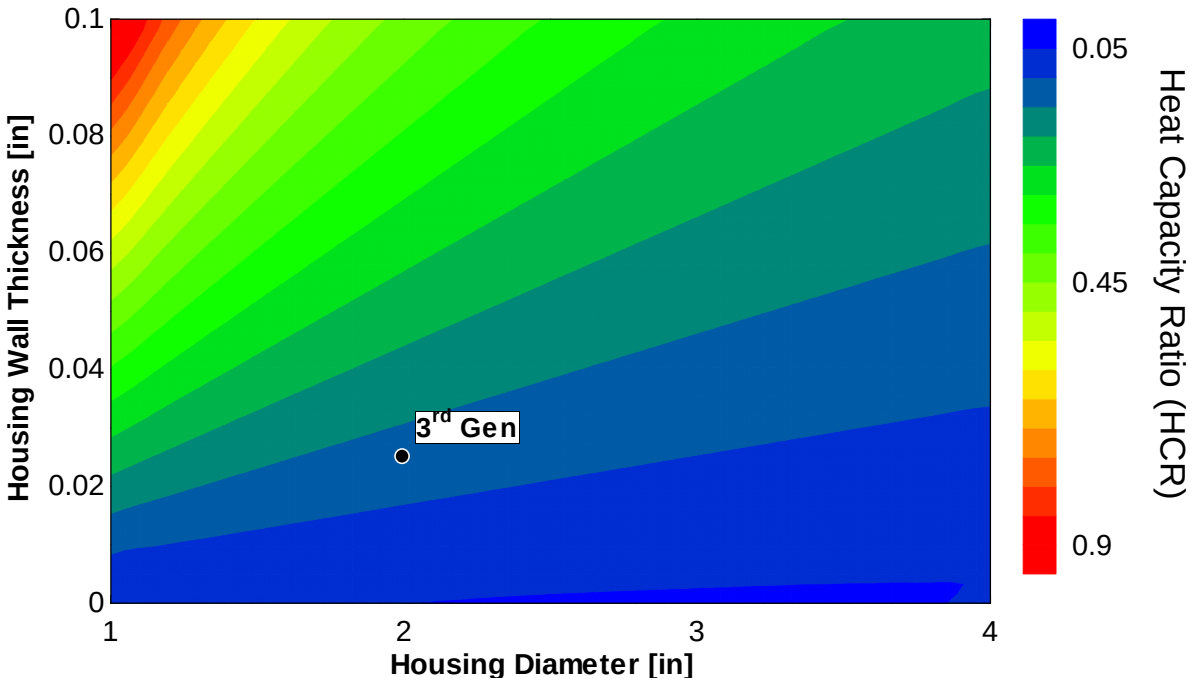

Figure 2.21: HCR as a function of housing outer diameter and wall thickness for the third generation regenerator.

By reducing the outer diameter of the housing to 2.0 in, it was possible to procure stainless tubing with a much smaller wall thickness of 0.020 inch. A 2.0 inch outer diameter piece of type 321 stainless steel tubing with a 0.020 inch wall thickness has an HCR that is less than 0.065.

In order to minimize the thermal communication that the test section has with the surroundings at the inlet and exit, a much larger void space is installed between the fluid inlet and exit ports and the test section. Figure 2.22 shows a picture of the inside of the regenerator. The end caps of the regenerator represent a large thermal mass. By increasing the distance between the end caps and the inlet of the test section (and where the thermocouples are placed), the impact of their thermal mass is reduced.

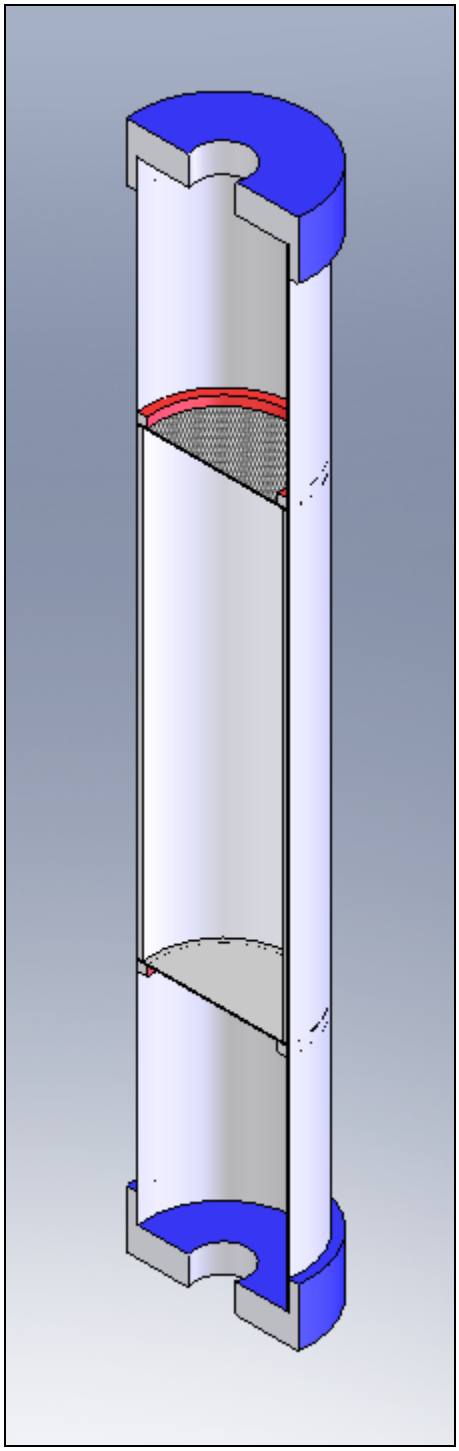

Figure 2.22: Computer model of a cross section of the third generation regenerator.

2.3.2 Third Generation Regenerator Fabrication

The fabrication process used to construct the third generation regenerator is similar to the process described for the second generation regenerator in Section 2.2.2. The end caps are machined from solid disks of aluminum. Each cap has a centered circular inset that is 2.0 inch in diameter and 0.375 inch deep and accepts the regenerator housing. There are three holes drilled in the caps. The largest, centered hole is 0.375 inch in diameter and accommodates the fluid flow (inlet or exit); this hole is tapped for 0.375 inch NPT thread in order to accept a fluid fitting. The two smaller holes allow access to the thermocouples and a pressure tap. These are each drilled and tapped for 0.125 inch NPT thread. Each end of the regenerator also receives an end cap to retain the packed spheres. The screen plugs are made from 20x20 screens with 0.02 inch diameter wire. Since the screen plugs are not located directly at the ends of the regenerator housing, welding the screen plugs into place is not an option. Instead, the screen plugs are held in place with epoxy, as shown in Figure 2.23.

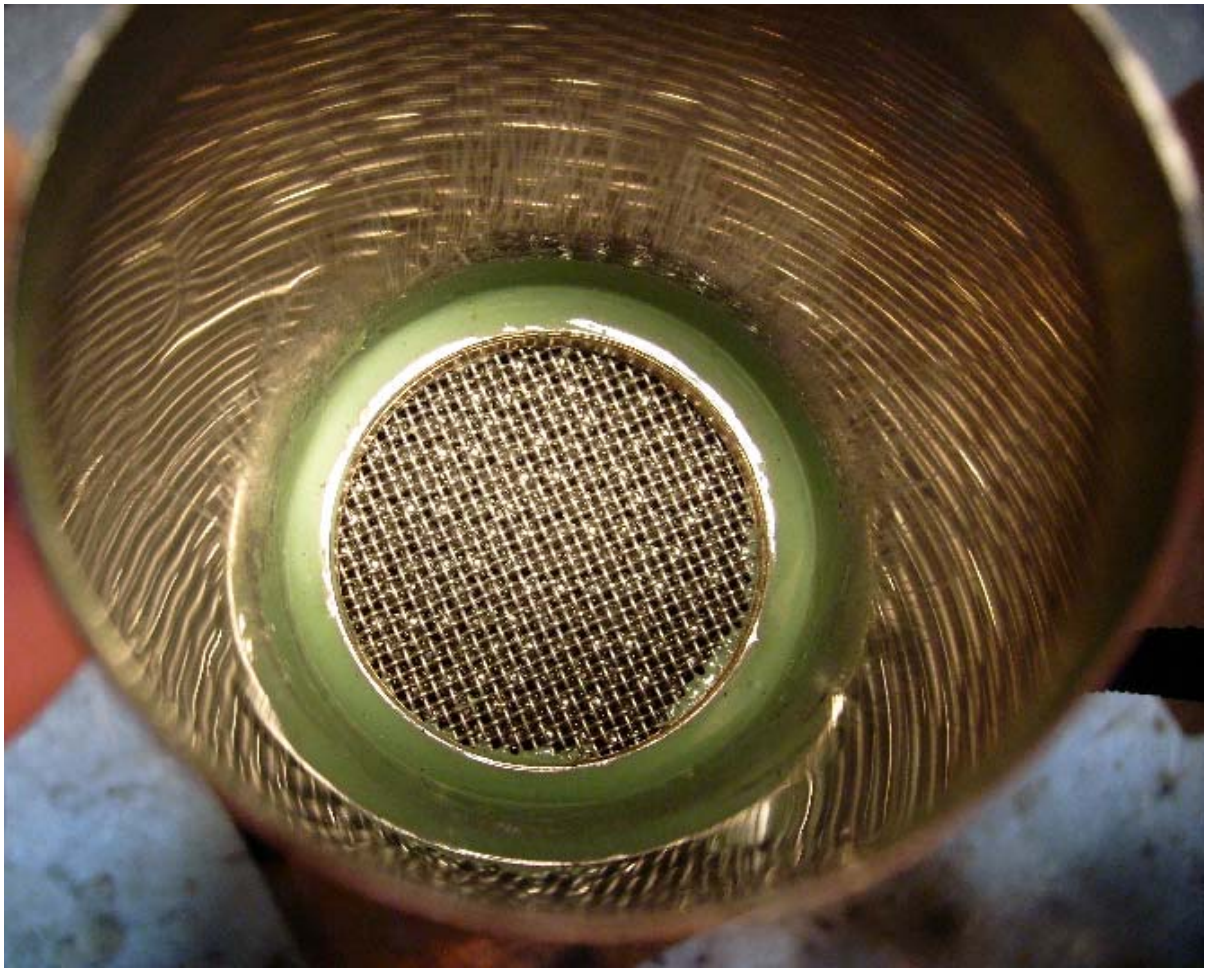

Figure 2.23: Photograph of one of the screen plugs after it was set in place with epoxy.

Foam lining was once again placed inside of the regenerator in order to reduce the effect of flow channeling along the wall. After the foam was installed, type 304 stainless steel spheres with 0.125 inch (3.1 mm) diameter were packed into the regenerator housing using the same technique described in Section 2.2.2.

Once the regenerator was fully packed and the second screen plug was installed, the thermocouples could be attached. Thermocouples are placed at the inlet and outlet of the regenerator in order to measure the temperature profiles. There are a total of seven

thermocouples at both the inlet and outlet spaced radially across the diameter of the flow path, as shown in Figure 2.24. The thermocouples used are Type-E (copper-constantin) with a wire diameter of 0.01 in. In addition to the thermocouples at the inlet and outlet, five thermocouples have been placed on the housing wall in order to monitor its temperature during the experiment. These thermocouples are electrically insulated from the housing using a sheet of Kimiwipe. This approach minimizes the electrical interference that might be caused by the housing acting as an antenna while providing good thermal communication. After the thermocouples were attached, the end caps of the regenerator were fixed to the top and bottom of the regenerator using epoxy to create a liquid tight seal. Fiberglass insulation was placed around the regenerator to insulate it from the surrounding conditions inside of the laboratory. A final picture of the regenerator showing the external thermocouples and attached end caps is shown in Figure 2.25.

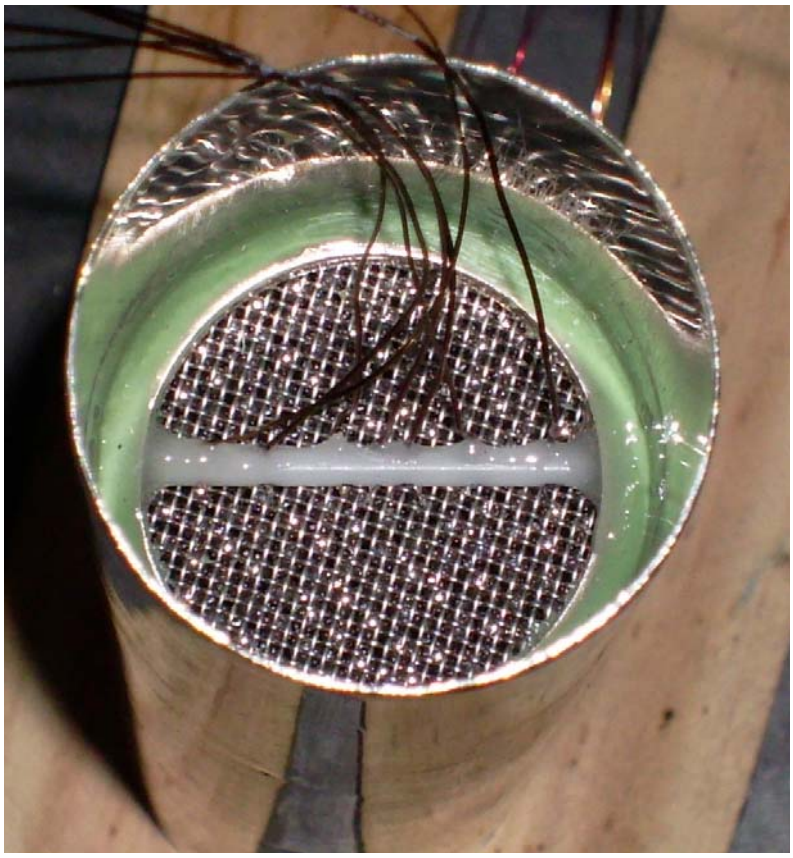

Figure 2.24: Thermocouple placement inside of the regenerator housing.

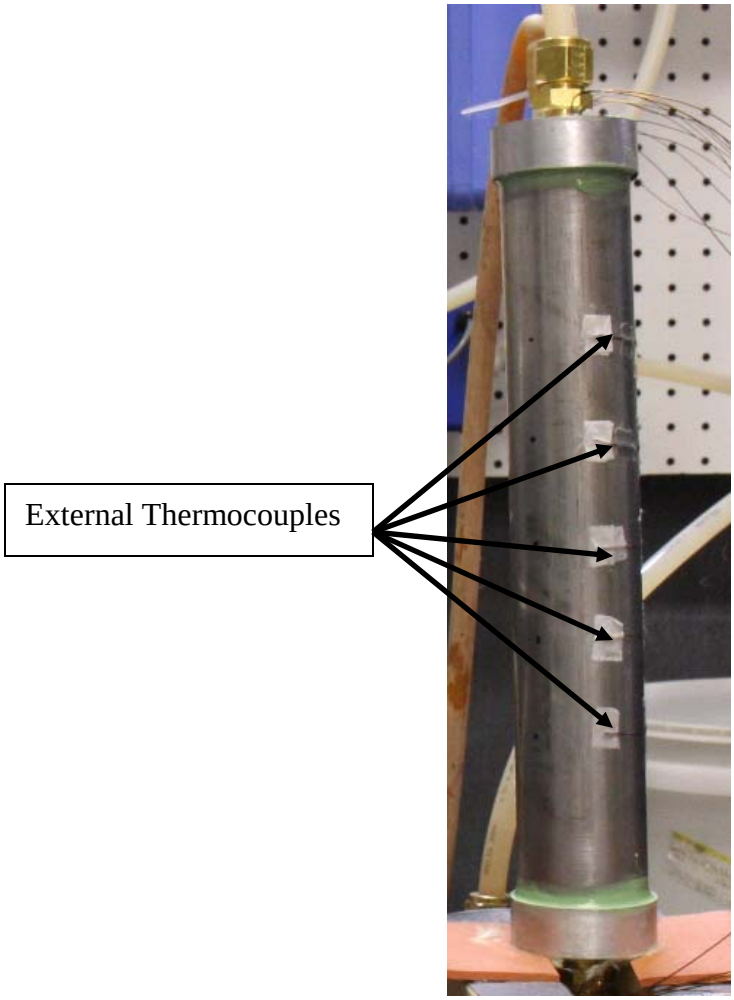

Figure 2.25: Completed third generation regenerator with the external thermocouples exposed and the fiberglass insulation removed.

2.3.3 Initial Trials

Once again initial tests were carried out in order to establish if the test section was functioning accurately. The temperature of the inlet and outlet as a function of time for a flow rate corresponding to a Reynolds number of 2 is shown in Figure 2.26. Note that the thermocouples agree very well at the start of the test. The thermocouples also agree very well with each other during a test. However, four of the thermocouples do not match as well as the others, indicated as the lagging thermocouples in Figure 2.26. These are the outer most

thermocouples at the inlet and outlet, and their disagreement is most likely due to flow variations caused by their close proximity to the screen plugs. Additionally, the thermocouples at the inlet and outlet do not converge completely at the end of the test. This is due to the termination of the test. Figure 2.27 shows the thermocouples after a long period of time where there is significant agreement between all of the thermocouples.

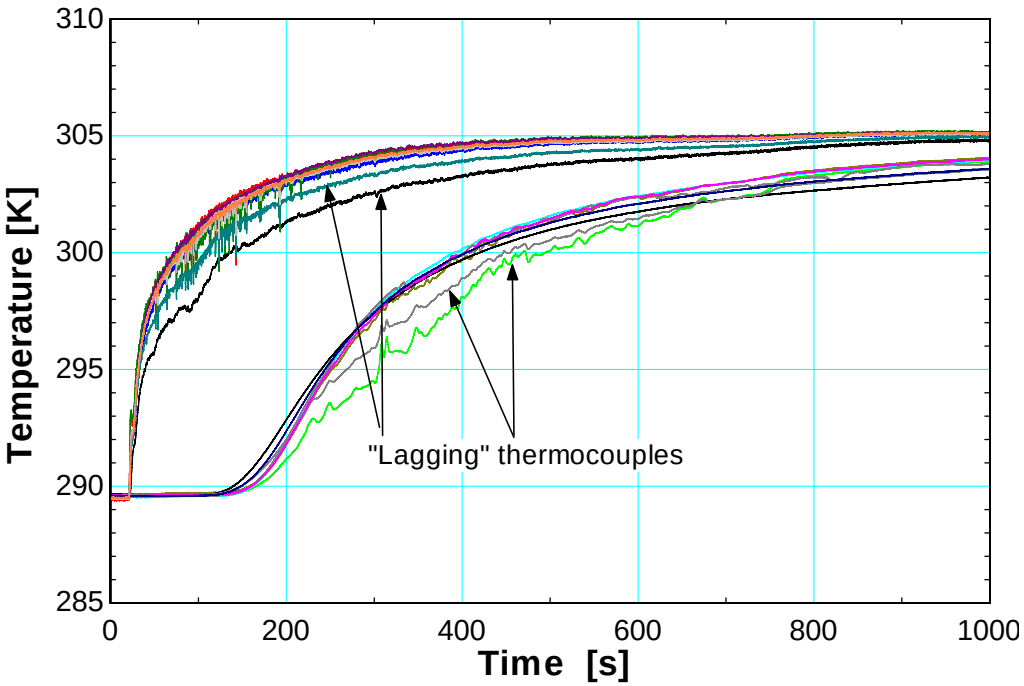

Figure 2.26: Experimental temperature measurements as a function of time for the inlet and outlet thermocouples during a test with a Reynolds number of 2.

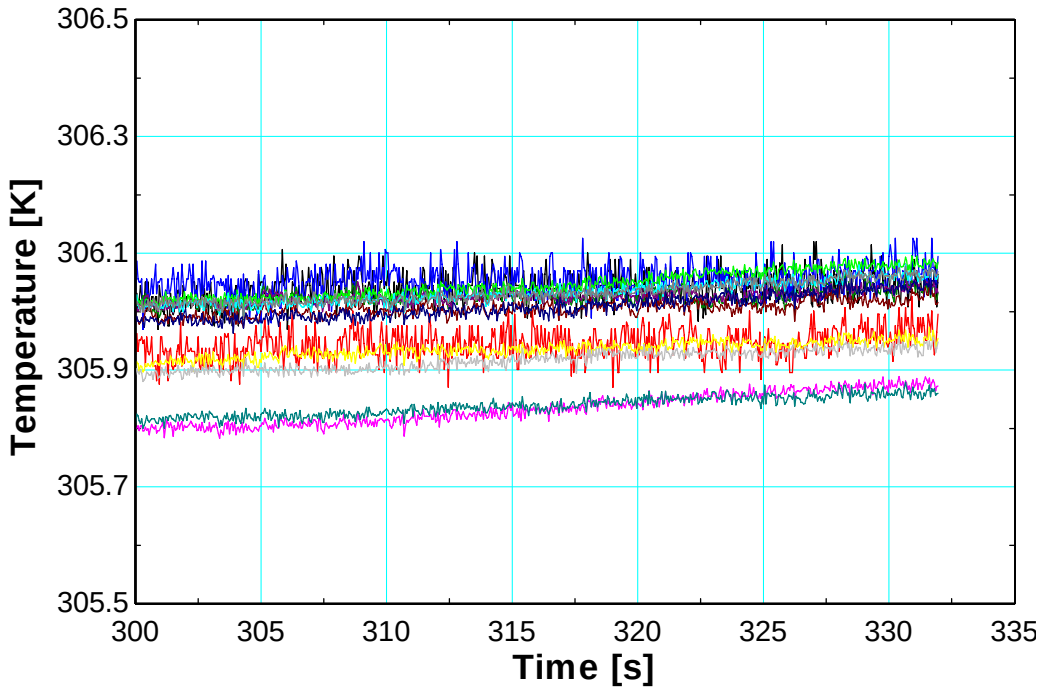

Figure 2.27: Thermocouple measurements after a sufficiently long period of time with a flow rate of 4.0 L/min.

Due to the fact that the model only requires one temperature at the inlet and outlet, the average of the inner five thermocouples at the inlet and outlet are used in data reduction (i.e. excludes the "lagging" thermocouples from Figure 2.26).

2.4 Instrumentation and Data Acquisition

Three different experimental measurements are required by the single - blow test: the mass flow rate of the fluid, the pressure drop across the regenerator, and the temperature at the inlet and outlet of the regenerator. The fluid flow rate is measured using an OMEGA FMG200 magnetic flow meter. The flow meter is calibrated for flows between 0.38 L/min and 3.8 L/min with an accuracy of 1% of the reading plus 0.02 L/min. The flow meter outputs a 4-20 mA signal which is converted to a 1-5 V signal using a 250 ohm shunt resistor. The voltage is read by a channel in the data acquisition system. The flow meter is

installed in the system upstream of the test section (symbol F in Figures 2.3-2.4, between Filter 1 and NV 1); this location is chosen because it ensures that the fluid passing through the flow meter during the test will remain at a relatively constant temperature. Figure 2.28 shows the location of the flow meter. A graduated cylinder and stop watch is used to supplement the magnetic flow meter and ensure that it is providing an accurate measurement of the average flow rate during the test.

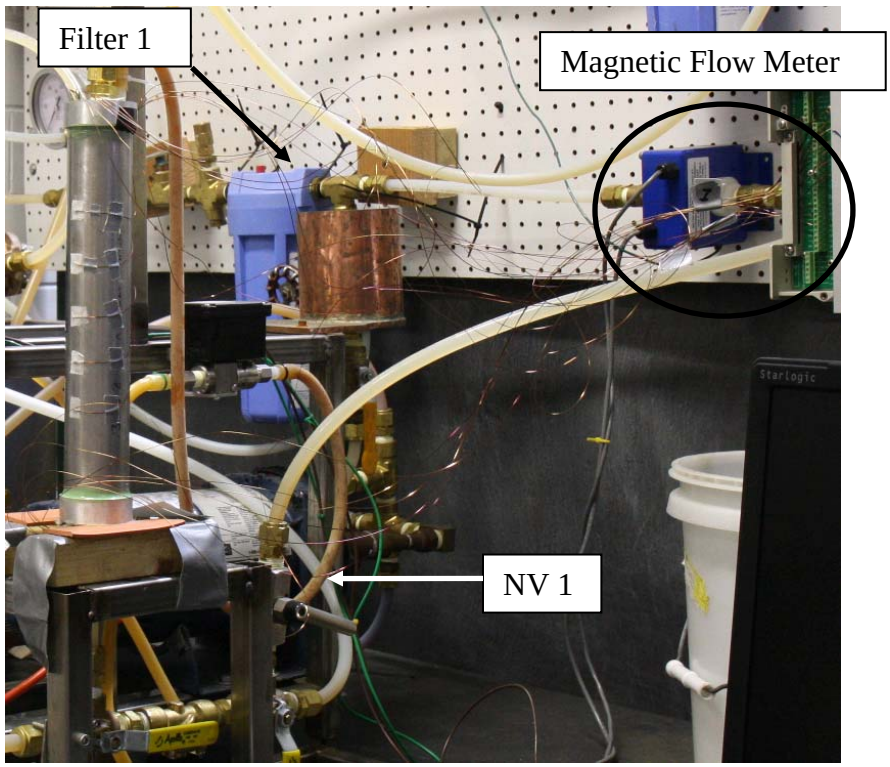

Figure 2.28: Photograph of the magnetic flow meter placement.

Pressure drop data across the regenerator are obtained using an OMEGA PX2300-01D differential pressure transducer. This pressure sensor measures differential pressure between 0 and 1 psid with an accuracy of 0.25% of full scale (0.0025 psid) and has a response time of 50 ms. During experimental tests, pressure drops ranging from 0.003 to 0.5 psid are expected

across the bed. The sensor outputs a 4-20 mA signal which is converted to a 1-5 V signal using a 250 ohm shunt resistor. The pressure sensor is connected to the regenerator via rubber tubing attached to the top and bottom end caps of the regenerator. Due to the very low pressure drop, the flexibility of the tubing has a negligible impact on the experimental results. However, care is taken to remove any air bubbles that could be trapped in the rubber tubing because the compressibility of the air trapped in the lines significantly reduces the accuracy of the measured pressure drop. Another important consideration is the hydrostatic head present due to the vertical orientation of the regenerator. The hydrostatic head present in the system is 0.41 psi, which is very near the largest pressure drop expected in the system of 0.5 psi. In order to correct for this, the initial pressure is subtracted from the remaining pressure data. As mentioned in Section 2.1, the data acquisition system is started before the hot blow process begins. This establishes a base line of temperature and pressure. Thus, the average pressure of the first second of data (roughly 40 data points) is subtracted from the entire pressure data set inside the model resulting in only the pressure drop across the test section.

The temperatures at the inlet and outlet of the regenerator are measured using type E thermocouples (discussed in Section 2.2.3 and Section 2.3.2). The thermocouples are enamel coated in order to prevent fluid from wicking through the space between the wires and the insulation and eventually reaching the data acquisition system (Marconnet, 2007). The non-junction side of each thermocouple is connected directly to the data acquisition system.

The data acquisition system consists of a desktop computer that is integrated with a National Instruments SCXI system. The desktop computer contains a supplementary PCI card (NI PCI

6034E) that communicates directly with the SCXI-1000 chassis. The SCXI chassis has two separate modules. One module accepts ±10 V signals. The other module is designed specifically for thermocouple inputs. The flow meter and differential pressure transducer voltage readouts are connected to the general voltage module (SCXI 1100) using wiring terminals provided by a SCXI 1300 wiring card. All of the thermocouples are attached to the thermocouple module (SCXI 1102) using thermocouple wiring terminals provided by a SCXI 1303 thermocouple wiring card. The thermocouple wiring card provides cold junction compensation via a high –accuracy thermistor, and is accurate to ±0.5 K.

All experiments are conducted with a cold soak temperature of 290 K, and a hot fluid temperature of 305 K, resulting in a 15 K temperature difference. It is important that the thermocouple response time is small compared to the time that an experiment takes to run. To test this, the thermocouples are placed in an ice bath, and then transferred to a room temperature water bath. Figure 2.29 shows the temperature of the thermocouples as a function of time when they are initially in an ice bath and transferred to a room temperature bath. Notice that all of the thermocouples reach a steady state temperature after 0.25 s, which is sufficiently small compared to the minimum breakthrough time of 26 s.

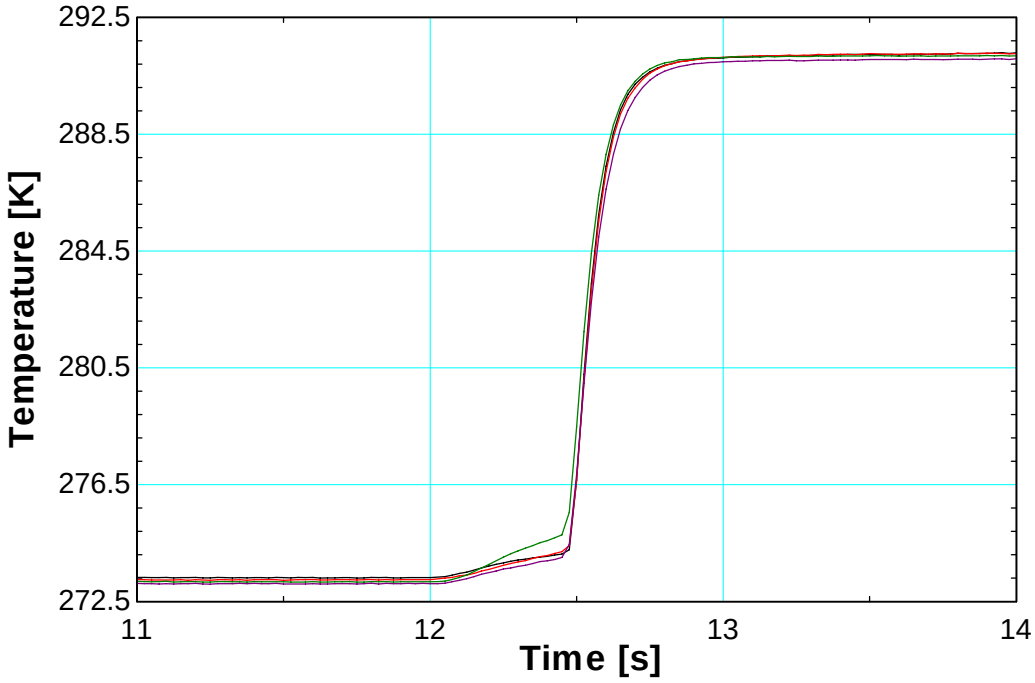

Figure 2.29: Thermocouple response over a 20 degree span,

The hardware is controlled and data is collected through the use of the LabView 8.0 software package. The data acquisition program can be started and stopped at any time by the user. The program also allows the user to specify the frequency of data collection, in Hz. Typically 40 Hz is used, which means there is one data point taken every 0.025 s. Marconnet (2007) showed that the experimental setup is capable of collecting data at frequencies that exceed 1000 Hz, resulting in one data point every 0.001 s. This is significantly faster than the response time of the flow meter and differential pressure transducer and indicates that the dynamic response of the measurement devices is the limiting factor of the data acquisition system. A photograph of the data acquisition system is shown in Figure 2.30.

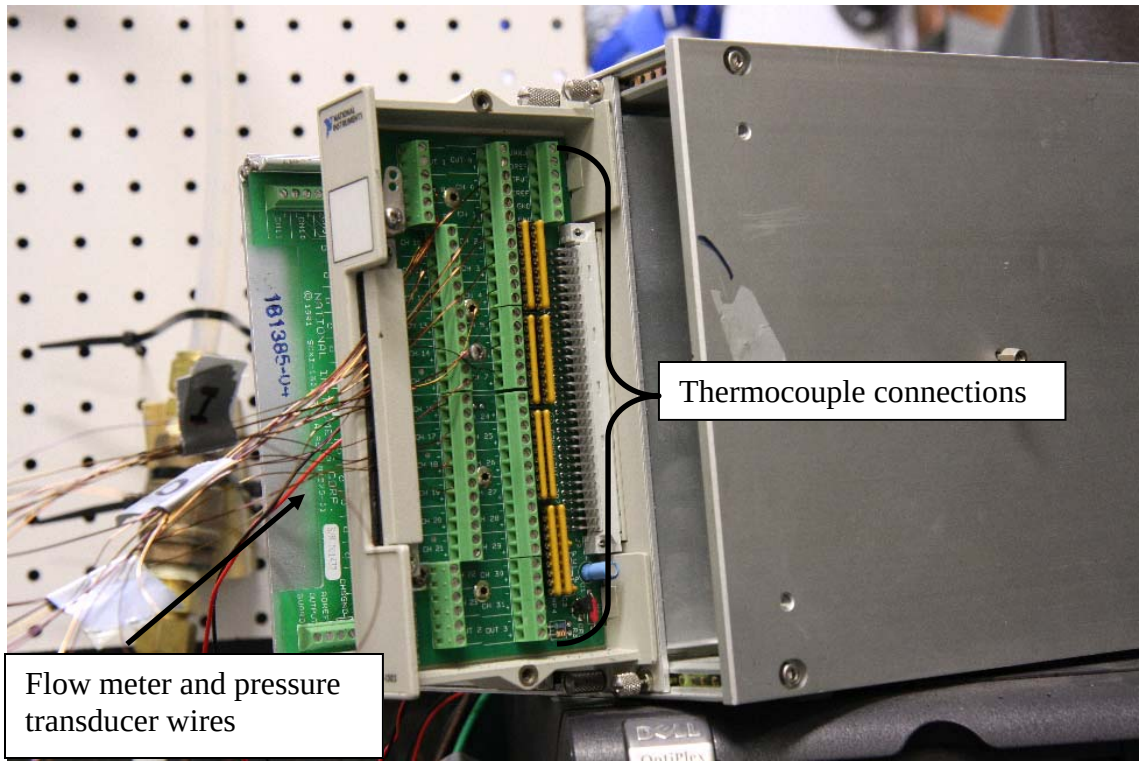

Figure 2.30: The SCXI chassis with the thermocouple, flow meter, and pressure transducer connections highlighted.

The primary measurement of the system is temperature, and as such, the most important uncertainty is in the temperature measurement. The uncertainty in the temperature measurement is the largest of several values; the uncertainty associated with calibration, the uncertainty in due to the time response of the thermocouple, and the resolution of the data acquisition system. All of the thermocouples were calibrated using the built – in calibration tool of LabView 8.0. Each thermocouple was calibrated using 4 data points; one at 0 C, 25 C, 60 C, and 100 C. However, the accuracy of the calibration is only as good as the accuracy of the reference temperature measurement. The reference temperatures were measured using an RTD with an uncertainty of ±0.1 K. Thus, the calibration uncertainty is given the same value. There is also uncertainty related to the response time of the thermocouples. The data acquisition system takes data points every 0.025 s, while the thermocouples have time

constants of 0.25 s (seen in Figure 2.29). Thus, the limiting factor is the time response of the thermocouples. During tests at the highest flow rate (Re = 100), the model predicted change of the outlet temperature over 0.25 s is 0.4 K. This is taken as the uncertainty associated with the time response of the system. The uncertainty in the resolution of the system is the accuracy of the components that comprise the data acquisition system. The accuracy of the SCXI 1303 thermocouple module is the limiting component with an accuracy of ±0.5 K. Comparing all the possible methods of uncertainty, the SCXI module has the highest value. Therefore, the uncertainty in the thermocouple measurements of these tests is ±0.5 K.

CHAPTER 3 – Numerical Models

Heggs and Burns (1988) report that the best method for determining the heat transfer coefficient from the data collected during a single-blow experiment is to adjust the Nusselt number used in a numerical model in order to match the predicted outlet fluid temperature from a passive regenerator model to the experimentally measured outlet fluid temperature. Two different passive regenerator models are used during this project. The first is the UW AMRR model that was developed by Engelbrecht (2005 and 2008) and the second is the dispersion concentric model developed by Steve Jacobs at the Astronautics Technology Center in Madison, WI.

3.1 UW AMRR Model

The AMRR model developed at the University of Wisconsin is a 1-D transient, numerical model that calculates the periodic steady state temperature of the regenerator material and the heat transfer fluid during a complete AMRR cycle (Engelbrecht, 2005 and Engelbrecht 2008). The temperatures as a function of position and time together with the prescribed mass flow rate allows the cycle performance parameters such as cooling load and coefficient of performance to be calculated. The model has been implemented in MATLAB, and is explicit with respect to time and implicit in position. A one-dimensional model is used because two-dimensional effects in well-designed regenerators are small and there is a significant savings in computational time required by a one-dimensional as compared to a complete, three-dimensional model of the flow through the porous media. However, because the model is 1-

D, the Navier-Stokes and energy equation for the fluid are not solved explicitly. Rather, correlations from the literature are used to calculate the axial dispersion parameter, the Nusselt number, and the local friction factor in the regenerator and these quantities are used to account for conduction and mixing, the fluid-to-solid heat transfer interaction, and pressure drop, respectively. Curve fits to experimental measurements of the material properties are used to calculate the specific heat, viscosity, and thermal conductivity of the fluid as a function of temperature (the effect of pressure on the fluid properties is neglected). The heat transfer fluid is assumed to be incompressible, therefore the density is constant and the mass flow rate does not change spatially because the amount of fluid entrained in the matrix remains constant. Experimental measurements of the properties of the magnetocaloric material are either used directly by interpolation or indirectly through curve fits to the data. The magnetocaloric material is assumed to be incompressible. The thermal conductivity of the magnetocaloric material is assumed to be unaffected by magnetic field and only a function of temperature Specific heat capacity and the partial derivative of entropy with respect to magnetic field are calculated by numerical differentiation of the magnetocaloric property data. The bed geometry is assumed to be spatially uniform so that bed parameters such as hydraulic diameter and porosity are constant. However, the bed material is allowed to vary spatially in order to allow studies of a layered bed in which the materials are selected so that the Curie temperature matches, approximately, the local operating temperature. There are several other assumptions and details that are thoroughly described by Engelbrecht (2008). The model can be downloaded from http://sel.me.wisc.edu/publications/publ.html.

3.1.1 Governing Equations

The behavior of the regenerator is described using a set of coupled differential equations. The differential equations are derived from an energy balance on a differential segment of fluid and a differential segment of the regenerator matrix. Figure 3.1 shows a differential fluid volume with the various energy transfers indicated (Engelbrecht, 2008).

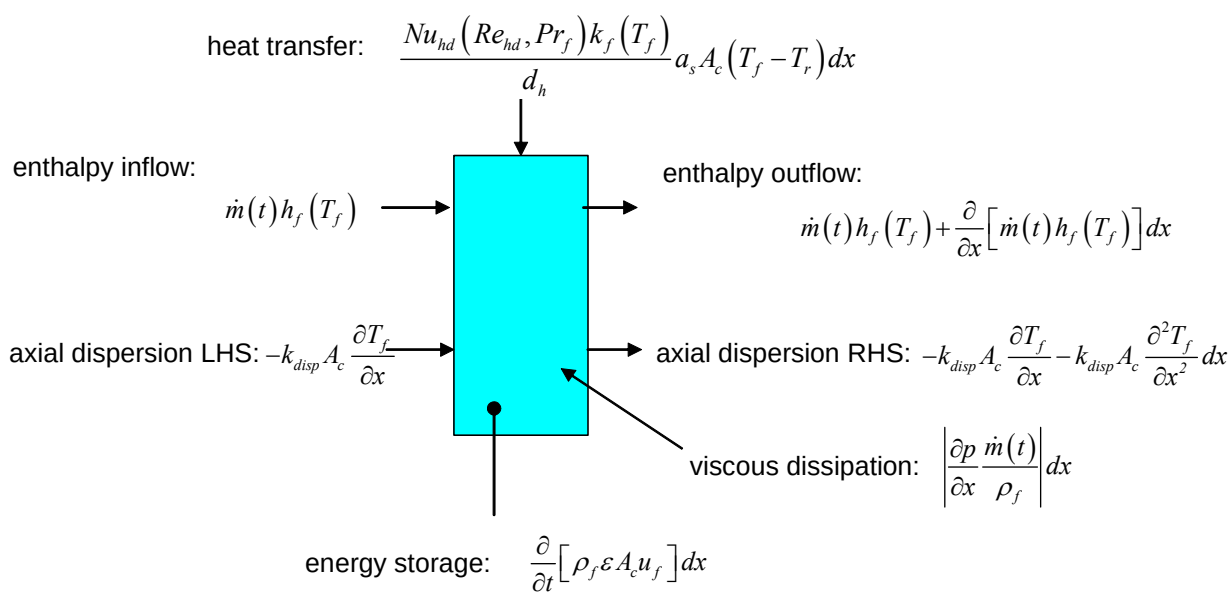

Figure 3.1: Differential segment of the fluid with all of the energy transfers indiated (Engelbrecht, 2008).

After substituting the definition of the friction factor for the pressure gradient, the final energy balance on the fluid can be written as:

$$k_{disp}\,A_c\frac{\partial^2 T_f}{\partial x^2}-\dot{m}\,c_f\frac{\partial T_f}{\partial x}-\frac{Nu_{hd}\,k_f}{d_h}a_s\,A_c\left(T_f-T_r\right)+\left|\frac{f_f\,\dot{m}^3}{2\,\rho_f^2\,A_c^2\,d_h}\right|=\rho_f\,A_c\,\varepsilon\,c_f\frac{\partial T_f}{\partial t} \qquad (3.1)$$

In (3.1), the parameter k_{disp} is the effective conductivity associated with the fluid (the dispersive conductivity, related primarily to mixing), Nu_{hd} is the Nusselt number based on hydraulic diameter that characterizes the fluid to solid heat transfer rate, and f_f is the friction

factor. These parameters are calculated using correlations that depend on the packing type as well as the local Reynolds number based on hydraulic diameter (Re_{hd}) and Prandtl number (Pr_f). The parameter A_c is the cross-sectional area, a_s is the specific surface area (the surface area per unit volume), d_h is the hydraulic diameter, and ε is the porosity of the regenerator matrix. The properties k_f, ρ_f, and c_f are the conductivity, density, and specific heat capacity of the fluid, respectively. The parameters T_f and T_r are the fluid and regenerator temperatures, respectively, and $\dot{m}$ is the mass flow rate.

Since AMRR systems operate cyclically, flow will enter the regenerator from either direction (i.e. be either positive or negative) during different portions of the cycle. When the mass flow rate is positive, the fluid is entering at the hot end (x = 0) with the prescribed hot reservoir temperature (T_H). When the flow is negative, the fluid enters at the cold end ($x = L$) with the cold reservoir temperature (T_C).

$$\begin{aligned} &if\ \dot{m}(t) \geq 0\, then\, T_f(x=0,t) = T_H \\ &if\ \dot{m}(t) \leq 0\, then\, T_f(x=L,t) = T_C \end{aligned} \tag{3.2}$$

Figure 3.2 shows a differential regenerator volume with all of the associated energy transfer mechanisms (Engelbrecht, 2008).

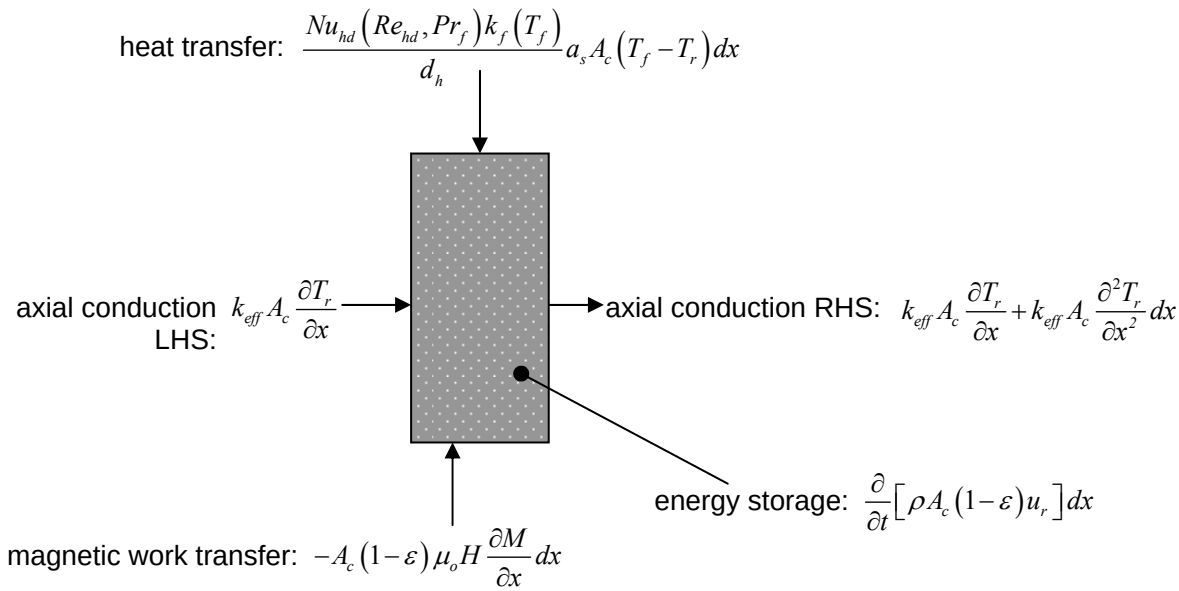

Figure 3.2: Differential segment of the regenerator material with all of the associated energy transfers shown.

Assuming that magnetization and demagnetization are internally reversible, the final energy balance on the regenerator material can be written as:

$$\frac{Nu\,k_f}{d_h}a_s\,A_s\left(T_f-T_r\right)+k_{eff}\,A_c\frac{\partial T_r}{\partial x^2}=A_c\left(1-\varepsilon\right)\rho_r\,T_r\frac{\partial^2 s_r}{\partial\mu_oH_T}\frac{\partial\mu_oH}{\partial t}+A_c\left(1-\varepsilon\right)\rho_r\,c_{\mu_oH}\frac{\partial T_r}{\partial t} \quad (3.3)$$

where k_{eff} is the effective conductivity of the matrix excluding the dispersive action of fluid mixing, s_r is the entropy of the matrix, and μ_oH is the magnetic field.

Both the fluid governing equation and the regenerator material governing equation are discretized and then implemented into the numerical model. The model begins from an arbitrary initial condition and integrates numerically through time until a cyclic steady state is achieved. The ends of the bed are assumed to be adiabatic during this process. A more detailed explanation of the model equation development is available from Engelbrecht (2008).

3.1.2 Correlations Used

Correlations from the literature are used to determine the local friction factor, axial dispersion parameter, and Nusselt number within the bed; these quantities are then used to model the axial conduction and mixing, the fluid-to-solid heat transfer, and the pressure drop, respectively. The regenerator bed is assumed to be composed of smooth, uniformly packed, spherical particles of uniform size.

The correlation developed by Ergun (1952) is used to determine the pressure drop through a bed of packed spheres, and is shown in equation (3.4).

$$\frac{dP}{dx} = \left(\frac{A\alpha\mu_f}{d_p^2}\right)v + \left(\frac{B\beta\rho_f}{d_p}\right)v^2$$
$$\alpha = \frac{(1-\varepsilon)^2}{\varepsilon^2} \quad \text{and} \quad \beta = \frac{1-\varepsilon}{\varepsilon^3} \tag{3.4}$$

where d_p is the particle diameter, and v is the superficial velocity. For smooth particles, A = 180 and B = 1.8 (Kaviany, 1995). The pressure gradient shown in equation (3.4) is then converted to a friction factor (f_f) as a function of Reynolds number based on hydraulic diameter (Re_{hd}) and bed porosity (ε), shown in equation (3.7) (Engelbrecht, 2008). This is done through the use of the definition of hydraulic diameter, shown in equation (3.5); and the definition of the friction factor, shown in equation (3.6) (Kaviany, 1995).

$$d_h = \frac{2}{3}\frac{\varepsilon}{(1-\varepsilon)}d_p \tag{3.5}$$

$$f_f = \frac{dP}{dx}\frac{d_p}{v_f^2\,\rho_f}\left(\frac{\varepsilon^3}{1-\varepsilon}\right) \tag{3.6}$$

$$f_f = 240\frac{(1-\varepsilon)}{\varepsilon^2 Re_{hd}} + 3.6\frac{(1-\varepsilon)}{\varepsilon^3} \tag{3.7}$$

As discussed in Section 1.3, the correlation developed by Wakao and Kaguei (1982) is used to determine the Nusselt number. The correlation is shown in equation 1.6, but is re-written here.

$$Nu_f = 2 + 1.1\mathrm{Re}_f^{0.6}\,\mathrm{Pr}_f^{1/3}$$

It is important to note that the Reynolds number used in the Wakao and Kaguei correlation is based on superficial fluid velocity and particle diameter instead of hydraulic diameter as in equation (3.7). Before the correlation is used by the model, the Reynolds number based on hydraulic diameter is converted to the Reynolds number based on particle diameter using equation 3.8 (Engelbrecht, 2008).

$$Re_f = \frac{3}{2}\frac{(1-\varepsilon)}{\varepsilon}Re_{dh} \tag{3.8}$$

The correlation is then used to predict the Nusselt number based on particle diameter. The resulting Nusselt number is then converted to the Nusselt number based on hydraulic diameter using equation (3.9).

$$Nu_{hd} = \frac{2}{3}\frac{\varepsilon}{(1-\varepsilon)}Nu_f \tag{3.9}$$

The final correlation is used to determine the axial conduction and dispersion within the bed. Kaviany (1995) suggests that the total effective thermal conductivity, k_{eff}, can be expressed as the sum of the dispersive and static components, shown in equation (3.10)

$$k_{eff} = k_{static} + k_f D_d \tag{3.10}$$

where k_{static} is the static thermal conductivity, k_f is the thermal conductivity of the fluid, and D_d is the dispersion coefficient. The static thermal conductivity is calculated via the correlation provided by Hadley (1986), shown in equations (3.11-3.13).

$$k_{static} = k_f \left[(1-\alpha_o) \frac{\varepsilon f_o + k_r / k_f (1-\varepsilon f_o)}{1-\varepsilon(1-f_o) + k_r / k_f \, \varepsilon (1-f_o)} + \alpha_o \frac{2(k_r/k_f)^2 (1-\varepsilon) + (1+2\varepsilon) k_r / k_f}{(2+\varepsilon) k_r / k_f + 1 - \varepsilon} \right] \quad (3.11)$$

$$f_o = 0.8 + 0.1\varepsilon \quad (3.12)$$

$$\begin{aligned} \log \alpha_o &= -4.898\varepsilon, & 0 \le \varepsilon \le 0.0827 \\ \log \alpha_o &= -0.405 - 3.154(\varepsilon - 0.0827), & 0.0827 \le \varepsilon \le 0.298 \\ \log \alpha_o &= -1.084 - 6.77(\varepsilon - 0.298), & 0.298 \le \varepsilon \le 0.580 \end{aligned} \quad (3.13)$$

where k_f is the thermal conductivity of the fluid, and k_r is the thermal conductivity of the regenerator material. The dispersion coefficient correlation used in the model is suggested by Kaviany (1995) and is given in equation (3.14) as a function of the Peclet number (Pe_{hd}). The Peclet number is the product of the Reynolds number and Prandtl number of the fluid ($Pe_{hd} = Re_{hd} \, Pr_f$). The correlation is only valid for cases where the Peclet number is greater than 1.

$$D_d = \varepsilon \frac{3}{4} Pe_{hd}, \qquad Pe_{hd} \gg 1 \quad (3.14)$$

3.1.3 Single-Blow adjustments

In order to use the single-blow model for data reduction, it had to be modified in several ways. The boundary conditions are adjusted in order to simulate continuous operation with flow in one direction rather than the cyclic flow that is experienced in an AMRR system. At the hot end of the regenerator, the temperature of the entering fluid is specified to be the experimentally measured inlet temperature (which varies slightly with time). Additionally,

there is assumed to be no dispersive heat transfer from the ends of the matrix (i.e., the matrix ends are adiabatic with respect to conduction heat transfer in either the fluid or the matrix).

The magnetic work term is removed from the governing differential equation associated with the regenerator material. Since this is a passive regenerator, there is no active magnetization or demagnetization taking place during an experiment. In order to remove the magnetic work term, the partial derivative of entropy with respect to magnetic field is set to 0 for all the materials used in the regenerator.

The model code was modified in order to read in the experimentally measured inlet and outlet temperature, mass flow rate, and pressure drop for a particular test from a data file. Since a perfect step change in inlet temperature and mass flow rate cannot be achieved during any practical single-blow test, it is important to consider the time variation of the inlet temperature and mass flow rate (Heggs and Burns, 1988). The initial temperature of the material in the test facility (i.e., the initial condition for the numerical model) is determined from the measured temperature data recorded immediately prior to the initiation of the hot blow process. The initial temperature is taken to be the average of the first 40 data points of the inlet temperature.

3.1.4 Determining Nusselt Number with the UW AMRR Model

The procedure to determine the best fit Nusselt number begins with a user-supplied vector of Nusselt number guesses (i.e., trial values that are used to predict the exit temperature

variation); the definition of the Nusselt number based on particle diameter, $Nu_{guess,i}$, is given in equation (3.15),

$$Nu_{guess,i} = \frac{h\ d_p}{k_f} \tag{3.15}$$

where h is the heat transfer coefficient, d_p is the particle diameter, and k_f is the thermal conductivity of the fluid. All of the governing equations that are used in the AMRR model are based on the hydraulic diameter of the regenerator. Therefore, it is necessary to convert the Nusselt number based on particle diameter to the Nusselt number based on hydraulic diameter using equation (3.16).

$$Nu_{hd,i} = \frac{2\varepsilon}{3(1-\varepsilon)} Nu_{guess,i} \tag{3.16}$$

where ε is the porosity of the regenerator matrix. The Nusselt number is subsequently adjusted in order to account for temperature gradients that are internal to the solid spheres using the technique described by Jefferson (1972). The corrected heat transfer coefficient is reduced by the degradation factor, DF

$$h^* = DF\ h \tag{3.17}$$

where h^* is the corrected heat transfer coefficient. The degradation factor derived by Jefferson for a spherical particle is

$$DF = \frac{1}{1+\frac{Bi}{5}} \tag{3.18}$$

where Bi is the Biot number of the solid. Since the Nusselt number is directly proportional to the heat transfer coefficient, the degradation factor can also be applied to the Nusselt number, as shown in equation (3.19).

$$Nu_{corr,i} = \frac{Nu_{guess,i}}{1 + \frac{Bi}{5}} \tag{3.19}$$

The fully corrected Nusselt number is then used by the model to calculate the heat transfer coefficient that is used in the simulation. The measured inlet fluid temperature and fluid mass flow rate (both functions of time) are input to the model, and the model is run for each of the Nusselt numbers contained in the array, $Nu_{guess,i}$. The result of the model is the prediction of the temperature at the regenerator exit as a function of time that would be obtained if the Nusselt number in the bed were constant (in space and time) and equal to $Nu_{guess,i}$. The agreement between the predicted exit temperature variation and the experimentally measured exit temperature is quantified by the root mean square error between the two curves. The root mean square error was provided in Equation (1.11) and is re-written here:

$$RMSE = \sqrt{\frac{\sum_{i=1}^{N_{exp}} \left(T_{exp,i} - T_{pre,i} \right)^2}{N_{exp}}}$$

where $T_{exp,i}$ and $T_{pre,i}$ are the experimentally measured and predicted exit temperatures at every experimental time i. Since the time steps used in the model and the time steps of the experimental data do not match up, the model predicted temperature data is interpolated using the experimental time steps. The experimentally measured exit temperature is taken to be the average of the three thermocouples located in the outlet plenum, as described in Section 2.2.3.

This process is repeated for all of the user supplied Nusselt number guess values, resulting in a vector containing the RMS error as a function of Nusselt number. The Nusselt number that produces the lowest RMS error is taken as the best fit Nusselt number for that test. Figure 3.3 shows the RMS error as a function Nusselt number for a test using water at a flow rate corresponding to a Reynolds number of 100.

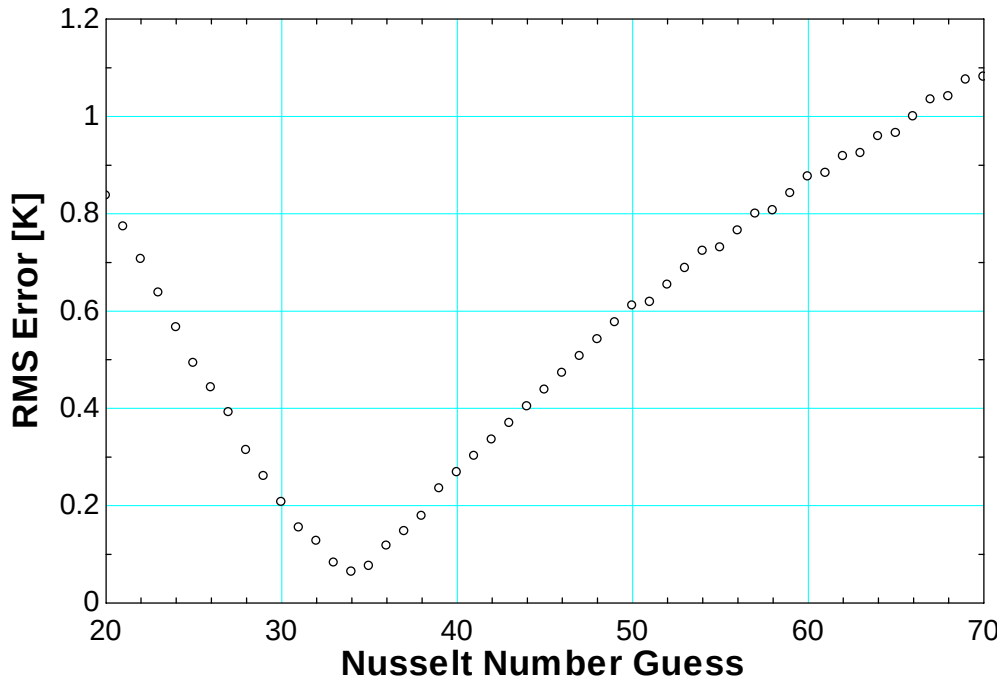

Figure 3.3: RMS error as a function of Nusslet number for a test corresponding to a Reynolds number of 100 with water.

Examination of Figure 3.3 reveals there is a clear and sharp minimum in the RMS error corresponding to a Nusselt number of 34. This trend is also apparent at low Reynolds numbers and the sharpness of the optimal value remains essentially unchanged. Figure 3.4 shows the RMS error as a function of guess Nusselt number for a test with a Reynolds number of 1.5 using water.

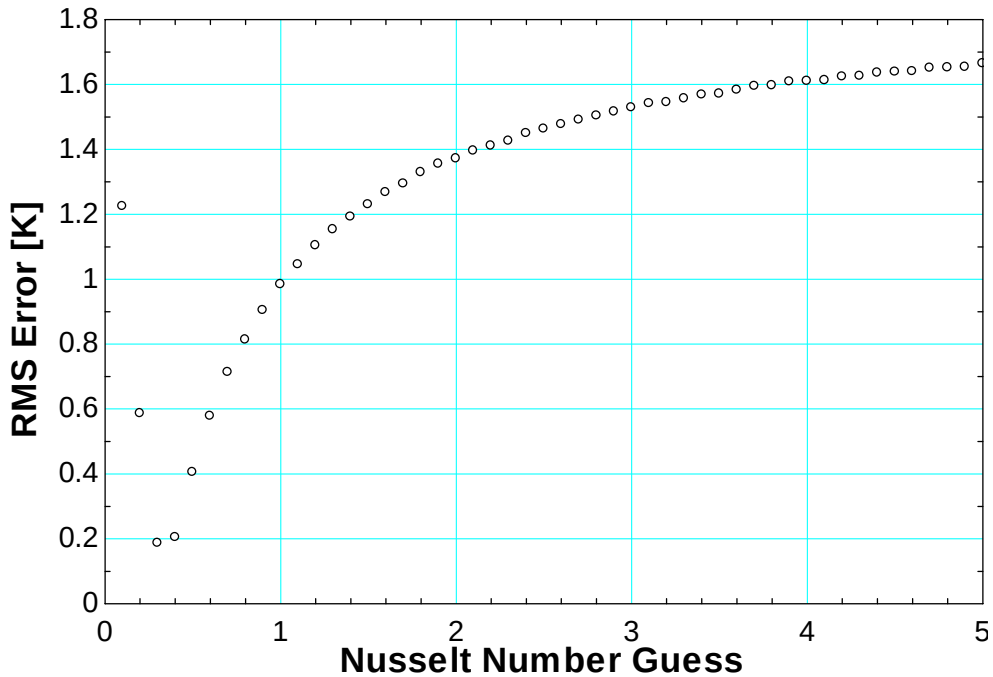

Figure 3.4: RMS error as a function of Nusselt number for a Reynolds number of 1.5 with water as the working fluid

The technique that is used to find the best fit Nusselt number works well for both high and low Reynolds number flows. Figures 3.3 and 3.4 show that the directly measured result - the predicted outlet temperature variation - is equally sensitive to the inferred quantity - the Nusselt number - at low Reynolds and high Reynolds number conditions.

3.2 Astronautics Dispersion Concentric Model

The dispersion concentric model (referred to as the DC Model) was also used to model the regenerator and reduce the data in order to infer the Nusselt number. The DC model focuses on a discrete solid with concentric temperature profiles in each particle (Kageui, 1977). This differs from the UW AMRR model where the solid phase is assumed to be continuous through which heat transfer takes place. This approach is consistent with a continuous solid phase model (CS Model).

Kaguei (1977) claims that when using a DC model, the fundamental differential equations are rather simple and can be easily solved. However, the DC model has a disadvantage in that heat conduction through the solid phase is not considered. This phenomenon is considered by the CS model; but the CS model boundary conditions are ambiguous and solving the differential equations can be complicated (Kaguei, 1977).

The dispersion concentric model was developed and used with the goal of explaining the anomalous behavior observed in the predicted Nusselt number at low Reynolds number based on the second generation experimental data evaluated with the UW model (this is discussed further in Chapter 4). The dispersion concentric model accounts for three different temperature gradients: the axial variation in temperature along the bed, the radial variation in temperature across the bed (from its center to its edge), and the internal temperature variation within each individual sphere. The model also explicitly includes the transient behavior of the foam that lines the regenerator as well as the regenerator housing. The model solves the partial differential equations using an eigenfunction expansion method and is implemented in Fortran90.

3.2.1 Governing Equations

The governing differential equations for the DC model are obtained by performing an energy balance on a differential segment of fluid. Unlike the UW model, the differential equations are solved in cylindrical coordinates. There are three separate computational domains inside the regenerator, shown in Figure 3.5. The interior of the regenerator, which extends from r =

0 to $r = r_1$, contains the packed particle bed and the heat transfer fluid. This region is enclosed by an insulating layer, which extends radially from $r = r_1$ to $r = r_2$. This region, in turn, is enclosed by the housing layer, which extends from $r = r_2$ to $r = r_3$, the outer radial boundary of the regenerator. The axis of the cylindrical regenerator extends along the x-direction. The inlet of the regenerator corresponds to $x = 0$ and the outlet corresponds to $x = L$. The particles in the PRS bed are spherical with outer radius R. The coordinate $\hat{r}$ denotes the radial location within a particle.

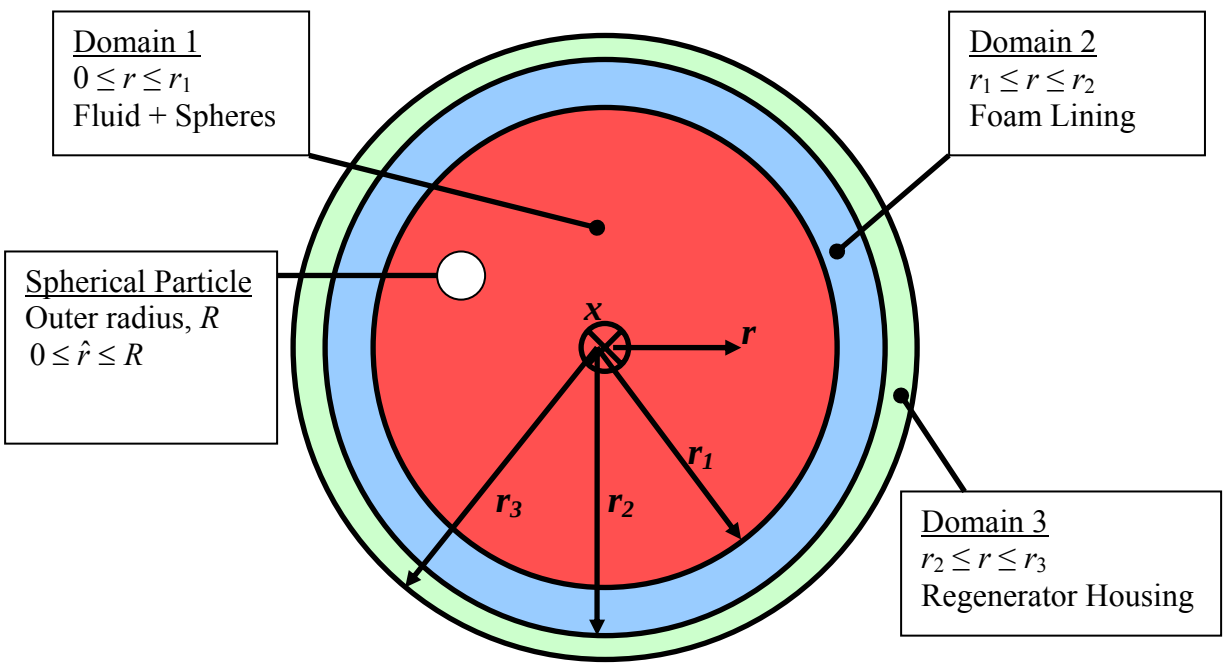

Figure 3.5: Computational domains of the dispersion concentric model including the spherical particles.

Within domain 1, the governing differential equation for the fluid is provided by equation (3.20).

$$\varepsilon \rho_f c_f \frac{\partial T_f}{\partial t} = k_{eff,x} \frac{\partial^2 T_f}{\partial x^2} + k_{eff,r} \frac{1}{r} \frac{\partial}{\partial r}\left(\frac{\partial T_f}{\partial r} \right) - \rho_f c_f v_f \frac{\partial T_f}{\partial x} - a_s k_p \frac{\partial T_p}{\partial \hat{r}}\left(\hat{r} = R; x, r \right) + F \quad (3.20)$$

Where v_f is the fluid velocity and k_p is the thermal conductivity of the spherical particles. The first term in equation (3.20) represents the energy storage inside of the differential fluid volume. The second and third terms define the conduction within the fluid in the axial and radial directions, respectively. The fourth term represents the enthalpy flow through the control volume. The fifth term represents the conduction to the outer surface of the spherical particles. The parameter F represents the viscous dissipation. Instead of carrying out a differential energy balance on a segment of the regenerator material, as is done with the UW model, each particle is modeled explicitly. Equation (3.21) shows the energy balance for a spherical particle inside the regenerator (still within domain 1). Equation (3.22) defines the boundary condition of a particle, which couples it with equation (3.20).

$$\rho_p c_p \frac{\partial T_p}{\partial t} = k_p \frac{1}{\hat{r}^2} \frac{\partial}{\partial \hat{r}}\left(\hat{r}^2 \frac{\partial T_p}{\partial \hat{r}} \right) \quad (3.21)$$

$$k_p \frac{\partial T_p}{\partial \hat{r}} = h\left[T_f\left(x, r, t \right) - T_p \right] \quad at \quad \hat{r} = R \quad (3.22)$$

The second computational domain deals with the foam lining that is inserted inside the regenerator between the spherical particles and the housing in order to reduce flow maldistribution along the wall. The governing differential equation for the foam lining is shown in equation (3.23).

$$\rho_1 c_1 \frac{\partial T_w}{\partial t} = k_1 \frac{\partial^2 T_w}{\partial x^2} + k_1 \frac{1}{r} \frac{\partial}{\partial r}\left(r \frac{\partial T_w}{\partial r} \right) \quad (3.23)$$

where T_w is the wall temperature, ρ_1 is the density of the foam lining, c_1 is the specific heat of the foam lining, and k_1 is the thermal conductivity of the foam lining. The third computational domain is the regenerator housing. The governing differential equation for the regenerator housing is shown in equation (3.24). The subscript *2* refers to the regenerator housing material.

$$\rho_2 c_2 \frac{\partial T_w}{\partial t} = k_2 \frac{\partial^2 T_w}{\partial x^2} + k_2 \frac{1}{r} \frac{\partial}{\partial r}\left(r \frac{\partial T_w}{\partial r} \right) \tag{3.24}$$

The regenerator is assumed to be adiabatic at the outlet surface ($x = L$), as well as the outer radius of the regenerator housing ($r = r_3$). Additionally, at the interface between the fluid and the foam lining, and the interface between the foam lining and the regenerator housing, the temperature is assumed to be continuous (i.e., an infinitely large heat transfer coefficient is assumed between the foam lining and the fluid and no contact resistance is modeled between the foam lining and the regenerator housing). Finally, the temperature of the regenerator housing and the foam lining at the inlet of the regenerator (the $x = 0$ plane) are assumed to remain constant at the hot fluid temperature, T_H. Since the DC model is transient, the initial conditions of each domain are required, as shown in equation (3.25).

$$T_f\left(x,r,t=0\right) = T_p\left(\hat{r};x,r,t=0\right) = T_w\left(x,r,t=0\right) = T_C \tag{3.25}$$

3.2.2 Determining Nusselt Number with the DC Model

Before the DC model can be run, the experimental data must be pre-processed. Since the DC model does not read in experimental data, the experimental inlet temperature and volumetric flow rate must be fit to functions of time. The inlet temperature is fit to the function shown in equation (3.26) and the volumetric flow rate is fit to the function is shown in equation (3.27).

$$T_f\left(x=0,r,t\right)=T_H-\left(P_3+P_5\,t+P_6\,t^2\right)e^{-t/P_2}-\left(T_H-T_C-P_3\right)e^{-t/P_4} \tag{3.26}$$

$$\Phi\left(t\right)=B_2-\left(B_2-B_1+B_4\,t+B_5\,t^2\right)e^{-t/B_5} \tag{3.27}$$

The curve fitting process is performed in MATLAB using the *lsqcurvefit* function. The *lsqcurvefit* function minimizes the least squares error by adjusting the fitting parameters P_i for the temperature equation, and B_i for the flow rate equation. Figure 3.6 shows the experimental inlet temperature and the completed curve fit, and Figure 3.7 shows the experimental volumetric flow rate with the completed curve fit.

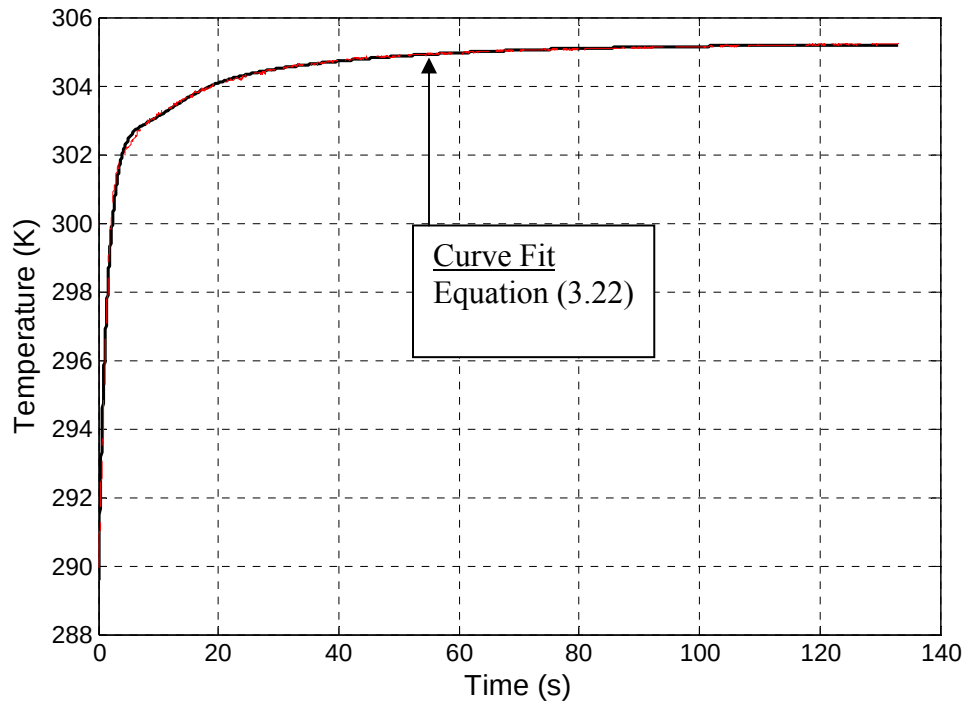

Figure 3.6: Experimental inlet temperature and the curve fit using equation (3.22).

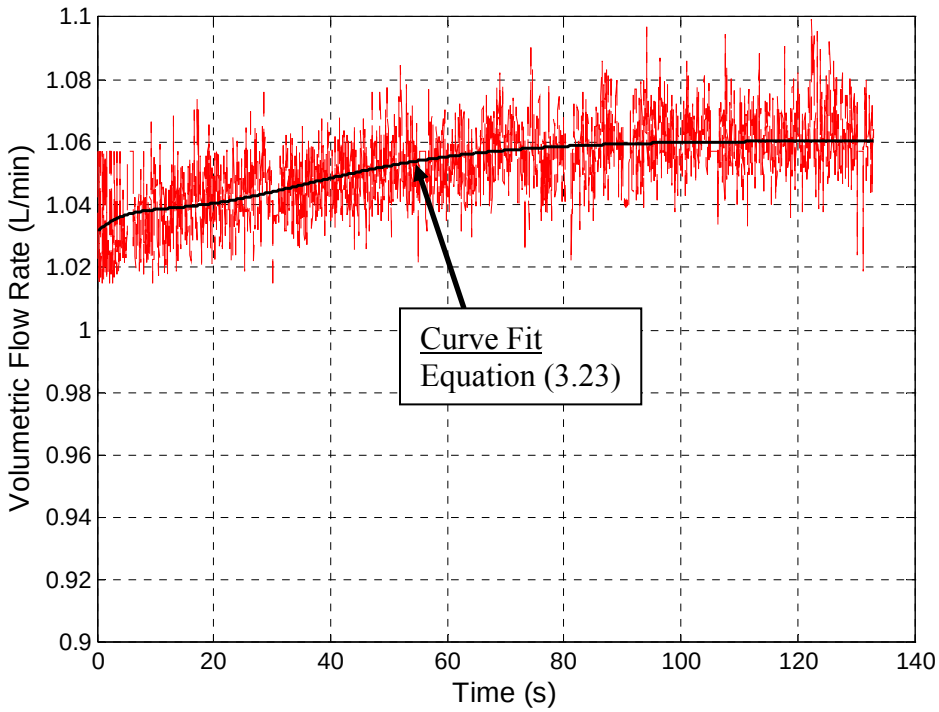

Figure 3.7: Experimental volumetric flow rate

Once the fitting parameters are calculated, they are entered into the DC model input file. The input text file contains all of the input parameters required to simulate the single-blow test facility; these include the regenerator dimensions, the regenerator material properties, the fluid properties, the hot and cold temperature of the current test, the best-fit parameters that characterize the input temperature and flow rate associated with the current test, and the Nusselt number guess values. The DC model input file is then read by the Fortran program and the model solves the governing differential equations. The model outputs the temperature of the regenerator material at a user specified axial location and three user specified radii, for each Nusselt number provided in the array of guess values. For the purposes of data reduction, the temperature at center ($r = 0$) of the outlet of the regenerator ($x = L$) is used.

The model returns the predicted outlet temperature as a function of time at the center of the regenerator for each Nusselt number guess value. These results are then post processed using MATLAB in order to quantify the agreement between the predicted and experimentally measured outlet temperature as a function of time. The Nusselt number that produces the minimum RMS error is taken as the best fit Nusselt number for that particular test. Figure 3.8 shows a graph of the RMS error as a function of the Nusselt number guess for a test where the Reynolds number is 5. Examination of Figure 3.8 shows that there is a clear minimum at a Nusselt number of 7.5 predicted by the model. This trend is observed for all flow rates tested.

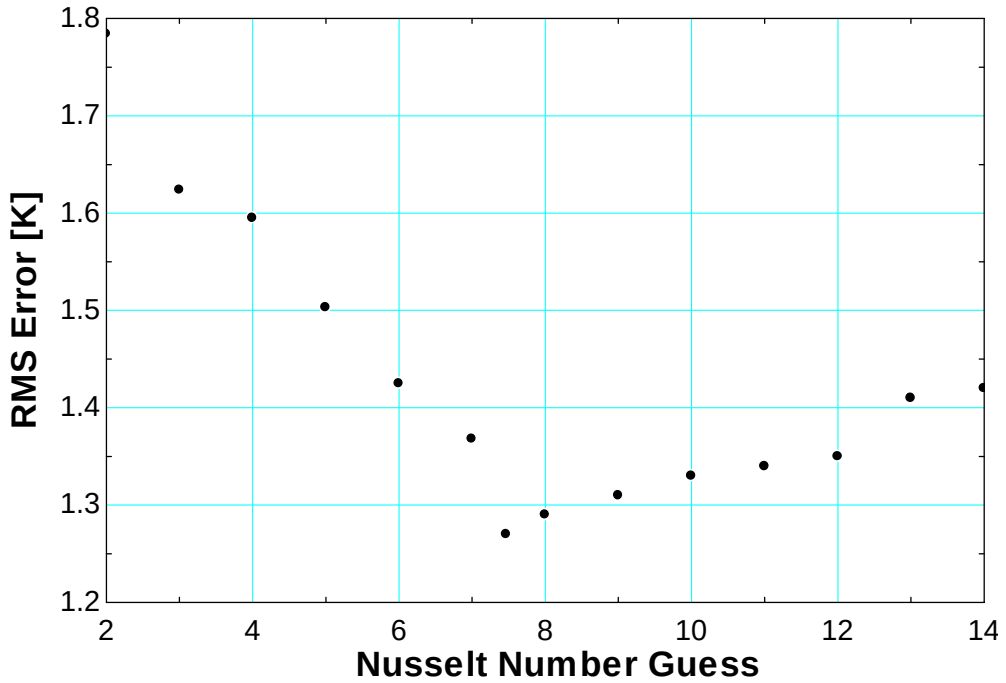

Figure 3.8: RMSE as a function of Nusselt number guess for a test with a Reynolds number of 5.

CHAPTER 4 – Second Generation Experiment Results

The second generation regenerator significantly reduces the heat capacity ratio of the regenerator housing. Experimental data were obtained for fluid flow rates corresponding to a Reynolds number range of 1 to 100 and different concentrations by mass of propylene glycol and water which correspond to difference values of the Prandtl number. For each flow rate and fluid (i.e., for each Reynolds number and Prandtl number), 10 independent experimental runs were performed in order to assess the repeatability of the results and reduce the uncertainty in the measurements. The results of reducing these data using the UW AMRR single blow model are discussed in the subsequent sections.

4.1 Experimental Data

The cold reservoir was held at 290 K and the hot reservoir was held at 305 K for all of the data sets. The flow rates used in the experimental matrix were selected in order to obtain data at Reynolds numbers that are logarithmically spaced from 1 to 100; the logarithmic spacing was selected in order to emphasize the low Reynolds numbers region which is of particular importance to AMRR applications. The Reynolds number used to characterize the experiments is based on the superficial velocity and particle diameter, originally defined in equation 1.4, but shown again below Re_f

$$Re_f = \frac{\rho_f \left(\frac{\dot{V}_f}{A_c} \right) d_p}{\mu_f}$$

where is the Reynolds number based on particle diameter, ρ_f is the fluid density, $\dot{V}_f$ is the fluid volumetric flow rate, A_c is the superficial cross sectional area of the regenerator, D_p is the particle diameter, and μ_f is the dynamic viscosity of the fluid. Tests were carried out using water, as well as 20%, 30%, and 40%, by mass, propylene glycol and water solutions. Table 4.1 shows the Reynolds number and the required experimental flow rates for all four of the fluids that were tested.

Table 4.1: Required flow rates in L/min. Entries that are grayed out exceed the maximum flow rate of the test facility.

Reynolds Number	Water	20% PG	30% PG	40% PG
1	0.03	0.07	0.10	0.14
2	0.07	0.14	0.19	0.28
3	0.10	0.21	0.29	0.42
5	0.17	0.35	0.49	0.70
7	0.24	0.48	0.68	0.97
10	0.35	0.69	0.97	1.39
15	0.54	1.04	1.46	2.09
20	0.69	1.38	1.94	2.78
30	1.04	2.07	2.91	4.17
50	1.74	3.45	4.86	6.96
70	2.43	4.83	6.81	9.74
100	3.47	6.90	9.72	13.91

The capability of the test facility places limitations on the maximum Reynolds number that can be achieved as the density of the working fluid increases. The maximum flow rate that can be generated by the pump used in the test facility is 5.0 L/min. This flow rate allows a maximum Reynolds number of 100 for water, but only 70 for 20%, by mass, propylene

glycol and water. Unattainable flow conditions are highlighted with gray backgrounds in Table 4.1. Figure 4.1 displays the maximum attainable Reynolds number as a function of the Prandtl number of the fluid.

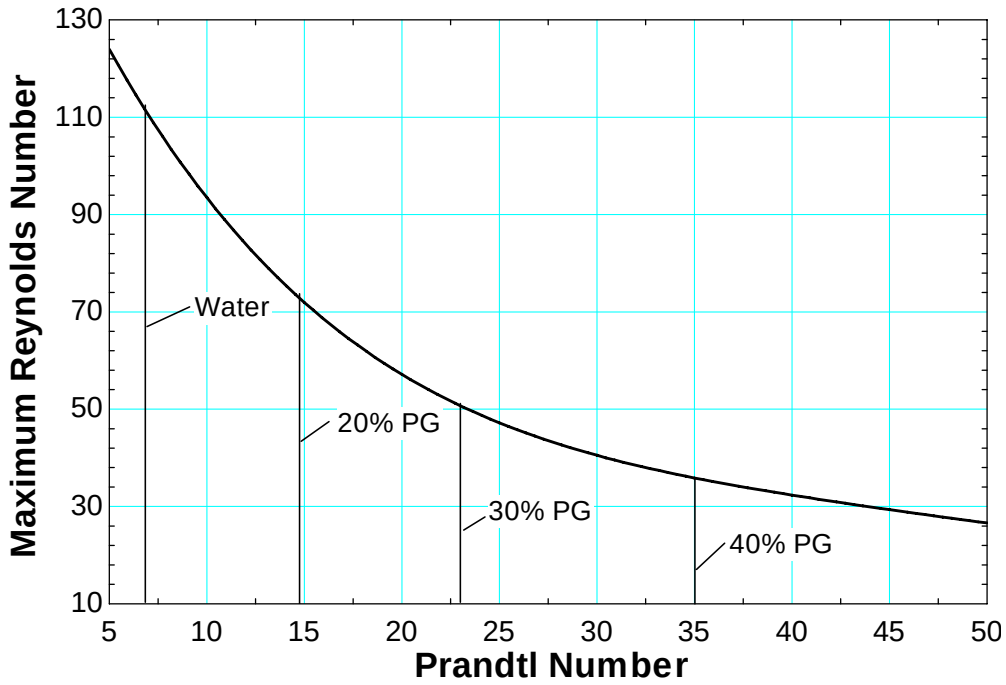

Figure 4.1: Maximum attainable Reynolds number of the test facility as a function of the Prandtl number of the fluid used. The fluids that are used in the experiment are indicated.

Examination of Figure 4.1 shows that the maximum achievable Reynolds number for water is 110. However as the concentration of propylene glycol increases to 20%, 30%, then 40%, the maximum possible Reynolds number decreases to 70, 50, and 40 respectively.

4.2 Repeatability Trials

The regenerator developed by Engelbrecht (2008) and Marconnet (2007) contained seven individual regenerator pucks; therefore, every run inherently resulted in seven separate measurements of the Nusselt number (one for each puck). The new regenerator consists of a

single regenerator matrix. Therefore, repeated experimental tests must be carried out in order to establish the repeatability of the measurements. Three different series of tests were carried out in order to examine the issue of repeatability. The first test series consisted of ten sequential experimental runs that were carried out on a single day. The repeatability of these data is shown in Figure 4.2 and it is clear that the tests result in very repeatable measurements, particularly when compared to data from the original regenerator facility developed by Engelbrecht and Marconnet, shown in Figure 4.3. Figure 4.3 illustrates the Nusselt number information obtained by reducing the data taken using water at a flow rate of 1.0 L/min with the original 7-puck regenerator (note that the same flow rate corresponds to a different Reynolds number and therefore a different Nusselt number due to dimensional differences between the facilities).

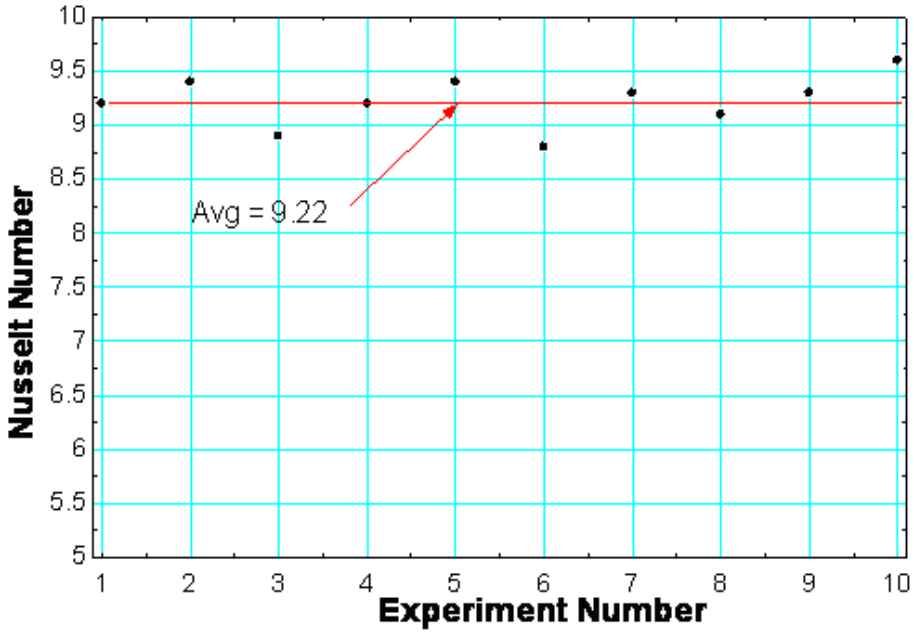

Figure 4.2: Nusselt numbers derived from ten individual sets of data using water at 1.0 L/min.

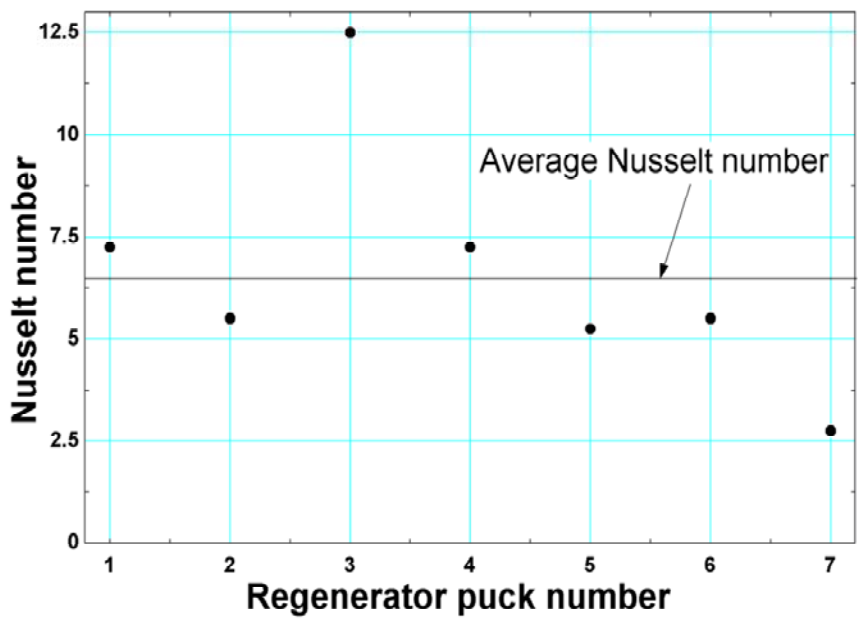

Figure 4.3: Nusselt numbers derived from data using water at 1.0 L/min with Engelbrecht's regenerator.

There is a significant reduction in the scatter of the data taken using the new regenerator. This in turn results in a much lower uncertainty in the average Nusselt number obtained from repeated testing using the new regenerator test facility. The uncertainty in the average Nusselt number is defined by equation 4.1

$$e_{Nu} = \frac{\sigma}{\sqrt{N-1}} \tag{4.1}$$

where e_{Nu} is the uncertainty in the average Nusselt number, σ is the standard deviation of the measured Nusselt numbers (which is taken to be the uncertainty in any single measurement), and N is the number of independent Nusselt number measurements. The uncertainty of the data from the original regenerator (shown in Figure 4.3) is approximately ±1.1 whereas the uncertainty of the data from the new regenerator (shown in Figure 4.2) is approximately ±0.06.

The next test series was carried out in order to establish the repeatability of the results obtained by carrying out tests on different days; the conditions in the lab may be slightly different from day-to-day and therefore these tests will identify uncertainty associated with these differences. Five tests were carried out using a flow rate of 1.0 L/min. The test facility was then shut down and the tests were repeated the next day under nominally the same test conditions. Figure 4.4 shows the Nusselt numbers derived from the data for the first two days of testing.

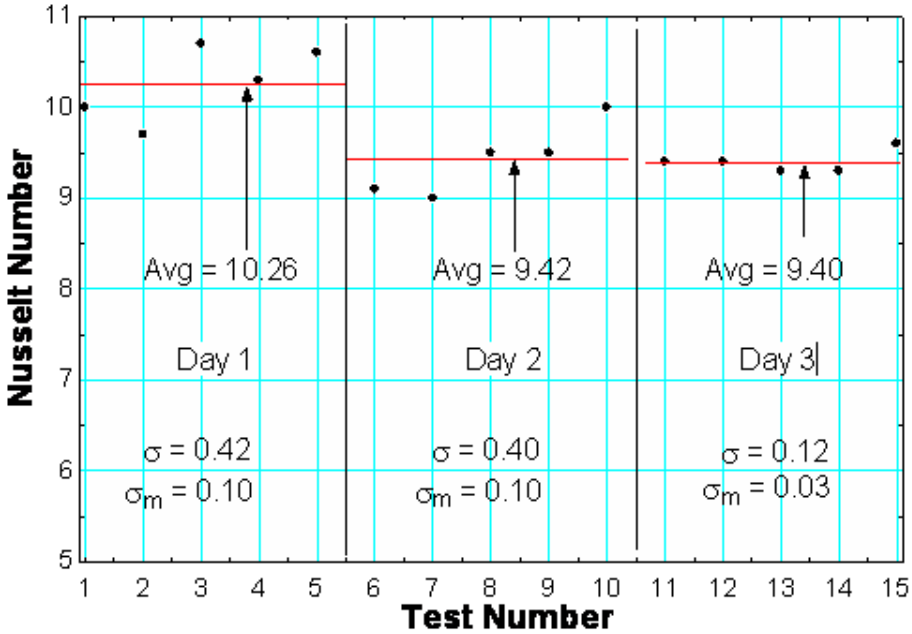

Figure 4.4: Nusselt numbers derived from ten sets of data using water with a flow rate of 1.0 L/min. Five sets of data were taken one day, and five more were taken the next two days.

The Nusselt number derived using the day 2 data is slightly lower than the value derived from day 1 data. The decrease in the measured Nusselt number motivated the collection of a third set of data on another, separate day; this was done in part to ensure that the results did not continue to decrease. Since the average Nusselt number on day 3 was very close to that

from day 2, the decrease in the results does not appear to be a consistent trend. Results from day 1 and day 2 differ by more than the standard deviation of the mean, σ_m. This observation suggests that a small difference in the experimental setup, for example, variations in the cold reservoir temperature setting or ambient air temperature, have a slight but measureable effect on the measured Nusselt number.

The third test series examined the impact of the temperature span (i..e., hot and cold reservoir temperatures) on the test results. Five sets of data were taken at a flow rate of 1.0 L/min with the same average temperature but three different temperature spans (i.e., hot to cold reservoir temperature difference): 9 K, 19 K, and 28 K. The cold reservoir temperature is the measured initial temperature of the regenerator bed (i.e. after cold soak), and hot reservoir temperature is the final steady state temperature of the regenerator (i.e. after hot blow). The measured cold and hot reservoir temperatures, and average experiment temperature are summarized in Table 4.2. The uncertainty associated with each of the measurements is the standard deviation of the five individual tests.

Table 4.2: Temperature Spans Summary.

Temperature Span	**Cold Reservoir Temperature**	**Hot Reservoir Temperature**	**Average Temperature**
Low, 9 K	288.6 K ± 0.2 K	298.1 K ± 0.1 K	293.3 K ± 0.1 K
Medium, 19 K	284.8 K ± 0.1 K	303.2 K ± 0.3 K	293.5 K ± 0.2 K
High, 28 K	280.0 K ± 0.3 K	308.0 K ± 0.3 K	294 K ± 0.2 K

The average temperature of the three tests was maintained the same in order to keep the average Prandtl number and Reynolds number experienced by the bed the same for all three

temperature spans. Figure 4.5 shows the Nusselt numbers measured for all three temperature spans.

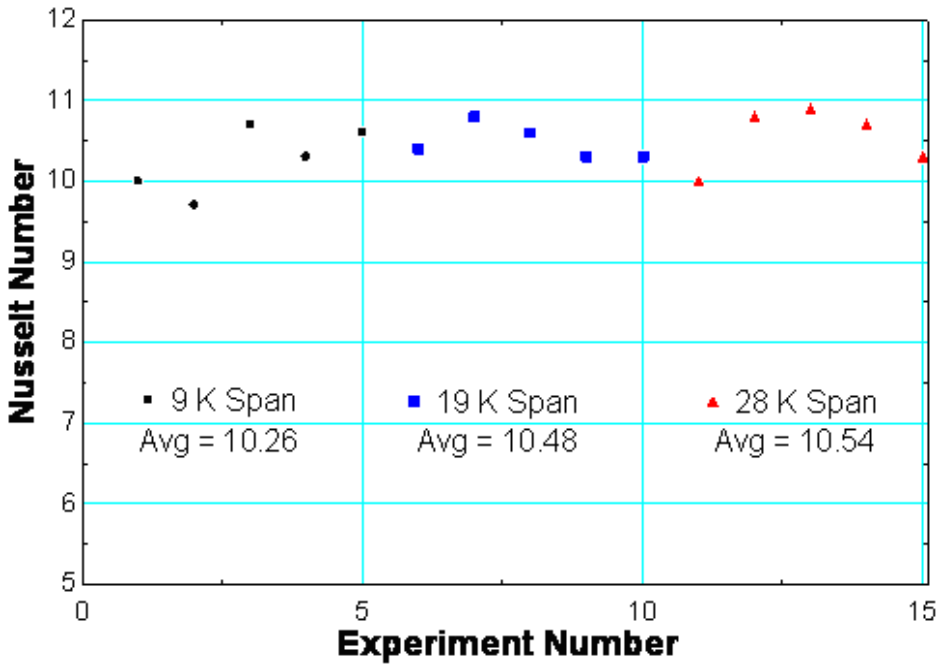

Figure 4.5: Measured Nusselt numbers for temperature spans of 9 K, 19 K, and 28 K.

The measured Nusselt numbers shown in Figure 4.5 suggests that the test facility is not affected by the temperature span used. Combining the results from all three repeatability tests yields the conclusion that the test facility produces results that are repeatable for any given trial and day and these results are not sensitive to the temperature span selected for the tests.

4.3 2nd Generation Results

Data reduction for the second generation experiment is performed using the UW AMRR model developed by Engelbrecht (2008). For every set of experimental data that is taken, an average Reynolds number and best fit Nusselt number is calculated according to the procedure discussed in Section 3.3.1. Figure 4.6 displays the best fit Nusselt number as a function of the average Reynolds number experienced during the test. The results shown are for each replicate at each flow rate with pure water as well as 20 and 30% propylene glycol and water solutions. Figure 4.6 illustrates the repeatability of the data taken at a given Reynolds number and Prandtl number.

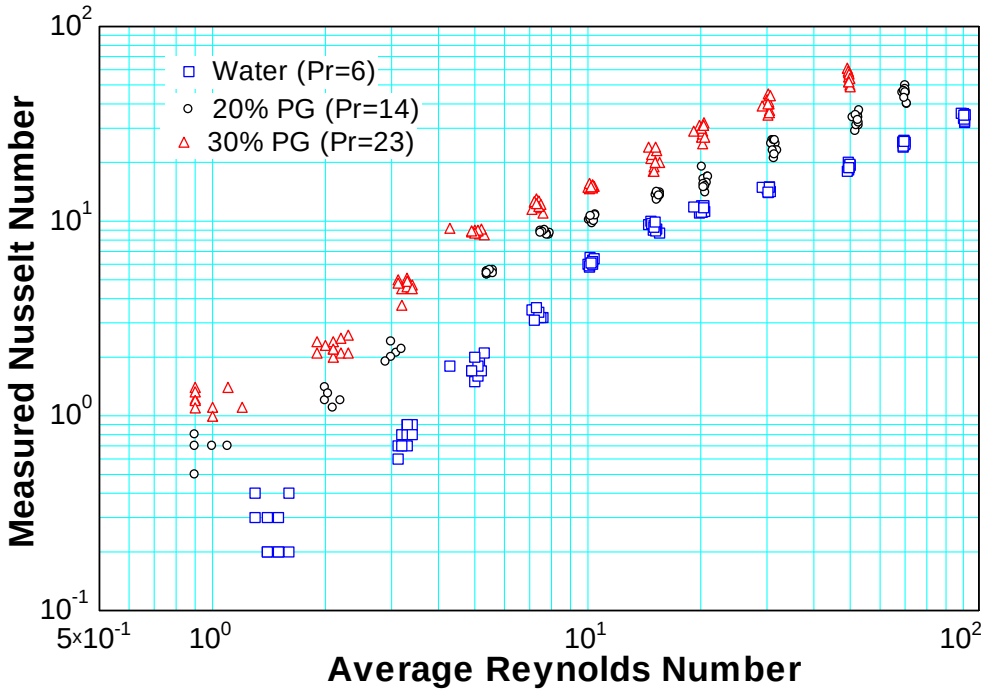

Figure 4.6: Experimentally determined Nusselt numbers for all data sets taken.

The results shown in Figure 4.6 follow the expected trends. The Nusselt number is an increasing function of both Prandtl number and Reynolds number. Wakao and Kaguei

developed a correlation for the Nusselt number as a function of Reynolds and Prandtl number; this correlation was previously provided by equation (1.3) and is shown again below:

$$Nu_{Wakao} = 2 + 1.1\,\mathrm{Re}^{0.6}\,\mathrm{Pr}^{1/3}$$

Measurements taken by Engelbrecht (2008) suggested that the Nusselt number for a packed bed of spheres with high Prandtl number fluids is approximately half of the value predicted by Wakao and Kaguei. The correlation developed by Engelbrecht based on his data is provided in equation 4.2

$$Nu_{UW} = 0.70\,\mathrm{Re}^{0.6}\,\mathrm{Pr}^{0.23} \tag{4.2}$$

Figures 4.7 and 4.8 compare the experimental data discussed in this chapter to the Nusselt numbers predicted by the Wakao and Engelbrecht (UW) correlations, respectively.

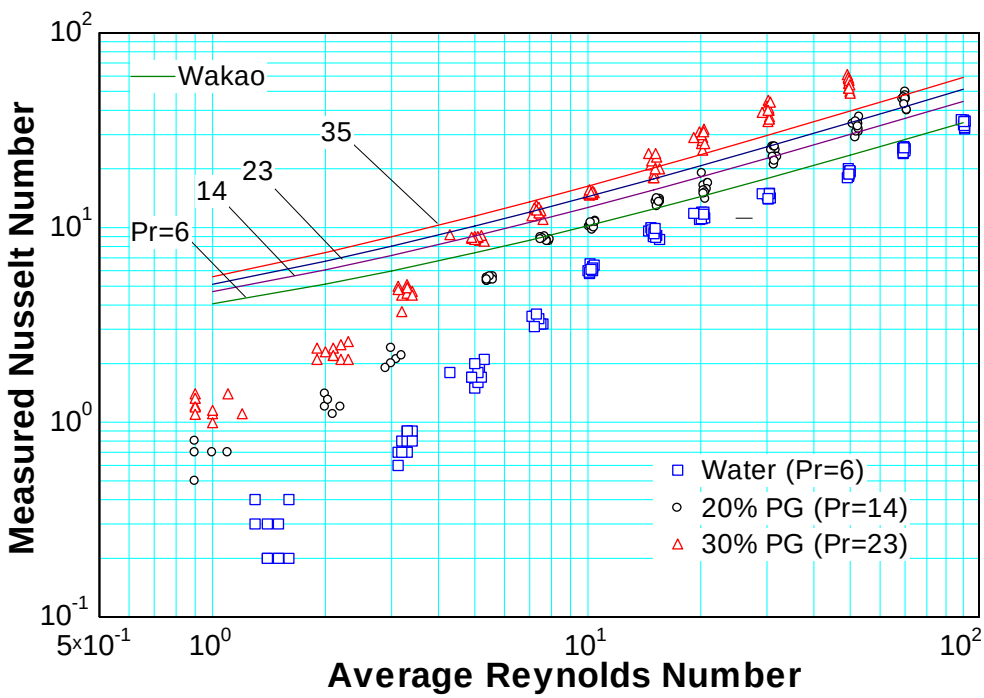

Figure 4.7: Experimental data along with Nusselt numbers predicted by Wakao and Kaguei.

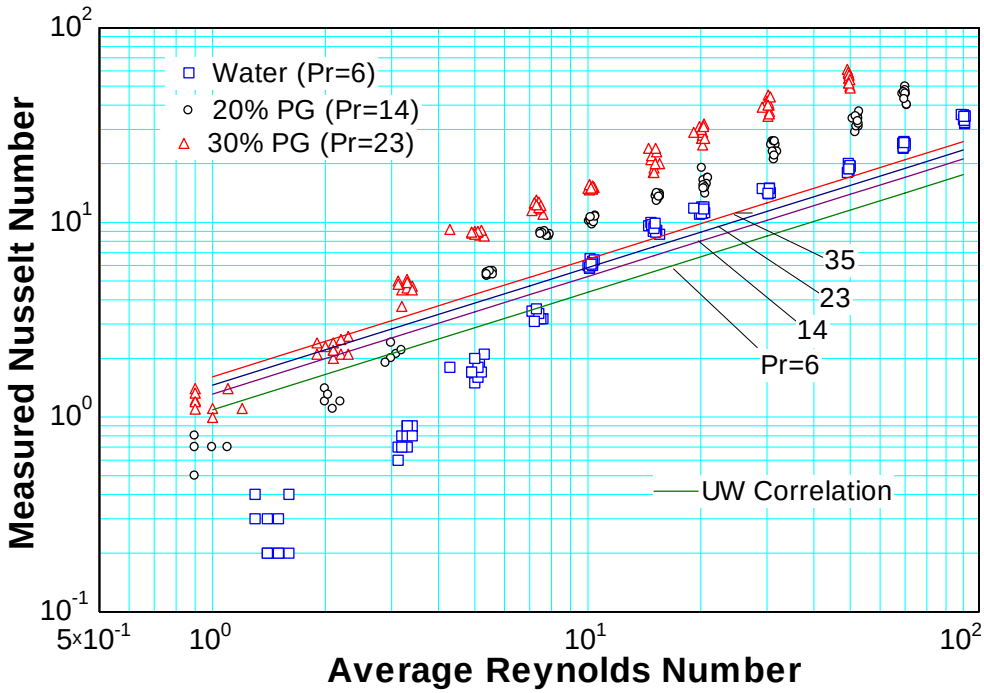

Figure 4.8: Experimental data along with Nusselt numbers predicted by Engelbrecht.

The experimental data tends to lie between the values predicted by these two correlations at moderate to high Reynolds number (i.e., at Reynolds number above approximately 5). At low Reynolds number, the data are below either of these correlations.

As previously mentioned, there were 10 replicate tests performed at each flow rate. In order to find the single best-fit Nusselt number for each test condition, the Nusselt number, Reynolds number, and Prandtl number associated with the replicates are averaged. The uncertainty associated with these averaged quantities is the uncertainty of the mean, defined by equation (4.3)

$$e = \frac{2\sigma}{\sqrt{N-1}} \tag{4.3}$$

where e is the uncertainty, σ is the standard deviation of the experimental data, and N is the number of samples taken. Using equation (4.3), the data is reduced to a single point at each Reynolds number and Prandtl number, as shown in Figure 4.9.

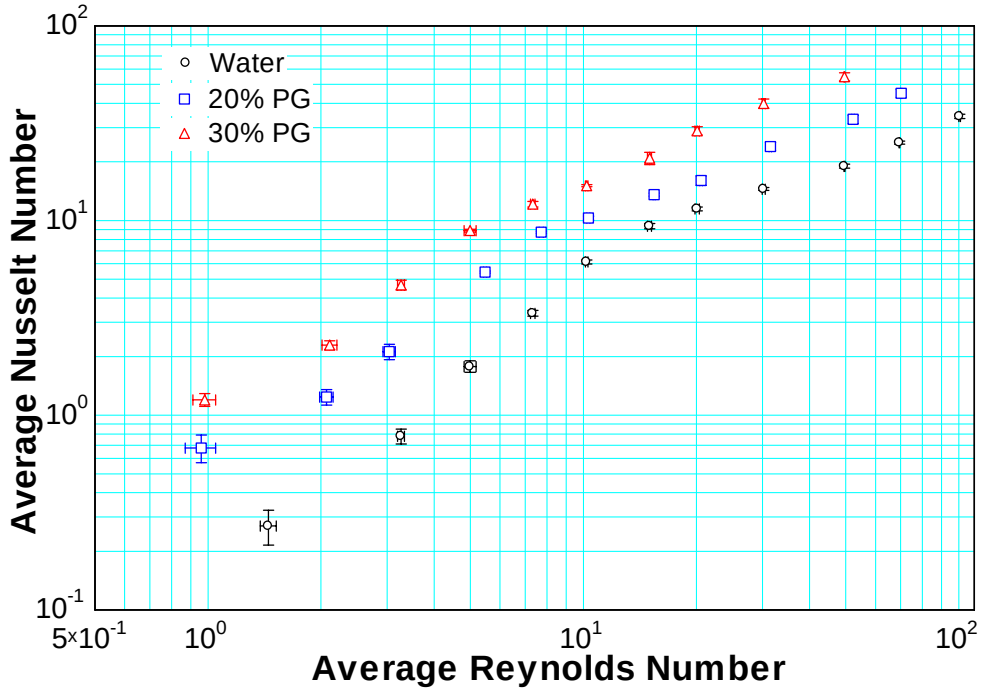

Figure 4.9: Average Nusselt number as a function of average Reynolds number.

The error bars in the x-direction represent the error in the average Reynolds number (due to variations from test-to-test), and the error bars in the y-direction represent the uncertainty in the Nusselt number (also due to variations from test-to-test). During a single test, the Reynolds number varies with time due to the property changes that are induced by varying fluid temperature. This leads to a range of Reynolds numbers over which the test occurs. Another method of quantifying the uncertainty in the Reynolds number is to take one-half the Reynolds number range experienced by the bed during each test. Figure 4.10 presents the same data seen in Figure 4.9; however, in Figure 4.9, the uncertainty in the Reynolds number

(i.e,. the magnitude of the error bars in the x-direction) is assigned based on the range of the Reynolds number experienced during each test.

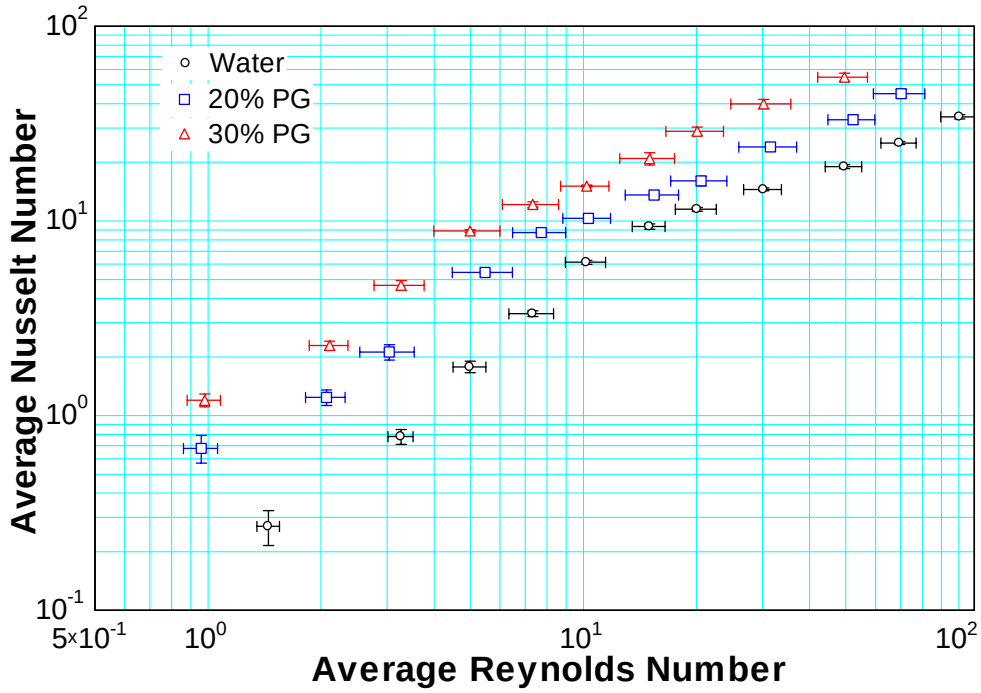

Figure 4.10: Average Nusselt number as a function of average Reynolds number using the range uncertainty.

There is a clear difference between the Reynolds number uncertainties in Figure 4.10 and Figure 4.9. The test-to-test average Reynolds number varies by a smaller amount than the Reynolds number range experienced by any single test. This observation indicates that each test was taken under nearly identical test conditions and reinforces the high level of repeatability that can be attained using this experiment.

It is important to note the dramatic reduction in the Nusselt number that occurs for Reynolds number below approximately 10. This decrease does not match well with either of the

previously mentioned correlations and causes the Nusselt number to drop below 2, which is the theoretical limit associated with a single sphere in an infinite medium. The subsequent sections explain several investigations that were carried out in order to (1) verify that the reduced Nusselt number is real and not the artifact of some flaw in the experimental apparatus, and (2) understand the underlying reason for this phenomenon.

4.4 Investigation of Results

There are several possible explanations for the precipitous decrease in the measured Nusselt number that is observed at low Reynolds number. This section describes the investigation of several of these potential causes.

4.4.1 Heat Transfer with the Environment

The model that is used to reduce the data and therefore infer the Nusselt number from the measured temperature variation does not consider the heat transfer with the surroundings during an experiment. In order to incorporate heat transfer into the model, a heat transfer term must be added the energy balance used to simulate each node. Figure 4.11 displays an energy balance on an internal node of the regenerator material, including heat loss to the surroundings.

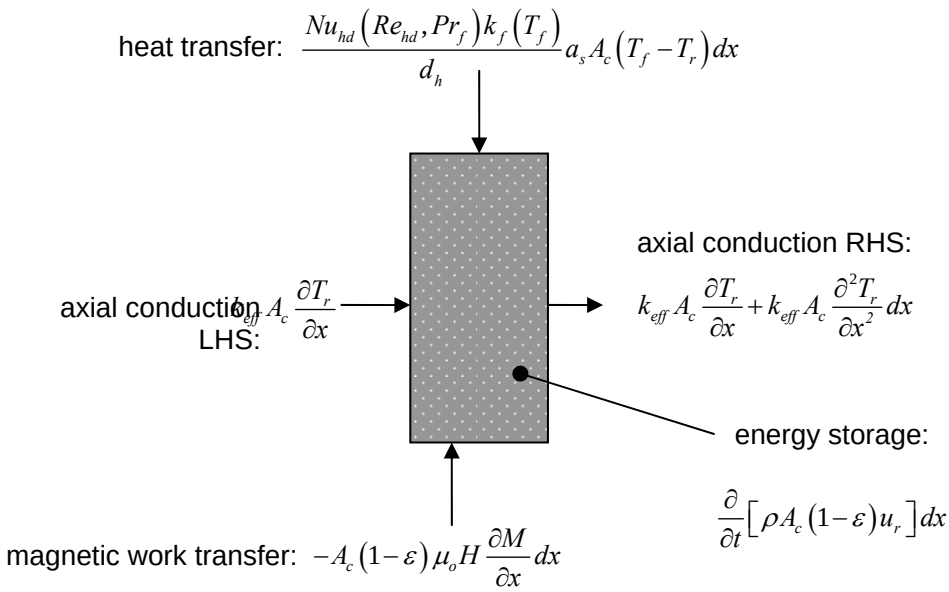

Figure 4.11: Energy balance on one node of the regenerator material including heat loss to the surroundings.

The heat loss to the surroundings is driven by the temperature difference between the regenerator material (T_r) and the surroundings (T_{sur}) and resisted by the thermal resistance to heat transfer between the external surface of the regenerator matrix and the surrounding air (R_{loss} - for the entire regenerator). The thermal resistance between the external surface of the regenerator and the surroundings is estimated according to Figure 4.12, which shows the resistance to conduction through each layer of the regenerator housing and the resistance to heat transfer between the exterior surface of the housing and the surroundings, which occurs due to both convection and radiation.

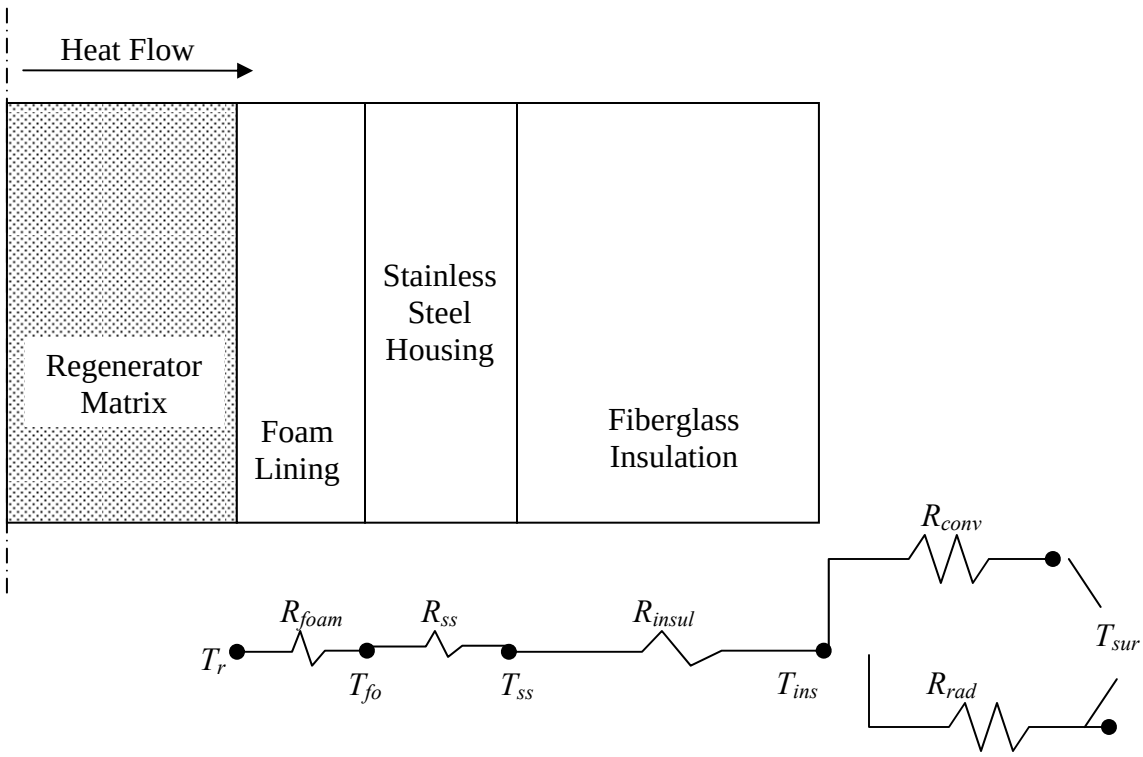

Figure 4.12: Diagram of the regenerator showing conduction heat loss through the thermal resistance network associated with the regenerator housing.

The thermal resistance network shown in Figure 4.12 includes conduction through several concentric cylinders. The thermal resistance through a cylinder is defined in equation (4.4)

$$R_{cyl} = \frac{\ln\left(\frac{r_{out}}{r_{in}}\right)}{2\pi\ L\ k} \tag{4.4}$$

where r_{out} is the outer radius of the cylinder, r_{in} is the inner radius of the cylinder, L is the length of the cylinder, and k is the thermal conductivity of the material. The equations for the resistance to convection and radiation are shown in equations (4.5) and (4.6) respectively.

$$R_{conv} = \frac{1}{\bar{h}\ A_s} \tag{4.5}$$

$$R_{rad} = \frac{1}{4A_s \ \sigma \ \varepsilon \ \overline{T}^3} \tag{4.6}$$

where $\overline{h}$ is the free convection heat transfer coefficient, A_s is the surface area of the outer surface of the regenerator, σ is Stephen-Boltzmann's constant, ε is the emissivity, and $\overline{T}$ is the average of the outer surface temperature and the surrounding temperature. The free convection heat transfer coefficient is calculated using the correlation for natural convection from a vertical cylinder, discussed by Rohsenow, Hartnett and Cho (1998). Inserting equations (4.4) through (4.6) into the resistance network shown in Figure 4.12 results in the total resistance to heat loss from the regenerator given by equation (4.7)

$$R_{Loss} = \frac{\ln\left(\frac{r_{fo}}{r_m}\right)}{2\pi \ k_{fo} \ L} + \frac{\ln\left(\frac{r_{ss}}{r_{fo}}\right)}{2\pi \ k_{ss} \ L} + \frac{\ln\left(\frac{r_{ins}}{r_{ss}}\right)}{2\pi \ k_{ins} \ L} + \left(\overline{h} \ A_s + 4A_s \ \sigma \ \varepsilon \ \overline{T}^3\right)^{-1} \tag{4.7}$$

where r_m is the outer radius of the regenerator packing, r_{fo} is the outer radius of the foam lining, r_{ss} is the outer radius of the stainless steel housing, and r_{ins} is the outer radius of the fiberglass insulation. Table 4.3 displays the values for each of the variables present in equation (4.7). The thermal conductivities for stainless steel and foam rubber, and emissivity of rubber are found in the property functions of Engineering Equation Solver (EES). The thermal conductivity of the fiberglass insulation is available from the distributor, McMaster-Carr. The average temperature $\overline{T}$ was calculated assuming that the regenerator temperature was the maximum temperature for any given test, 305 K, and the surroundings inside the laboratory were at 292 K. Thus, the value of R_{Loss} remains constant for the heat loss equation described in Figure 4.11. Table 4.4 displays the nominal values of each resistance in the thermal network.

Table 4.3: Variable values used in equation (4.7).

Variable Name	Description	Value (units)
r_m	Outer radius of packing	2.93 (cm)
r_{fo}	Outer radius of foam lining	3.01 (cm)
r_{ss}	Outer radius of housing	3.18 (cm)
r_{ins}	Outer radius of insulation	5.72 (cm)
L	Regenerator length	27.94 (cm)
A_s	Outer surface area of insulation	1000 (cm^2)
k_{fo}	Thermal conductivity of foam lining	0.40 (W/m-K)
k_{ss}	Thermal conductivity of stainless steel	14.94 (W/m-K)
k_{ins}	Thermal conductivity of fiberglass insulation	0.04 (W/m-K)
$\bar{h}$	Free convection heat transfer coefficient	3.01 (W/m^2-K)
σ	Stephan-Boltzmann's constant	5.67E-08 (W/m^2-K^4)
ε	Emissivity of outer insulation surface	0.89 (-)
$\bar{T}$	Average temperature	297.3 (K)

Table 4.4: Nominal thermal resistances.

Name	Symbol	Thermal Resistance [K/W]
Foam Lining	R_{fo}	0.038
Steel Housing	R_{ss}	0.002
Fiberglass Insulation	R_{ins}	4.17
Free Convection	R_{conv}	4.18
Radiation	R_{rad}	2.42

The values listed in Table 4.4 suggest that the fiberglass insulation is the largest resistance (note that the resistance to free convection and radiation are combined in parallel). The final

value of R_{Loss} was substituted into the energy balance for the control volume, shown in equation (4.8).

$$\frac{Nu\ k_f}{d_h} a_s\ A_s \left(T_f - T_r\right) + k_{eff}\ A_c \frac{\partial^2 T_r}{\partial x^2} = A_c \left(1-\varepsilon\right) \rho_r \left(\frac{\partial u_r}{\partial t} - \mu_o H \frac{\partial \left(v_r\ M\right)}{\partial t} \right) + \frac{\left(T_r - T_{sur}\right)}{R_{Loss}\ L} \quad (4.8)$$

Equation 4.8 is the governing equation solved by the UW-AMR model modified to include the heat loss to the surroundings. The total rate of heat transfer to the surroundings as a function of time is shown in Figure 4.13 for the test with water at a Reynolds number of 100.

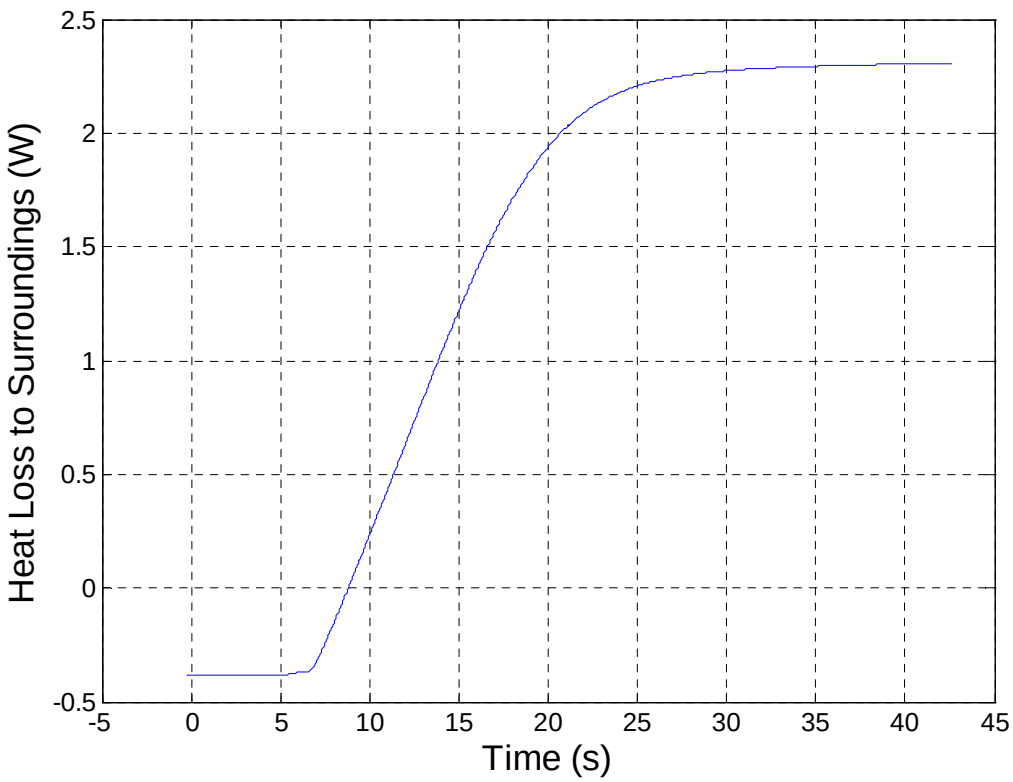

Figure 4.13: Heat loss to surrounding as a function of time for Re = 100 with water.

The rate of heat transfer is initially a small negative value because the temperature of the regenerator material is slightly less than that of the surroundings, causing heat to be transferred into the regenerator. However as time progresses and the regenerator begins to

increase in temperature due to the hot blow process, the rate of heat transfer becomes more and more positive and asymptotes to a constant value when the regenerator has reached the hot fluid temperature. This follows the expected behavior. Due to the insulation surrounding the regenerator, only a small amount of heat is transferred to the surroundings; the heat loss to the surroundings is 2 W compared to the approximately 375 W of heat transfer that took place inside the regenerator under the same test conditions. Therefore including the heat transfer in the data reduction procedure leads to only a very small change in the experimentally determined Nusselt number, as seen in Figure 4.14.

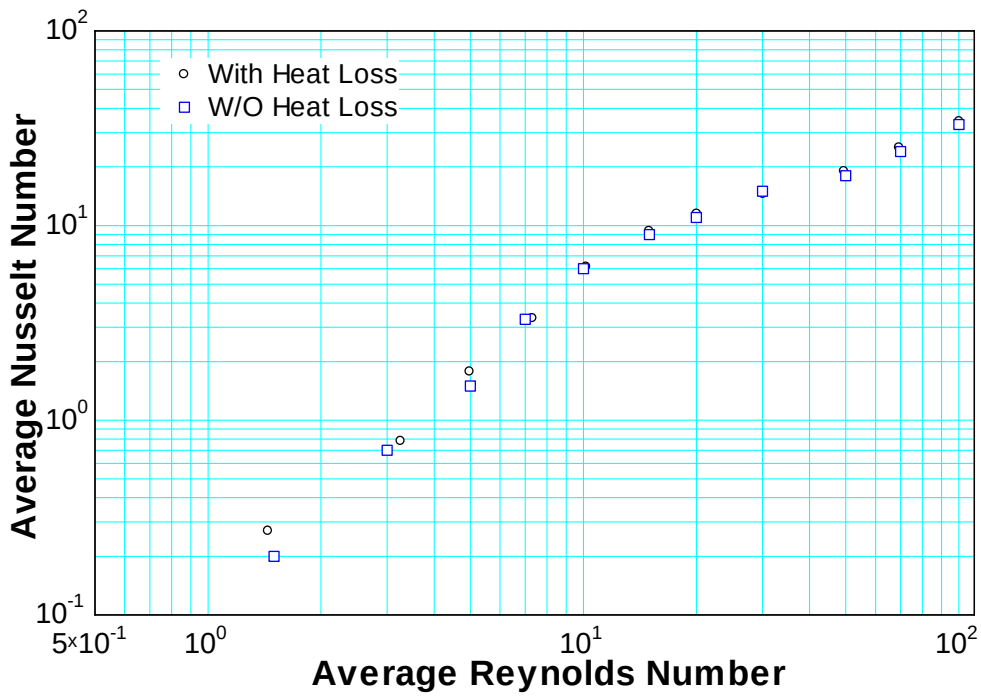

Figure 4.14: Nusselt numbers for water before and after the heat loss term is included.

4.4.2 Nusselt Number as a Function of Re and Pr

The Nusselt number values that are used by the model to reduce the data come from a vector of parametric values that are supplied by the user. This Nusselt number is used during the

simulation and assumed to be constant throughout the entire experiment, even though the local Reynolds number and Prandtl number vary somewhat during a test due to the temperature change of the fluid. In order to verify this approach, the Nusselt number used during the simulation was allowed to vary with the local Reynolds and Prandtl number. The equation used to compute the local Nusselt number given the local Reynolds number and Prandtl number is shown in Equation (4.9).

$$Nu_{fun(i,j)} = Nu_{guess,i}\left(\frac{Re_{f(i,j)}}{Re_{nom}}\right)^{A}\left(\frac{Pr_{f(i,j)}}{Pr_{nom}}\right)^{B} \tag{4.9}$$

where $Nu_{guess,i}$ is the user-supplied Nusselt number value that is being evaluated, $Re_{f(i,j)}$ is the local Reynolds number, and $Pr_{f(i,j)}$ is the local Prandtl number. Re_{nom} and Pr_{nom} are the nominal Reynolds number and Prandtl number associated with that particular test. For example, if the first set of data taken at a target Reynolds number of 100 is used, then the average Reynolds number and Prandtl number computed for that test are taken to be the values of Re_{nom} and Pr_{nom}, respectively. The exponents A and B that are used in equation (4.9) are consistent with the Nusselt number correlation for flow through a bed of packed spheres developed by Wakao and Kaguei. As with any test reduction, the RMS error between the measured and predicted temperature is calculated as a function of the Nusselt number guess value and the Nusselt number that produces the smallest error is taken to be the Nusselt number that is "measured" by the test. Figures 4.15 and 4.16 illustrate the RMS error as a function of the guess Nusselt number associated with a constant and varying Nusselt number technique for Reynolds numbers of 100 and 1.5, respectively.

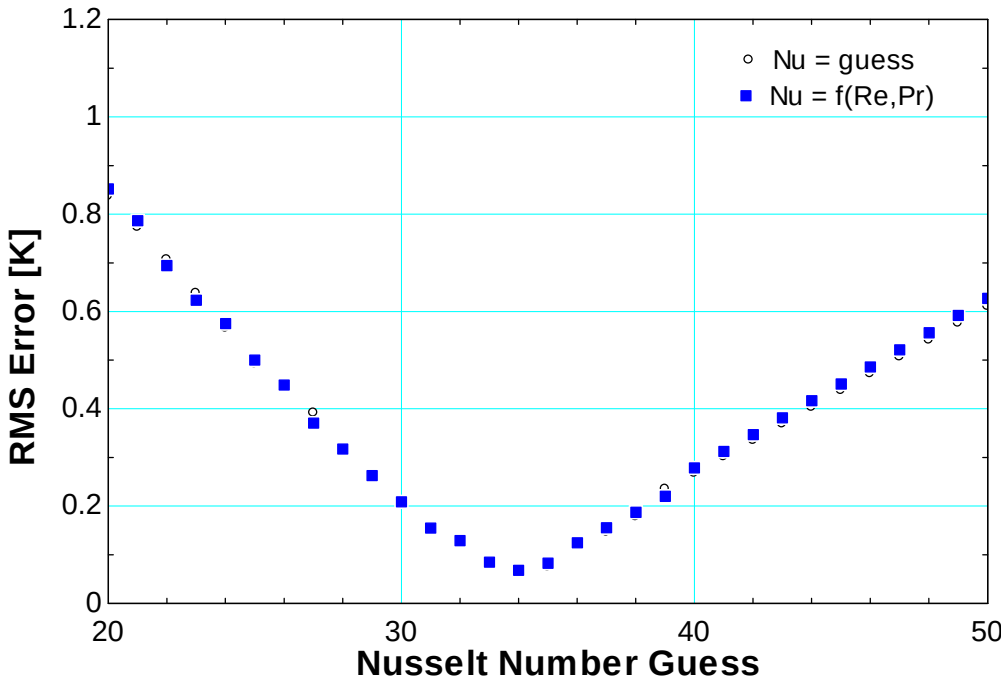

Figure 4.15: RMS error as a function of Nusselt number guess for both the constant Nusselt number and Nu=f(Re,Pr) for experimental data taken with a Reynolds number of 100 with A and B taken from Wakao and Kaguei.

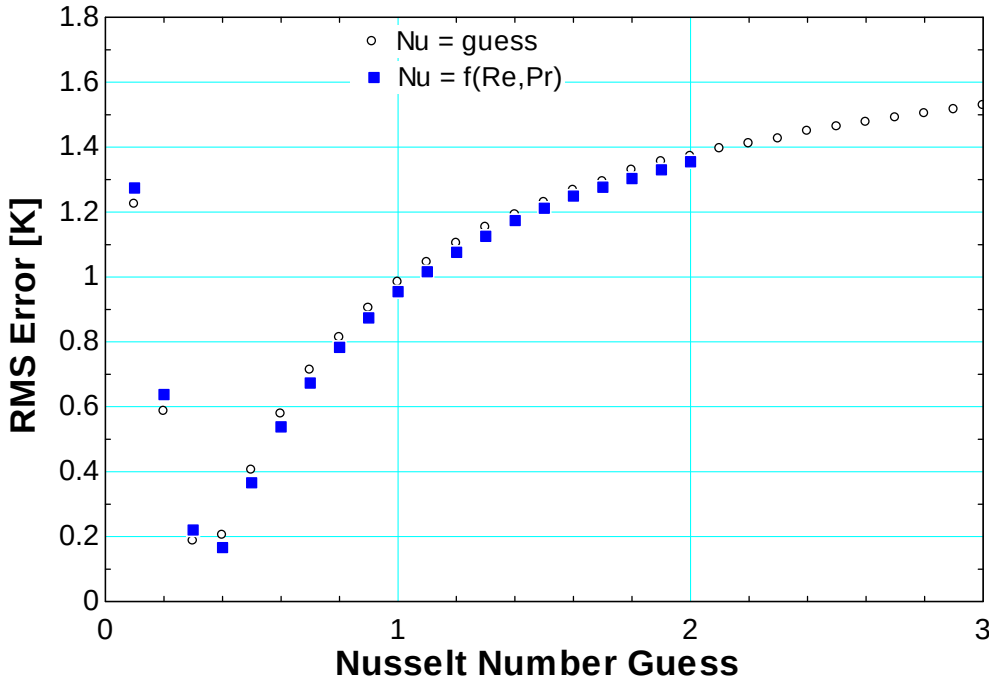

Figure 4.16: RMS error as a function of Nusselt number guess for both the constant Nusselt number and Nu=f(Re,Pr) for experimental data taken with a Reynolds number of 1.5 with A and B taken from Wakao and Kaguei.

The data presented in Figures 4.15 and 4.16 demonstrate that the results do not change regardless of whether the Nusselt number is assumed to be constant or allowed to vary with the Reynolds number and Prandtl number during any single test. This result is found to be true even if the exponents used in equation (4.9) are changed. Figures 4.17 and 4.18 show the RMS error as a function of Nusselt number for a Reynolds exponent of A = 0.8 and a Prandtl exponent of B = 0.1.

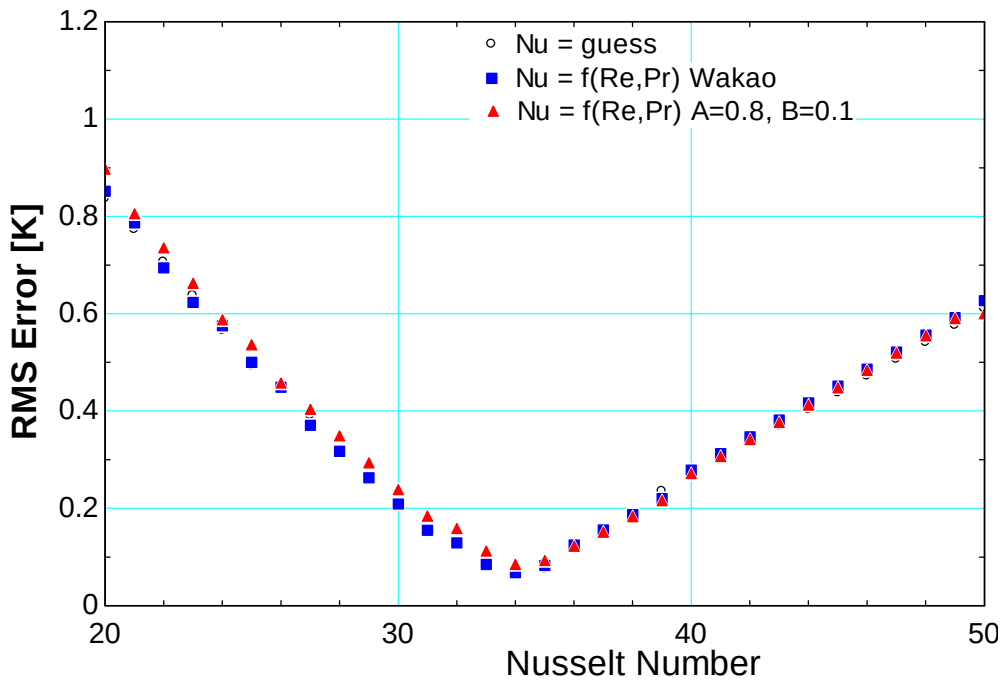

Figure 4.17: RMS error as a function of Nusselt number guess for constant Nusselt number and Nu=f(Re,Pr) for experimental data taken with a Reynolds number of 100 with A=0.8 and B=0.1.

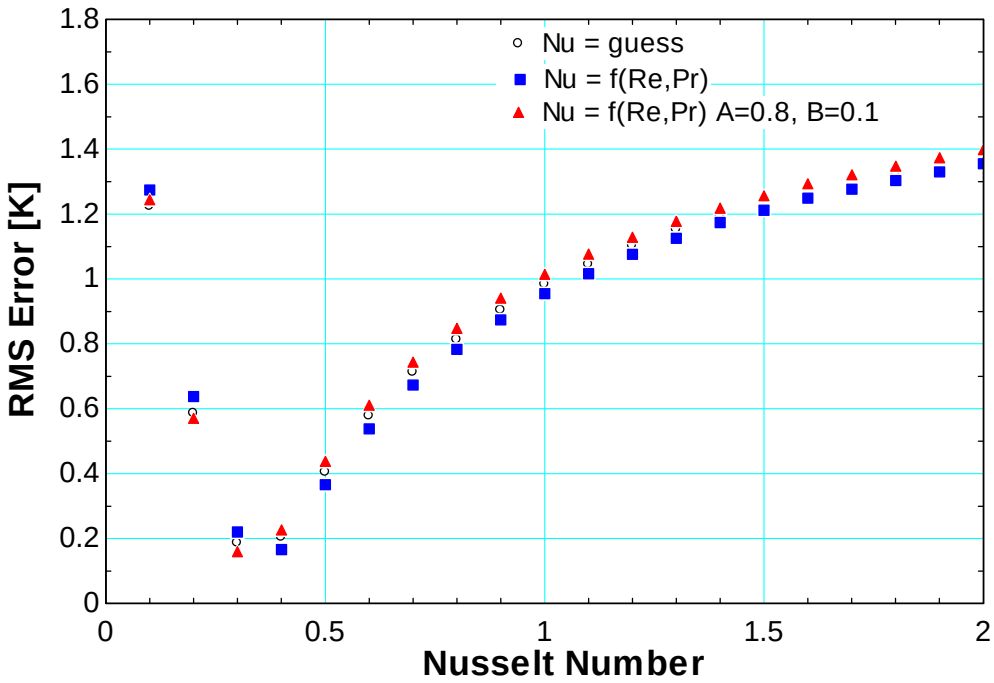

Figure 4.18: RMS error as a function of Nusselt number guess for constant Nusselt number and Nu=f(Re,Pr) for experimental data taken with a Reynolds number of 1.5 with A=0.8 and B=0.1.

4.4.3 Flow Maldistribution

Flow maldistribution can significantly impact the performance of a regenerator. Therefore, it is possible that the sharp decrease in measured Nusselt number at low Reynolds number is actually an artifact of an actual reduction in the performance of the regenerator due to flow maldistribution (which is not accounted for in the model). The impact of flow maldistribution is examined by performing a CFD analysis using Fluent to describe the flow characteristics inside of the regenerator bed. Credit for the Fluent model creation, analysis, and plots is given to Ryan Taylor. The results discussed in this section are the product of personal communication with Mr. Taylor. The Fluent model considers the entire passive regenerator and its inlet and outlet plumbing, as shown in Figure 4.19. The structure of the

regenerator is not considered explicitly; rather, a porous media model is used in which the momentum loss coefficients are based on the Ergun pressure drop equation (Taylor, 2008). The packed bed of spheres is assumed to be isotropic. The screens used to hold the spheres in place are not considered; this is a conservative assumption because the screens themselves should act to distribute the flow. However, the screens have a small spatial extent and therefore will likely have a small effect on the flow distribution. The steady state flow distribution is predicted by the CFD model. All of the material properties are assumed to remain constant and the flow is assumed to be laminar.

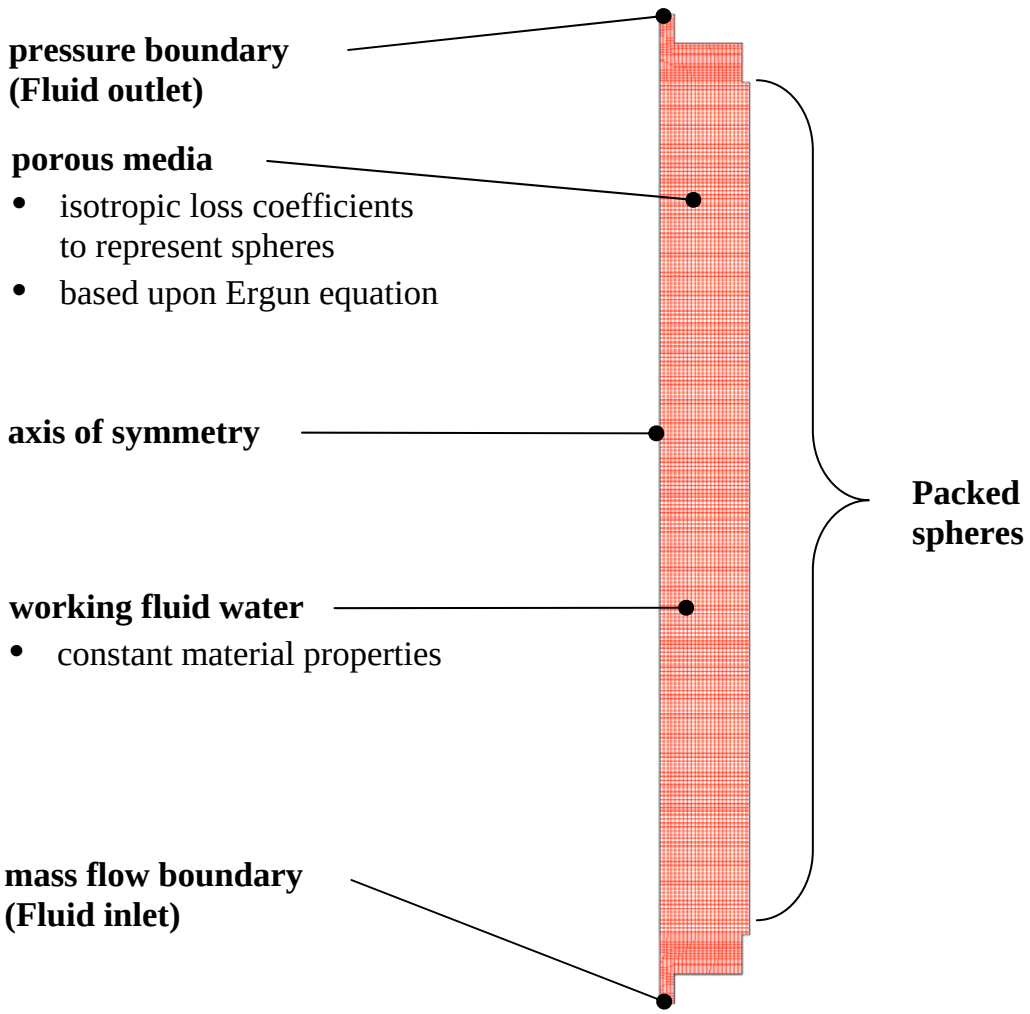

Figure 4.19: CFD model of the passive regenerator used to study flow maldistribution effects.

The CFD model is used to study the operation of the facility for Reynolds numbers ranging from 1 to 100 with water. The analysis only considered the hydrodynamic characteristics of the facility; heat transfer was neglected. Figure 4.20 illustrates the pressure drop predicted by the Fluent model and measured in the tests as a function of Reynolds number. The agreement shows that the data agree approximately with the Ergun correlation for the friction factor and therefore that the momentum loss coefficients used in the CFD model were extracted from the correlation correctly.

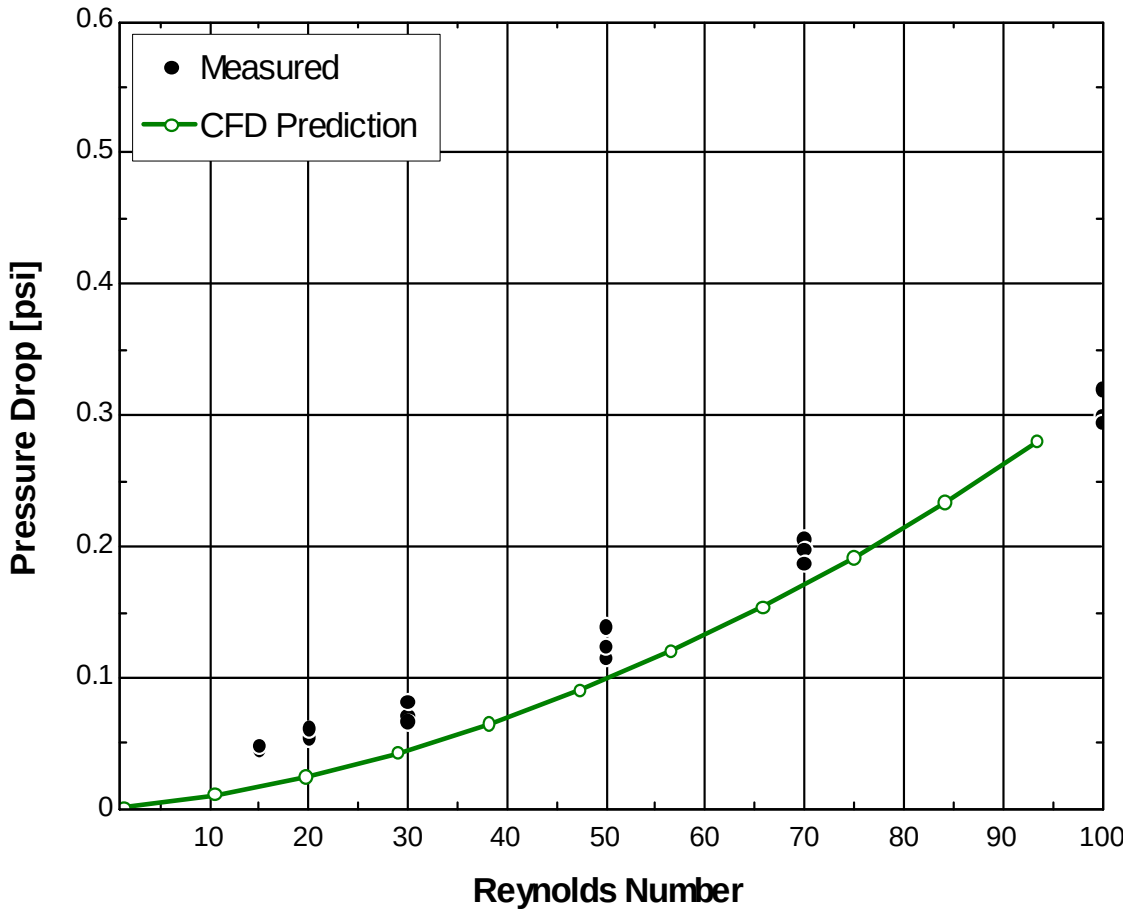

Figure 4.20: Total pressure drop across the bed predicted by the CFD model and experimentally measured as a function of Reynolds number.

The velocity profiles of the fluid inside the regenerator are examined in order to determine if there is significant flow maldistribution. Figures 4.21, 4.22, and 4.23 show contour plots of the magnitude of the *x*-velocity of the fluid within the regenerator for high, medium, and low Reynolds number cases, respectively. The velocity profiles shown in Figures 4.21 to 4.23 indicate that the flow is essentially uniform everywhere except very near the inlet, even for very low Reynolds number test conditions. The Fluent simulation suggests that the overall geometry of the regenerator does not induce flow maldistribution and adversely affect the results.

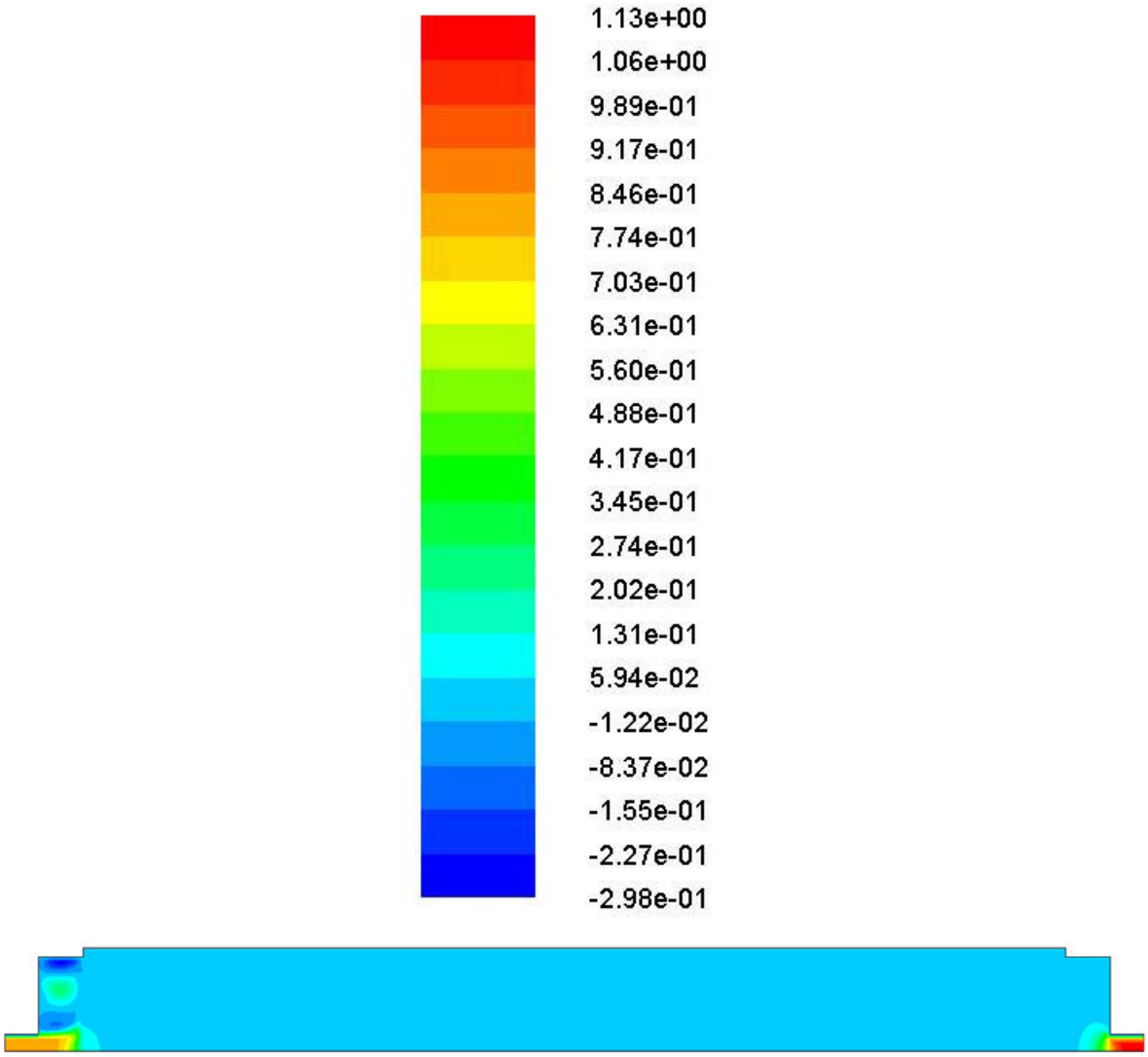

Figure 4.21: Fluid velocity in m/s inside regenerator for a Reynolds number of 100

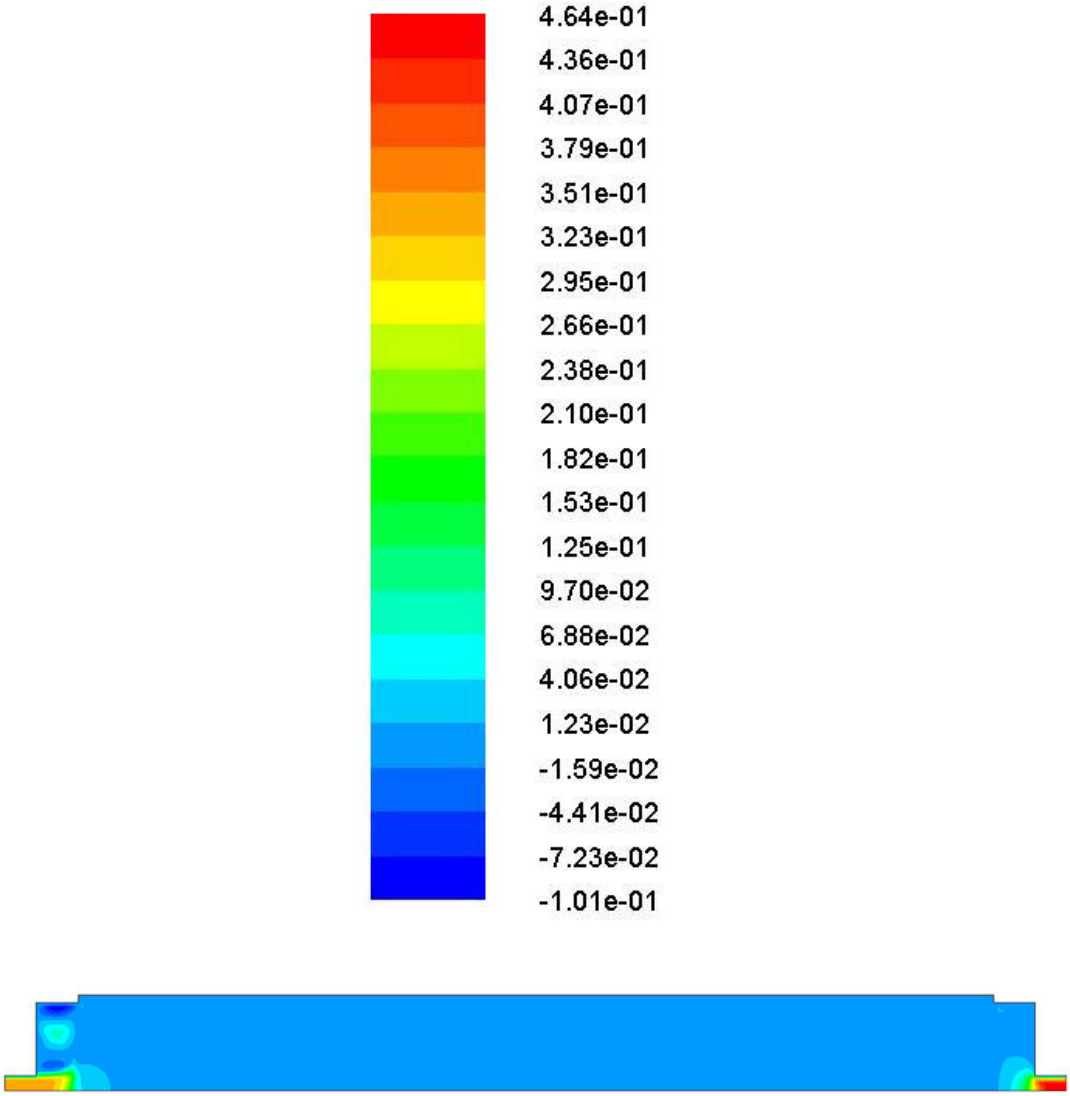

Figure 4.22: Fluid velocity in m/s inside regenerator for a Reynolds number of 38

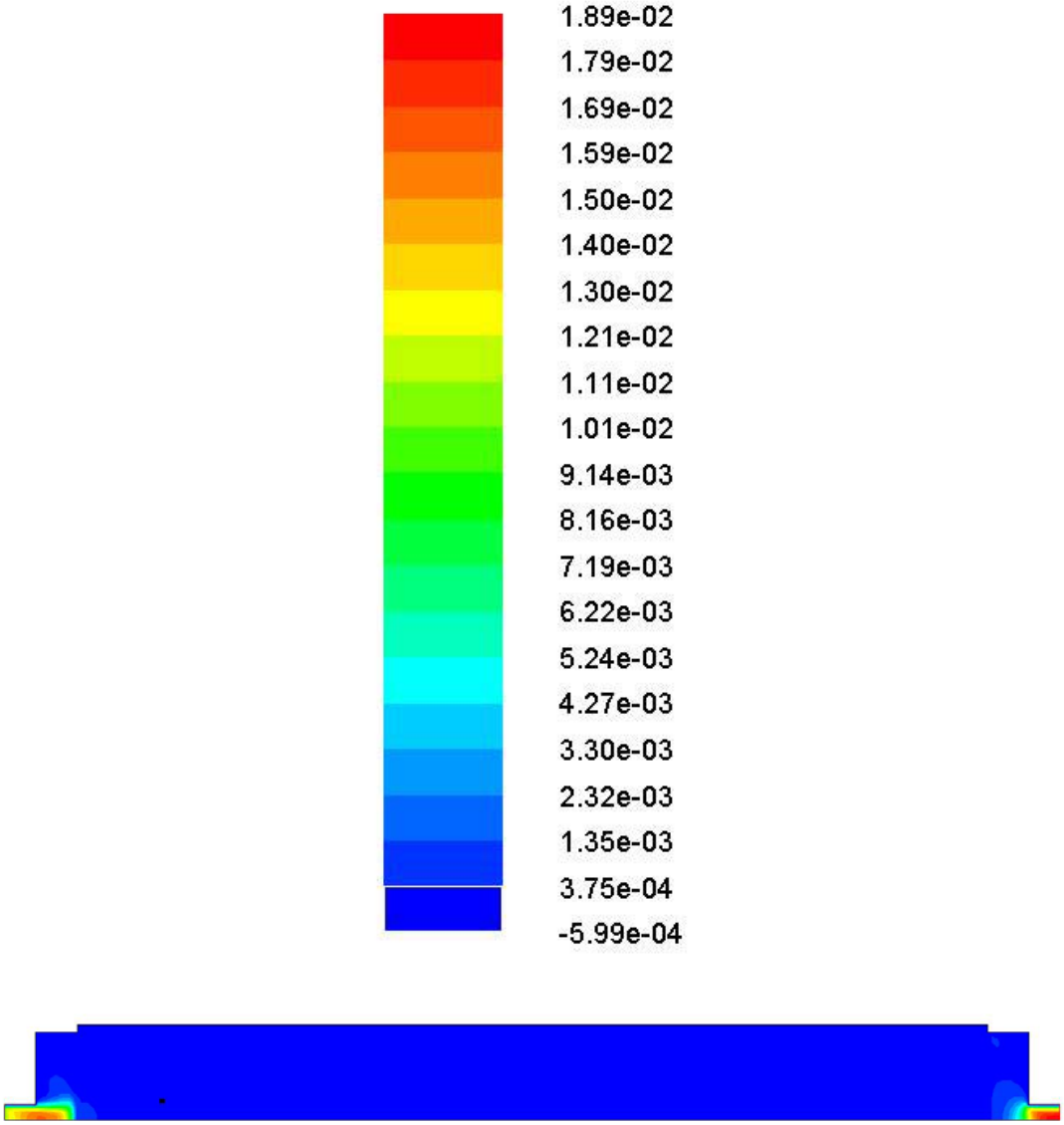

Figure 4.23: Fluid velocity in m/s inside regenerator for a Reynolds number of 1.

Chapter 5 – Third Generation Experiment Results

Due to the non-physical behavior observed in the data from the second generation regenerator at low Reynolds number, discussed in Chapter 4, the third generation regenerator (discussed in Section 2.3) was developed in order to provide another, independent data set. In addition, the dispersion concentric (DC) model developed by Astronautics is used to reduce the data in order to provide a method for determining Nusselt number that explicitly includes the impact of the housing and foam heat capacity on the behavior of exit temperature. Experimental data were obtained for flow rates corresponding to a Reynolds number range of 1 to 100 for different concentrations of propylene glycol and water that correspond to a range of Prandtl numbers. At each flow rate, three independent tests were run using the third generation regenerator. The experimental data from the third generation regenerator and the experimental data from the second generation regenerator are both reduced using the DC model. The results of this analysis are discussed in the subsequent sections of this chapter.

5.1 Experimental Data

During experimental data acquisition with the third generation experiment, the cold reservoir temperature was held at 280 K and the warm reservoir temperature was held at 305 K in order to be consistent with data obtained using the second generation experiment. Experimental flow rates for this experiment were chosen to match the Reynolds numbers used in the second generation experiment, discussed in Section 4.1. Tests were once again

carried out using water, 20%, 30%, and 40% by mass solutions of propylene glycol and water. Table 5.1 shows the required flow rates for all four fluids tested.

Table 5.1: Required flow rates in L/min. Entries that are grayed out exceed the maximum flow rate of the test facility.

Reynolds Number	Water	20% PG	30% PG	40% PG
1	0.03	0.06	0.09	0.13
2	0.06	0.12	0.17	0.25
3	0.09	0.19	0.26	0.38
5	0.16	0.31	0.44	0.63
7	0.22	0.43	0.61	0.88
10	0.31	0.62	0.87	1.25
15	0.47	0.93	1.31	1.88
20	0.62	1.24	1.75	2.50
30	0.94	1.86	2.62	3.76
50	1.56	3.10	4.37	6.26
70	2.19	4.35	6.12	8.76
100	3.12	6.21	8.75	12.52

The maximum flow rate achievable on the test facility is 5.0 L/min. Therefore, the maximum Reynolds number attainable for each fluid is different (seen as the grayed out flow rates in Table 5.1). For water, the maximum Reynolds number of 100 is achievable, however for 20% propylene glycol the maximum Reynolds number is only 70, for 30% the maximum is 50, and for 40% the maximum is 40. Figure 5.1 displays the maximum achievable Reynolds number for the third generation experiment, compared to that of the second generation experiment.

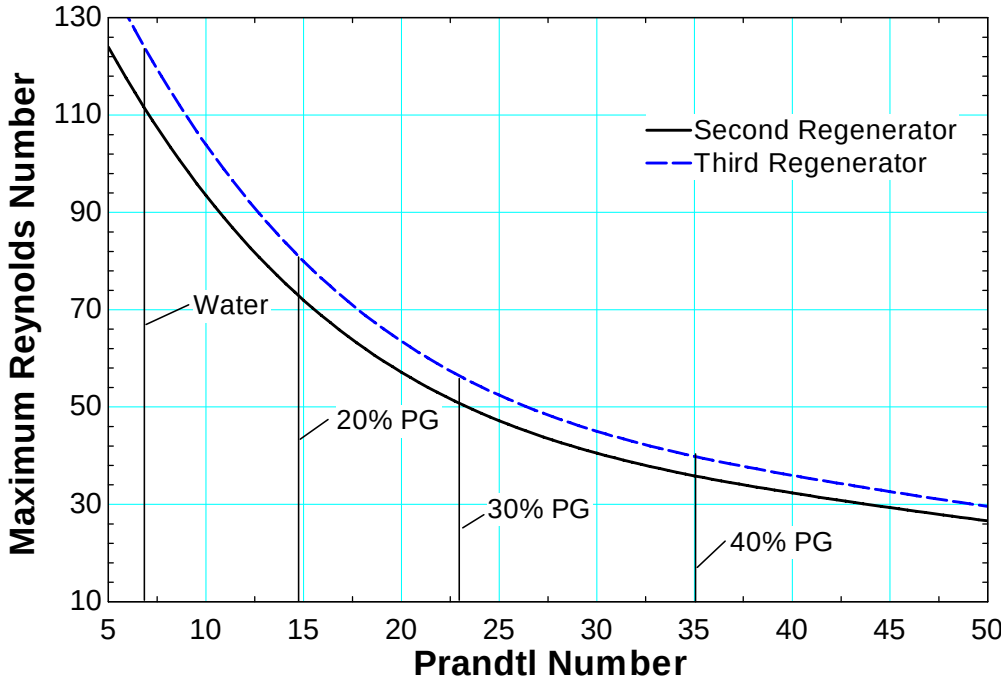

Figure 5.1: Maximum achievable Reynolds number for the second and third generation experiment.

5.2 Repeatability Experiment

Two tests were performed in order to establish the repeatability of the results obtained with this facility. The experimental results are reduced using the dispersion concentric model. The first test carries out 10 individual experimental data sets on the same day. The tests were performed at a flow rate corresponding to a Reynolds number of 10 (which corresponds to approximately 0.3 L/min with water), and the results are shown in Figure 5.2. The results show very good repeatability, especially when compared to the results obtained by Engelbrecht (2008) and Marconnet (2007), shown in Figure 5.3.

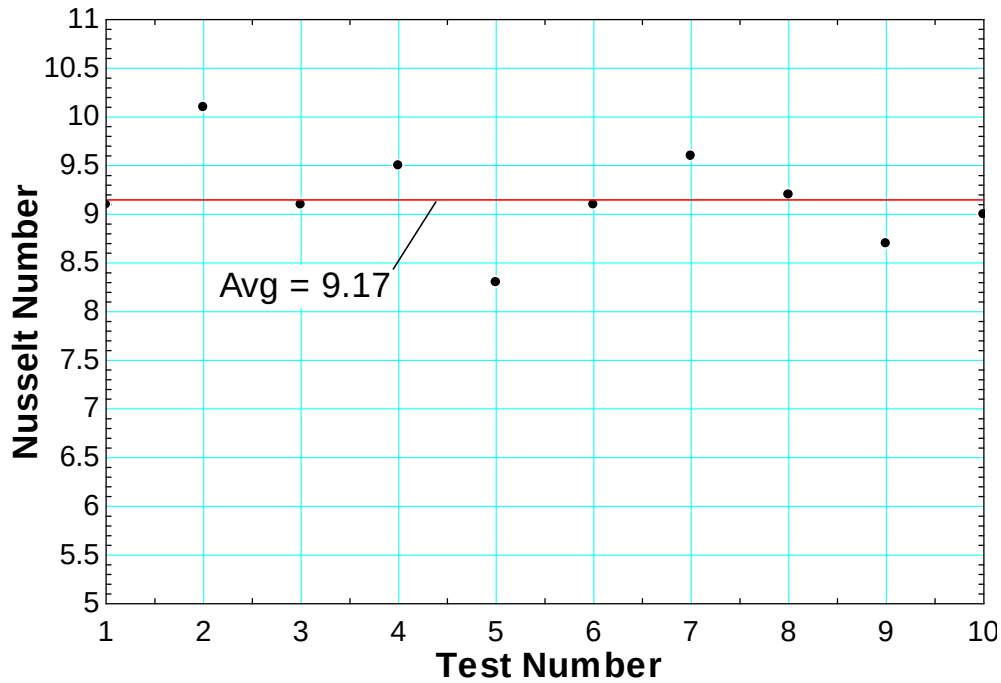

Figure 5.2: Nusselt number results for 10 individual tests performed at a flow rate of 0.3 L/min (Re = 10).

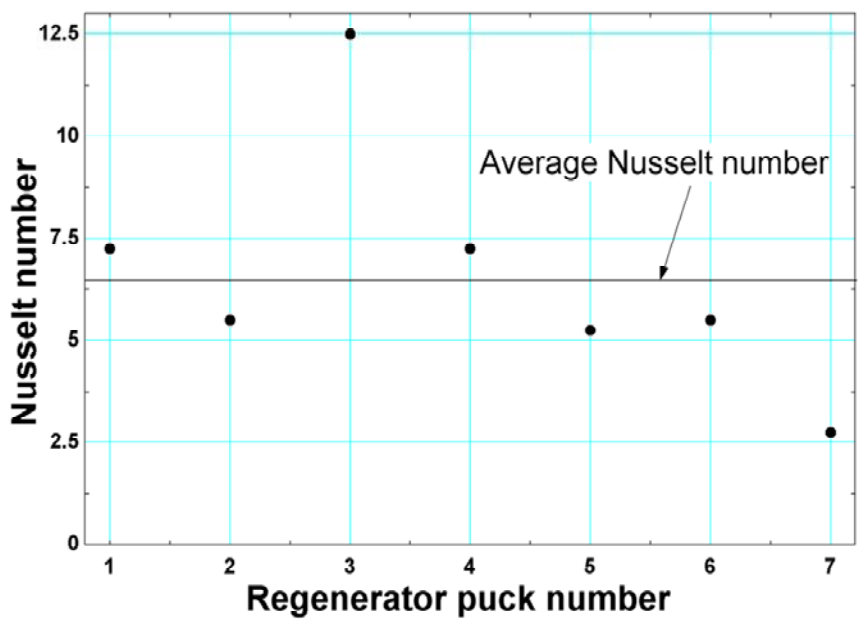

Figure 5.3: Nusselt numbers derived from data using water at 1.0 L/min with Engelbrecht's regenerator.

The repeatability associated with the results obtained on the third regenerator suggests that there is a small uncertainty in the measured Nusselt number. The uncertainty in the average Nusselt number is defined in equation 4.1, re-written here:

$$e_{Nu} = \frac{\sigma}{\sqrt{N-1}}$$

The uncertainty in the average Nusselt number of the first generation regenerator (Figure 5.3) is approximately ±1.1, while the uncertainty in the average Nusselt number of the third generation regenerator is approximately ±0.16.

The second repeatability test was carried out in order to determine the day-to-day repeatability of the regenerator test facility. Ten additional sets of data were taken on a separate day after the test facility being completely shut down and restarted. Figure 5.4 displays the results of the Nusselt number derived from the data taken on both days.

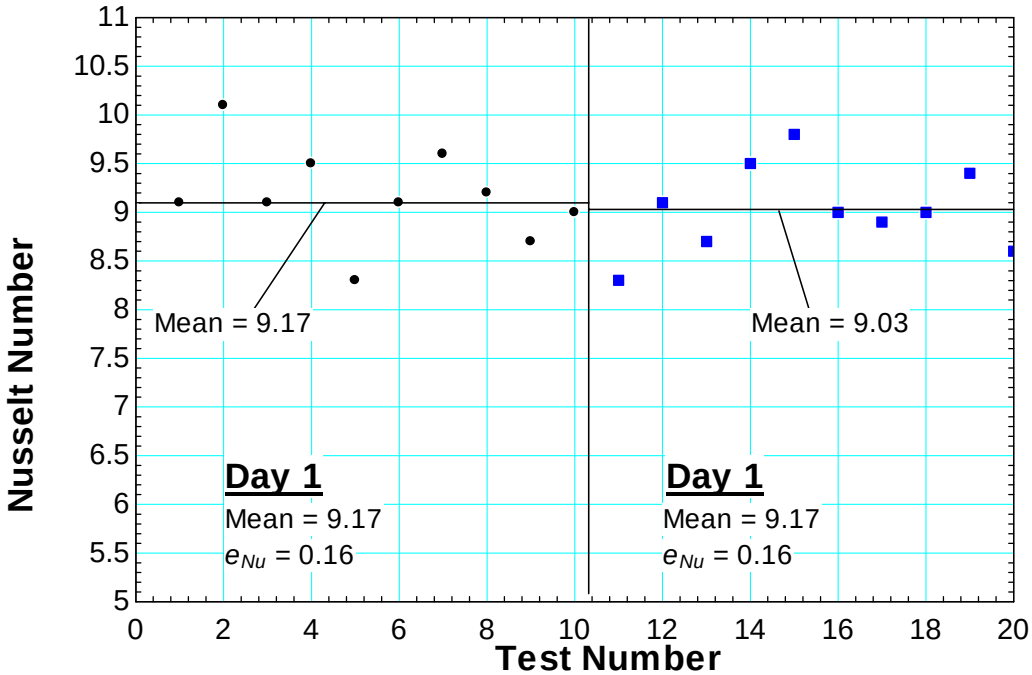

Figure 5.4: Nusselt number derived from 10 sets of data taken on separate days with a flow rate of 0.3 L/min.

The mean of the results taken on day 2 is slightly less than that of the data taken on day 1. However, it is within the uncertainty in the mean Nusselt number. Combining the results of the two repeatability trials shows that the results obtained with the third regenerator are repeatable for any given trial on any given day.

5.3. Nusselt Number Results

Each set of experimental data obtained using the third generation regenerator, as well as the data obtained earlier with the second generation regenerator has been reduced using the DC model developed by Astronautics. For each experimental data point, the average Nusselt number and Reynolds number is calculated using the procedure outlined in Section 3.2.2.

5.3.1 Third Generation Regenerator Results

Figure 5.5 shows the best fit Nusselt number as a function of Reynolds number for the data obtained using the third generation regenerator. The data obtained for pure water, as well as 20%, 30%, and 40% solutions of propylene glycol and water are shown. Each data point obtained from the three separate tests are plotted in order to show the repeatability of the experiment.

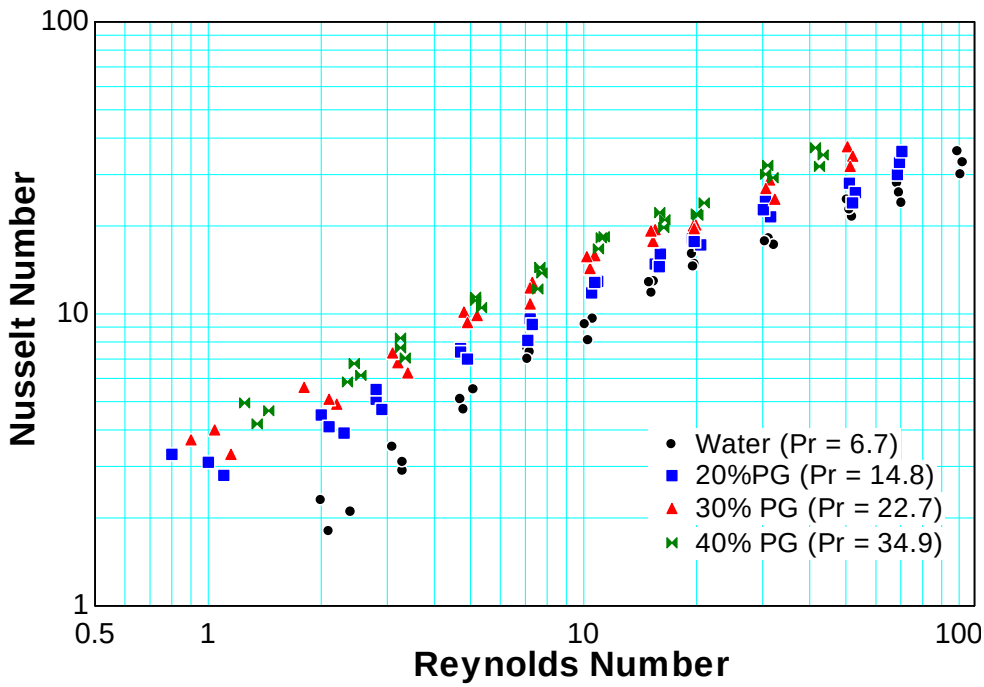

Figure 5.5: Best fit Nusselt number as a function of average Reynolds number for all data sets taken on the third regenerator.

Examination of Figure 5.5 shows that the Nusselt number follows the expected trends. As the Reynolds number and/or the Prandtl number increase, the Nusselt number increases. Figure 5.6 shows the experimental results overlaid onto the correlation developed by Wakao and Kaguei (1982).

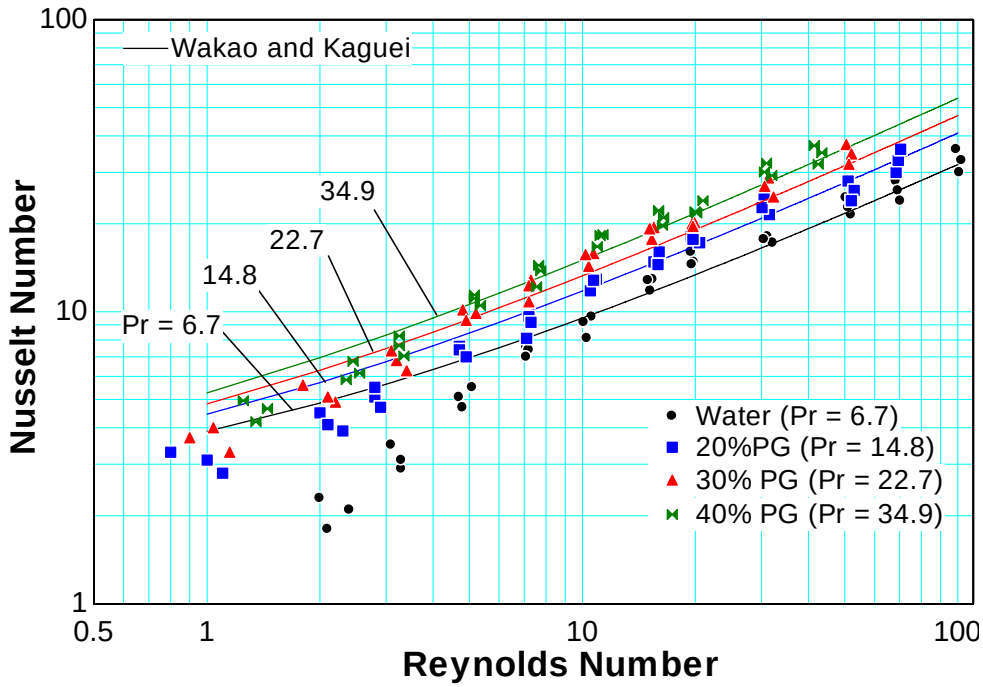

Figure 5.6: Best fit Nusselt numbers along with the Nusselt number predicted by the Wakao and Kaguei correlation.

Figure 5.6 shows that the data matches the correlation at large Reynolds numbers. At lower Reynolds numbers, the data decreases below the predicted value, but this trend decreases with increasing Prandtl number. Additionally, the experimental Nusselt numbers do not drop below the theoretical limit for a sphere in an infinite medium, 2.0, in the same way as the results obtained by reducing the data with the UW model.

Three individual tests performed at each test condition using the third regenerator. In order to determine the best fit Nusselt number for each test condition, the Nusselt, Reynolds, and Prandtl number of the three individual tests are averaged. The uncertainty associated with each of these quantities is the uncertainty in the mean defined previously.

$$e_{Nu} = \frac{\sigma}{\sqrt{N-1}}$$

Each group of experimental data is reduced to a single data point for each Reynolds number and Prandtl number, shown in Figure 5.7.

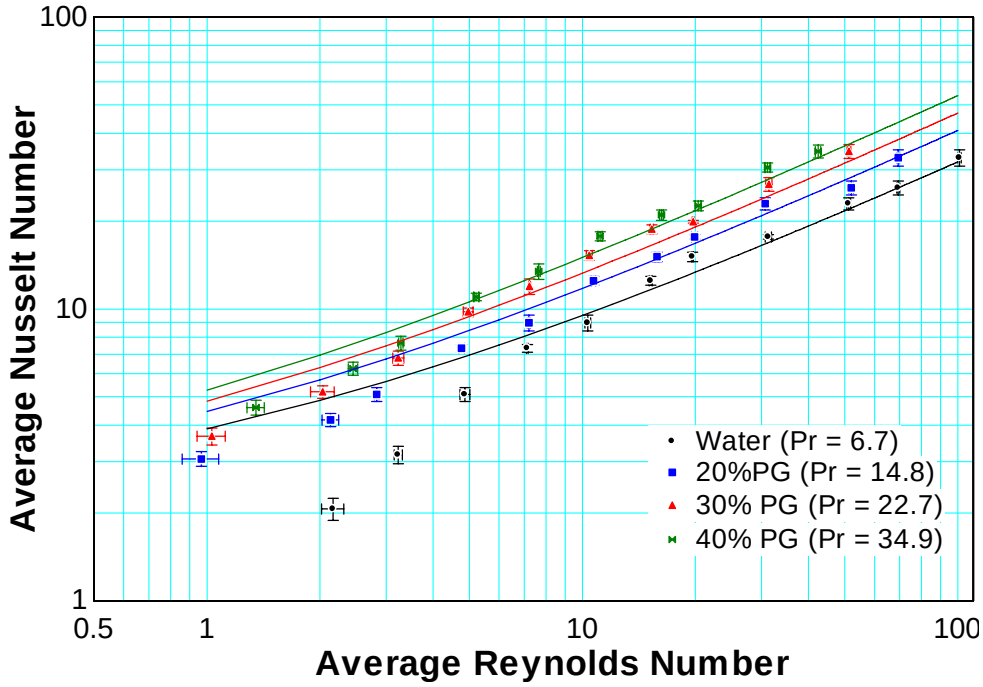

Figure 5.7: Average Nusselt number as a function of average Reynolds number.

In Figure 5.7, the error bars in the *y*-direction represent the uncertainty in the experimentally determined Nusselt number, and the error bars in the *x*-direction represent the error in the average Reynolds number. The small magnitude of the error bars associated with the Reynolds number and Nusselt number once again reinforce the repeatability of this experiment. The results obtained on the third regenerator confirm the Wakao and Kaguei (1982) correlation for the high Reynolds number high Prandtl number tests. Since there was not complete agreement, the data obtained on the second generation regenerator is reduced as well.

5.3.2 Second Generation Regenerator Results

Figure 5.8 shows the best fit Nusselt number as a function of Reynolds number for the data obtained using the second generation regenerator. The data obtained using pure water, as well as 20%, 30%, and 40% solutions of propylene glycol and water are shown.

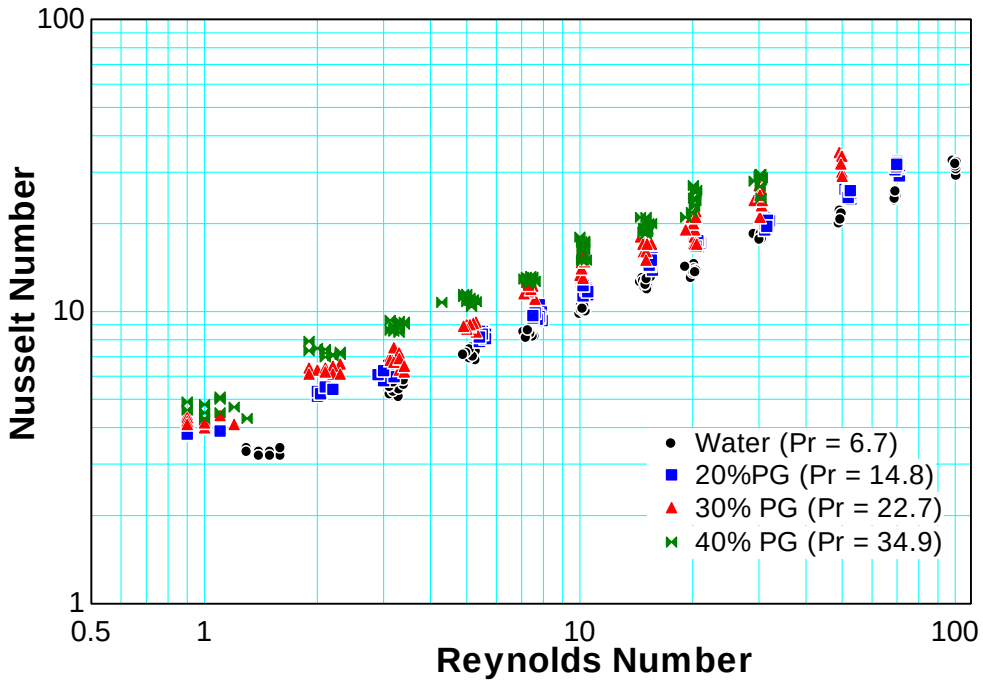

Figure 5.8: Best fit Nusselt number as a function of average Reynolds number for all data sets taken on the third regenerator.

Examination of Figure 5.8 shows that the Nusselt number once again follows the expected trends; the Nusselt number is an increasing function of Reynolds number and Prandtl number. The significant clustering of the data reinforces the repeatability of the second generation experiment, discussed in Chapter 4. The results of the 10 individual sets of data are again averaged to determine the best fit Nusselt number, average Reynolds number, and average Prandtl number at each test condition. The average Nusselt number as a function of

Reynolds number for all the Prandtl numbers tested is shown in Figure 5.9, along with the correlation developed by Wakao and Kageui.

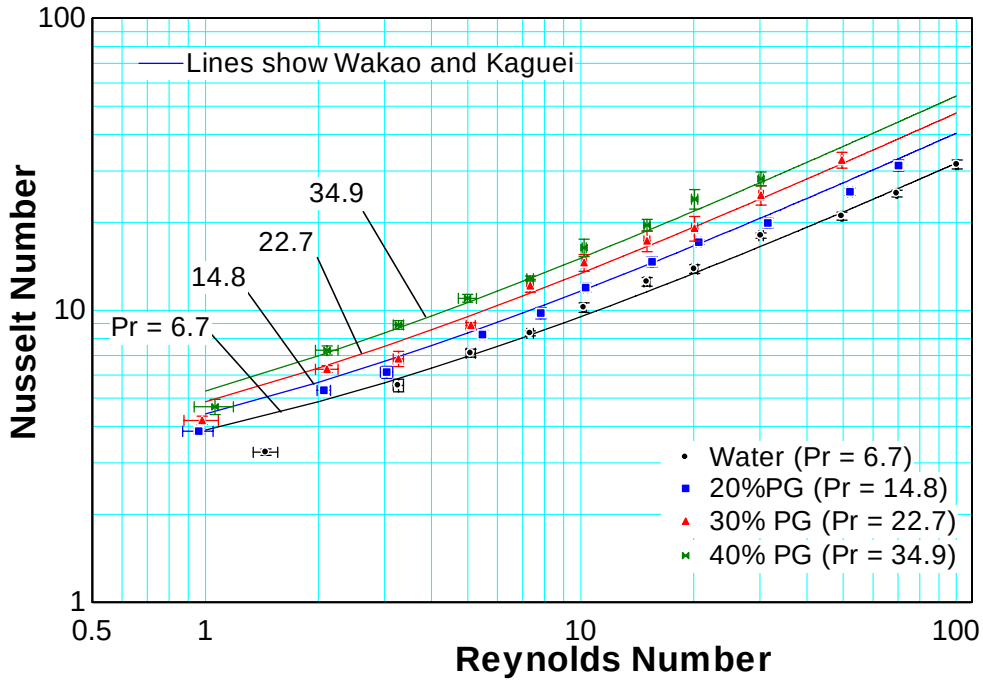

Figure 5.9: Average Nusselt number as a function of average Reynolds number compared with the Wakao and Kaguei correlation.

The error bars in the *y*-direction represent the uncertainty in the measured Nusselt number, and the error bars in the *x*-direction represent the error in the average Reynolds number. The magnitude of the error is once again small due to the repeatability of the experiment. The results seen in Figure 5.9 agree well with the Wakao and Kaguei correlation regardless of Reynolds and Prandtl number. By coupling these results with the results of the third regenerator seen in Figure 5.7, the correlation determined by Wakao and Kaguei proves to be the most accurate correlation for heat transfer in a packed bed of spheres using a liquid heat transfer fluid.

5.4 Friction Factor

Another feature of the test facility is the ability to measure the pressure drop across the regenerator bed. Using the measured pressure drop, it is possible to calculate the friction factor of the flow through the regenerator bed. The friction factor is related to the pressure drop using equation (5.1)

$$f_f = \frac{\Delta P\, d_p}{L\, v_f^2\, \rho_f}\left(\frac{\varepsilon^3}{1-\varepsilon}\right) \tag{5.1}$$

where f_f is the friction factor, ΔP is the measured pressure drop, L is the length of the regenerator, v_f is the superficial fluid velocity calculated from the experimental volumetric flow rate data, ε is the bed porosity, and ρ_f is the fluid density (Kaviany, 1995). The experimental data are compared to the widely used correlation for friction factor through beds of packed smooth spheres developed by Macdonald et al. (1979)

$$f_f = \frac{180(1-\varepsilon)}{Re_d} + 1.8 \tag{5.2}$$

where Re_d is the Reynolds number based on particle diameter and superficial velocity. Several tests are carried out at each flow rate so that several values of the friction factor are obtained for each test condition. Figure 5.10 displays the experimental friction factor determined from each experimental test that was conducted.

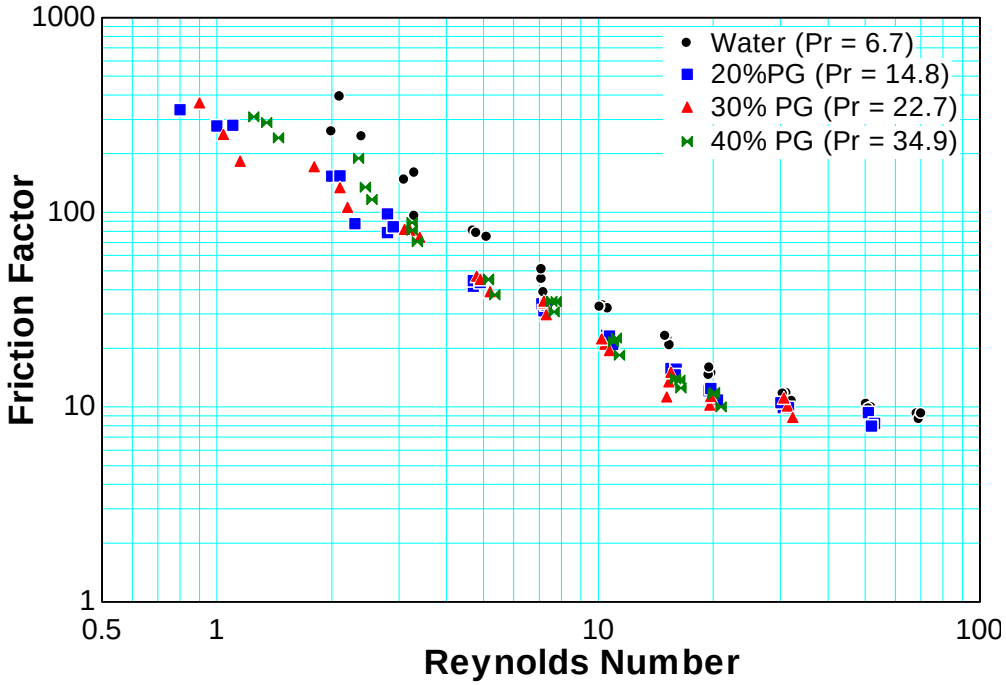

Figure 5.10: Experimental friction factor as a function of Reynolds number for all fluids tested.

In an identical process to averaging the Nusselt number (discussed in Section 4.3), the average friction factor for each test condition is found. Figure 5.11 shows the average friction factor as a function of the average Reynolds number for each test fluid.

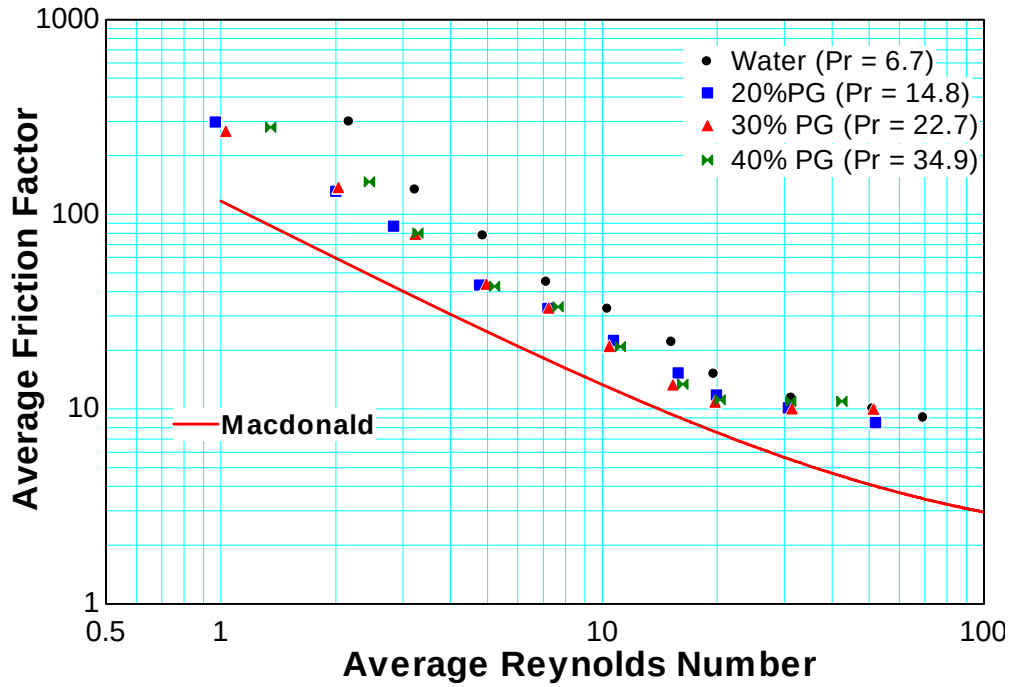

Figure 5.11: Average friction factor as a function of average Reynolds number along with the Macdonal *et al.* correlation.

Examination of Figure 5.8 shows very good agreement between the 20% and 30% propylene glycol and water solutions. The experimental data for water is consistently higher. This is most likely due to the uncertainty in the pressure measurement. As the Prandtl number of the fluid increases, the measured pressure drop across the regenerator also increases, allowing for more accurate measurement. The agreement between the data is expected due to the fact that friction factor is only a function of Reynolds number. However, there is discrepancy between the experimental values and those predicted by the Macdonald correlation. The subsequent sections explore some possible causes of the discrepancy.

5.4.1 Uncertainty in the Friction Factor

Since the friction factor is an experimental quantity, there is an associated uncertainty. The friction factor is calculated using equation (5.1), re-written here.

$$f_f = \frac{\Delta P\, d_p}{L\, v_f^2\, \rho_f}\left(\frac{\varepsilon^3}{1-\varepsilon}\right)$$

Assuming that the fluid properties and nominal particle size are known accurately, there is not uncertainty in the friction factor associated with these quantities. However, the remaining terms in equation (5.1) are measured quantities with some associated uncertainty. The pressure drop is measured using a 0-1 psid pressure transducer with an uncertainty of ±0.0025 psid. The signal output of the pressure transducer is a 4-20 mA current that is converted to a voltage (0 to 5 V) using a shunt resistor with a 250 ohm nominal resistance. This voltage is collected by the data acquisition system (discussed in Section 2.4) which has 14 bit resolution. The uncertainty of the voltage measured by the data acquisition system (*DA*) is then calculated using equation (5.3).

$$\delta DA = \frac{Volt\ Range}{2^{\#bits}} \tag{5.3}$$

Substituting the voltage range (5 V) and the number of bits (14) into equation (5.3) results in an uncertainty in the data acquisition system of ±0.0003 V. This results in an uncertainty in the pressure reading of ±0.00006 psid. The limiting factor for the pressure measurement is the uncertainty of the pressure transducer itself; therefore the uncertainty in the pressure measurement is ±0.0025 psid.

Since the friction factor has a cubic dependence on the porosity, small changes in the porosity of the bed can result in substantial changes in the prediction of the experimental friction factor. The current porosity of the regenerator bed is 0.368. Reducing this value by 20% gives the experimental data significantly improved agreement with the Macdonald *et al.*

correlation, as shown in Figure 5.12. Therefore, it is important to accurately measure the porosity of the regenerator.

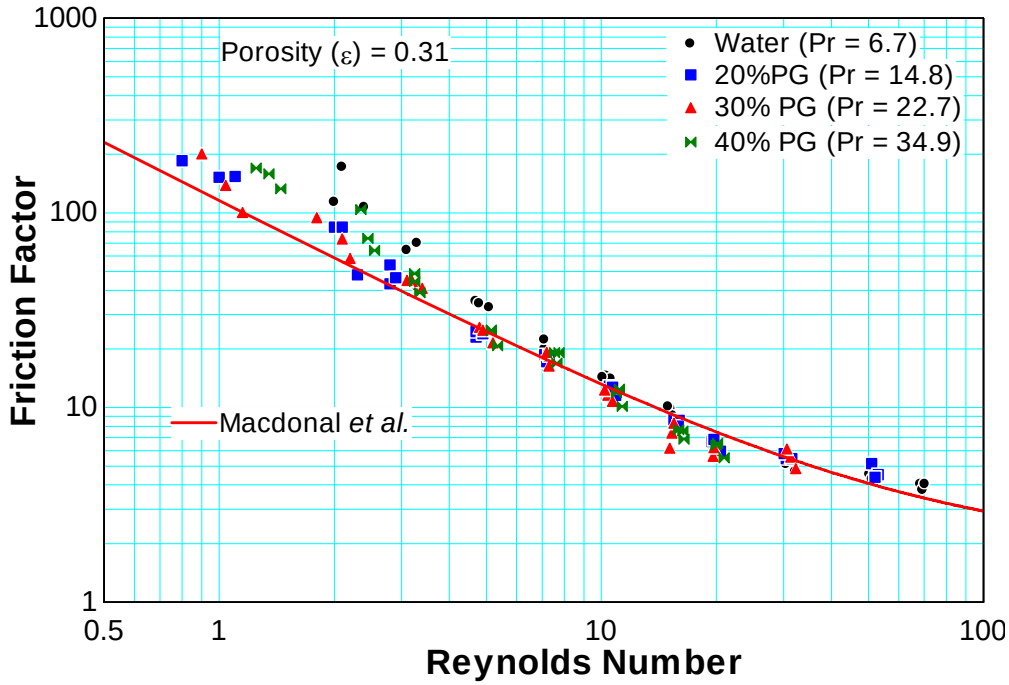

Figure 5.12: Experimental friction factors using a bed porosity of 0.31 instead of the measured value of 0.368.

The porosity of the bed (ε) is the ratio of the void volume (V_V) to the total volume (V_T):

$$\varepsilon = \frac{V_V}{V_T} \tag{5.4}$$

The void and total volume are inferred by measuring the dimensions of the regenerator, and the amount of water required to fill the regenerator with the packing. Due to the headers inside the regenerator, the total void volume must be inferred rather than directly measured. First, the entire regenerator volume is measured using calipers to determine the inner diameter and a ruler to determine the length; these measurements result in a total volume of 575.0 mL. After the regenerator is packed, the length of each header is measured using a

ruler, and the volume of each header is determined; 142.5 mL for the top, and 154.5 mL for the bottom. The header volume is subtracted from the total volume in order to find the starting total volume for the test section, 278.0 mL. Once the regenerator is completed, the remaining volume inside the regenerator is measured to be 398.0 mL by plugging the outlets in the bottom end cap and filling the regenerator with water. By once again subtracting the header volumes, the void volume of the test section is determined (105.0 mL). The bed porosity is then equal to the ratio of the test section void volume (105 mL) to the initial test section total volume (278.0 mL). The porosity of the regenerator is found to be 0.368. The graduated cylinder used to measure the volume of water is readable to the nearest 0.5 mL. The uncertainty in the bed porosity can then be calculated using the uncertainty propagation technique shown in equations (5.5) through (5.7).

$$\delta\varepsilon = \sqrt{\left(\delta\varepsilon_{V_V}\right)^2 + \left(\delta\varepsilon_{V_T}\right)^2} \tag{5.5}$$

$$\delta\varepsilon_{V_V} = \frac{\partial\varepsilon}{\partial V_V}\delta V_V = \frac{1}{V_T}\delta V_V \tag{5.6}$$

$$\delta\varepsilon_{V_T} = \frac{\partial\varepsilon}{\partial V_T}\delta V_T = -\frac{V_V}{V_T^2}\delta V_T \tag{5.7}$$

Substituting in 278.0 mL for V_T, 105.0 mL for V_V, and 0.25 mL for both δV_V and δV_T results in an uncertainty in the porosity of ±0.001. The final measured quantity is the length of the regenerator. This is measured using a ruler that is measured to the nearest 0.5 mm, resulting in an uncertainty in the length of the regenerator of ±0.25 mm.

The friction factor is also dependent on the measured fluid velocity. The fluid velocity is calculated from the measured volumetric rate and the cross sectional area of the regenerator.

In order to improve the agreement between the experimental data and the correlation, the diameter of the regenerator must be decreased by 24%, to 0.0366 m (from the original 0.0482 m). The decrease in diameter results in very good agreement between the experimental values and the correlation as shown in Figure 5.13.

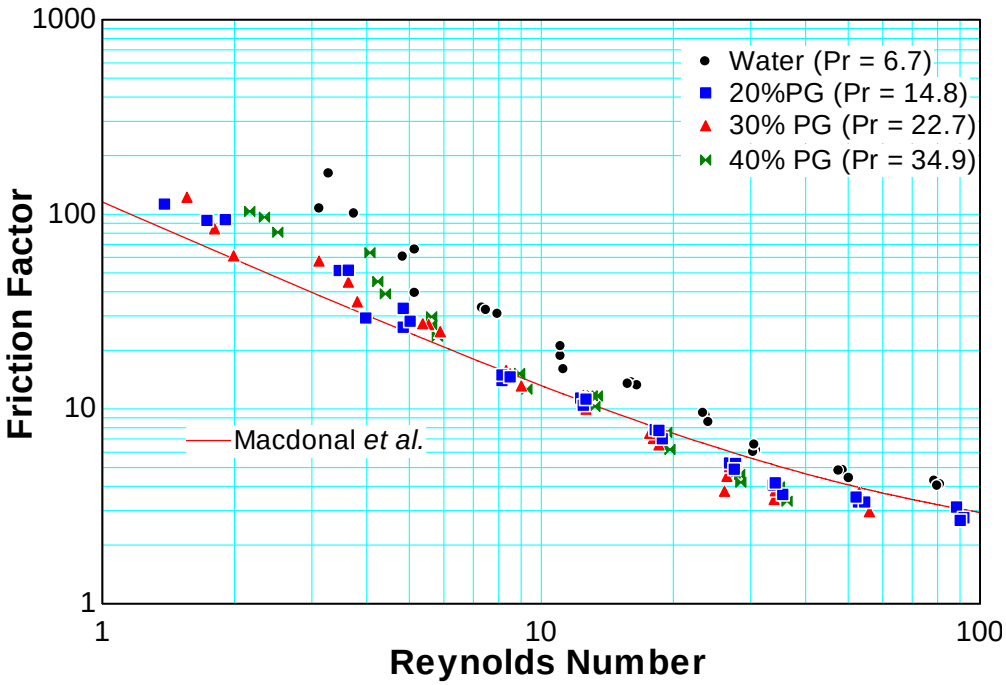

Figure 5.13: Friction factor as a function of Reynolds number after the diameter of the regenerator has been adjusted from 0.0482 m to 0.0366 m (24 % change).

The uncertainty of the superficial velocity is related to the uncertainty in the volumetric flow rate. The volumetric flow meter has an accuracy of ±0.02 L/min. The flow meter has the same 4-20 mA output as the pressure transducer which is converted to a voltage again using a shunt resistor with a 250 ohm nominal resistance. The voltage signal is collected using the same data acquisition system as the pressure transducer signal, which results in a resolution of ±0.0002 L/min. Therefore, the limiting factor for the flow meter is the accuracy of the flow meter itself, ±0.02 L/min. It is possible to calculate the uncertainty in the superficial

fluid velocity (δv_f) using the equations for uncertainty propagation shown in equations (5.8) through (5.10).

$$\delta v_f = \sqrt{\left(\delta v_{f,\dot{V}}\right)^2 + \left(\delta v_{f,A_c}\right)^2} \tag{5.8}$$

$$\delta v_{f,\dot{V}} = \frac{\partial v_f}{\partial \dot{V}} \delta \dot{V} = \frac{1}{A_c} \delta \dot{V} \tag{5.9}$$

$$\delta v_{f,A_c} = \frac{\partial v_f}{\partial A_c} \delta A_c = -\frac{\dot{V}}{A_c^2} \delta A_c \tag{5.10}$$

where $\delta v_{f,\dot{V}}$ is the uncertainty in the velocity associated with volumetric flow rate, $\delta \dot{V}$ is the uncertainty in the volumetric flow rate, $\delta v_{f,A_c}$ is the uncertainty in the velocity associated with the cross sectional area, δA_c is the uncertainty in the cross sectional area, $\dot{V}$ is the volumetric flow rate, and A_c is the cross sectional area of the regenerator. Substituting 0.02 L/min in for the uncertainty in volumetric flow rate (converted to 3.33x10^{-7} m^3/s) and 0.0019 m^2 in for the cross sectional area, and 3.0E-5 m^2 in for the uncertainty in cross sectional area, results in an uncertainty in the velocity measurement of ±0.0002 m/s.

The uncertainty in the friction factor is then calculated using the uncertainty propagation technique, shown in equations (5.11) through (5.15).

$$\delta f_f = \sqrt{\left(\delta f_{f,\Delta P}\right)^2 + \left(\delta f_{f,v_f}\right)^2 + \left(\delta f_{f,\varepsilon}\right)^2 + \left(\delta f_{f,L}\right)^2} \tag{5.11}$$

$$\delta f_{f,\Delta P} = \frac{\partial f_f}{\partial \Delta P} \delta \Delta P = \frac{d_p}{L v_f^2 \rho_f} \left(\frac{\varepsilon^3}{1-\varepsilon} \right) \delta \Delta P \tag{5.12}$$

$$\delta f_{f,v_f} = \frac{\partial f_f}{\partial v_f}\delta v_f = -\frac{\Delta P\, d_p}{L\, v_f^3\, \rho_f}\left(\frac{\varepsilon^3}{1-\varepsilon}\right)\delta v_f \tag{5.13}$$

$$\delta f_{f,L} = \frac{\partial f_f}{\partial L}\delta L = -\frac{\Delta P\, d_p}{L^2\, v_f^2\, \rho_f}\left(\frac{\varepsilon^3}{1-\varepsilon}\right)\delta L \tag{5.14}$$

$$\delta f_{f,\varepsilon} = \frac{\partial f_f}{\partial \varepsilon}\delta \varepsilon = \left[\frac{3\,\Delta P\, d_p\, \varepsilon^2}{L\, v_f^2\, \rho_f\left(1-\varepsilon\right)} + \frac{\Delta P\, d_p\, \varepsilon^3}{L\, v_f^2\, \rho_f\left(1-\varepsilon\right)^2}\right]\delta \varepsilon \tag{5.15}$$

A summary of the values used in this calculation is shown in Table 5.2. Based on the values listed in Table 5.2, the uncertainty in the friction factor associated with the pressure transducer is the most significant. The values shown in Table 5.2 are for a flow rate of 1.0 L/min using water as the working fluid.

Table 5.2: Summary of uncertainty values.

Variable	Description	Value (units)
δf_f	Total uncertainty in the friction factor	0.396
$\delta f_{f,\Delta P}$	Uncertainty in friction factor associate with pressure drop	0.346
$\delta f_{f,v_f}$	Uncertainty in friction factor associate with fluid velocity	0.179
$\delta f_{f,\varepsilon}$	Uncertainty in friction factor associate with porosity	0.073
$\delta f_{f,L}$	Uncertainty in friction factor associate with length	0.013
$\delta \Delta P$	Uncertainty in pressure drop	2.50E-3 (psid)
δv_f	Uncertainty in fluid velocity	2.00E-4 (m/s)
δL	Uncertainty in length	2.50E-4 (m)
$\delta \varepsilon$	Uncertainty in porosity	0.001
ΔP	Pressure drop (@ 1.0 L/min)	407.3 (Pa)
d_p	Particle diameter	0.003 (m)
ε	Bed porosity	0.368
L	Length	0.152 (m)
v_f	Fluid velocity (@ 1.0 L/min)	0.009 (m/s)
ρ_f	Fluid density	997.2 (kg/m^3)

Figure 5.14 shows the friction factor results obtained using water and a 40% propylene glycol and water solution including error bars associated with the uncertainties in friction factor and average Reynolds number. Only the highest and lowest Prandtl number fluid are shown in order to make the error bars more visible.

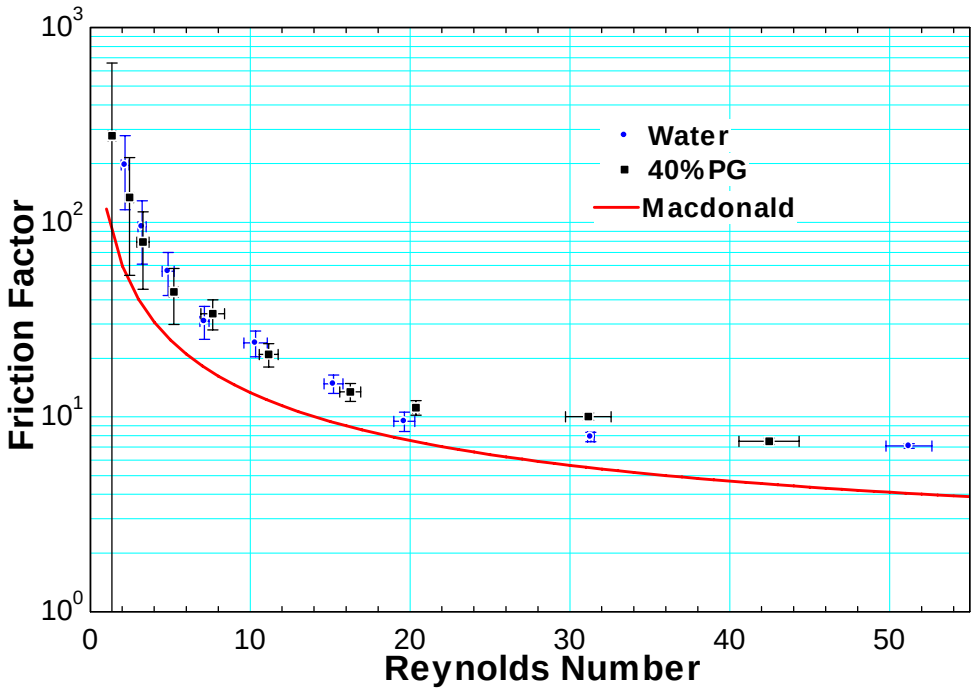

Figure 5.14: Friction factor as a function of average Reynolds number.

The error bars in the *x*-direction represent the error in the average Reynolds number described in Section 5.3.1. The error bars in the *y*-direction represent the uncertainty in the friction factor. The uncertainty in the fiction factor varies with the Reynolds number due to its dependence on fluid velocity and pressure drop. The large uncertainty at low Reynolds number is caused by the accuracy of the pressure transducer. The correlation developed by Macdonald et al. predicts a pressure drop of 0.0008 psi at a Reynolds number of 1. This is lower than the accuracy of the current pressure transducer (±0.0025 psi). The large

uncertainty may account for some of the disagreement between the Macdonald correlation and the experimental data at low flow rates. However, as the Reynolds number increases, the uncertainty in the measurement becomes very small and the discrepancy remains. Therefore, the uncertainty cannot account for the disagreement of the entire data set.

Chapter 6 – Conclusions and Future Work

Two different passive regenerators were built and tested using the passive single-blow test facility at the University of Wisconsin. During this investigation, the main objective was to confirm one of the existing correlations in the literature for the heat transfer inside packed sphere regenerators, or if none could be confirmed, develop a new correlation. Experimental data was obtained using water and three different propylene glycol and water solutions; 20%, 30% and 40% by mass. The experimental data was reduced using two different models; the AMRR model developed by Engelbrecht (2008), and the dispersion concentric model developed by Astronautics Corp. After reducing the experimental data using both of the models, the correlation proposed by Wakao and Kaguei has been found to provide the most accurate prediction of the heat transfer inside a packed sphere regenerator. The experimental friction factor was also measured and compared to the correlation developed by Macdonald (1979). The experimental values are consistently higher than those predicted by the correlation. The uncertainty in the experimental measurement could explain the deviation at low flows but not at higher flow rates.

There are many areas for future work related to this project:

1) Variations to the geometry of the passive regenerator matrix should be tested. This includes non-uniform sphere sizes, loosely packed or sintered beds of spheres, and crushed particles. This can be accomplished by using the current test facility, and fabricating additional regenerators to be put in place of the current ones.

2) Additional tests and calculations should be carried out in order to ensure that the pressure loss related to the inlet and exit plenums and screen plugs are not the underlying cause of the discrepancy in the measured and correlated friction factor.
3) The reason behind the precipitous drop in the predicted Nusselt numbers obtained when reducing the data with the UW AMRR model should be determined. This can be done by adjusting the parameters on the dispersion concentric model to so that it does not include the transient response of the housing and foam lining, or the temperature gradients inside the spheres. The dispersion concentric model can then be used to reduce the experimental data again and try to emulate the results seen when using the UW model.
4) A transient model of the regenerator housing should be implemented into the UW model. While the heat capacity of the housing is minimized during this investigation, it can never be eliminated. As such, in order to maximize the accuracy of the UW model, this effect should be included in both the single-blow and AMRR versions of the model.

References

Baclic, B.S., Heggs, P.J., Ziyan, H.A., 1986, The Differential Fluid Enthalpy Method, *Proc. 8th International Heat Transfer Conf.*, San Francisco, v. 5, p. 2616-1622.

Balakrishnan, A.R., Pei, D.C.T, 1978, Heat Transfer in Gas-Solid Packed Bed Systems, *Ind. Eng. Chem.*, v. 37, p. 30-40.

Brown, G. V., 1976, Magnetic Heat Pumping Near Room Temperature, *Journal of Applied Physics* 47:3673-3680.

Engelbrecht, K., 2005, *A Numerical Model of an Active Magnetic Regenerator Refrigeration System*, M.S. Thesis, University of Wisconsin Madison.

Engelbrecht, K., Nellis, G.F., Klein, S.A., 2007, Recent Developments in Room Temperature Active Magnetic Regenerative Refrigeration, *HVAC&R Research*, vol. 13, n 4:525-542.

Engelbrecht, K., 2008, *A Numerical Model of an Active Magnetic Regenerator Refrigerator with Experimental Validation*, Ph.D. Thesis, University of Wisconsin Madison.

Ergun, S., 1952, Fluid Flow through Packed Column, *Chemical Engineering Progress*, 48(2):125-127.

Heggs, P.J., Burns, D., 1988, Single-Blow Experimental Prediction of Heat Transfer Coefficients, *Exper Therm Fluid Sci*, vol. 1, n 3:243-251.

Giauque, W. F. and D. P. MacDougall, 1933, Attainment of temperatures below 1º absolute by demagnetization of $Gd_2(SO_4)_3$ $8H_2O$, *Phys. Rev.* 43:7768.

Gschneidner, K.A., Pcharsky, V.K., Tsokol, A.O., 2005, Recent Developments in Magnetocaloric Materials, *Rep. Prog. Phys.*, vol. 68:1479-1539.

Jeffreson, C. P., 1972, Prediction of Breakthrough Curves in Packed Beds: I. Applicability of Single Parameter Models, *AIChE Journal*, 18:409-416.

Kaguei, S., Shiozawa, B., Wakao, N., 1977, Dispersion-Concentric Model for Packed Bed Heat Transfer, *Chem. Eng. Sci.*, v. 32, p. 507-513.

Kaviany, M., 1995, *Principles of Heat Transfer in Porous Media*, Springer, New York, NY, p. 33, 46-47, 130, 228-229.

Kitanovski, A., Egolf, P., 2006, Thermodynamics of magnetic refrigeration, *International Journal of Refrigeration*, v. 29, p. 3-21.

Klein, S.A., 2009, *EES – Engineering Equation Solver*, F-Chart Software, www.fchart.com.

Kunii, D., Levenspeil, O., 1969, *Fluidization Engineering*, Wiley, New York, NY, 534.

Locke, G. L., 1950, *Heat Transfer and Flow Friction Characteristics of Porous Solids*, Tech. Report. No. 10, Dept. Mech. Eng., Stanford University.

Macdonald, I.F., El-Sayed, M.S., Mow, K., Dullien, F.A.L., 1979, Flow Through Porous Media – Ergun Equation Revisited, *Ind. Eng. Chem. Fund.*, v. 18, p. 199-208.

Macias-Machin, A., Oufer, L., Wannenmacher, N., 1991, Heat Transfer between an Immersed Wire and a Liquid Fluidized Bed, *Powder Technology*, vol. 66:281-284.

Marconnet, A., 2007, *Predicting Regenerator Performance with a Single-Blow Experiment*, M.S. Thesis, University of Wisconsin Madison.

Rohsenow, W. M., J. P. Hartnett and Y. I. Cho, 1998, *Handbook of Heat Transfer*, McGraw-Hill, New York, NY.

Rowe, A., Tura, A., 2007, Active Magnetic Regenerator Performance Enhancement Using Passive Magnetic Materials, *2nd International Conference on Magnetic Refrigeration at Room Temperature*, Portoroz, Slovenia.

Taylor, R.P., 2009, Personal correspondence regarding flow maldistribution simulation using FLUENT.

Wakao, N., Kaguei, S., 1982, *Heat and Mass Transfer in Packed Beds*, Gordon and Breach Science Publishers, New York, NY, 364.

Wen, D., Cong, T. N., He, Y., Chen, H., Ding, Y., 2007, Heat transfer of gas-solid two-phase mixtures flowing through a packed bed. *Chem. Eng. Sci.*, v. 62, 4241-4249

Zimm, C., Boeder, A., Chell, J., Sternberg, A., Fujita, A., Fujieda, S., Fukamichi, K., 2006, Design and Performance of a Permanent Magnet Rotary Refrigerator, *International Journal of Refrigeration*, vol. 29, 8:1302-1306.

Appendix A

UW Single-Blow Front End Script

```
%%%
```

```
[Ntime,
Ncol,t_exp,mdot_exp,Tin_exp,Tout_exp,dtimebreak_exp,T_start,T_inlet,t_fina
l,TBL,TBH,Tbreak_exp,tbreak_exp,nBL_exp,nBH_exp]=detopcondmultBT_SmallRege
n(datafile,BT);

figure(1)
plot(t_exp,T_inlet,t_exp,Tout_exp)

eps=0.3604; %porosity of the regenerator
dp = 0.00396875; %m particle diameter
D = 0.05681; %0.0635 outer diameter of pipe, 0.0602 inner diameter of
pipe, 0.05681 inner dia of foam; %m, regenerator diameter
L = 0.2794; %m length of regenerator (packed section)
ar = L/D; %aspect ratio of the regenerator -> L/D
bed_vol =pi*(D/2)^2*L; %volume per bed
nbed = 1; %number of beds lump all seven pucks into one bed
Volume = nbed*bed_vol*1000; %L, total volume of the regenerator material
Ac=pi/4*D.^2; %m2, cross sectional area of the regenerator

%%parameters for the void volume
Total_Void_volume = 0.000271681; %m^3 volume of void space in the
regenerator not including the inlet and outlet gap

%% Model parameters

%scaling factors

cff = 1;    %friction factor scaling factor
cnk = 1;    %axial conduction scaling factor
cdp = 1;    %dispersion scaling factor
%Qloss = 1.422; %W,Heat loss to the surroundings through housing
Qloss = 0;

Nx=70; %number of spatial steps
Nt=2000; %number of time steps for the model
%        Nt=400; %number of time steps for the model
fluidfun=@props_water; %the fluid is a 10% ethylene glycol and water
mixture
fluid = '_water'; %used for file name, place underscore before the name
bedcorrfun=@SphPart_SB_1par; %regenerator correlation function
magpropfun=@SS304nonconst;%@SS304nonconst;
mcmfun={@SS304nonconst}; % {@SS304nonconst}; %magnetocaloric material
property function - need to use {} brackets
mcm_inp=[300, 1]; %inputs for bed composition [Curie temp, fraction of
bed], this can be used to model a multiple material regenerator
numlayer=1; %number of layers in the regenerator bed
magmat = 'SS304nonconst'; % 'ss304nonconst';

modelcheck=1; %plot results of the regenerator function

TC = T_start; % TC=285; %K - see above this temperature is averaged from
the first few
```

```
%% determine mass flow profile
ii=1:Nx;
jj=0:Nt;
t_final=tbreak_exp(length(tbreak_exp))+20;
t_node=(jj(1:Nt)'+0.5)/Nt*t_final; %time grid at center of time step
xr=L*(ii'-1/2)/Nx; %regenerator spatial grid

%% determine characteristic fluid length
[muf,kf,cf,rhof,hf,sf]=fluidfun(T_inlet(1));
dt=t_node(2)-t_node(1);
CFL=median(mdot_exp)*dt*Nx/(60000*Ac*L);

mdot=interp1(t_exp,mdot_exp,t_node); %mass flow rate read in from files
(Liter/min)
TH=interp1(t_exp,Tin_exp,t_node); % the hot temp (inlet) is read in from
the file
TH_plot = TH;
[muf,kf,cf,rhof,hf,sf]=fluidfun(TC); %evaluate fluid properties at the
cold reservoir temperature
mdot=mdot*rhof/(1000*60); %convert Liter/min to kg/s
[mdot_filtered]=mdotfilter(mdot); %function that removes numerical
outliers from the measured mass flow rate
t_transport=Total_Void_volume/(mean(mdot_exp)/rhof); %seconds, determines
time for a slug of fluid to travel from the regenerator inlet to the exit
%T_meas_breakthrough=interp1(t_exp,T_meas_exp,t_node); %measured
temperature at end of regenerator
muoH=zeros(Nx,Nt+2);

%%%%%%%%%%%%%%%%%%%%%%%%%%%%%%%%%%%%%%%%%%%%%%%%%%%%%%%%%%%%%%%%%%%%%%%%%%%%
%% Call the AMR bed model - using the two Nusselt correlation coefficients
%%%%%%%%%%%%%%%%%%%%%%%%%%%%%%%%%%%%%%%%%%%%%%%%%%%%%%%%%%%%%%%%%%%%%%%%%%%%

[Na] = length(Nu_guess);

for i=1:Na

    Nu=Nu_guess(i);
    fprintf('\n Nusselt guess = %.3f \n',Nu) %display Nusselt correlation
parameters
    pacRAW=[eps, 0, dp, 0]; %[eps, dummy, dp, dummy] for packed sphere
regenerator

[Tr,Tf,TCedg,t_node,mdot,xf,deltaP,Ref,Prf,Ref_Dp]=SingleBlowregen_3_8_2(L
,Ac,t_final,TC,TH,Qloss,Nx,Nt,pacRAW,mcmfun,mcm_inp,numlayer,fluidfun,bedc
orrfun,modelcheck,mdot_filtered,muoH,Nu,cnk,cff,cdp);

    %%%%%%%%%%%%%%%%%%%%%%%%%%%%%%%%%%%%%%%%%%%%%%%%%%%%%%%%%%%%%%%%%%%%%%%%%
    %% Find 20% and 80% breakthrough times from the predicted regenerator
    %% outlet temperature profile.
    %%%%%%%%%%%%%%%%%%%%%%%%%%%%%%%%%%%%%%%%%%%%%%%%%%%%%%%%%%%%%%%%%%%%%%%%%

    foundBL = 0;
    foundBH = 0;
    n=0;
```

```
    timeBL=0;
    timeBH=0;
    nBL=0;
    nBH=0;

    while foundBL==0
        n=n+1;
        if TCedg(n)>=TBL
            timeBL = t_node(n)
            nBL = n;
            foundBL = 1;
        end
    end
    while foundBH==0
        n=n+1;
        if TCedg(n)>=TBH
            timeBH = t_node(n)
            nBH = n;
            foundBH = 1;
        elseif n==Nt
            timeBH = t_node(n)
            nBH = n;
            foundBH = 1;
            fprintf('did not find actual breakthrough\r')
        end
    end
    Tbreak=TCedg(nBL:nBH); %predicted 20% to 80% breakthrough temperatures
    t2080=t_node(nBL:nBH); %time of predicted 20% to 80% breakthrough
temperatures
    dtimebreak=timeBH-timeBL; %predicted time between 20% and 80%
breakthrough times
    deltatime(i)=dtimebreak-dtimebreak_exp; %difference in time between
predicted breakthrough time and experimental breakthrough time

    %%%%%%%%%%%%%%%%%%%%%%%%%%%%%%%%%%%%%%%%%%%%%%%%%%%%%%%%%%%%%%%%%%%%%%%%%%%%
    %% Interpolate predicted data to determine the predicted temperature
    %% at same points in time as the experimental fluid temperature in
order to
    %% calculate the RSS error value.
    %%%%%%%%%%%%%%%%%%%%%%%%%%%%%%%%%%%%%%%%%%%%%%%%%%%%%%%%%%%%%%%%%%%%%%%%%%%%

    toff=timeBL-tbreak_exp(1) %offset in time between the experimental and
predicted values for the 20% breakthrough time
    t_node=t_node-toff;
    tbreak_exp(1);
    Tbreak=interp1(t_node,TCedg,tbreak_exp,'cubic');

    %%%%%%%%%%%%%%%%%%%%%%%%%%%%%%%%%%%%%%%%%%%%%%%%%%%%%%%%%%%%%%%%%%%%%%%%%%%%
    %% calculates the RSS error value between the predicted and
experimental
    %% exiting fluid temperature between the experimental 20% and 80%
    %% breakthrough times.
    %%%%%%%%%%%%%%%%%%%%%%%%%%%%%%%%%%%%%%%%%%%%%%%%%%%%%%%%%%%%%%%%%%%%%%%%%%%%
```

```
    RSS_SB(i) = sqrt(sum((Tbreak_exp-Tbreak).^2)/(nBH_exp-nBL_exp))
%calculates the RSS error value between the predicted and experimental
exiting fluid

end

%    done = 1;
% end

%%%
```

```
dlmwrite(outputfile,writedat1,'-append','delimiter','\t','precision', 6)
fid=fopen(outputfile,'a');
fprintf(fid,'Time difference between 20 percent and 80 percent
breakthrough for model and experiment \n');
fclose(fid);
dlmwrite(outputfile,writedat2,'-append','delimiter','\t','precision', 6)
dlmwrite(outputfile,best,'-append','delimiter','\t','precision', 6)

%dlmwrite('output\exitTemp.dat',TCedg','delimiter','\t','precision',6)

fclose('all');
% r='Finsihed';

% end

%%%
```

```
end
```

UW Single Blow Model

```
%% This function is based on the cyclical AMR regenerator model.  The
%% function has been modified to analyze a transient, single-blow
%% regenerator.  This function takes
%% inputs that define the system and forcing functions, such as mass flow
%% profile, and calculates the regenerator performance.  This model does
%% not account for heat exchangers.  The main outputs of the model are the
%% temperatures profiles of the fluid and solid during transient
operation.
%%
%% 3_7_1 starts from the amr model version 3_7 and adds functionality
%% needed for the single-blow test facility analysis at UW.
%% 3_7_2 added a calculation for Reynolds number based on particle
diameter
%% 3_8_3 starts with 3_7_2 and adds a term to account for heat loss to the
%% surroundings
%% 3_8_5 adds a term that accounts for conduction at the cold and hot ends
%% of the regnerator bed

function[Tr,Tf,TCedg,t_node,mdot,xf,deltaP,Ref,Prf,Ref_Dp,Qloss,PDrop,PDro
p_Mac]=SingleBlowregen_3_8_5(L,Ac,t_final,TC,TH,Rloss,Tsur,Nx,Nt,pacRAW,mc
mfun,mcm_inp,numlayer,fluidfun,bedcorrfun,modelcheck,mdot,muoH,cNu,cnk,cff
,cdp);
%        [Tr_bed,Tf_bed,mdot_bed,muoH_bed,t_bed,xr_bed,Nu_avg_bed,
Re_dp_bed,
deltaP_bed]=SingleBlowregen_3_6_1_augment_ratio(L,Ac,t_final,TC,overallT(:
,gap+pucks),Nx,Nt,pacRAW,magpropfun,mcmfun,fluidfun,bedcorrfun,modelcheck,
mdot,muoH,cNu,cnk,cff,cdp,augment_ratio(pucks));

%%Bed paramters

tic %start timer to determine clock time needed to achieve convergence

t_final
TC
[dh,eps,as]=pack_geom(pacRAW,bedcorrfun);
n_motor=.9; %electric motor efficiency
n_pump=.7; %pump efficiency
imp=1; %1=run implicit to generate guess values, 0=don't run implicit
%tau=1000; %set to an arbitrarily large number

%%Conditions
% cnk=1; %axial conduction scaling factor
% cff=1; %friction factor scaling factor
% cNu=1; %Nusselt number scaling factor
% layer=0; %0 not layered 1=layered

dt=t_final/Nt; %time step in s
```

```
%% Allocate the sparse matrices A and B.
N=2*Nx;
A=spalloc(N,N,8*N);
B=spalloc(N,1,N);
%%

i=1:Nx;
xf=L*(i'-1/2)/Nx; %fluid spatial grid
xr=xf; %regenerator spatial grid
j=0:Nt;
t=j'*t_final/(Nt);
t_node=(j(1:Nt)'+0.5)/Nt*t_final; %time grid at center of time step
dt=t(2)-t(1);
TCurie=292*ones(Nx,1);
dx=xr(2)-xr(1);

Tr(:,1)=TC*ones(size(xf)); %initial regenerator temp
Tf(:,1)=TC*ones(size(xf));  %initial fluid temp

%% inputs for new mcmprops

magpropfun=@mcmprops;
% numlayer=1; %number of layers in the regenerator
% mcm_inp=[294, 1];
% mcmfun={@Gdcom}; %property function used for each layer.  This array
must use the curly brackets {} to stay compatible with other matlab
versions

%calculate energy difference between fluid at TH and TC.  These properties
%are also used to calculated heat flux at the hot and cold reservoirs.
[mufC,kfC,cfC,rhofC,hfC,sfC]=fluidfun(TC);
[mufH,kfH,cfH,rhofH,hfH,sfH]=fluidfun(TH);
deltaUf=hfH-hfC;

% initialize variables before beginning the main loop.  These variables
are
% used to check for co
done=0;
j=0;
pacCOOKED=[pacRAW,as,eps,dh,cNu,cff,cnk,cdp];
%    pacCOOKED=[pacRAW,epsX,epsY,as,eps,dh,FAR,PAR,cNu(1),cff,cnk,cdp];
%regenerator parameters that are generalized in terms of hydraulic
diameter, etc.


% ref_load=[-500 -500];
% Er=[0 0]; %this matrix stores the total energy in the fluid for this
past two cycles
% Ef=[0 0];%this matrix stores the total energy in the solid material for
this past two cycles
% Etot=[0 0];%this matrix stores the total energy in the fluid and solid
for this past two cycles
% count=0;
% count2=0;
```

```
% iteration(1)=1;
% deltaE=zeros(extrapnum,1);

while(done==0)
    j=j+1;
    time=t(j);
    [muf(:,j),kf(:,j),cf(:,j),rhof,hf(:,j),sf(:,j)]=fluidfun(Tf(:,j));
    v=-mdot/(Ac*rhof);
    Prf(:,j)=cf(:,j).*muf(:,j)./(kf(:,j)); %Prandtl number
    Ref(:,j)=4*abs(v(j))*rhof./(as*muf(:,j)); %Reynolds number based on
hydraulic diameter
    Ref_Dp(:,j)=(rhof*abs(v(j))*pacRAW(3))./muf(:,j); %Reynolds number
based on particle diameter

[cmuoH(:,j),dsdmuoH(:,j),rhor,kr(:,j),sr(:,j),hr(:,j)]=magpropfun(xr,L,Tr(
:,j),muoH(:,j),numlayer,mcm_inp,mcmfun);
    cf_av=mean(mean(cf)); %average fluid specific heat over the entire
cycle
    muf_av=mean(mean(muf)); %average fluid viscosity over the entire cycle
    cmuoH_av=mean(mean(cmuoH)); %average solid specific heat over the
entire cycle


[Nuf(:,j),ff(:,j),kstat(:,j),kdisp(:,j),f_Mac(:,j)]=bedcorrfun(pacCOOKED,R
ef(:,j),Prf(:,j),kf(:,j), kr(:,j),v,muf(:,j),rhof,cf(:,j));
    %Nuf=0*Nuf+1;
    dP(:,j)=ff(:,j).*(Ref(:,j)).^2*2/dh^3.*(muf(:,j)/rhof).^2*rhof*L/Nx;
%Pressure drop in Pa, based on hydraulic diameter


dP_Mac(:,j)=f_Mac(:,j).*(Ref(:,j)).^2*2/dh^3.*(muf(:,j)/rhof).^2*rhof*L/Nx
; %Pressure drop in Pa, based on hydraulic diameter,Macdonald friction
factor
    PDrop_Mac=sum(dP_Mac);
    PDrop=sum(dP);

    %% Fill the A and B matrices according to the system governing
    %% equations.  A and B are used to solve for the temperature of every
    %% node in the regenerator at each time step in the cycle.

    %     if(mdot(j)>=0)

    %% fluid flow is always assumed to enter at the x=0 end of the
regenerator

    % fluid energy equations
    for i=2:Nx-1;
        h(i,j)=Nuf(i,j).*kf(i,j)/dh; %convection coefficient in node i,j

A(i,i)=eps*rhof*Ac*L/Nx*cf(i,j)/dt+h(i,j)*as*Ac*L/Nx+2*kdisp(i,j)*Ac*Nx/L;
%energy balance for center node
        A(i,i-1)=-kdisp(i,j)*Ac*Nx/L-mdot(j)*cf(i,j)/2; %energy balance
for left node
```

```
        A(i,i+1)=-kdisp(i,j)*Ac*Nx/L+mdot(j)*cf(i,j)/2; %energy balance
for right node
        A(i,Nx+i)=-h(i,j)*as*Ac*L/Nx; %energy balance for regenerator

B(i)=Tf(i,j)*eps*rhof*Ac*L/Nx*cf(i,j)/dt+dP(i,j)*abs(mdot(j))/rhof; %right
hand side of energy balance
    end
    i=1; %hot end
    h(i,j)=Nuf(i,j).*kf(i,j)/dh;

A(i,i)=eps*rhof*Ac*L/Nx*cf(i,j)/dt+cf(i,j)*mdot(j)/2+h(i,j)*as*Ac*L/Nx+1*k
disp(i,j)*Ac*Nx/L;
    A(i,i+1)=-kdisp(i,j)*Ac*Nx/L+mdot(j)*cf(i,j)/2;
    A(i,Nx+i)=-h(i,j)*as*Ac*L/Nx;

B(i)=Tf(i,j)*eps*rhof*Ac*L/Nx*cf(i,j)/dt+dP(i,j)*abs(mdot(j))/rhof+TH(j)*c
f(i,j)*mdot(j);
    i=Nx; %cold end
    h(i,j)=Nuf(i,j).*kf(i,j)/dh;

A(i,i)=eps*rhof*Ac*L/Nx*cf(i,j)/dt+cf(i,j)*mdot(j)+h(i,j)*as*Ac*L/Nx+1*kdi
sp(i,j)*Ac*Nx/L;
    A(i,i-1)=-kdisp(i,j)*Ac*Nx/L-mdot(j)*cf(i,j);
    A(i,Nx+i)=-h(i,j)*as*Ac*L/Nx;
    B(i)=Tf(i,j)*eps*rhof*Ac*L/Nx*cf(i,j)/dt+dP(i,j)*abs(mdot(j))/rhof;

    %     else
    %         if(mdot(j)<0)
    %             %cold-to-hot flow
    %             % fluid energy equations
    %             for i=2:Nx-1;
    %                 h(i,j)=Nuf(i,j).*kf(i,j)/dh; %convection coefficient
in node i,j
    %
A(i,i)=eps*rhof*Ac*L/Nx*cf(i,j)/dt+h(i,j)*as*Ac*L/Nx+2*kdisp(i,j)*Ac*Nx/L;
%energy balance for center node
    %                 A(i,i-1)=-kdisp(i,j)*Ac*Nx/L-mdot(j)*cf(i,j)/2;
%energy balance for right node
    %                 A(i,i+1)=-kdisp(i,j)*Ac*Nx/L+mdot(j)*cf(i,j)/2;
%energy balance for right node
    %                 A(i,Nx+i)=-h(i,j)*as*Ac*L/Nx; %energy balance for
regenerator
    %
B(i)=Tf(i,j)*eps*rhof*Ac*L/Nx*cf(i,j)/dt+dP(i,j)*abs(mdot(j))/rhof; %right
hand side of energy balance
    %             end
    %             i=1; %hot end
    %             h(i,j)=Nuf(i,j).*kf(i,j)/dh;
    %             A(i,i)=eps*rhof*Ac*L/Nx*cf(i,j)/dt-
cf(i,j)*mdot(j)+h(i,j)*as*Ac*L/Nx+1*kdisp(i,j)*Ac*Nx/L;
    %             A(i,i+1)=-kdisp(i,j)*Ac*Nx/L+mdot(j)*cf(i,j);
    %             A(i,Nx+i)=-h(i,j)*as*Ac*L/Nx;
    %
B(i)=Tf(i,j)*eps*rhof*Ac*L/Nx*cf(i,j)/dt+dP(i,j)*abs(mdot(j))/rhof;
    %             i=Nx; %cold end
```

```
    %             h(i,j)=Nuf(i,j).*kf(i,j)/dh;
    %             A(i,i)=eps*rhof*Ac*L/Nx*cf(i,j)/dt-
cf(i,j)*mdot(j)/2+h(i,j)*as*Ac*L/Nx+1*kdisp(i,j)*Ac*Nx/L;
    %             A(i,i-1)=-kdisp(i,j)*Ac*Nx/L-mdot(j)*cf(i,j)/2;
    %             A(i,Nx+i)=-h(i,j)*as*Ac*L/Nx;
    %
B(i)=Tf(i,j)*eps*rhof*Ac*L/Nx*cf(i,j)/dt+dP(i,j)*abs(mdot(j))/rhof-
TC*mdot(j)*cf(i,j);
    %
    %         else
    %             %no flow
    %
    %         end
    % end

    for i=2:Nx-1
        % regenerator energy equations
        A(Nx+i,Nx+i)=Ac*L/Nx*(1-
eps)*rhor(i)*cmuoH(i,j)/dt+h(i,j)*as*Ac*L/Nx+2*kstat(i,j)*Ac*Nx/L; %energy
equation for center node
        A(Nx+i,Nx+i-1)=-kstat(i,j)*Ac*Nx/L; %energy equation for left node
        A(Nx+i,Nx+i+1)=-kstat(i,j)*Ac*Nx/L; %energy equation for right
node
        A(Nx+i,i)=-h(i,j)*as*Ac*L/Nx; %energy equation for fluid
        Qloss(i,j) = (Tr(i,j)-Tsur)/(L/dx*Rloss);
        B(Nx+i)=Ac*L/Nx*(1-eps)*rhor(i)*cmuoH(i,j)*Tr(i,j)/dt-Ac*L/Nx*(1-
eps)*rhor(i)*Tr(i,j)*dsdmuoH(i,j)*(muoH(i,j+1)-muoH(i,j))/dt - Qloss(i,j);
%right hand side of energy equation
    end
    i=1; %hot end
    A(Nx+i,Nx+i)=Ac*L/Nx*(1-
eps)*rhor(i)*cmuoH(i,j)/dt+h(i,j)*as*Ac*L/Nx+kstat(i,j)*Ac*Nx/L+kstat(i,j)
*Ac*Nx/L;
    A(Nx+i,Nx+i+1)=-kstat(i,j)*Ac*Nx/L;
    A(Nx+i,i)=-h(i,j)*as*Ac*L/Nx;
    Qloss(i,j) = (Tr(i,j)-Tsur)/(L/dx*Rloss);
    B(Nx+i)=Ac*L/Nx*(1-eps)*rhor(i)*cmuoH(i,j)*Tr(i,j)/dt-Ac*L/Nx*(1-
eps)*rhor(i)*Tr(i,j)*dsdmuoH(i,j)*(muoH(i,j+1)-muoH(i,j))/dt -
Qloss(i,j)+kstat(i,j)*Ac*Nx/L*Tf(i,j);
    i=Nx; %cold end
    A(Nx+i,Nx+i)=Ac*L/Nx*(1-
eps)*rhor(i)*cmuoH(i,j)/dt+h(i,j)*as*Ac*L/Nx+kstat(i,j)*Ac*Nx/L+kstat(i,j)
*Ac*Nx/L;
    A(Nx+i,Nx+i-1)=-kstat(i,j)*Ac*Nx/L;
    A(Nx+i,i)=-h(i,j)*as*Ac*L/Nx;
    Qloss(i,j)=(Tr(i,j)-Tsur)/(L/dx*Rloss);
    B(Nx+i)=Ac*L/Nx*(1-eps)*rhor(i)*cmuoH(i,j)*Tr(i,j)/dt-Ac*L/Nx*(1-
eps)*rhor(i)*Tr(i,j)*dsdmuoH(i,j)*(muoH(i,j+1)-muoH(i,j))/dt -
Qloss(i,j)+kstat(i,j)*Ac*Nx/L*Tf(i,j);

    %%invert matrix A to calculate the temperature of the fluid and solid
    %%for the current time step then pull fluid and regenerator
    %%temperatures from the resulting X matrix.
```

```
    X=A\B; %the matrix X contains the fluid temp in rows 1 to Nx, and
regenerator temp in rows Nx + 1 to 2Nx

    %% extract the fluid and solid temps from the sparse matrix X using
the
    %% matlab command 'full'

    i=1:Nx;
    Tf(:,j+1)=full(X(i));
    i=1:Nx;
    Tr(:,j+1)=full(X(Nx+i));

    if j==Nt %end of flow period
        %% calculate properties for Nt+1 time step
        j=Nt+1;
        [muf(:,j),kf(:,j),cf(:,j),rhof,hf(:,j),sf(:,j)]=fluidfun(Tf(:,j));
        Prf(:,j)=cf(:,j).*muf(:,j)./(kf(:,j)); %Prandtl number

[cmuoH(:,j),dsdmuoH(:,j),rhor,kr(:,j),sr(:,j),hr(:,j)]=magpropfun(xr,L,Tr(
:,j),muoH(:,j),numlayer,mcm_inp,mcmfun);

        %calculate temperature of fluid exiting the regenerator
        TCedg=0.5*(1.5*Tf(Nx,1:Nt)-0.5*Tf(Nx-
1,1:Nt))+0.5*(1.5*Tf(Nx,2:Nt+1)-0.5*Tf(Nx-1,2:Nt+1)); %Fluid temperature
at the cold edge of the bed.  This temp is extrapolated from the last two
nodes in the bed
        [mufCedg,kfCedg,cfCedg,rhof,hfCedg,sfCedg]=fluidfun(TCedg); %Use
the fluid temp at the cold end of the bed to determine fluid properties at
the cold end of the bed.

        %calculate pressure drop in the regenerator and pump work
        for j=1:Nt
            dWpump(:,j)=abs(mdot(j)/rhof*dP(:,j)); %W
            deltaP(j)=sum(dP(:,j));
        end
        figure(5)
        plot(deltaP)
        Wpump=sum(sum(dWpump,1),2)*dt %pump work in J
        done=1; %routine is done when the it reaches t_final

%         Ef=eps*rhof*hf*Ac*L/Nx; %fluid energy entrained in one bed of
the regenerator
%         Er=(1-eps)*rhor(1)*hr*Ac*L/Nx; %regenerator energy for one bed
%         dE_cycle=sum(abs(Er(:,Nt+1)-Er(:,1)))+sum(abs(Ef(:,Nt+1)-
Ef(:,1))) %absolute value of the change in energy over one cycle
%         Wmag=dE_cycle-Wpump+heat_load-ref_load; %magnetic work during
the previous cycle
%         Emax=max(sum(Ef,1)+sum(Er,1)); %maximum energy in the solid and
fluid during previous cycle
%         Emin=min(sum(Ef,1)+sum(Er,1)); %minimum energy in the solid and
fluid during previous cycle
%         err=abs(dE_cycle/(Emax-Emin)) %figure of merit for cyclical
steady state convergence
%         count=count+1
```

```
%         count2=count2+1;
%         if count==1
%             E0=Ef(Nt+1)+Er(Nt+1);
%         end
%         deltaE(count2)=dE_cycle/E0;
%         if err<tol %system has reached steady state, exit while loop.
%             %         if deltaU<tol
%             done=1;
%         else %steady state has not been achieved, continue to next
cycle.
%             j=0; A=0*A; B=0*B; %reset matrices A and B
%             cycle=(1:1:extrapnum)';
%             dE=mean(deltaE);
%             Tr(:,1)=Tr(:,Nt+1); %initial regenerator temp for next cycle
%             Tf(:,1)=Tf(:,Nt+1);  %initial fluid temp for next cycle
%             Tr_log(:,count)=Tr(:,Nt+1);
%             Tf_log(:,count)=Tf(:,Nt+1);
%             Tr_log2(:,count2)=Tr(:,Nt+1);
%             Tf_log2(:,count2)=Tf(:,Nt+1);
%
%         end
        %done=1
    end
    %     done=1
end

TCedg=0.5*(1.5*Tf(Nx,1:Nt)-0.5*Tf(Nx-1,1:Nt))+0.5*(1.5*Tf(Nx,2:Nt+1)-
0.5*Tf(Nx-1,2:Nt+1)); %Fluid temperature at the hot edge of the bed.  This
temp is extrapolated from the last two nodes in the bed
[mufCedg,kfCedg,cfCedg,rhof,hfCedg,sfCedg]=fluidfun(TCedg);

t_conv=toc %this determines how long the model took to finish

cf_avg=mean(mean(cf));
Nu_avg=mean(Nuf);
NTU=Nu_avg*kf(1,19)*Ac*L*as/(dh*mean(mdot)*cf_avg);

%% Calculate net enthalpy and entropy fluxes

%THedg=0.5*(1.5*Tf(1,1:Nt)-0.5*Tf(2,1:Nt))+0.5*(1.5*Tf(1,2:Nt+1)-
0.5*Tf(2,2:Nt+1)); %Fluid temperature at the hot edge of the bed.  This
temp is extrapolated from the last two nodes in the bed

% %Calculate system performance
% Qpump=Wpump/(n_pump*tau); %rate of work applied to the pump in W for all
beds in the regenerator

%% plot selected model results, if modelcheck is set to a value of 1.

% if modelcheck==1
%
%     figure(1)
%     hold off
%     plot(t_node,TH, 'k')
```

```
%     hold on
%     plot(t_node,TCedg, 'r')
%     xlabel('time (s)')
%     ylabel('Temperature (K)')
%
%     figure(2)
%     plot(t_node,mdot)
%
% end
```

Appendix B

Dispersion Concentric Input File

```
Parameter file for 2-D DC PRS Model
All properties should be in MKS units unless specified otherwise
*** PRS Properties ***
 2.901700D+02                !Cold soak temperature (Kelvin)
 3.043400D+02                !Hot blow temperature (Kelvin)
 4.180000D+03                !Specific heat of fluid
 6.043323D-01                !Thermal conductivity of fluid
 1.000000D+03                !Density of fluid
 8.978600D-04                !Viscosity of fluid
 1.800000D+02                !Ergun "A" coefficient
 1.800000D+00                !Ergun "B" coefficient
 7.900000D+03                !Density of regenerator bed material
 4.970000D+02                !Specific heat of bed material
 1.454510D+01                !Thermal conductivity of bed material
 3.600000D-01                !Porosity
 3.970000D-03                !Particle diameter
 2.794000D-01                !Bed length
 2.994000D-02                !Radius of regenerator
 1.100000D+03                !Density of insulating material
 2.010000D+03                !Specific heat of insulating material
 1.300000D-01                !Thermal conductivity of insulating material
 1.600000D-04                !Thickness of insulating material
 7.900000D+03                !Density of housing material
 4.970000D+02                !Specific heat of housing material
 1.454510D+01                !Thermal conductivity of housing material
 3.175000D-02                !Outer radius of housing
 1.000000D+00  1.000000D+01  2    !Start Nusselt number, End Nusselt number, Number of
Nu to run
 2.794000D-01                !Axial position for temperature evaluation
 0.000000D+00                !Radius for temperature evaluation
 1.000000D-02                !Radius for temperature evaluation
 2.000000D-02                !Radius for temperature evaluation
*** Properties of inlet temperature ***
 1                      !Type of inlet housing temperature (1 for "Warm Housing", 2 for "Cold
Housing")
 1.137000D+01                !Inlet parameter P2
 6.720000D+00                !Inlet parameter P3
 1.081800D+02                !Inlet parameter P4
 0.000000D+00                !Inlet parameter P5
 0.000000D+00                !Inlet parameter P6
*** Properties of time-dependent flow ***
 1.770000D-01                !Flow parameter P1 in lit/min
```

```
 1.770000D-01                !Flow parameter P2 in lit/min
 8.053600D+00                !Flow parameter P3
 0.000000D+00                !Flow parameter P4
 0.000000D+00                !Flow parameter P5
*** Numerical solution parameters ***
 32                     !Number of radial eigenfunctions
 64                     !Number of axial eigenfunctions
  1                     !Number of spherical eigenfunctions
 7.000000D+02                !Ending time
 14000                  !Number of time steps
*** Output file name. Must not already exist or will prompt for different name***
 test.dat
```

Dispersion Concentric Source Code

```
program Run_DC_PRS_2D_ee_UW
!-----------------------------------------------------------------------
-------------------------
! Program for driving the DC_PRS_2D subroutine, which solves the 2D
Dispersion-Concentric equations
! for the temperature profiles in a passive regenerator. The predicted
outlet temperature is then
! compared to a measured outlet temperature provided by the UW.
!-----------------------------------------------------------------------
-------------------------
    use DC_PRS_2D_ee_UW_mod
    implicit none
!-----Variables defining the PRS.
    type (PRS_vars) pvs
!-----Numerical solution parameters.
    type (num_vars) nvs
!-----Variables storing results.
    type (result_vars) rslts
!-----Miscellaneous variables.
    integer i,j,k,nNu
    real*8 T_avg,ht,time,ratio,f0,alpha0,krat,x,x1,x2,Nu0,Nu1,hNu
    character*40 tfile
    logical ex
    real*8, dimension(:,:), allocatable :: Tf_outlet_Nu
!
!-----Read and check PRS properties (all units are MKS unless noted
otherwise).
!
    open(unit=1,file='PRS_Nu_Cycle.par',status='old')
    read(1,*); read(1,*); read(1,*)
    read(1,*)pvs%Tc                           !Cold soak temperature
    read(1,*)pvs%Th                           !Hot blow temperature
    read(1,*)pvs%cf                           !Specific heat of fluid
    read(1,*)pvs%avg_kf                       !Thermal conductivity of
fluid
    read(1,*)pvs%rhof                         !Density of fluid
    read(1,*)pvs%avg_visc                     !Viscosity of fluid
    read(1,*)pvs%Ergun_a                      !Ergun "A" coefficient
```

```
    read(1,*)pvs%Ergun_b                        !Ergun "B" coefficient
    read(1,*)pvs%rhos                           !Density of regenerator
material
    read(1,*)pvs%cs                             !Specific heat of
regenerator material
    read(1,*)pvs%avg_ks                         !Thermal conductivity of
regenerator material
    read(1,*)pvs%eps                            !Porosity of regenerator
    read(1,*)pvs%pdiam                          !Particle diameter
    pvs%aspec=6.d0*(1.d0-pvs%eps)/pvs%pdiam     !Specific area of packed
particle bed
    read(1,*)pvs%bedlen                         !Bed length
    read(1,*)pvs%r1                             !Bed radius
    read(1,*)pvs%rho1                           !Density of first housing
layer (soft rubber)
    read(1,*)pvs%c1                             !Specific heat of first
housing layer (soft rubber)
    read(1,*)pvs%k1                             !Thermal conductivity of
first housing layer
    read(1,*)pvs%r2                             !Thickness of first housing
layer
    pvs%r2=pvs%r1+pvs%r2                        !Radius to end of first
housing layer
    read(1,*)pvs%rho2                           !Density of 2nd housing
layer (type 304 stainless steel)
    read(1,*)pvs%c2                             !Specific heat of 2nd
housing layer
    read(1,*)pvs%k2                             !Thermal conductivity of 2nd
housing layer
    read(1,*)pvs%r3                             !Radius to end of housing
    pvs%Ac=pi*pvs%r1**2                         !Cross-sectional area of bed
    read(1,*)Nu0,Nu1,nNu                        !Start Nusselt number, end
Nusselt number, number of Nu to run
    read(1,*)pvs%outlet_position                !Position of outlet
temperature
    if(pvs%outlet_position .lt. 0.d0 .or. pvs%outlet_position .gt.
pvs%bedlen)then
       write(*,*)'Invalid position for evaluation of outlet
temperature',pvs%outlet_position
       stop
    endif
    read(1,*)pvs%rchek(1)                       !Radius for evaluating
outlet fluid temperature
    if(pvs%rchek(1) .lt. 0.d0 .or. pvs%rchek(1) .gt. pvs%r3)then
       write(*,*)'Invalid radius for evaluation of outlet
temperature',pvs%rchek(1)
       stop
    endif
    read(1,*)pvs%rchek(2)                       !Radius for evaluating
outlet fluid temperature
    if(pvs%rchek(2) .lt. 0.d0 .or. pvs%rchek(2) .gt. pvs%r3)then
       write(*,*)'Invalid radius for evaluation of outlet
temperature',pvs%rchek(1)
       stop
    endif
```

```
    read(1,*)pvs%rchek(3)                      !Radius for evaluating
outlet fluid temperature
    if(pvs%rchek(3) .lt. 0.d0 .or. pvs%rchek(3) .gt. pvs%r3)then
       write(*,*)'Invalid radius for evaluation of outlet
temperature',pvs%rchek(1)
       stop
    endif
!
!-----Read inlet temperature properties.
!
    read(1,*)
    read(1,*)pvs%inlet_housing_type            !Type of inlet housing
temperature (1 for warm housing, 2 for cold housing)
    read(1,*)pvs%tau1
    read(1,*)pvs%delta1
    read(1,*)pvs%tau2
    read(1,*)pvs%aic
    read(1,*)pvs%bic
!
!-----Read flow properties.
!
    read(1,*)
    read(1,*)pvs%flow1
    read(1,*)pvs%flow2
    read(1,*)pvs%tauf
    read(1,*)pvs%afc
    read(1,*)pvs%bfc
!
!-----Read numerical parameters.
!
    read(1,*)
    read(1,*)nvs%nr
    read(1,*)nvs%nx
    read(1,*)nvs%ns
    read(1,*)nvs%tmax       !Ending time
    read(1,*)nvs%tsteps     !Number of time steps
    read(1,*)
    read(1,'(a40)')tfile    !Output file name
    close(unit=1)
!
!-----Evaluate properties, Reynolds, and Prandtl numbers at average
temperature.
!
    x1=exp(-nvs%tmax/pvs%tauf)
    pvs%aflow=(pvs%flow2-
pvs%flow1+pvs%afc*pvs%tauf+2*pvs%bfc*pvs%tauf**2)*(1.d0-x1)
    pvs%aflow=pvs%aflow-
nvs%tmax*x1*(pvs%afc+pvs%bfc*(2*pvs%tauf+nvs%tmax))
    pvs%aflow=pvs%flow2-pvs%tauf*pvs%aflow/nvs%tmax   !Average flow rate
    pvs%aflow=pvs%aflow*flow_conversion               !Convert flow rate
from lit/min to m^3/s
    pvs%avg_Re=pvs%pdiam*(pvs%aflow/pvs%Ac)*pvs%rhof/pvs%avg_visc
    pvs%avg_Pr=pvs%cf*pvs%avg_visc/pvs%avg_kf
!
!-----Evaluate effective thermal conductivity.
```

```
!
    ratio=pvs%avg_ks/pvs%avg_kf
    f0=0.8d0+0.1d0*pvs%eps
    alpha0=10.d0**(-1.084d0-6.778d0*(pvs%eps-0.298d0))
    krat=(1-alpha0)*(pvs%eps*f0+ratio*(1-pvs%eps*f0))
    krat=krat/(1-pvs%eps*(1-f0)+ratio*pvs%eps*(1-f0))
    x=alpha0*(2*ratio**2*(1-pvs%eps)+(1+2*pvs%eps)*ratio)
    krat=krat+x/((2+pvs%eps)*ratio+1-pvs%eps)    !Ratio of effective
quiescent axial thermal conductivity to fluid thermal conductivty
    pvs%kx=pvs%avg_kf*(krat+0.5d0*pvs%avg_Pr*pvs%avg_Re)
    pvs%kr=pvs%avg_kf*(krat+0.1d0*pvs%avg_Pr*pvs%avg_Re)
!
!-----Evaluate viscous dissipation.
!
    pvs%avg_viscdiss=pvs%Ergun_a+pvs%Ergun_b*pvs%avg_Re/(1-pvs%eps)

pvs%avg_viscdiss=pvs%avg_viscdiss*(pvs%aflow/pvs%Ac)**2*(pvs%avg_visc/pvs%
pdiam**2)*(1-pvs%eps)**2/pvs%eps**3
!
!-----Cycle over average Nusselt number and heat transfer coefficient.
!
    hNu=0.d0
    if(nNu .gt. 1)hNu=(Nu1-Nu0)/(nNu-1)
    allocate(TF_outlet_Nu(0:nvs%tsteps,nNu))
    do k=0,nNu-1
       pvs%avg_Nu=Nu0+k*hNu
       pvs%avg_htc=pvs%avg_Nu*pvs%avg_kf/pvs%pdiam
!
!-----Solve for temperature profiles.
!
       call DC_PRS_2D_ee(pvs,nvs,rslts)
!
!-----Store outlet temperature profile.
!
       do i=0,nvs%tsteps
          Tf_outlet_Nu(i,k+1)=rslts%tf_outlet(i,1)
       end do
       deallocate(rslts%tf_outlet)
    end do
!
!-----Write out outlet temperature.
!
    do
       inquire(file=tfile,exist=ex)
       if(ex)then
          write(*,*)'Requested output file already exists. Enter new file
name:'
          read(*,'(a40)')tfile
       else
          exit
       endif
    end do
    open(unit=2,file=tfile,status='new')
    ht=nvs%tmax/nvs%tsteps
    do i=0,nvs%tsteps
```

```
       write(2,'(1x,1p2000e16.6)')i*ht,(Tf_outlet_Nu(i,j),j=1,nNu)
    end do
    close(unit=2)
!
!-----End of program.
!
    deallocate(Tf_outlet_Nu)
    stop
end program Run_DC_PRS_2D_ee_UW
!-----------------------------------------------------------------------
 module DC_PRS_2D_ee_UW_mod
!-----------------------------------------------------------------------
! This module contains constants and derived type definitions needed
! for solving the 2D DC PRS model equations governing a passive
! regenerator system (PRS). The housing of the PRS consists of 2 layers.
! These equations are solved by eigenfunction expansion in the two
! spatial variables, leading to a system of ODEs in time. These ODEs
! are solved with a Runge-Kutta method.
!
! The flow is assumed to be time dependent.
!
! Unless specified otherwise, all dimensioned variables have MKS units.
! SAJ 02/04/2009
!-----------------------------------------------------------------------
!
!-----Constants/parameters.
!
    real*8, parameter :: pi=3.14159265358979d0          !Pi
    real*8, parameter :: flow_conversion=0.001d0/60.d0  !Convert lit/min
to m^3/s
!
!-----Derived type with PRS properties.
!
    type PRS_vars
       real*8 rhos                                  !Density of solid phase
particles
       real*8 rho1                                  !Density of first housing
layer
       real*8 rho2                                  !Density of second
housing layer
       real*8 r1                                    !Radial extent of bed
       real*8 r2                                    !Radius to end of first
housing layer
       real*8 r3                                    !Radius to end of 2nd
housing layer
       real*8 bedlen                                !Bed length
       real*8 Ac                                    !Cross-sectional area of
bed normal to flow
       real*8 pdiam                                 !Particle diameter
       real*8 eps                                   !Porosity
       real*8 aspec                                 !Specific area
       real*8 rhof                                  !Fluid density
       real*8 cf                                    !Fluid heat capacity
       real*8 cs                                    !Solid phase heat
capacity
```

```
       real*8 c1                                !Specific heat of first
housing layer
       real*8 c2                                !Specific heat of 2nd
housing layer
       real*8 k1                                !Thermal conductivity of
first housing layer
       real*8 k2                                !Thermal conductivity of
2nd housing layer
       real*8 Tc                                !Cold inlet fluid
temperature
       real*8 Th                                !Hot inlet fluid
temperature
       real*8 tau1                              !Fluid inlet temperature
time constant
       real*8 tau2                              !Fluid inlet temperature
time constant
       real*8 delta1                            !Fluid inlet temperature
constant
       real*8 aic                               !Fluid inlet coefficient
       real*8 bic                               !Fluid inlet coefficient
       real*8 aflow                             !Average flow rate
       real*8 flow1                             !Initial flow rate
       real*8 flow2                             !Asymptotic flow rate
       real*8 tauf                              !Flow time constant
       real*8 afc                               !Flow coefficient
       real*8 bfc                               !Flow coefficient
       real*8 avg_kf                            !Axial thermal
conductivity of fluid at average PRS temperature
       real*8 avg_ks                            !Thermal conductivity of
solid phase at average PRS temperature
       real*8 avg_visc                          !Viscosity at average PRS
temperature
       real*8 avg_Re                            !Reynolds number at
average PRS temperature
       real*8 avg_Pr                            !Prandtl number at
average PRS temperature
       real*8 avg_Nu                            !Nusselt number at
average PRS temperature
       real*8 avg_htc                           !Heat transfer
coefficient at average PRS temperature
       real*8 Ergun_a                           !Ergun equation
coefficient
       real*8 Ergun_b                           !Ergun equation
coefficient
       real*8 avg_viscdiss                      !Viscous dissipation at
average PRS temperature
       real*8 kx                                !Effective axial thermal
conductivity
       real*8 kr                                !Effective radial thermal
conductivity
       real*8 outlet_position                   !Axial position to
evaluate the outlet temperature
       real*8 rchek(3)                          !Radii to evaluate the
outlet temperature
```

```
       integer inlet_housing_type                !Type of inlet housing
temperature (1 for warm housing, 2 for cold housing)
    end type PRS_vars
!
!-----Derived type with variables that control the numerical solution.
!
    type num_vars
       real*8 tmax                                !Ending time
       integer tsteps                             !Number of time steps
       integer nr                                 !Number of radial
eigenfunctions
       integer nx                                 !Number of axial
eigenfunctions
       integer ns                                 !Number of spherical
eigenfunctions
    end type num_vars
!
!-----Derived type with radial eigenfunction variables.
!
    type radial_eigenfunction_vars
       real*8 g0,g1,g2                              !Gamma0, Gamma1,
Gamma2
       real*8 norm                                  !Common norm of
eigenfunctions
       real*8, dimension(:), allocatable :: eta     !Array of eigenvalues
       real*8, dimension(:,:), allocatable :: a     !Array storing
eigenfunction coefficients
       real*8, dimension(:), allocatable :: F       !Viscous dissipation
inner products
       real*8, dimension(:,:), allocatable :: P     !Matrix of inner
products of radial eigenfunctions
       real*8, dimension(:,:), allocatable :: Alpha  !Thermal diffusivity
matrix
       real*8, dimension(:,:), allocatable :: reI    !Integrals of radial
eigenfunctions needed for x = 0 boundary condition
    end type radial_eigenfunction_vars
!
!-----Derived type with spherical eigenfunction variables
!
    type spherical_eigenfunction_vars
       real*8, dimension(:), allocatable :: root      !Spherical
eigenvalues
       real*8, dimension(:), allocatable :: norm      !Norm of
eigenfunctions
       real*8, dimension(:), allocatable :: beta      !Expansion
coefficients
       real*8, dimension(:), allocatable :: seR       !Eigenfunctions at
particle radius
       real*8, dimension(:), allocatable :: lambdasq  !Modified
eigenvalues
    end type spherical_eigenfunction_vars
!
!-----Derived type storing results.
!
    type result_vars
```

```
       real*8, dimension(:,:), allocatable :: Tf_outlet  !Array storing
outlet fluid temperature
    end type result_vars
!
!-----Module subprograms.
!
contains
!-----------------------------------------------------------------------
---------------------
subroutine DC_PRS_2D_ee(pvs,nvs,rslts)
!-----------------------------------------------------------------------
---------------------
! Solves the 2-D Dispersion-Concentric (DC) equations governing the
temperatures
! of the regenerator material and the heat transfer fluid. The fluid
temperature is represented
! as an expansion in radial and axial eigenfunctions with time-dependent
coefficients. The
! solid phase material temperature is represented as an expansion in *Ns*
spherical
! eigenfunctions of the heat diffusion operator, with time, x-, and r-
dependent coefficients.
! The equations of the model then reduce to a system of ODEs in time,
which are solved with a
! Runge-Kutta method.
!
! The time-dependent coefficient of the *(i,m)*th radial-axial
eigenfunction is stored in
! element *theta((i-1)Nx + m)*.
!-----------------------------------------------------------------------
---------------------
    implicit none
!-----Variables defining the PRS.
    type (PRS_vars), intent(in) :: pvs
!-----Numerical solution parameters.
    type (num_vars), intent(inout) :: nvs
!-----Results.
    type (result_vars), intent(out) :: rslts
!-----Variables for radial eigenfunctions.
    type (radial_eigenfunction_vars) revs
!-----Variables for spherical eigenfunctions.
    type (spherical_eigenfunction_vars) sevs
!-----Variables for time derivatives.
    real*8, dimension(:), allocatable :: thetavec,psivec,dvect,dvecp
!-----Variables governing the time integration.
    integer istep
    real*8 ht,time
!-----Arrays storing the time-dependent coefficients.
    real*8, dimension(:), allocatable :: theta0,theta1
    real*8, dimension(:), allocatable :: psi0,psi1
!-----Miscellaneous variables.
    integer i,j,k,m,nsys,npsi
    real*8 phi,csimx,tf_inlet,x1,x2,r(3),Ti0
    real*8 dbesj0,dbesy0
!
```

```
!-----Set size of systems of ODEs in time.
!
    nsys=nvs%nx*nvs%nr
    npsi=nvs%ns*nvs%nr*nvs%nx
!
!-----Check porosity.
!
    if(pvs%eps .ge. 1.d0 .or. pvs%eps .le. 0.d0)then
       write(*,*)'DC_PRS: Invalid porosity',pvs%eps
       stop
    endif
!
!-----Evaluate radial eigenfunctions and the matrices that depend on them.
!
    call radial_eigenfunctions(pvs,nvs,revs)
!
!-----Evaluate spherical eigenfunctions.
!
    call spherical_eigenfunctions(pvs,nvs,sevs)
!
!-----Allocate array for storing the solution.
!
    allocate(theta0(nsys),theta1(nsys),psi0(npsi),psi1(npsi))
!
!-----Allocate arrays for storing the time derivatives.
!
    allocate(thetavec(nsys),psivec(npsi),dvect(nsys),dvecp(npsi))
!
!-----Allocate array for fluid outlet temperature.
!
    allocate(rslts%Tf_outlet(0:nvs%tsteps,3))
!
!-----Set initial conditions (*t = 0*).
!
    theta0=0.d0
    psi0=0.d0
    rslts%Tf_outlet=pvs%Tc
!
!-----Set initial time and time step.
!
    time=0.d0
    ht=nvs%tmax/nvs%tsteps
!
!-----Integrate in time using RK4.
!
    do istep=0,nvs%tsteps-1
!
!-----First stage of RK4. Evaluate the time derivatives of the expansion
coefficients.
!
       do i=1,nsys
          thetavec(i)=theta0(i)
          theta1(i)=theta0(i)
       end do
       do i=1,npsi
```

```
          psivec(i)=psi0(i)
          psi1(i)=psi0(i)
       end do
       call setdvec(pvs,nvs,revs,sevs,time,thetavec,psivec,dvect,dvecp)
!
!-----Update solution and perform second stage of RK4.
!
       do i=1,nsys
          theta1(i)=theta1(i)+ht*dvect(i)/6
          thetavec(i)=theta0(i)+ht*dvect(i)/2
       end do
       do i=1,npsi
          psi1(i)=psi1(i)+ht*dvecp(i)/6
          psivec(i)=psi0(i)+ht*dvecp(i)/2
       end do
       time=time+ht/2
       call setdvec(pvs,nvs,revs,sevs,time,thetavec,psivec,dvect,dvecp)
!
!-----Update solution and perform third stage of RK4.
!
       do i=1,nsys
          theta1(i)=theta1(i)+ht*dvect(i)/3
          thetavec(i)=theta0(i)+ht*dvect(i)/2
       end do
       do i=1,npsi
          psi1(i)=psi1(i)+ht*dvecp(i)/3
          psivec(i)=psi0(i)+ht*dvecp(i)/2
       end do
       call setdvec(pvs,nvs,revs,sevs,time,thetavec,psivec,dvect,dvecp)
!
!-----Update solution and perform fourth stage of RK4.
!
       do i=1,nsys
          theta1(i)=theta1(i)+ht*dvect(i)/3
          thetavec(i)=theta0(i)+ht*dvect(i)
       end do
       do i=1,npsi
          psi1(i)=psi1(i)+ht*dvecp(i)/3
          psivec(i)=psi0(i)+ht*dvecp(i)
       end do
       time=time+ht/2
       call setdvec(pvs,nvs,revs,sevs,time,thetavec,psivec,dvect,dvecp)
!
!-----Update solution.
!
       do i=1,nsys
          theta1(i)=theta1(i)+ht*dvect(i)/6
          theta0(i)=theta1(i)
       end do
       do i=1,npsi
          psi1(i)=psi1(i)+ht*dvecp(i)/6
          psi0(i)=psi1(i)
       end do
       x1=time/pvs%tau1
       x2=time/pvs%tau2
```

```
       tf_inlet=pvs%Th-(pvs%delta1+pvs%aic*time+pvs%bic*time**2)*exp(-x1)-
(pvs%Th-pvs%Tc-pvs%delta1)*exp(-x2)
       do k=1,3
          rslts%Tf_outlet(istep+1,k)=0.d0
          do i=1,nvs%nr
             if(i .eq. 1)then
                phi=1.d0
             else if(pvs%rchek(k) .le. pvs%r1)then
                phi=revs%a(1,i)*dbesj0(revs%eta(i)*revs%g0*pvs%rchek(k))
             else if(pvs%rchek(k) .le. pvs%r2)then

phi=revs%a(2,i)*dbesj0(revs%eta(i)*revs%g1*pvs%rchek(k))+revs%a(3,i)*dbesy
0(revs%eta(i)*revs%g1*pvs%rchek(k))
             else

phi=revs%a(4,i)*dbesj0(revs%eta(i)*revs%g2*pvs%rchek(k))+revs%a(5,i)*dbesy
0(revs%eta(i)*revs%g2*pvs%rchek(k))
             endif
             do m=1,nvs%nx
                j=(i-1)*nvs%nx+m
                csimx=(2*m-1)*pi*pvs%outlet_position/(2*pvs%bedlen)

rslts%Tf_outlet(istep+1,k)=rslts%Tf_outlet(istep+1,k)+theta1(j)*sqrt(2.d0)
*sin(csimx)*phi
             end do
             Ti0=revs%reI(1,i)*tf_inlet+revs%reI(2,i)*(pvs%Tc-
tf_inlet)+revs%reI(3,i)*pvs%Tc
             rslts%Tf_outlet(istep+1,k)=rslts%Tf_outlet(istep+1,k)+phi*Ti0
          end do
       end do
       if(mod(istep,100) .eq. 0)write(*,*)'Time =',time
       if(abs(theta1(1)) .gt. 100.d0*pvs%Th)then    !Check for proper
behavior of solution
          write(*,*)'Improper behavior of solution. Increase number of
time steps'
          stop
       endif
    end do
!
!-----Deallocate storage that is no longer needed.
!
    deallocate(thetavec,psivec,dvect,dvecp)
!
!-----End of subroutine.
!
    deallocate(revs%eta,revs%a,revs%F,revs%P,revs%Alpha,revs%reI)
    deallocate(sevs%root,sevs%norm,sevs%beta,sevs%seR,sevs%lambdasq)
    deallocate(theta0,theta1,psi0,psi1)
    return
end subroutine DC_PRS_2D_ee
!-----------------------------------------------------------------------
---------------
subroutine setdvec(pvs,nvs,revs,sevs,time,theta,psi,dvect,dvecp)
!-----------------------------------------------------------------------
---------------
```

```
! Evaluates the time derivatives of the expansion coefficients at *time*.
The arrays
! *theta,psi* store the current values of the coefficients. The arrays
*dvect,dvecp*
! store the time derivatives for the *theta,psi* coefficients,
respectively.
!-----------------------------------------------------------------------
---------------
    implicit none
    type (PRS_vars), intent(in) :: pvs                    !PRS properties
    type (num_vars), intent(in) :: nvs                    !Variables
controlling the numerical solution
    type (radial_eigenfunction_vars), intent(in) :: revs     !Radial
eigenfunction variables
    type (spherical_eigenfunction_vars), intent(in) :: sevs  !Spherical
eigenfunction variables
    real*8, intent(in) :: time                            !Time
    real*8, intent(in) :: theta(*)                        !Expansion
coefficients of temperatures at *time*
    real*8, intent(in) :: psi(*)                          !Spherical
expansion coefficients at *time*
    real*8, intent(out) :: dvect(*)                       !Vector of
*theta* time derivatives
    real*8, intent(out) :: dvecp(*)                       !Vector of *psi*
time derivatives
!-----Local variables.
    integer i,j,k,m,n,l,q
    real*8
tf_inlet,dtf_inlet,x1,x2,x3,x4,sum,phi,cv,gm,etasq,prd,prd1,ti0,dti0,flow,
v_pore
    real*8, dimension(:), allocatable :: csi,csisq,fac,T0,dT0
    real*8, dimension(:,:), allocatable :: G,Gtheta
!
!-----Check input.
!
    if(time .lt. 0.d0)then
       write(*,*)'SETDVEC: Invalid time',time
       stop
    endif
!
!-----Evaluate fluid inlet temperature and its time derivative.
!
    x1=time/pvs%tau1
    x2=time/pvs%tau2
    tf_inlet=pvs%Th-(pvs%delta1+pvs%aic*time+pvs%bic*time**2)*exp(-x1)
    tf_inlet=tf_inlet-(pvs%Th-pvs%Tc-pvs%delta1)*exp(-x2)
!Fluid inlet temperature
    dtf_inlet=(pvs%Th-pvs%Tc-pvs%delta1)*exp(-x2)/pvs%tau2
!Time derivative of fluid inlet temperature
    dtf_inlet=dtf_inlet+(pvs%delta1+pvs%aic*time+pvs%bic*time**2)*exp(-
x1)/pvs%tau1
    dtf_inlet=dtf_inlet-(pvs%aic+2*pvs%bic*time)*exp(-x1)
!
!-----Evaluate flow velocity.
!
```

```
    flow=pvs%flow2-(pvs%flow2-
pvs%flow1+pvs%afc*time+pvs%bfc*time**2)*exp(-time/pvs%tauf)
    flow=flow*flow_conversion
    v_pore=flow/(pvs%eps*pvs%Ac)
!
!-----Allocate space for auxiliary arrays. Evaluate auxiliary arrays.
!
    allocate(G(nvs%nx,nvs%nx),Gtheta(nvs%nr,nvs%nx))
    do m=1,nvs%nx
       do n=1,nvs%nx
          if(m .eq. n)then
             G(m,n)=1.d0
          else if(mod(m-n,2) .eq. 0)then
             G(m,n)=(2.d0*n-1.d0)/(m+n-1.d0)
          else
             G(m,n)=(2.d0*n-1.d0)/(m-n)
          endif
          G(m,n)=G(m,n)/pvs%bedlen
       end do
    end do
    do j=1,nvs%nr
       do m=1,nvs%nx
          Gtheta(j,m)=0.d0
          do l=1,nvs%nx
             Gtheta(j,m)=Gtheta(j,m)+G(m,l)*theta((j-1)*nvs%nx+l)
          end do
          Gtheta(j,m)=v_pore*Gtheta(j,m)
       end do
    end do
    allocate(csi(nvs%nx),csisq(nvs%nx),fac(nvs%nx),T0(nvs%nr),dT0(nvs%nr))
    do m=1,nvs%nx
       csi(m)=(2*m-1)*pi/(2*pvs%bedlen)
       csisq(m)=csi(m)**2
       fac(m)=2.d0*sqrt(2.d0)/(pi*(2*m-1))
    end do
    do i=1,nvs%nr
       T0(i)=revs%reI(1,i)*tf_inlet+revs%reI(2,i)*(pvs%Tc-
tf_inlet)+revs%reI(3,i)*pvs%Tc
       dT0(i)=dtf_inlet*(revs%reI(1,i)-revs%reI(2,i))
    end do
!
!-----Evaluate time derivatives.
!
    cv=pvs%eps*pvs%rhof*pvs%cf
    do i=1,nvs%nr
       etasq=revs%eta(i)**2
       do m=1,nvs%nx
          l=(i-1)*nvs%nx+m
          dvect(l)=-etasq*theta(l)+(revs%F(i)-etasq*T0(i)-dT0(i))*fac(m)
          x1=0.d0
          x3=0.d0
          do j=1,nvs%nr
             x1=x1+revs%Alpha(i,j)*theta((j-
1)*nvs%nx+m)*csisq(m)+revs%P(i,j)*Gtheta(j,m)
```

```
             x3=x3+revs%P(i,j)*theta((j-
1)*nvs%nx+m)*(csisq(m)*pvs%kx/cv+revs%eta(j)**2)
             x3=x3+revs%P(i,j)*(Gtheta(j,m)+revs%eta(j)**2*T0(j)*fac(m))
          end do
          dvect(l)=dvect(l)-x1
          x1=0.d0
          do k=1,nvs%ns
             n=(k-1)*nvs%nr*nvs%nx+(i-1)*nvs%nx+m
             x1=x1+psi(n)*sevs%seR(k)
          end do
          x1=pvs%aspec*pvs%avg_htc*x1/cv
          dvect(l)=dvect(l)-x1
          do k=1,nvs%ns
             n=(k-1)*nvs%nr*nvs%nx+(i-1)*nvs%nx+m
             dvecp(n)=-
sevs%lambdasq(k)*psi(n)+sevs%beta(k)*(revs%F(i)*fac(m)-x3-x1)
          end do
       end do
    end do
!
!-----End of subroutine.
!
    deallocate(G,csi,csisq,fac,Gtheta,T0,dT0)
    return
end subroutine setdvec
!-----------------------------------------------------------------------
-----
subroutine radial_eigenfunctions(pvs,nvs,revs)
!-----------------------------------------------------------------------
-----
! Evaluates the radial eigenfunctions used in the solution of the 2-D DC
! equations.
!-----------------------------------------------------------------------
-----
    implicit none
    type (PRS_vars), intent(in) :: pvs
    type (num_vars), intent(in) :: nvs
    type (radial_eigenfunction_vars), intent(out) :: revs
!-----Local variables.
    real*8, parameter :: etamx=100.d0 !Upper limit of eigenvalue search
region
    integer, parameter :: npts=2000   !Number of mesh points for
eigenvalue search
    real*8, parameter :: tol=1.d-12   !Eigenvalue tolerance
    integer, parameter :: maxit=200   !Maximum number of bisections
    real*8, parameter :: isq3=0.577350269189626d0  !1/sqrt(3) needed for
quadrature
    real*8 h,ratio,eta1,eta2,eta3,f1,f2,f3,eta2str,f2str,rq
    integer iroots,i,iter,j,q,nq,q2
    real*8
j001,j101,j011,j111,y011,y111,j012,j112,y012,y112,j022,j122,y022,y122,j023
,y023
    real*8, dimension(:), allocatable:: phi1m,dphi1m,phi2m,dphi2m,phi3
    real*8 dtrmnt
    real*8 dbesj0,dbesy0,dbesj1,dbesy1
```

```
!
!-----Allocate space for eigenfunction variables.
!

allocate(revs%eta(nvs%nr),revs%a(5,nvs%nr),revs%F(nvs%nr),revs%P(nvs%nr,nv
s%nr),revs%Alpha(nvs%nr,nvs%nr))
    allocate(revs%reI(3,nvs%nr))

allocate(phi1m(nvs%nr),dphi1m(nvs%nr),phi2m(nvs%nr),dphi2m(nvs%nr),phi3(nv
s%nr))
!
!-----Set layer constants.
!
    revs%g0=sqrt(pvs%eps*pvs%rhof*pvs%cf/pvs%kr)
    revs%g1=sqrt(pvs%rho1*pvs%c1/pvs%k1)
    revs%g2=sqrt(pvs%rho2*pvs%c2/pvs%k2)
!
!-----First eigenfunction is a constant.
!
    iroots=1
    revs%eta(iroots)=0.d0

revs%norm=pvs%eps*pvs%rhof*pvs%cf*pvs%r1**2+pvs%rho1*pvs%c1*(pvs%r2**2-
pvs%r1**2)
    revs%norm=revs%norm+pvs%rho2*pvs%c2*(pvs%r3**2-pvs%r2**2)
    revs%norm=0.5d0*revs%norm
    do i=1,5
       revs%a(i,iroots)=1.d0
    end do
!
!-----If more roots are needed, search through *eta* to find roots.
!
    if(nvs%nr .gt. 1)then
       h=etamx/npts
       eta1=h

f1=dtrmnt(revs%g0,revs%g1,revs%g2,pvs%kr,pvs%k1,pvs%k2,pvs%r1,pvs%r2,pvs%r
3,eta1)
       do i=1,npts
          eta2=eta1+h

f2=dtrmnt(revs%g0,revs%g1,revs%g2,pvs%kr,pvs%k1,pvs%k2,pvs%r1,pvs%r2,pvs%r
3,eta2)
!
!-----If bracket for root has been found, refine with bisection.
!
          if(f1*f2 .lt. 0.d0)then
             eta2str=eta2   !Store upper bound on root
             f2str=f2       !Store function value at root upper bound
             do iter=1,maxit
                eta3=(eta1+eta2)/2.d0

f3=dtrmnt(revs%g0,revs%g1,revs%g2,pvs%kr,pvs%k1,pvs%k2,pvs%r1,pvs%r2,pvs%r
3,eta3)
                if(eta2-eta1 .lt. tol*eta3 .or. f3 .eq. 0.d0)then
```

```
                   iroots=iroots+1
                   revs%eta(iroots)=eta3
                   j001=dbesj0(eta3*revs%g0*pvs%r1);
j101=dbesj1(eta3*revs%g0*pvs%r1)
                   j011=dbesj0(eta3*revs%g1*pvs%r1);
j111=dbesj1(eta3*revs%g1*pvs%r1)
                   y011=dbesy0(eta3*revs%g1*pvs%r1);
y111=dbesy1(eta3*revs%g1*pvs%r1)
                   j012=dbesj0(eta3*revs%g1*pvs%r2);
j112=dbesj1(eta3*revs%g1*pvs%r2)
                   y012=dbesy0(eta3*revs%g1*pvs%r2);
y112=dbesy1(eta3*revs%g1*pvs%r2)
                   j022=dbesj0(eta3*revs%g2*pvs%r2);
j122=dbesj1(eta3*revs%g2*pvs%r2)
                   y022=dbesy0(eta3*revs%g2*pvs%r2);
y122=dbesy1(eta3*revs%g2*pvs%r2)
                   revs%a(1,iroots)=1.d0
                   revs%a(2,iroots)=j001*y111-
j101*y011*revs%g0*pvs%kr/(revs%g1*pvs%k1)
                   revs%a(2,iroots)=-
revs%a(1,iroots)*revs%a(2,iroots)*pi*eta3*revs%g1*pvs%r1/2.d0

revs%a(3,iroots)=j011*j101*revs%g0*pvs%kr/(revs%g1*pvs%k1)-j111*j001
                   revs%a(3,iroots)=-
revs%a(1,iroots)*revs%a(3,iroots)*pi*eta3*revs%g1*pvs%r1/2.d0
                   ratio=revs%g1*pvs%k1/(revs%g2*pvs%k2)

revs%a(4,iroots)=y122*(revs%a(2,iroots)*j012+revs%a(3,iroots)*y012)-
y022*(revs%a(2,iroots)*j112+revs%a(3,iroots)*y112)*ratio
                   revs%a(4,iroots)=-
pi*eta3*revs%g2*pvs%r2*revs%a(4,iroots)/2.d0

revs%a(5,iroots)=j022*ratio*(revs%a(2,iroots)*j112+revs%a(3,iroots)*y112)-
j122*(revs%a(2,iroots)*j012+revs%a(3,iroots)*y012)
                   revs%a(5,iroots)=-
pi*eta3*revs%g2*pvs%r2*revs%a(5,iroots)/2.d0
                   exit
                else
                   if(f3*f1 .lt. 0.d0)then
                      f2=f3
                      eta2=eta3
                   else
                      f1=f3
                      eta1=eta3
                   endif
                endif
             end do
             if(iter .gt. maxit)then
                write(*,*)'RADIAL_EIGENFUNCTIONS: Convergence Failure'
                stop
             endif
             if(iroots .eq. nvs%nr)exit
             f2=f2str
             eta2=eta2str
          endif
```

```
          f1=f2
          eta1=eta2
       end do
    endif
    if(iroots .lt. nvs%nr)then
       write(*,*)'RADIAL_EIGENFUNCTIONS: Cannot find all requested roots'
       write(*,*)'  *** Increase *etamx* and refine search grid ***'
       stop
    endif
!
!-----Normalize.
!
    do i=2,nvs%nr
       j001=dbesj0(revs%eta(i)*revs%g0*pvs%r1);
j101=dbesj1(revs%eta(i)*revs%g0*pvs%r1)
       j012=dbesj0(revs%eta(i)*revs%g1*pvs%r2);
j112=dbesj1(revs%eta(i)*revs%g1*pvs%r2)
       y012=dbesy0(revs%eta(i)*revs%g1*pvs%r2);
y112=dbesy1(revs%eta(i)*revs%g1*pvs%r2)
       j023=dbesj0(revs%eta(i)*revs%g2*pvs%r3);
y023=dbesy0(revs%eta(i)*revs%g2*pvs%r3)
       h=pvs%eps*pvs%rhof*pvs%cf*(revs%a(1,i)*pvs%r1)**2*(j001**2+j101**2)
       h=h-
pvs%rho1*pvs%c1*(revs%a(1,i)*pvs%r1)**2*(j001**2+(revs%g0*pvs%kr*j101/(rev
s%g1*pvs%k1))**2)

h=h+pvs%rho1*pvs%c1*pvs%r2**2*((revs%a(2,i)*j012+revs%a(3,i)*y012)**2+(rev
s%a(2,i)*j112+revs%a(3,i)*y112)**2)
       h=h-
pvs%rho2*pvs%c2*pvs%r2**2*((revs%a(2,i)*j012+revs%a(3,i)*y012)**2+((revs%g
1*pvs%k1/(revs%g2*pvs%k2))*(revs%a(2,i)*j112+revs%a(3,i)*y112))**2)

h=h+pvs%rho2*pvs%c2*pvs%r3**2*(revs%a(4,i)*j023+revs%a(5,i)*y023)**2
       h=h/2.d0
       do j=1,5
          revs%a(j,i)=revs%a(j,i)*sqrt(revs%norm/h)
       end do
    end do
!
!-----Evaluate integrals of eigenfunctions needed for solution of thermal
equations.
!
    do i=1,nvs%nr
       if(i .eq. 1)then
          revs%F(i)=0.5d0*pvs%r1**2/revs%norm
          phi1m(i)=1.d0
          dphi1m(i)=0.d0
          phi2m(i)=1.d0
          dphi2m(i)=0.d0
          phi3(i)=1.d0
          if(pvs%inlet_housing_type .eq. 2)then

revs%reI(1,i)=pvs%eps*pvs%rhof*pvs%cf*pvs%r1**2+pvs%rho1*pvs%c1*(pvs%r2**2
-pvs%r1**2)
             revs%reI(1,i)=0.5d0*revs%reI(1,i)/revs%norm
```

```
            revs%reI(3,i)=1.d0-revs%reI(1,i)
         endif
      else
         phi1m(i)=revs%a(1,i)*dbesj0(revs%eta(i)*revs%g0*pvs%r1)
         dphi1m(i)=-
revs%a(1,i)*dbesj1(revs%eta(i)*revs%g0*pvs%r1)*revs%eta(i)*revs%g0

phi2m(i)=revs%a(2,i)*dbesj0(revs%eta(i)*revs%g1*pvs%r2)+revs%a(3,i)*dbesy0
(revs%eta(i)*revs%g1*pvs%r2)
         dphi2m(i)=-
(revs%a(2,i)*dbesj1(revs%eta(i)*revs%g1*pvs%r2)+revs%a(3,i)*dbesy1(revs%et
a(i)*revs%g1*pvs%r2))*revs%eta(i)*revs%g1

phi3(i)=revs%a(4,i)*dbesj0(revs%eta(i)*revs%g2*pvs%r3)+revs%a(5,i)*dbesy0(
revs%eta(i)*revs%g2*pvs%r3)
         revs%F(i)=-pvs%r1*dphi1m(i)/(revs%eta(i)*revs%g0)**2
         revs%F(i)=revs%F(i)/revs%norm
         if(pvs%inlet_housing_type .eq. 2)then
            revs%reI(1,i)=-
pvs%r2*pvs%k1*dphi2m(i)/(revs%norm*revs%eta(i)**2)
            revs%reI(3,i)=-revs%reI(1,i)
         endif
      endif
      do j=1,i
         if(i .eq. 1 .and. j .eq. 1)then
            revs%P(i,j)=pvs%eps*pvs%rhof*pvs%cf*0.5d0*pvs%r1**2/revs%norm
            revs%Alpha(i,j)=pvs%r1**2*(pvs%kx-pvs%k1)+pvs%r2**2*(pvs%k1-
pvs%k2)+pvs%r3**2*pvs%k2
            revs%Alpha(i,j)=0.5d0*revs%Alpha(i,j)/revs%norm
         else if(i .eq. j)then

revs%P(i,j)=0.5d0*pvs%r1**2*pvs%eps*pvs%rhof*pvs%cf*(phi1m(i)**2+(dphi1m(i
)/(revs%eta(i)*revs%g0))**2)
            revs%P(i,j)=revs%P(i,j)/revs%norm
            revs%Alpha(i,j)=pvs%r1**2*((pvs%kx-
pvs%k1)*phi1m(i)**2+((pvs%kx/pvs%kr)/(pvs%eps*pvs%rhof*pvs%cf)-
1.d0/(pvs%rho1*pvs%c1))*(pvs%kr*dphi1m(i)/revs%eta(i))**2)
            revs%Alpha(i,j)=revs%Alpha(i,j)+pvs%r2**2*((pvs%k1-
pvs%k2)*phi2m(i)**2+(1.d0/(pvs%rho1*pvs%c1)-
1.d0/(pvs%rho2*pvs%c2))*(pvs%k1*dphi2m(i)/revs%eta(i))**2)
            revs%Alpha(i,j)=revs%Alpha(i,j)+pvs%k2*(pvs%r3*phi3(i))**2
            revs%Alpha(i,j)=0.5d0*revs%Alpha(i,j)/revs%norm
         else
            revs%P(i,j)=pvs%r1*pvs%kr*(phi1m(i)*dphi1m(j)-
phi1m(j)*dphi1m(i))/(revs%eta(i)**2-revs%eta(j)**2)
            revs%P(i,j)=revs%P(i,j)/revs%norm

revs%Alpha(i,j)=pvs%r1*pvs%kr*(pvs%kx/(pvs%eps*pvs%rhof*pvs%cf)-
pvs%k1/(pvs%rho1*pvs%c1))*(phi1m(i)*dphi1m(j)-phi1m(j)*dphi1m(i))

revs%Alpha(i,j)=revs%Alpha(i,j)+pvs%r2*pvs%k1*(pvs%k1/(pvs%rho1*pvs%c1)-
pvs%k2/(pvs%rho2*pvs%c2))*(phi2m(i)*dphi2m(j)-phi2m(j)*dphi2m(i))
            revs%Alpha(i,j)=revs%Alpha(i,j)/(revs%norm*(revs%eta(i)**2-
revs%eta(j)**2))
         endif
```

```
        end do
    end do
    do i=1,nvs%nr
        do j=i+1,nvs%nr
            revs%P(i,j)=revs%P(j,i)
            revs%Alpha(i,j)=revs%Alpha(j,i)
        end do
    end do
    do i=1,nvs%nr
        revs%F(i)=revs%F(i)*pvs%avg_viscdiss
    end do
!
!-----Quadrature for evaluation of radial eigenfunction integral needed
for x = 0 boundary condition.
!
    if(pvs%inlet_housing_type .eq. 2)then
        nq=8*nvs%nr+8
        h=(pvs%r2-pvs%r1)/(2.d0*nq)
        f1=h*pvs%rho1*pvs%c1/revs%norm
        do i=1,nvs%nr
            revs%reI(2,i)=0.d0
            do q=0,2*nq-1
                q2=q/2
                if(mod(q,2) .eq. 0)then
                    rq=pvs%r1+h*(1.d0+isq3+2*q2)
                else
                    rq=pvs%r1+h*(1.d0-isq3+2*q2)
                endif
                if(i .eq. 1)then
                    f2=1.d0
                else

f2=revs%a(2,i)*dbesj0(revs%eta(i)*revs%g1*rq)+revs%a(3,i)*dbesy0(revs%eta(
i)*revs%g1*rq)
                endif
                f3=(rq-pvs%r1)/(pvs%r2-pvs%r1)
                revs%reI(2,i)=revs%reI(2,i)+f3**2*(3.d0-2.d0*f3)*rq*f2
            end do
            revs%reI(2,i)=f1*revs%reI(2,i)
        end do
    else if(pvs%inlet_housing_type .eq. 1)then
        revs%reI=0.d0; revs%reI(1,1)=1.d0
    else
        write(*,*)'RADIAL_EIGENFUNCTIONS: Invalid Value of
inlet_housing_type',pvs%inlet_housing_type
        stop
    endif
!
!-----End of subroutine.
!
    deallocate(phi1m,dphi1m,phi2m,dphi2m,phi3)
    return
end subroutine radial_eigenfunctions
!-----------------------------------------------------------------------
-----
```

```
function dtrmnt(g0,g1,g2,kr,k1,k2,r1,r2,r3,eta)
!-----------------------------------------------------------------------
-----
! Evaluates the determinant whose roots give the radial eigenvalues.
!-----------------------------------------------------------------------
-----
    implicit none
    real*8, intent(in) :: g0,g1,g2,kr,k1,k2,r1,r2,r3,eta
    real*8 dtrmnt
    real*8
j001,j101,j011,j111,y011,y111,j012,j112,y012,y112,j022,j122,y022,y122,j123
,y123
    real*8 x0,x1,x2,cp1,cp2
    real*8 dbesj0,dbesj1,dbesy0,dbesy1
!
!-----Evaluate Bessel functions.
!
    j001=dbesj0(eta*g0*r1); j101=dbesj1(eta*g0*r1)
    j011=dbesj0(eta*g1*r1); j111=dbesj1(eta*g1*r1);
y011=dbesy0(eta*g1*r1); y111=dbesy1(eta*g1*r1)
    j012=dbesj0(eta*g1*r2); j112=dbesj1(eta*g1*r2);
y012=dbesy0(eta*g1*r2); y112=dbesy1(eta*g1*r2)
    j022=dbesj0(eta*g2*r2); j122=dbesj1(eta*g2*r2);
y022=dbesy0(eta*g2*r2); y122=dbesy1(eta*g2*r2)
    j123=dbesj1(eta*g2*r3); y123=dbesy1(eta*g2*r3)
!
!-----Evaluate determinant.
!
    x0=g0*kr; x1=g1*k1; x2=g2*k2
    cp1=x2*(j122*y123-j123*y122); cp2=x1*(y022*j123-y123*j022)
    dtrmnt=(y012*cp1+y112*cp2)*(x1*j001*j111-x0*j101*j011)
    dtrmnt=dtrmnt+(j012*cp1+j112*cp2)*(x0*j101*y011-x1*j001*y111)
!
    return
end function dtrmnt
!-----------------------------------------------------------------------
-----
subroutine spherical_eigenfunctions(pvs,nvs,sevs)
!-----------------------------------------------------------------------
-----
! Evaluates the radial eigenfunctions of the spherical heat diffusion
operator.
!-----------------------------------------------------------------------
-----
    implicit none
    type (PRS_vars), intent(in) :: pvs      !PRS variables
    type (num_vars), intent(in) :: nvs      !Numerical solution parameters
    type (spherical_eigenfunction_vars), intent(out) :: sevs   !Output:
spherical eigenfunction parameters
!-----Local variables.
    real*8 b,yk,fyk,dfyk,zk
    real*8, parameter :: eps=1.d-12         !Tolerance for root
convergence
    integer k,n,icnvrg
```

```
    integer, parameter :: maxit=100         !Maximum iterations of
Newton's method
!
!-----Check input.
!
    b=0.5d0*(pvs%avg_kf/pvs%avg_ks)*pvs%avg_Nu-1.d0
    if(b .le. -1.d0)then                    !b < -1 corresponds to a
negative Nusselt number
       write(*,*)'Spherical_eigenfunctions: Invalid b',b
       stop
    endif
!
!-----Allocate storage for eigenfunction variables.
!

allocate(sevs%root(nvs%ns),sevs%norm(nvs%ns),sevs%beta(nvs%ns),sevs%seR(nv
s%ns),sevs%lambdasq(nvs%ns))
!
!-----Find roots using Newton's method.
!
    do k=1,nvs%ns
       zk=(2*k-1)*pi/2
       yk=zk+(sqrt(zk**2+4*b*(1+b/2))-zk)/(b+2)  !Initial guess for root
based on second order expansion of eigenvalue equation
       icnvrg=0
       do n=1,maxit
          fyk=b*sin(yk)+yk*cos(yk)
          dfyk=(b+1)*cos(yk)-yk*sin(yk)
          if(abs(dfyk) .lt. 1.d-12)then
             write(*,*)'Radial_eigenfunctions: Newton method failure',dfyk
             stop
          else if(abs(fyk/dfyk) .gt. pi/2)then
             write(*,*)'Radial_eigenfunctions: Newton step too
large',abs(fyk/dfyk)
             stop
          else
             yk=yk-fyk/dfyk
             if(abs(fyk/dfyk) .lt. eps*abs(yk))then
                icnvrg=1
                exit
             endif
          endif
       end do
       if(icnvrg .eq. 0)then
          write(*,*)'Spherical_eigenfunctions: Newton method fails to
converge'
          stop
       endif
       if(k .gt. 1)then
          if(yk .le. sevs%root(k-1))then
             write(*,*)'Radial_eigenfunctions: Eigenvalue sequence not
increasing'
             write(*,*)yk,sevs%root(k-1)
             stop
          endif
```

```
        endif
        sevs%root(k)=yk
        sevs%norm(k)=yk*sqrt(2.d0/(1.d0-sin(2*yk)/(2*yk)))
        sevs%beta(k)=(b+1)*sevs%norm(k)*sin(yk)/yk**3
        sevs%seR(k)=sevs%norm(k)*sin(yk)/yk

sevs%lambdasq(k)=(pvs%avg_ks/(pvs%cs*pvs%rhos))*(sevs%root(k)/(pvs%pdiam/2
))**2
    end do
!
!-----End of subroutine.
!
    return
end subroutine spherical_eigenfunctions
!
!-----End module.
!
end module DC_PRS_2D_ee_UW_mod
```

Appendix C

Single-Blow Operating Instructions

The system schematic for the single blow test stand is shown in Figure A2.1. Each valve is numbered in Figure A2.1 for reference purposes. Valves 1, 3 and 4 are manual 3-way valves and Valve 2 is a solenoid valve. Bath 1 and Bath 2 are temperature controlled baths. BV 1 and BV 2 are bleeder valves used to purge air from the system. SV is a shutoff valve, and AF 1 and AF 2 are quick-connect air fittings. For the purpose of describing the state of each valve, each valve will be referred to as being in state 1 when the cold soak flow loop is used and position 2 when the main pump flows through the test section into the graduated cylinder. For example, when Valve 1, the on/off solenoid valve, is in the off position, it is in position 1. In Figure A2.1, Valve 1 is in Position 1 and Valve 4 is in Position 2. A photograph of the test stand is shown in Figure A2.2.

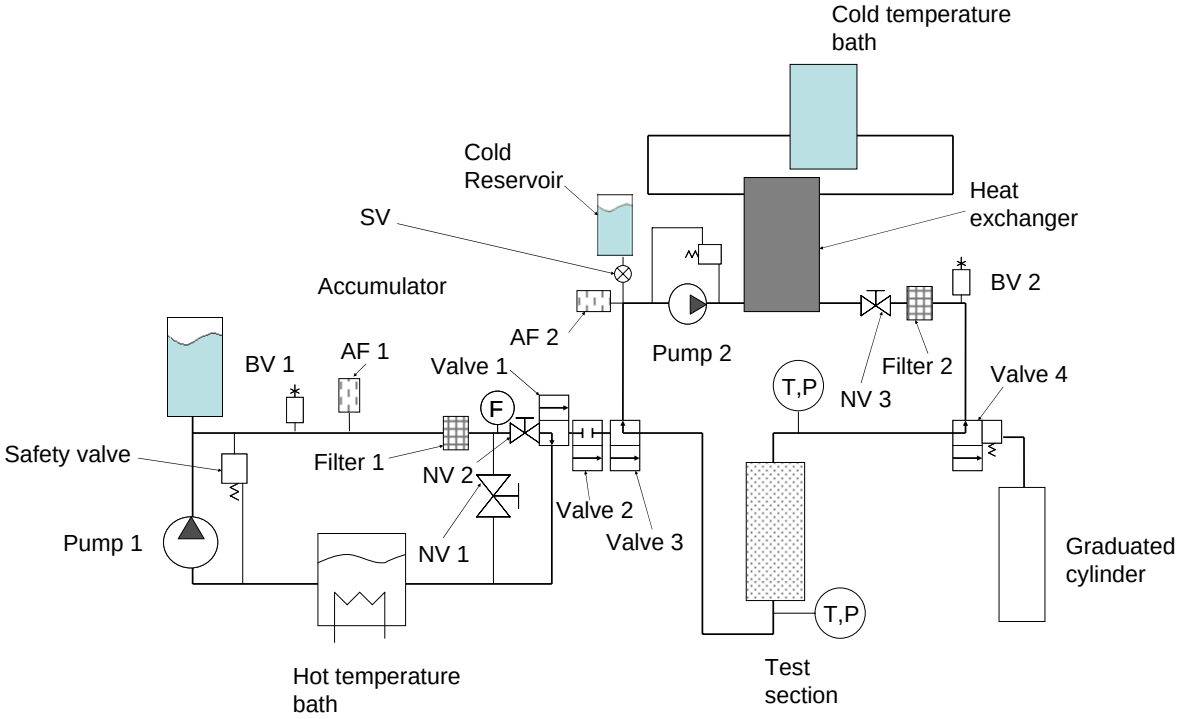

Figure A2.1. Schematic of the single blow test facility

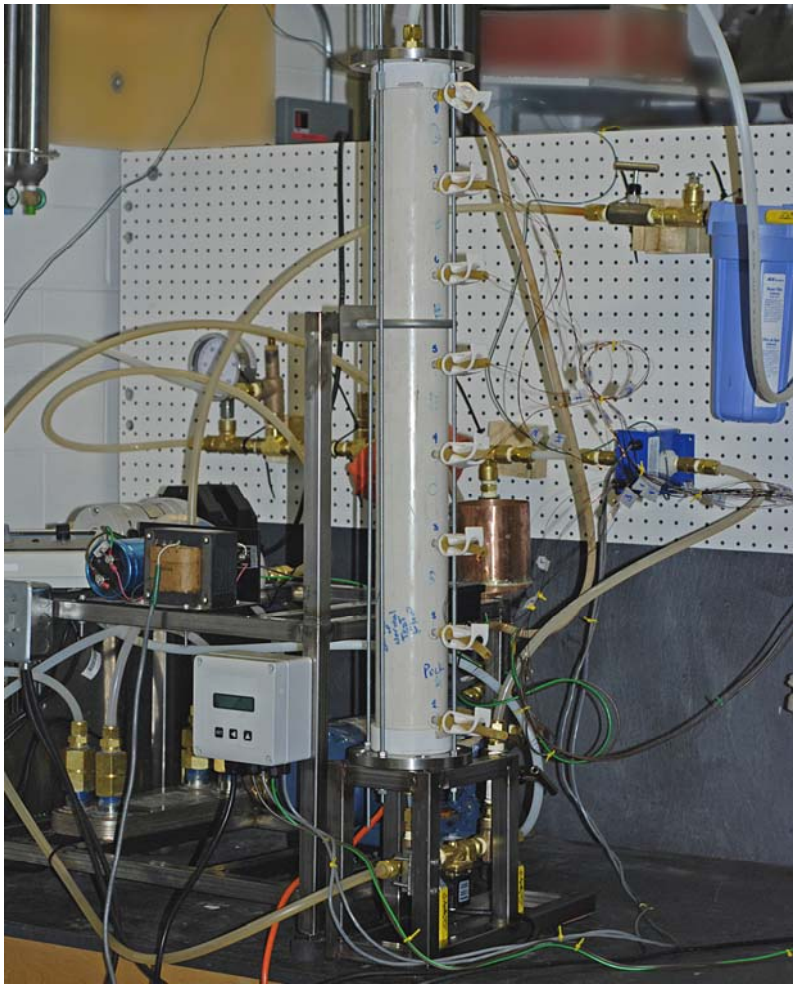

Figure A2.2. Single blow test facility

Below are operating procedures for the single blow test stand.

Filling the System

It is very important to system performance that the system have as few bubbles as possible. Bubbles tend to accumulate in the regenerator and can cause significant measurement error. It is acceptable if there are standing bubbles in the cold soak system that do not pass through the regenerator. However, any bubbles in the flow loop used to conduct an experiment must be purged.

The system should be as dry as possible before filling. Start with power to the pumps and controlled temperature baths off. The following steps should be taken to purge all air from the system during filling:

1. Begin with both pumps off and the valves in the following positions.

Valve Name	Position
Valve 1	2
Valve 2	1
Valve 3	1
Valve 4	1
NV 1	partially open
BV 1	closed
BV 2	open
SV	open

The valves should be positioned as shown in Figure A2.3. The flow schematic in this position is shown in Figure A2.1.

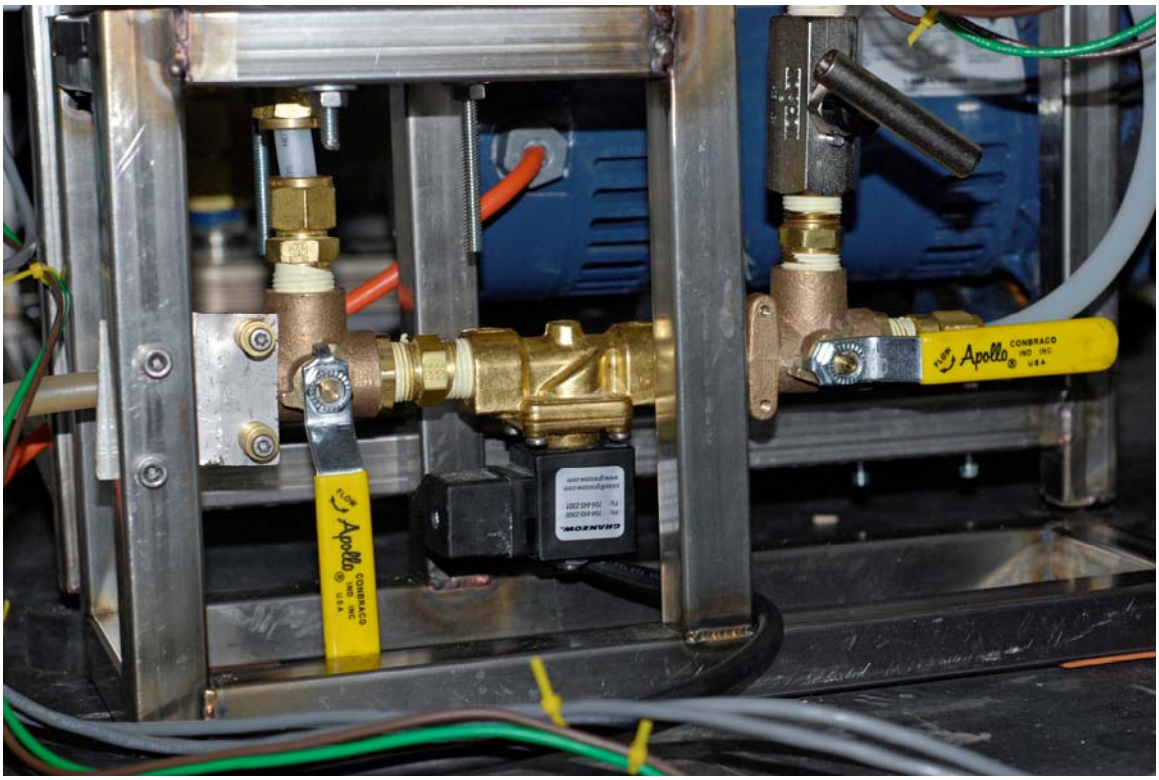

Figure A2.3. Photograph of 3-way valve positions during filling.

2. Fill Bath 1. Slowly fill the cold reservoir with the bleeder valve, BV 2, open. A photograph of BV 2 is shown in Figure A2.4. Ensure that the shut-off valve below the cold reservoir is open. Fill the cold reservoir then close BV 2. Pump 1 is self priming so no efforts to prime the pump are necessary.

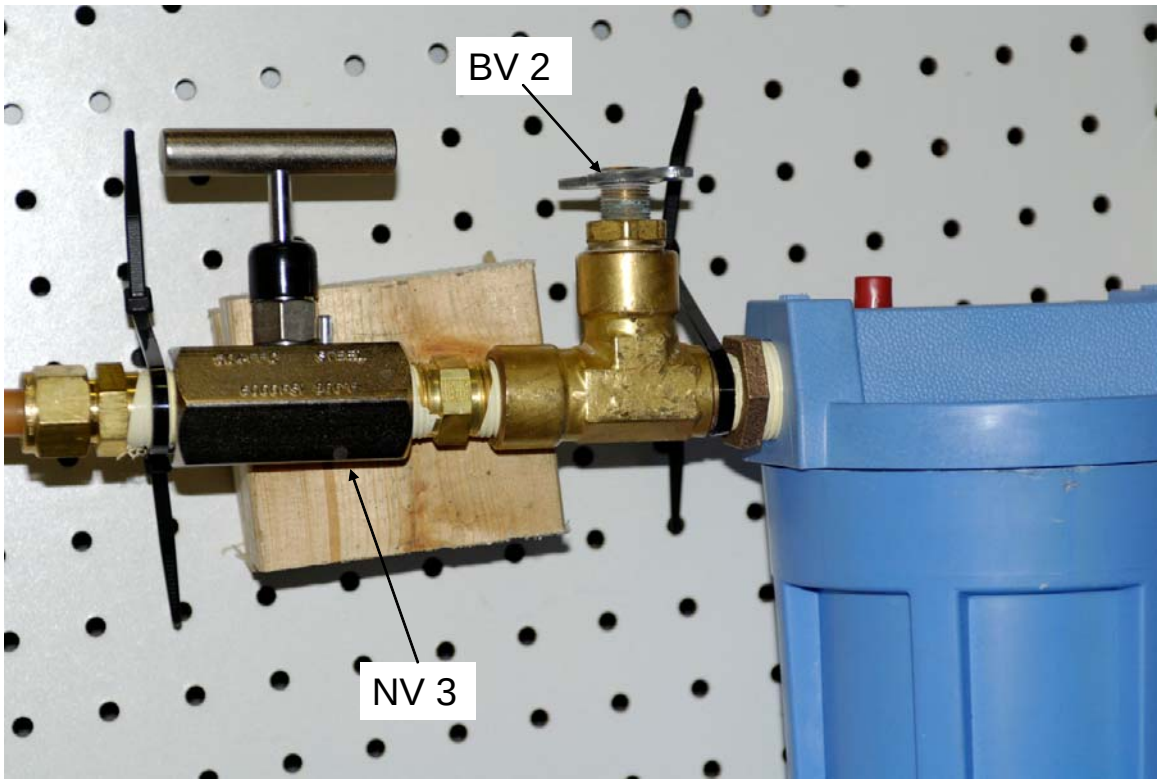

Figure A2.4. Photograph of bleed valve, BV 2.

3. Slowly increase the speed of Pump 1. Allow the pump to run until there are no visible bubbles in the return flow to Bath 1. Be sure that the fluid level in Bath 1 remains at an adequate level. Open valve 5 and allow the pump to run until there are no visible in the return flow to Bath 1. Crack BV 1 to purge any trapped air in the system. A photograph of BV 1 is shown in Figure A2.5.

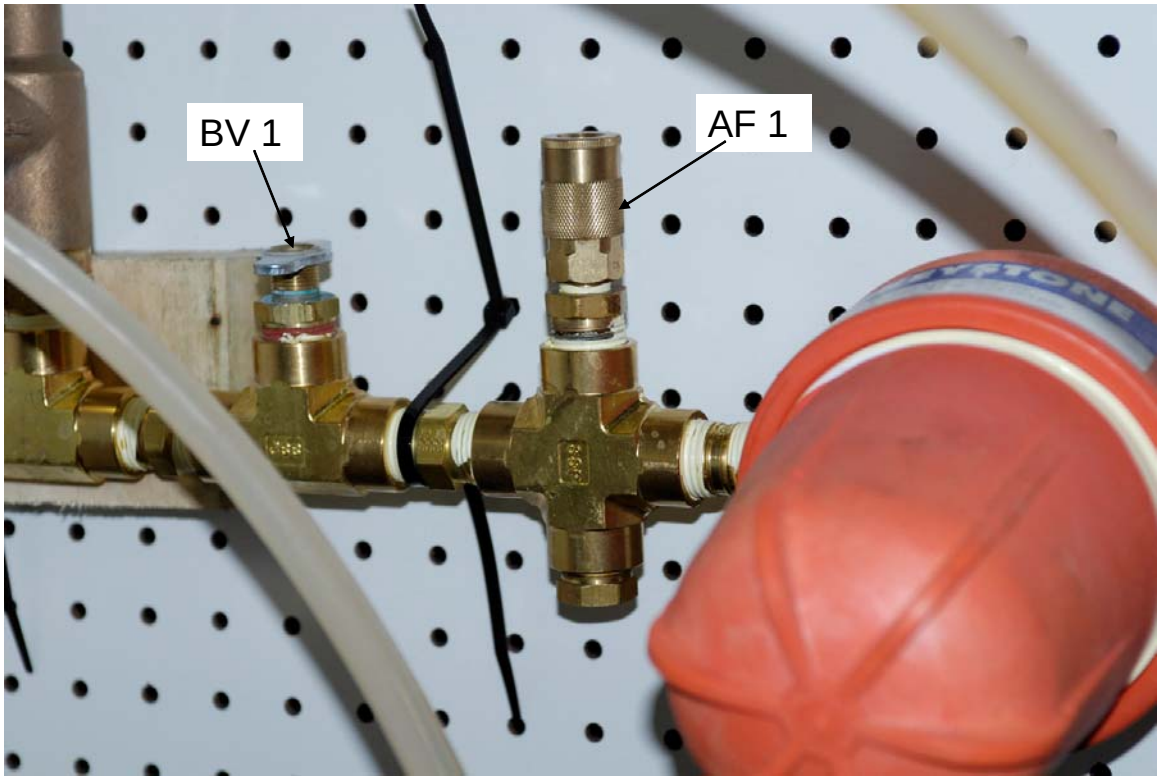

Figure A2.5. Photograph of bleed valve, BV 2.

4. Turn Pump 2 on to a slow flow rate and allow the pump to run. Add fluid to the cold reservoir as needed and be sure not to allow the level to drop below the bottom of the reservoir. Crack BV 2 while the pump is running and allow bubbles to escape. Add fluid to the cold reservoir as necessary. It may be necessary to start and stop the pump several times to purge some of the bubbles. It will likely be necessary to repeat step 3 in order to purge air from the regenerator.
5. Switch Valve 5 to position 2 by energizing the solenoid. Allow Pump 1 to run until there are no visible bubbles in the flow to the graduated cylinder. De-energize the solenoid and increase the pump speed. Switch the solenoid valve on and off several times until no additional bubbles flow out of the regenerator when the solenoid is energized.
6. There is often a bubble that gets trapped near valve 1. One way to purge this bubble is to run pump 1 at a moderate rate and slowly switch the position in valve 1 until the bubble is purged are reduced to a very small size that will not flow into the regenerator.

Emptying the System

If the fluid mixture is to be changed, it is necessary to purge as much of the fluid in the system as possible. All power to the pumps and controlled temperature baths should be off. The following steps should be taken to purge the system:

1. Drain Bath 1. Position the valves as follows:

Valve Name	Position
Valve 1	1
Valve 2	2
Valve 3	2
Valve 4	1
NV 1	closed
BV 1	closed
BV 2	closed
SV	open

2. Reverse polarity to the pump motor so it will pump in the opposite direction. Turn Pump 1 on and allow it to pump fluid from the regenerator and connecting piping into Bath 1. Turn Pump 1 off once fluid ceases to flow into Bath 1.
3. Close the cold reservoir shut-off valve, SV.
4. Apply a regulator hooked to shop air to the quick connect coupling, AF 1, and allow the compressed air to push the fluid out into the graduated cylinder. Move Valve 1 into position 2 and allow the compressed air to purge the fluid into Bath 1. Close Valve 5 and wait until liquid no longer exits into the graduated cylinder. Remove the regulator from AF 1.
5. Move Valve 3 into position 1. Move Valve 2, the solenoid valve, to position 1 by de-energizing it. Apply a regulator hooked to shop air to the quick connect coupling, AF 2, and open the bleeder valve, BV 2. A piece of ¼" tubing can be placed in the outlet of the bleeder valve to reduce fluid spray. Allow the compressed air to push the fluid out the bleeder valve for several minutes. Remember to drain the cold reservoir. This can be done by setting the air pressure to 0 and opening the shut-off valve, SV, to let the fluid drain into the piping. Increase the air pressure again to purge as much of the remaining fluid as possible. Remove the compressed air line from AF 2.
6. Empty the filters for the hot and cold systems. Inspect the filter elements and change them, if necessary.

Setting flow rate through regenerator

The flow rate through the regenerator can be controlled through a combination of varying the speed of pump 1, opening the bypass needle valve (NV1), setting the flow resistance to the regenerator by opening the needle valve upstream of the regenerator (NV2). The flow rate should be set in such a way as to maintain a sufficiently low pressure drop across the system and reduce the flow spike when the solenoid valve is opened. To set the flow rate through the regenerator:

1. Set the speed of pump 1. Generally it should be set to a value of 5 or higher.
2. Set the flow restriction of NV2.
3. Adjust the flow rate to the desired value by opening the bypass needle valve (NV1).
4. De-energize the solenoid valve (Valve 2), allow the system to stabilize, then re-energize it and ensure that the flow rate is still the desired value.

Temperature Soaking the System

Before each test, the system must be thermally soaked to achieve a uniform initial cold temperature in the test section and uniform initial warm temperature in the rest of the system. To thermally soak the system:

1. Before the system is set to cold soak mode, the flow rate through the regenerator must be set to the desired value in order to run the test after the system has been soaked. See above for setting flow rate before beginning the cold soak process.
2. Set the desired temperature of Bath 1 and Bath 2.
3. Set the valves to the following positions. It is generally best to switch the position of Valve 4 first.

Valve Name	**Position**
Valve 1	2
Valve 2	1
Valve 3	1
Valve 4	1
BV 1	closed
BV 2	closed

The valves should now be in the positions shown in Figure A2.6. The flow schematic for cold soak operation is shown in Figure A2.7.

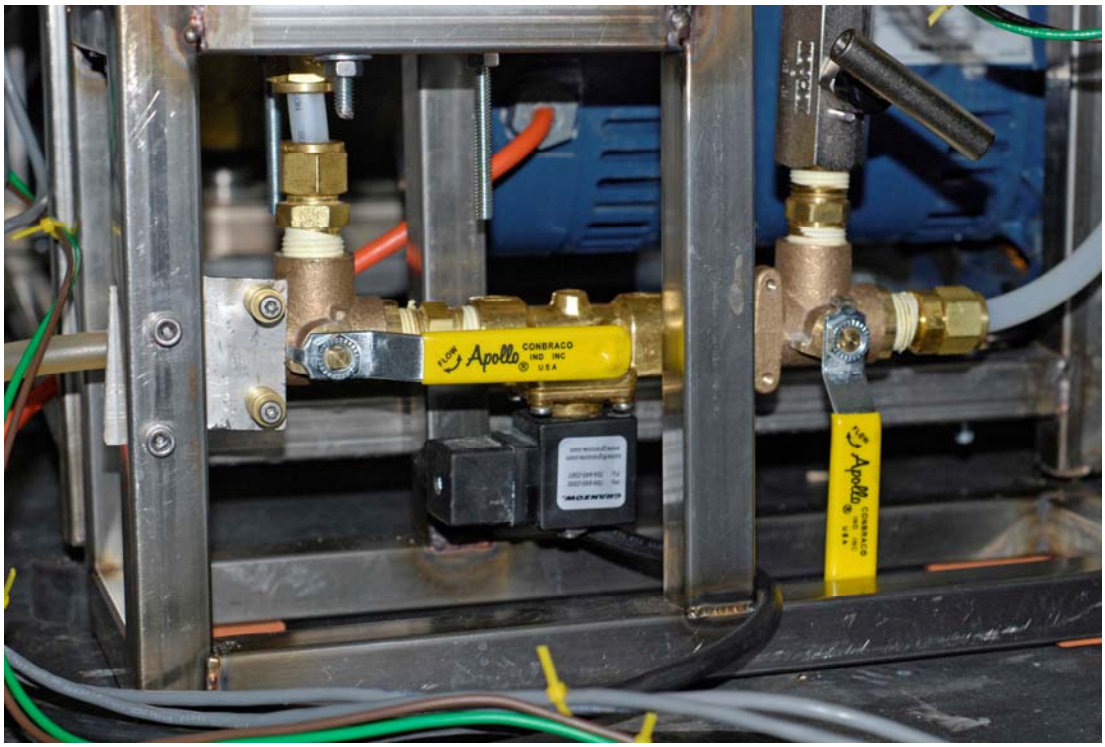

(a)

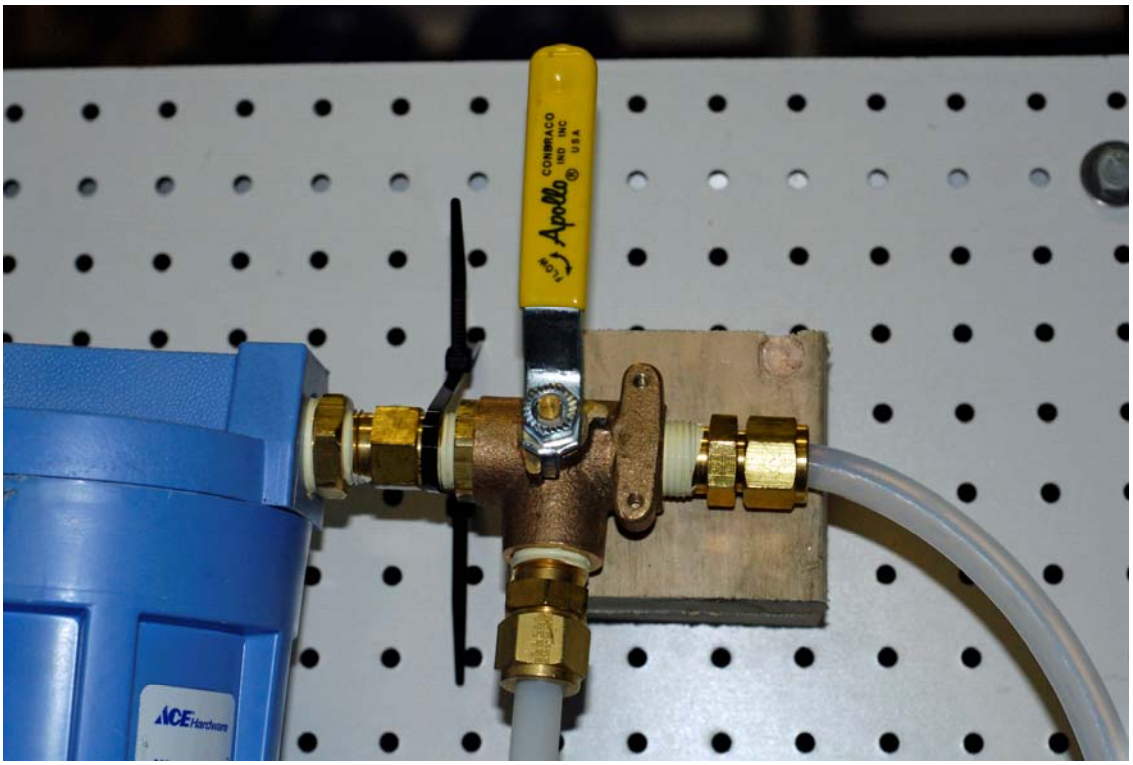

(b)

Figure A2.6. Photograph of (a) Valves 1 – 3 and (b) Valve 4 during the cold soak operation.

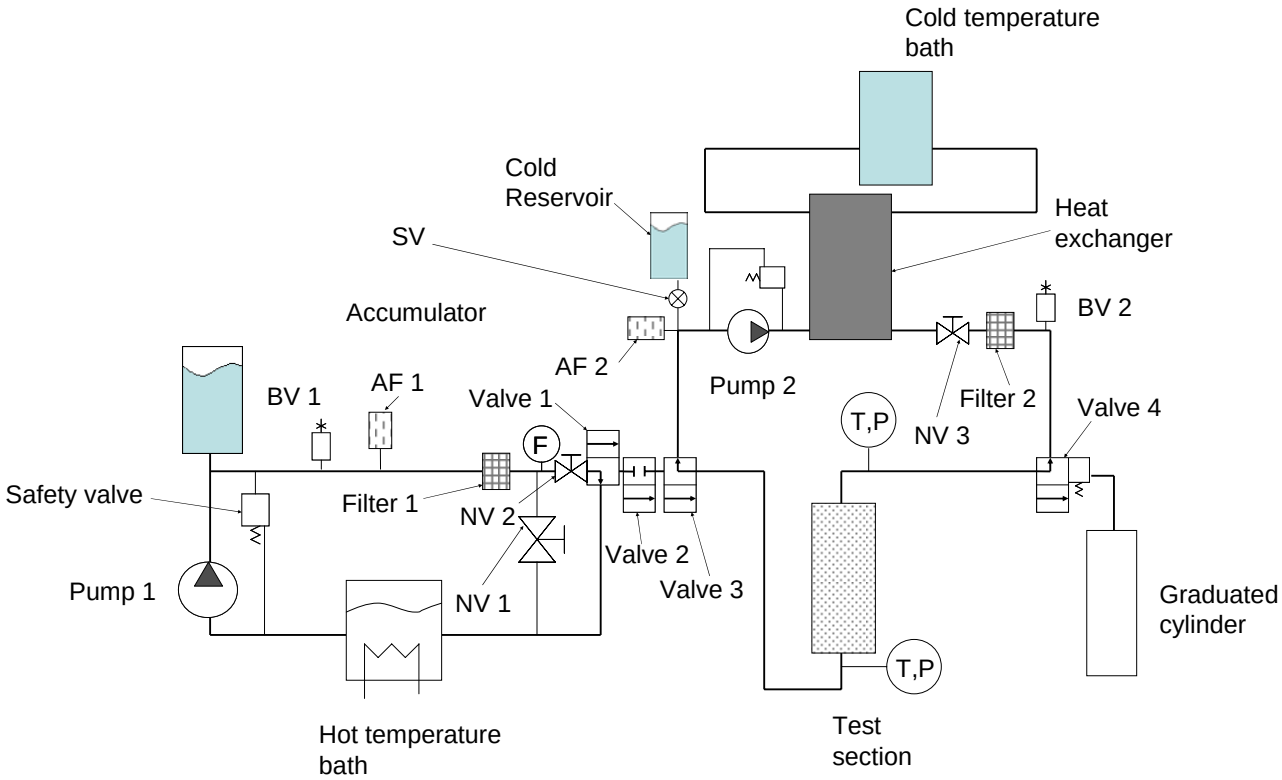

Figure A2.7. System flow schematic cold soak.

4. Turn on Pump 1 and Pump 2 and allow the entire system to reach thermal equilibrium. This will take approximately 15 minutes depending on the temperatures of the hot and cold reservoirs.

Running an Experiment

1. Ensure that Bath 1 and Bath 2 are set to the correct temperatures and that Pump 1 is set to the correct speed. Pump 2 should be turned off. The system should have attained thermal equilibrium in the soak mode and should not have been exposed to ambient temperature for an extended period of time.
2. Before the experiment begins, the valves should be in the following positions.

Valve Name	Position
Valve 1	1
Valve 2	1
Valve 3	2
Valve 4	2
BV 1	closed
BV 2	closed

The valves should be in the positions shown in Figure A2.8. The flow schematic for cold soak operation is shown in Figure A2.9.

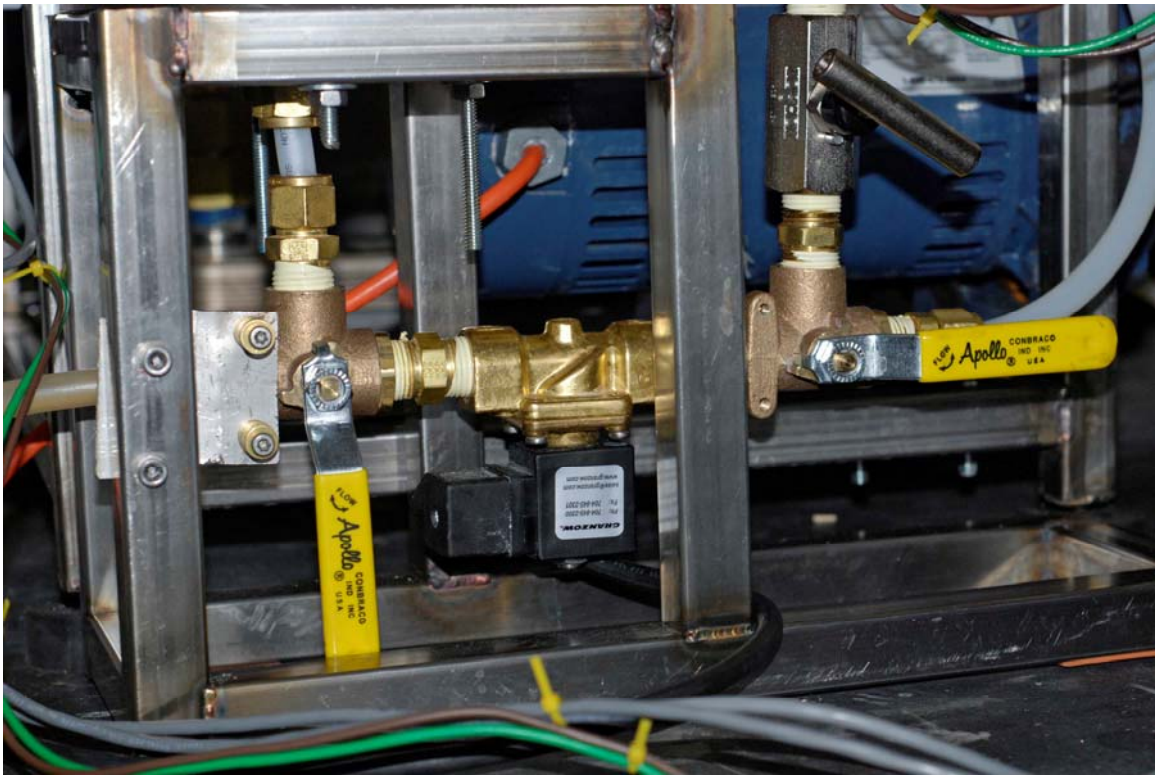

(a)

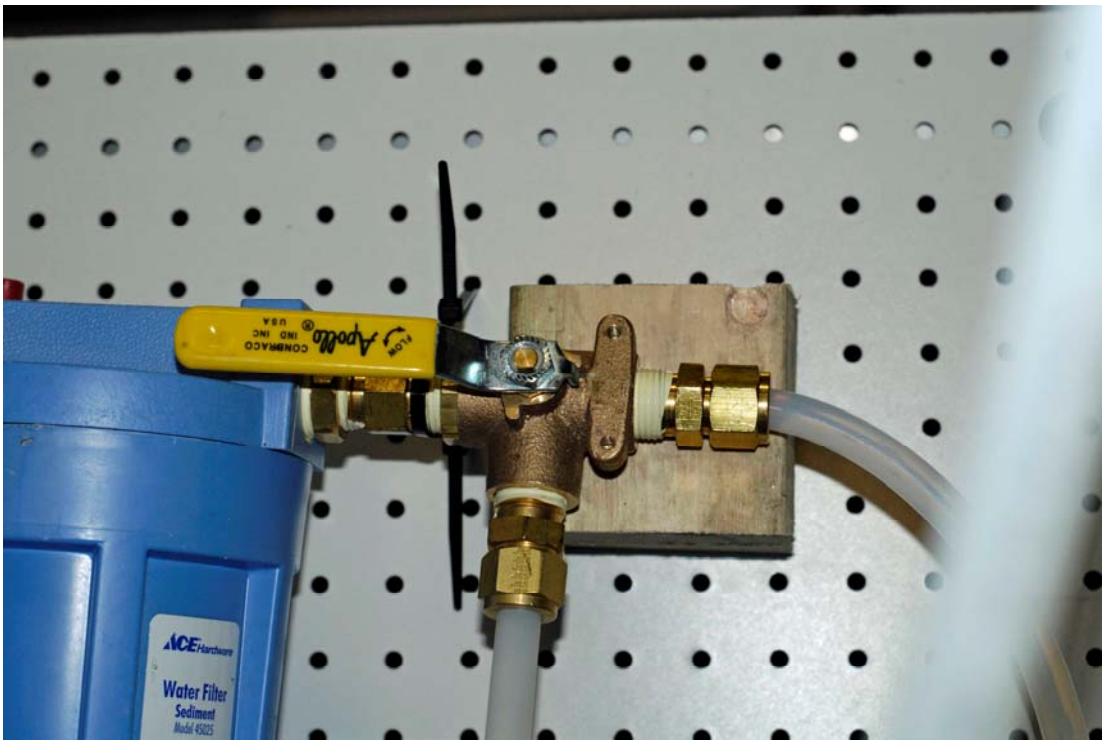

(b)

Figure A2.8. Photograph of (a) Valves 1 – 3 and (b) Valve 4 during an experiment.

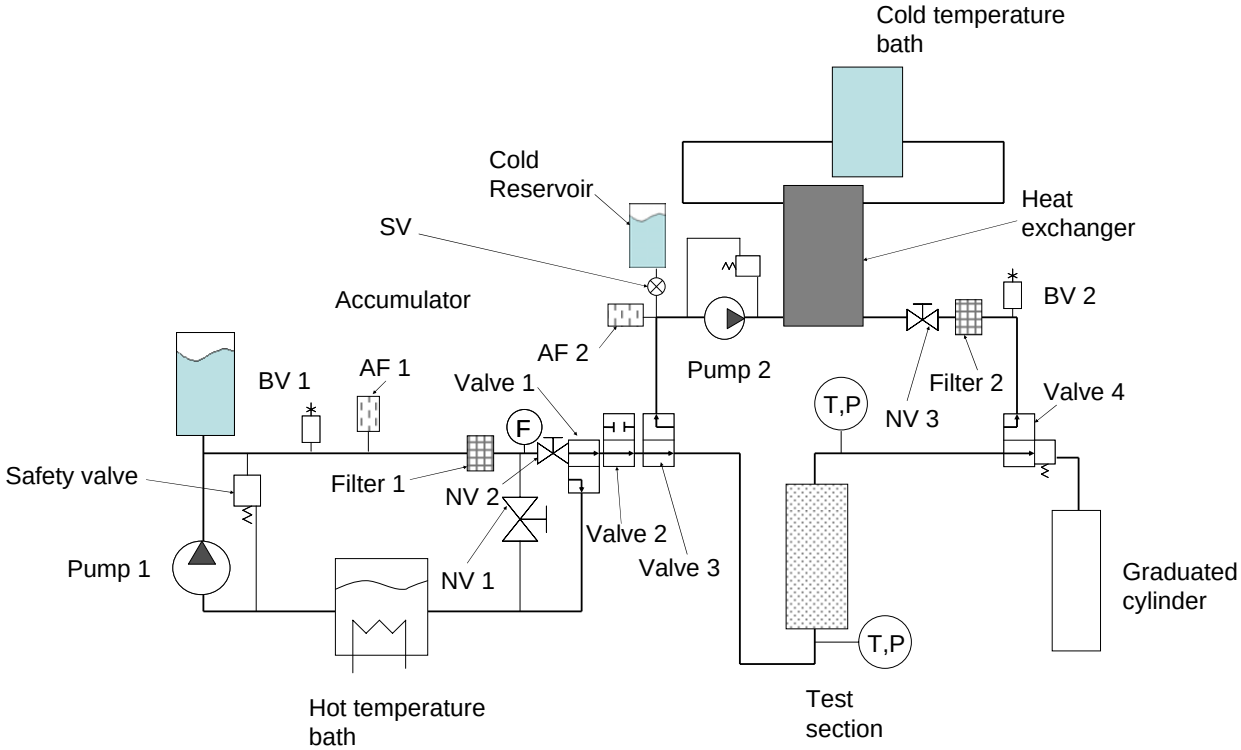

Figure A2.9. System flow schematic during an experiment.

3. Start data collection.
4. The test begins when Valve 2 (the solenoid valve) opens and allows fluid to flow from the pump to the test section.
5. After an appropriate amount of time, switch Valve 2 to Position 1 (closed) to stop the test.
6. Record the amount of fluid collected in the graduated cylinder and transfer the fluid to Bath 1.

Description of System Components

Label	Description	Function
safety valve	adjustable crack pressure check valve	relieve pressure on pump 1 to prevent failure
pump 1	peristaltic pump	pump used during experiment
pump 2	centrifugal pump	cold soak pump
BV 1	bleed valve	purge bubbles from main flow path
BV 2	bleed valve	purge bubbles from the cold soak circuit
AF 1	quick-connect air fitting	purge heat transfer fluid from the main flow loop
AF 2	quick-connect air fitting	purge from the cold soak circuit
Filter 1	water filter	protect flow meter from particulates
Filter 2	water filter	protect the regenerator and the cold soak circuit from particulates from pump 2
NV 1	needle valve	allows fluid to bypass the regenerator during an experiment, which allows for precise flow rate control and can reduce flow spikes when the solenoid valve is opened
NV 2	needle valve	controls the restriction of the regenerator in order to reduce flow spikes when the solenoid valve opens
NV 3	needle valve	controls the restriction of the cold soak circuit, which controls the flow rate through Filter 2 and the regenerator during the cold soak process
Valve 1	3 way valve	controls the direction of flow from pump 1
Valve 2	solenoid valve	is energized to provide a step change in flow across the regenerator
Valve 3	3 way valve	controls flow direction into the regenerator
Valve 4	3 way valve	controls flow direction out of the regenerator
SV	shut-off valve	allows the cold soak circuit reservoir to be shut off from the rest of the system
Heat exchanger	counter-flow heat exchanger	provides thermal communication between the cold temperature bath and the cold soak circuit
Cold reservoir	Reservoir	provides a fluid reservoir for the cold soak circuit and allows the cold soak circuit to be filled independently of the main circuit